

LIBRARY Michigan State University

This is to certify that the thesis entitled

MULTIPOINT OPTIMIZATION OF A 3D RADIAL COMPRESSOR IMPELLER

presented by

Steven C. Kowalski Jr.

has been accepted towards fulfillment of the requirements for the

M.S. degree in Mechanical Engineering

Major Professor's Signature

MSU is an Affirmative Action/Equal Opportunity Institution

Date

PLACE IN RETURN BOX to remove this checkout from your record.

TO AVOID FINES return on or before date due.

MAY BE RECALLED with earlier due date if requested.

DATE DUE	DATE DUE	DATE DUE

2/05 c:/CIRC/DateDue.indd-p.15

MULTIF

MULTIPOINT OPTIMIZATION OF A 3D RADIAL COMPRESSOR IMPELLER

Ву

Steven C. Kowalski Jr.

A THESIS

Submitted to
Michigan State University
in partial fulfillment of the requirements
for the degree of

MASTER OF SCIENCE

Department of Mechanical Engineering

2005

In this we geometry at the concepts. In mumerical tool

- Artifici
- Genetic
- Vavier-

With this s

as an Artificia accurate but slo design being a (

Optimum g

case which we

geometry. Thus,

operating point v

ABSTRACT

MULTIPOINT OPTIMIZATION OF A 3D RADIAL COMPRESSOR IMPELLER

By

Steven C. Kowalski Jr.

In this work, one has attempted to find an optimum radial compressor impeller geometry at both single and multi-point operation by utilizing advanced numerical concepts. In particular the optimization that was attempted is based on advanced numerical tools applied to aerodynamics such as:

- Artificial Neural Network (ANN)
- Genetic Algorithm (GA)
- Navier-Stokes Solver (NS)

With this system the performance is predicted using a fast approximate model known as an Artificial Neural Network (ANN), and then subsequently verified by a very accurate but slow computing Navier-Stokes Solver, the core of this knowledge based-on design being a Genetic Algorithm (GA).

Optimum geometries were found for both the single point case and multiple point case which were different and have improved efficiencies relative to the baseline geometry. Thus, the main conclusion is that the geometry that works well for one operating point will not necessarily work well for multiple point operation.

Copyright by Steven C. Kowalski Jr. 2005

This

This thesis is dedicated to my parents, Steve and Sue Kowalski.

I would 1 all the suppor for recommen Karman Instit following peop I would 1: gratitude for th supervision, hi academic year. I would also advice that I rece a doubt that I we Thanks as well provided me.

Thanks as well
provided me.
Next, so as to
come to know are
work environmes:
Last, but by
support.

ACKNOWLEDGMENTS

I would like to thank Professor A. Engeda of Michigan State University (MSU) for all the support and advice he has given me during my academic years at MSU and also for recommending me to be a participant of this prestigious institution known as the von Karman Institute (VKI). It has definitely been an opportunity of a lifetime. The following people that are greatly acknowledged are all from the world famous VKI.

I would like to express Professor R.A. Van den Braembussche all my sincere gratitude for the opportunity he has given me to work on this project, for his help and his supervision, his knowledge and wisdom, which he shared with me throughout the academic year.

I would also like to thank Dr. Z. Alsalihi for his kindness, patience and the great advice that I received countless times throughout the duration of this project. It is without a doubt that I would have never been able to complete this project without his guidance. Thanks as well to Mr. J. Prinsier and Mr. T. Verstraete for all their help that they provided me.

Next, so as to not leave anyone out, I am very thankful for all the students that I have come to know and appreciate during my period of study here at the VKI, for the positive work environment they have created, and for their friendships.

Last, but by no means least, I would like to thank my parents for all there loving support.

Steven C. Kowalski Jr.

LIST OF TAB

LIST OF FIGU

KEY TO SYM

INTRODUCTI

CHAPTER 1 BACKGROUN

1.1 Air Cor

1.2 Limitin

1.3 Technic

14 Need fo

CHAPTER 2 OPTIMIZATIO:

2.1 General

2.2 Databas 2.3 Artificia

2.4 Genetic

2.5 Objectiv

CHAPTER 3
BASELINE GE(

3.1 Geometr 3.2 Fundame

3.3 Meshing 3.4 Navier-S

3.4.1 Sol

3.4.2 Bo

3.4.3 Pos

3.4.4 Ba

CHAPTER 4
SINGLE POINT

4.1 Geometr

42 Design S 43 ANNS U

4.4 Objectiv

4.4.1 On

4.4.2 G.

TABLE OF CONTENTS

LIST OF TABLES	viii
LIST OF FIGURES	ix
KEY TO SYMBOLS AND ABBREVIATIONS	xiii
INTRODUCTION	1
CHAPTER 1	
BACKGROUND AND MOTIVATION	3
1.1 Air Conditioning Fundamentals	
1.2 Limiting factors of flow range	
1.3 Techniques to extend the flow range	
1.4 Need for Multi-point optimization	
CHAPTER 2	
OPTIMIZATION METHOD	24
2.1 General Philosophy	24
2.2 Database	
2.3 Artificial Neural Network	31
2.4 Genetic Algorithm	36
2.5 Objective Function	38
CHAPTER 3	
BASELINE GEOMETRY	41
3.1 Geometric Fitting	41
3.2 Fundamentals of the TRAF3D Program	
3.3 Meshing approach and parameters	46
3.4 Navier-Stokes Solver Parameterization	54
3.4.1 Solution Parameters	54
3.4.2 Boundary Conditions	56
3.4.3 Post-Processing Parameters	
3.4.4 Baseline Performance	
CHAPTER 4	
SINGLE POINT OPTIMIZATION	67
4.1 Geometry Definition	67
4.2 Design Space	
4.3 ANNs Utilized	
4.4 Objective Function and GA Settings	
4.4.1 Objective Function	
4.4.2 GA Settings	0.4

4.5 Presen 4.5.1 D

4.5.2 C 4.5.3 z

4.6 Perform

CHAPTER 5 MULTIPOINT

5.1 Objects 5.1.1 O

5.1.2 G

5.2 Present 5.2.1 D

5.2.2 Co

5.2.3 At 5.3 Perform

CHAPTER 6 OVERALL CO:

REFERENCES

4.5 Presentation of the Optimization	87
4.5.1 Database	
4.5.2 Convergence History	
4.5.3 Analysis of Optimized Geometries	
4.6 Performance of Optimum Geometry and conclusion	on122
CHAPTER 5	
MULTIPOINT OPTIMIZATION	130
5.1 Objective Function and GA Settings	130
5.1.1 Objective Function	130
5.1.2 GA Settings	
5.2 Presentation of the Optimization	
5.2.1 Database	137
5.2.2 Convergence History	
5.2.3 Analysis of Optimized Geometries	
5.3 Performance of Optimum Geometry and conclusion	on176
CHAPTER 6	
OVERALL CONCLUSIONS AND FUTURE WORK	181
REFERENCES	184

Table 2.1

Table 3.1

Table 3.2

Table 3.3

Table 4.1

Table 4.2 V

Table 4.3 G

Table 4.4 D.

Table 4.5 Na

Table 4.6 Ch.

Table 5.1 Wes

Table 5.2 GA

Table 5.3 NS re

Table 5.4 NS re

Table 5.5 NS R

Table 5.6 NS Re

Table 5.7 NS Ru

Table 5.8 NS Ru

Table 5.9 Chara

LIST OF TABLES

Table 2.1	GA's Terminology	36
Table 3.1	Characteristics of the Baseline Geometry	45
Table 3.2	Impeller Mesh Parameters (number of cells)	49
Table 3.3	Near wall parameters	52
Table 4.1	Geometric Variables	73
Table 4.2	Weights used in Single point Optimization	84
Table 4.3	GA and ANN Parameters	84
Table 4.4	Database Navier-Stokes Results	91
Table 4.5	Navier-Stokes calculations of Optimized Geometries	116
Table 4.6	Characteristics of Single Point Optimum	124
Table 5.1	Weights used in Multiple Point Optimization	134
Table 5.2	GA and ANN Parameters	134
Table 5.3	NS results of the Database at IGV Setting Angle = 0 Degrees	139
Table 5.4	NS results of the Database at IGV Setting Angle = 40 Degrees	140
Table 5.5	NS Results of the Database at IGV Setting Angle = 60 Degrees	141
Table 5.6	NS Results of the Optimizations at Pre-rotation = 0 Degrees	152
Table 5.7	NS Results of the Optimizations at Pre-Rotation = 40 Degrees	153
Table 5.8	NS Results of the Optimizations at Pre-Rotation = 60 Degrees	154
Table 5.9	Characteristics of the Multi-Point Optimum Geometry	177

Figure 1.1 Ge

Figure 1.2 Air

Figure 1.3 Sch

Figure 1.4 Imp

Figure 1.5 Effi

Figure 1.6 Con

Figure 1.7 Wor

Figure 1.8 Perf

Figure 1.9 Perti

Figure 1.10 Intl

Figure 1.11 Per

Figure 1.12 Ma

Figure 1.13 Illu

Figure 1.14 Uni separated flow.

Figure 1.15 Nor

Figure 2.1 Flow

Figure 2.2 Com

Figure 2.3 A Th

Figure 2.4 Sigm

Figure 2.5 Propo

Figure 2.6 Flow

LIST OF FIGURES

Figure 1.1 Generalized phase change process	4
Figure 1.2 Air Conditioning cycle	6
Figure 1.3 Schematic of an air conditioning unit	7
Figure 1.4 Impeller Nomenclature. [6]	.10
Figure 1.5 Effect of incidence on boundary layer accumulation. [6]	.12
Figure 1.6 Components that are capable of extending the flow range	.13
Figure 1.7 Working principle of IGVs [6]	.14
Figure 1.8 Performance map with variable inlet swirl using a vaneless diffuser	.15
Figure 1.9 Performance map with peripheral speeds using a vaneless diffuser	.17
Figure 1.10 Influence of a diffuser vane on the flow in a radial diffuser. [9]	.19
Figure 1.11 Performance map with variable inlet angle of diffuser. Swirl free inflow	.19
Figure 1.12 Mach number distribution illustrating incidence of IGV. [3]	.21
Figure 1.13 Illustration of flow separation of an IGV . [3]	.21
Figure 1.14 Unbalance of Centrifugal and pressure gradient forces and radial shift of separated flow. Suction side.	.22
Figure 1.15 Non-uniform impeller total pressure distribution	.23
Figure 2.1 Flowchart of optimization system. [2]	.25
Figure 2.2 Comparison of DOE and Random database generation. [2]	.30
Figure 2.3 A Three-Layer Artificial Neural Network. [2]	.31
Figure 2.4 Sigmoid Transfer function. [2]	.32
Figure 2.5 Properly trained (a) and improperly trained (b) data	.35
Figure 2.6 Flow Chart of the working principle of a GA. [2]	.38

Figure 3.1 Definitions of the meridional contour geometric parameters. [4]	41
Figure 3.2 Baseline Geometry: (a) Meriodinal contours. (b) Blade profiles	43
Figure 3.3 Main Grid Parameters. H-type Grid. [5]	48
Figure 3.4 Boundary layer mesh parameters. [5]	50
Figure 3.5 Typical Blade to Blade Plane Grids. (a) Shroud (b) Hub	53
Figure 3.6 Convergence History	55
Figure 3.7 Non-Uniform Inlet Profiles. (a). Pressure (b). Flow Angle	57
Figure 3.8 Post-Processing Planes and numerical pinch	60
Figure 3.9 Performance Maps. (a) π , (b) η_{ts} , (c) η_{tt}	61
Figure 3.10 Mach Number Distributions at various Pre-Rotations: (a) 0 degrees	(b) 40
degrees, (c) 60 degrees	64
Figure 4.1 Geometry definition and baseline. (a) Geometry Definition, (b) Baseline.	ine67
Figure 4.2 Illustration of design space concept	70
Figure 4.3 Inducer stalling and choking incidence as a function of leading edge a	ıngle and
inlet Mach number	72
Figure 4.4 Main Blade and splitter blade contours	75
Figure 4.5 Definition of (a) outlet lean (b) inlet lean	76
Figure 4.6 Illustration of Splitter channels	78
Figure 4.7 Neural Network Structure	79
Figure 4.8 Mach number distribution demonstrating unwanted features	83
Figure 4.9 General Working Principle of the Genetic Algorithm. [2]	86
Figure 4.10 The operating point chosen, P2/P01 _{imposed} = 1.4	88

Figure 4.11 Mach Number Distribution Database sample 1	92
Figure 4.12 Mach number distribution of Database sample 20	93
Figure 4.13 Mach number distribution of Database sample 24	94
Figure 4.14 Total Penalty. (a) With database. (b) Without database	96
Figure 4.15 Total-Static Efficiency Penalty. (a) With database (b) Without database	98
Figure 4.16 Channel mass difference Penalty. (a) With database (b) Without database 1	00
Figure 4.17 Mass Penalty. (a) With database (b) Without database1	02
Figure 4.18 Negative Loading Penalty. (a) With database (b) Without database1	04
Figure 4.19 Negative Loading Penalty. (a) With database (b) Without database1	06
Figure 4.20 Loading Unbalance Penalty. (a) With database (b) Without database1	08
Figure 4.21 Loading Unbalance Penalty. (a) With database (b) Without database1	10
Figure 4.22 Comparison of efficiencies(T-S and T-T) of the database and iterations1	13
Figure 4.23 Meridional Contours (left) and Mach distributions (right) of Iterations1	17
Figure 4.24 Baseline Mach number distribution. Illustrates the improvement	23
Figure 4.25 Performance Maps. (a) π (b) η_{ts} (c) η_{tt}	25
Figure 4.26 Mach Number Distributions at various Pre-Rotations: (a) 0 degrees (b) 40	
degrees, (c) 60 degees12	28
Figure 5. 1 The operating points chosen for optimization. (a). PI (b). TS	36
Figure 5.2 Convergence History of Total Penalty at the three operating points1	42
Figure 5.3 Convergence History. Efficiency Penalty at the three operating points1	43
Figure 5.4 Convergence History. Mass Penalty at the three operating points1	44
Figure 5.5 Convergence History. Unbalance Penalty at the three operating points1	45

Figure 5.6	Convergence History. Neg. Loading Penalty at the three operating points.	146
Figure 5.7	Plots of the efficiencies at Various IGV Setting angles. (a) 0° (b) 40° (c) 60°	149
Figure 5.8	Meridional Contours (left) and blade profiles (right) of the Iterations	155
Figure 5.9	Mach number distributions at various IGV settings of Iterations	162
Figure 5.10	Mach number distributions of the Baseline and Single Point Optimum	
geometries		171
Figure 5.11	Performance Map: (a) Pressure ratio (b) η _{ts} (c) η _{tt}	178

KEY TO SYMBOLS AND ABBREVIATIONS

SYMBOLS: NOTE (SI UNITS ARE USED THROUGHOUT THE TEXT)

α : Absolute Flow angle (Degrees)

β : Relative Flow angle (Degrees)

b : blade height

BC : Boundary Condition Vector

C : absolute velocity

C_P : Specific heat at Constant Pressure

COP : Coefficient of Performance

D : Diameter

 \vec{G} : Geometry Vector

H : Enthalpy

h : Specific enthalpy

M : Mach number

 \dot{m} : Total Mass flow rate

m1, m2 : Mass Flow rate in a splitter channel

N : Rotational Speed (RPM)

lη : Efficiency

P : Pressure, Penalty

 \vec{P} : Performance Vector

ρ : Density

 \dot{Q} : Heat Transfer Rate

R : Radius of Curvature, Radial coordinate direction

RE : Reynolds Number

S : Curvilinear length

T : Temperature

W: Weights, Weight Matrix, Relative Velocity

γ : Ratio of Specific Heats

Z : Blade number

SUBSCRIPTS

0 : Value related to the total conditions

: Value related to the inlet of the computational domain (impeller inlet)

2 : Value related to the outlet of the computational domain (diffuser outlet)

fb : Full Blade

H : High Temperature Reservoir

hub : Hub

L : Low Temperature Reservoir

Le : Leading edge

lu : Loading unbalance

Min : Minimum Value

Max : Maximum Value

mass diff: Mass Difference

OF : Objective Function

nl : Negative Loading

ps : Pressure Side

Ref : Reference Value

Req : Required value

shr : Shroud

sb : Splitter Blade

ss : Suction Side

Te : Trailing edge

ts: : Total to Static

tt : Total to Total

U : Value related to the circumferential direction

X : Value related to the axial direction

ABBREVIATIONS

2D, 3D : Two-dimensional, Three-dimensional

ANN : Artificial Neural Network

CFD : Computational Fluid Dynamics

DOE : Design of Experiment

GA : Genetic Algorithm

IGV : Inlet Guide Vane

NS : Navier-Stokes or Navier-Stokes Solver

RANS : Reynolds averaged Navier-Stokes Equations

TRAF : Transonic Reynolds averaged flow solver

INTRODUCTION

Computational Science has provided the building blocks necessary to design innovative engineering systems at every level of sophistication.

Nowadays, performances of a given geometry and their associated boundary conditions can easily and quite reliably be evaluated using computational fluid dynamic (CFD) codes using state of the art computer systems. Although experimental testing will never become extinct, the digital evaluation and development of new products and technologies may eventually begin to overtake experimental testing as the dominant analysis method. This is mainly due to the fact that state of the art computational systems save companies much time and money, which attracts many of them to invest more in these systems every year.

This project combines two recent design tools together with a CFD solver, in order to get the full benefit of computational methods in the design of turbomachinery components. The first new tool that was applied to the design problem is based on a method known as function approximation. The expert system used to implement this concept, an artificial neural network (ANN), has the capability of analyzing design variables and of predicting the performance that can be expected from a new proposed geometry. This is done by creating a network of non-linear relations between inputs and outputs by utilizing a learning process. This learning process provides the capability of the ANN to predict the performance accurately for existing, and more importantly, new geometries with much less computational effort than a full Navier-Stokes computation. A

database conta train the ANN. The other t geometric mod capable of find to find the gev That is, in a no: In the follo case, a 3D rad impeller geome provided by an with a fundame readers. Follow will then take chapters. Subse Finally, some o Provided.

database containing full three-dimensional Navier-Stokes (NS) computations is used to train the ANN, which then classifies the system as one that is self-learning.

The other tool that has been utilized is the genetic algorithm, or GA. This tool makes geometric modifications that are based on biological and genetic evolution, making it capable of finding the geometry that demonstrates superior performance. Its main goal is to find the geometry that corresponds to maximum performance in a statistical manner. That is, in a non-deterministic way.

In the following chapters, the above mentioned design system is applied to a selected case, a 3D radial compressor impeller. For this case one will attempt to optimize an impeller geometry to accommodate multiple operating points. These operating points are provided by an inlet guide vane (IGV). Before attempting this however, one will start with a fundamental background which is aimed specifically at completely uninitiated readers. Following this a more complete description of the general optimization system will then take place, leaving the unique aspects of our particular optimization to later chapters. Subsequently, the results of the optimizations will be presented and discussed. Finally, some overall conclusions will be drawn and suggestions for future work will be provided.

CHAPTER 1

BACKGROUND AND MOTIVATION

In the following subsections the author would like to provide a short overview regarding the fundamentals of air conditioning cycles, and aerodynamics of compressors in order to provide a sufficient background for readers of all levels and motivation to perform an optimization.

1.1 Air Conditioning Fundamentals

Everyone knows from experience that heat flows in the direction of decreasing temperature, that is, from high temperature regions to the low temperature regions. This heat transfer process occurs in nature without requiring any devices. The reverse process, however, cannot occur by itself. This leads us to special devices known as air conditioners and refrigerators which operate on a thermodynamic cycle. These air conditioners and refrigerators are essentially the same in that the objective of their design and application is to utilize work to move heat from a cooled space to a hot space using a refrigerant. To do this, one can choose to use many different types of cycles. However, the one discussed here will be the more common vapor compression cycle.

In order to understand the vapor compression cycle, and other similar cycles, it is important to understand about the phase changes that the refrigerant experiences. This is best illustrated through the use of the pressure-enthalpy diagram displayed in Figure 1.1 below.

Pressure vs. Enthalpy Diagram

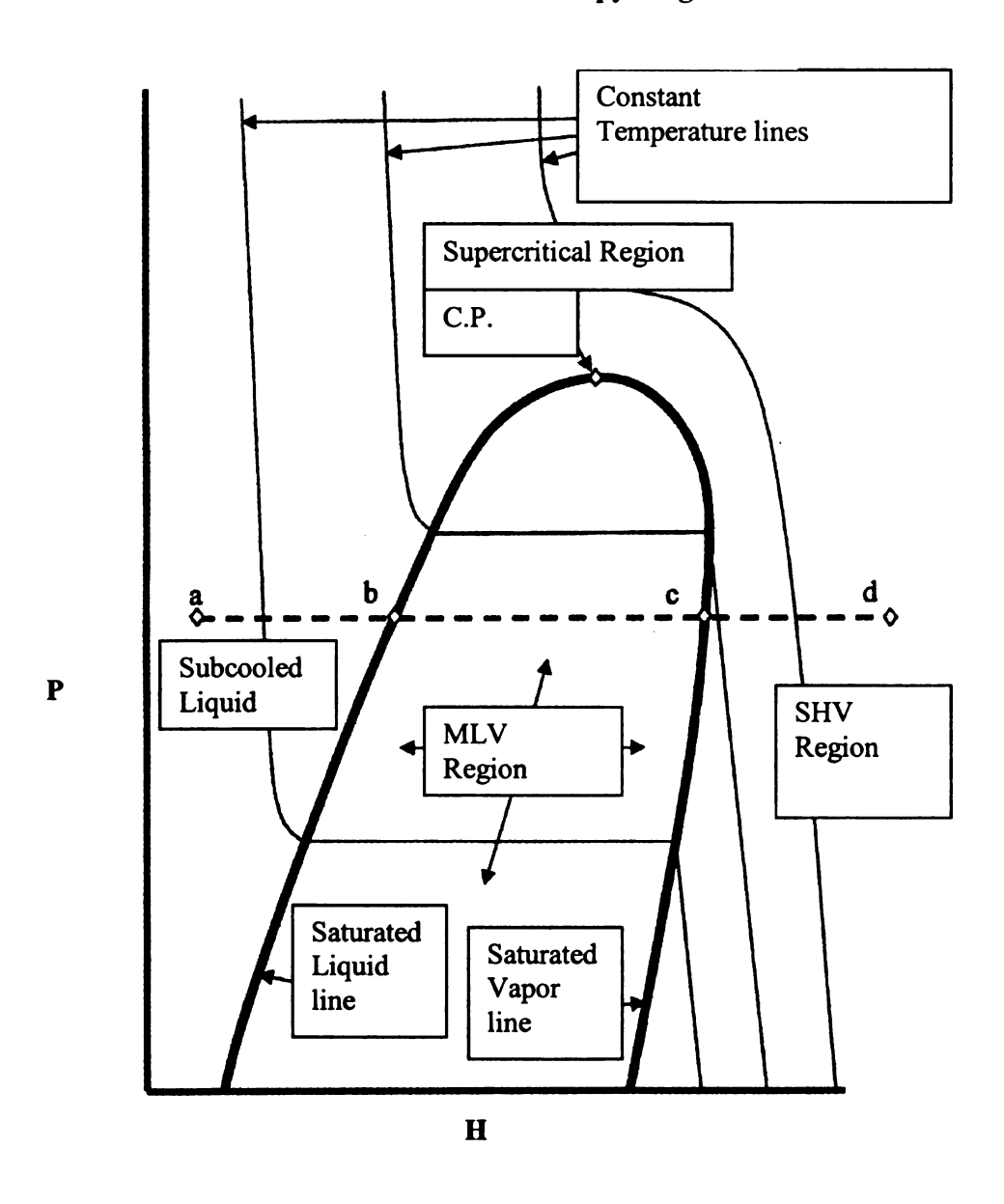


Figure 1.1 Generalized phase change process

In this figure, a refrigerant in the subcooled liquid region (point a), is at a temperature that is below its boiling point. If one adds heat while maintaining constant pressure, the refrigerants temperature will rise which leads to a corresponding enthalpy rise. This

enthalpy rise corresponds to a change of state from point "a" to "b", where at point "b" the liquid is about to vaporize. As heat is continually added, the refrigerant will start to vaporize and its enthalpy will increase, but its temperature will remain constant as it moves through the mixed vapor and liquid range, which is located between points "b" and "c". As the process continues the state of the fluid will soon reach the saturated vapor condition at point "c", where there is only refrigerant in the vapor phase. Finally, with more heat addition, the refrigerant state moves into the superheated vapor region (point d) where the temperature of fluid begins to rise again.

This concept of phase changes is applied to the well known ideal air conditioning cycle. Figure 1.2 illustrates the ideal vapor compression cycle on a pressure-enthalpy diagram. The starting point of the cycle is at point 1 in the saturated vapor phase, where the refrigerant enters a compressor and is compressed adiabatically from point 1 to point 2. The compressor is a device which increases the pressure, enthalpy, and temperature of the refrigerant. Once the refrigerant leaves the compressor, it then enters the condenser. The condenser is essentially a heat exchanger that transfers heat from the high temperature refrigerant and rejects it to the environment. As heat removal from the refrigerant begins, the fluid cools until the saturated vapor state is reached which corresponds to point 2a. As heat continues to be removed, the enthalpy continues to decrease but the temperature and pressure remain constant. During this part of the process, the refrigerant begins to condense to the liquid phase. This condensation continues until the saturated liquid line is reached at point 3, whereupon the refrigerant consists entirely of liquid. At this point, the refrigerant leaves the condenser as a saturated liquid.

Ideal Vapor Compression Cycle

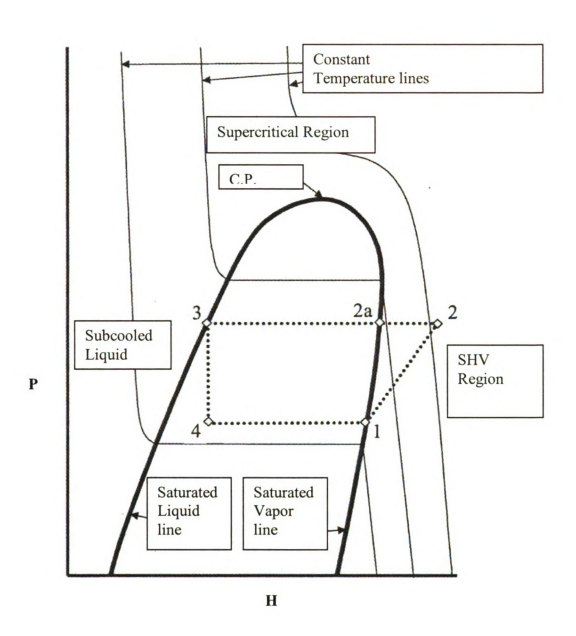


Figure 1.2 Air Conditioning cycle

The next part of the cycle consists of an isenthalpic expansion process, which is usually provided by an expansion valve or capillary tube (see Figure 1.3). This expansion

valve dramatically reduces the temperature and pressure of the refrigerant while holding its enthalpy level constant. Some of the liquid vaporizes during the expansion process until the end of the process is reached at state 4. Now the refrigerant is a low quality mixture of liquid and vapor at a temperature somewhat below the temperature of the space to be cooled.

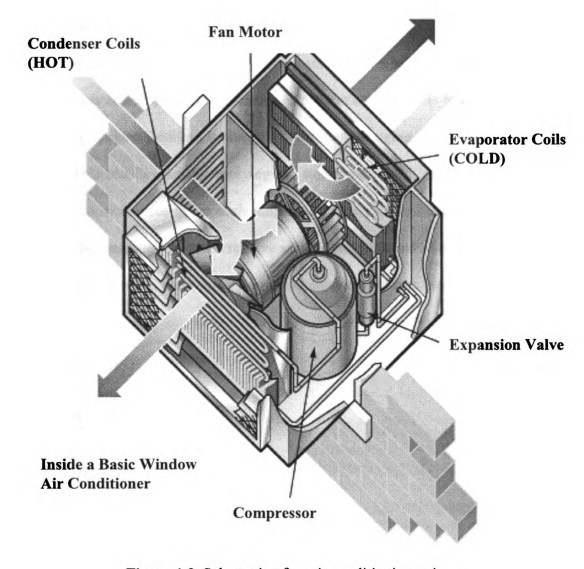


Figure 1.3 Schematic of an air conditioning unit

Next, the refrigerant flows through an evaporator, which is another heat exchanger that transfers heat from the space to be cooled to the refrigerant. The refrigerant absorbs this heat, increasing its enthalpy during this process, although its temperature and pressure remain constant. Finally the liquid gradually vaporizes until the saturated vapor line is reached at state 1, whereupon the refrigerant enters the compressor in order to repeat the cycle.

The heat load or the amount of heat that an air conditioner must remove from a room varies throughout the year. More specifically, a small heat load in the spring and autumn changes to a larger heat load in the summer. How can one vary this heat load? Well the way in which the heat load can be controlled without changing the cycle is to vary the mass flow. This can be seen by applying the steady flow form of the conservation of energy to the flow devices while neglecting kinetic and potential energy changes of the fluid. This is because they are small relative to the work input and heat transfer processes. The rate of heat supplied, rejected, and power input can be written below as

$$\dot{Q}_L = \dot{m}(h_1 - h_4) \tag{1.1}$$

$$\dot{Q}_H = \dot{m}(h_2 - h_3) \tag{1.2}$$

$$\dot{W}_{in} = \dot{m}(h_2 - h_1) \tag{1.3}$$

From these equations it can be seen that for a fixed cycle, the only way to increase or decrease the heat transfer rate and the corresponding amounts of heat is to vary the mass flow. Thus, a designer should select a compressor that is capable of delivering the mass

flow efficiently at constant outlet pressure, which will result in a high coefficient of performance (COP) for the air conditioner. That is, for the same Q_L, the COP will increase if the work input is at a minimum. The work input will be a minimum only if the compressor is able to perform efficiently at a particular operating point.

$$COP_{AC} = \frac{Q_L}{W_{in}}$$
 [1.4]

This section ends with a question. How can one vary the mass flow efficiently using a centrifugal compressor without changing the pressure rise?

1.2 Limiting factors of Flow range

The need for multiple point operation of an air conditioner is dictated by the seasons as discussed above. So the component of major concern is then the flow range of the compressor. A definition of a typical impeller can be seen in Figure 1.4.

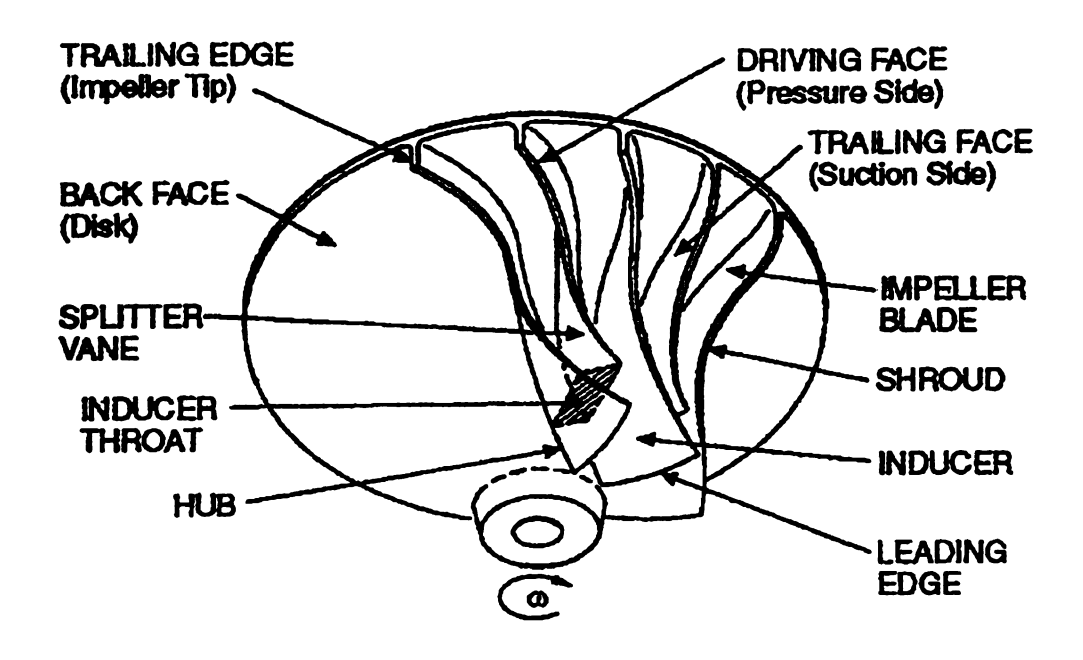


Figure 1.4 Impeller Nomenclature. [6]

Before discussing how to increase the flow range of the compressor, we will first discuss the limiting factors of the flow range in basic detail. One of the factors is known as compressor choke, which is defined as the maximum mass flow that the compressor can swallow and is relatively easy to predict and control. This choking occurs because of two reasons:

- Sonic velocity in the throat of the inducer or vaned diffuser
- Negative stalling incidence of the inducer. The passage area decreases due to boundary layer blockage. This can be seen in Figure 1.5.

The other limiting factor is known as surge or stall, which is the complete breakdown of the flow, or alternatively called separation or return flow. This normally occurs at low mass flows and is a much more complex and difficult phenomena to predict and control. There are many types or sources of stall, a few of which are listed here for the sake of brevity.

However, some basic ideas will be discussed in the following paragraphs.

- Impeller rotating stall.
- Stall in the vaneless or vaned diffuser
- Surge

At lower mass flows, the compressor provides a higher pressure ratio, and thus higher diffusion rates. The impeller channels act as rotating diffusers that generally exhibit large relative velocity decelerations. These large relative velocity decelerations in the impeller channels cause large boundary buildup. The thicker the boundary layer, the weaker and more sensitive to separation it becomes. The Coriolis and curvature effects tend to make the boundary layer more turbulent and thus more resistant to flow separation on the pressure side of the blades and at the hub. However, the reverse situation of less flow stability occurs at the suction side of the blades and at the shroud. That is, the boundary

layer tends to remain laminar which means that it is more susceptible to flow separation due to adverse pressure gradients. The situation can become more serious when the inlet relative flow angle does not coincide with the inlet blade angle. This situation can lead to high velocity peaks which will inevitably cause flow separation. This non-flow alignment to the blades is known as incidence and effects are illustrated in Figure 1.5.

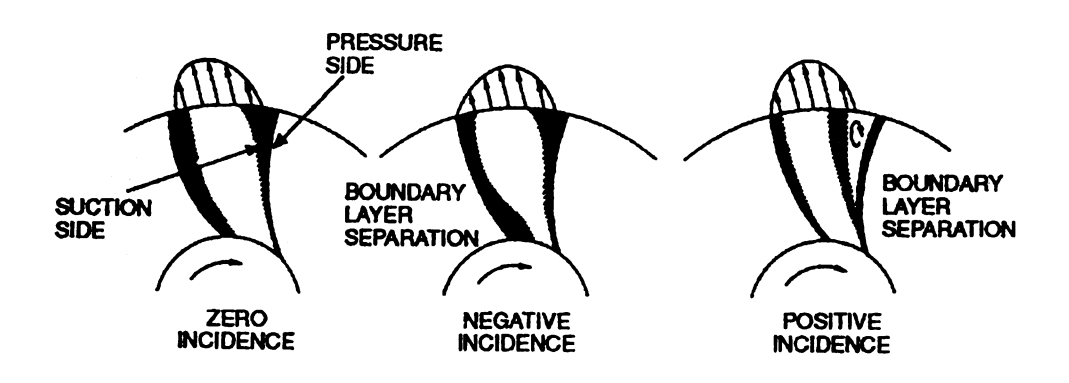


Figure 1.5 Effect of incidence on boundary layer accumulation. [6]

In this figure an excessive positive incidence means that the flow impinges on the pressure side which will in turn lead to a high velocity peak on the suction side. This high peak has to be decelerated with an opposing adverse pressure gradient in order to achieve a pressure rise, which inevitably leads to flow separation and thus limits the flow range. Finally, for a more detailed treatment of stall, one should consult references [12-13].

1.3 Techniques to increase the flow range

A few ways in which to circumvent this problem of limited flow range is by using one or more of the following techniques all of which are illustrated in Figure 1.6:

- Variable inlet guide vanes (IGVs)
- Variable Speed Motors
- · Variable vaneless or vaned diffusers
- · Active control of surge and stall

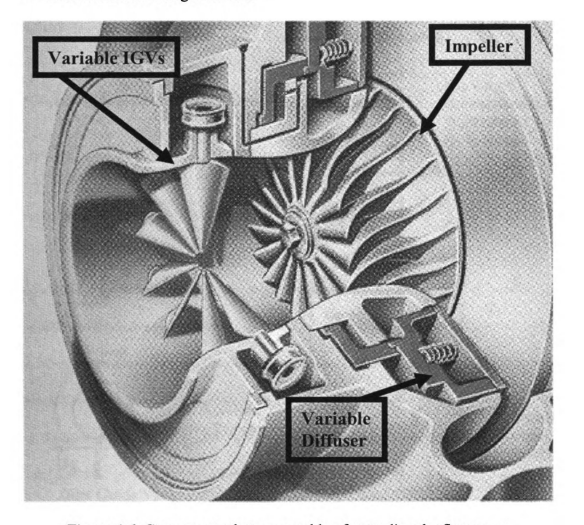


Figure 1.6 Components that are capable of extending the flow range

Variable IGVs:

Installing a fixed or variable inlet guide vanes (IGVs) allows circumventing the incidence problem by aligning the flow to the blades. In other words, the IGV extends the flow range by introducing pre-rotation to the flow so as to maintain the optimum incidence at different mass flows. Figure 1.7 shows the basic working principle of inlet guide vanes in a self-explanatory manner.

INLET GUIDE VANE $U_1x Cu_1>0$ $\mathbf{W_1}$ With Rotation (Lower Head) (Positive Prewhirl) W₁ Reduced **Type "1"** O₁ Reduced $\mathbf{U_1}$ Cu₁ $\mathbf{W_1}$ $Cu_1 = 0$ Zero Prewhirl **Type "2"** \mathbf{U}_1 Wheel U₁x Cu₁<0 $\mathbf{W_1}$ **Against Rotation** (Higher Head) (Negative Prewhirl) W₁ Increased **Type "3"** Q₁ Increased $\mathbf{U_1}$ Cu_1 Inlet Guide Vane

Figure 1.7 Working principle of IGVs [6]

Error!

As one can see above, when positive pre-rotation is introduced it leads to a reduction in mass flow and in turn to a slightly less enthalpy rise (or pressure ratio). The opposite is the case for negative pre-rotation. That is, a higher mass flow and a slightly increased pressure ratio results. One can understand this by studying Figure 1.7 along with considering the Euler equation. Both effects on performance can be seen in Figure 1.8.

Euler Equation:

$$H = \Delta(UC_u) = U_2C_{u2} - U_1C_{u1}$$
[1.5]

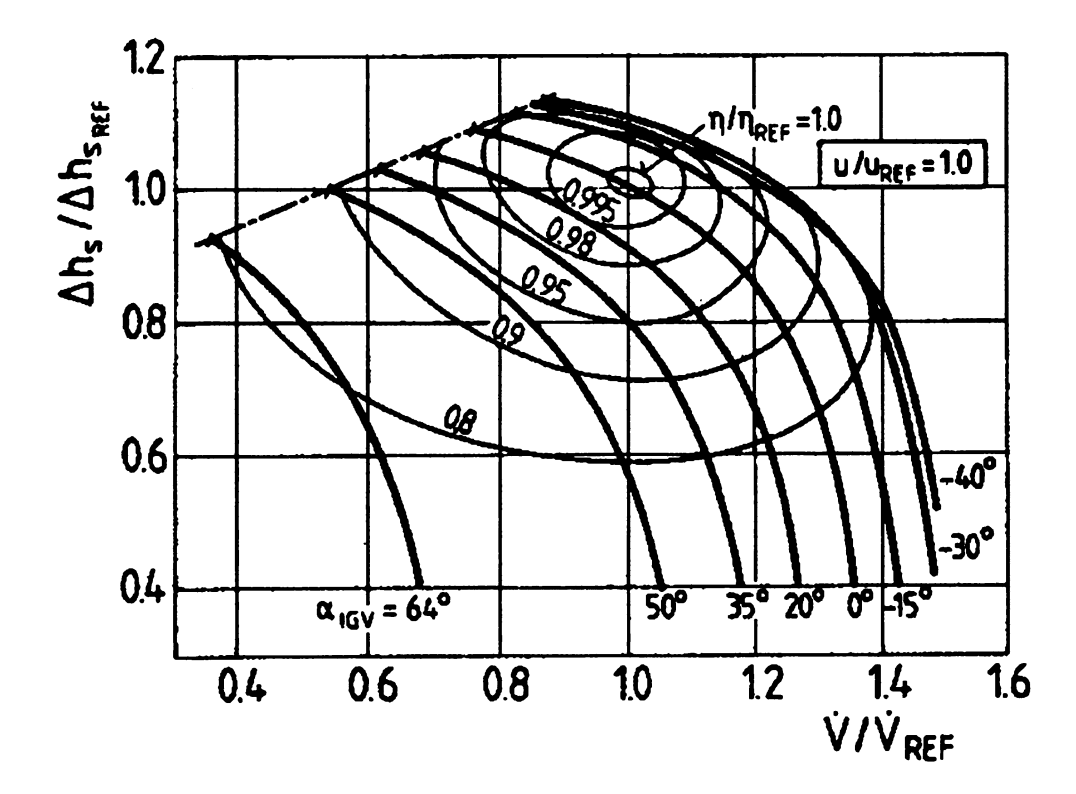


Figure 1.8 Performance map with variable inlet swirl using a vaneless diffuser

Variable Speed Motor:

Another potential solution is to vary the rotational speed. However this is more expensive because one needs to use a variable speed motor. Also the pressure ratio varies in accordance with the Euler equation (equation [1.5]) and consequently produces a higher pressure ratio mainly due to the change in peripheral speed. This can be a problem if one considers that the condenser needs to have roughly the same inlet pressure over a wide flow range. Figure 1.9 shows the effect of varying the rotation speed on the performance of compressor. [10]

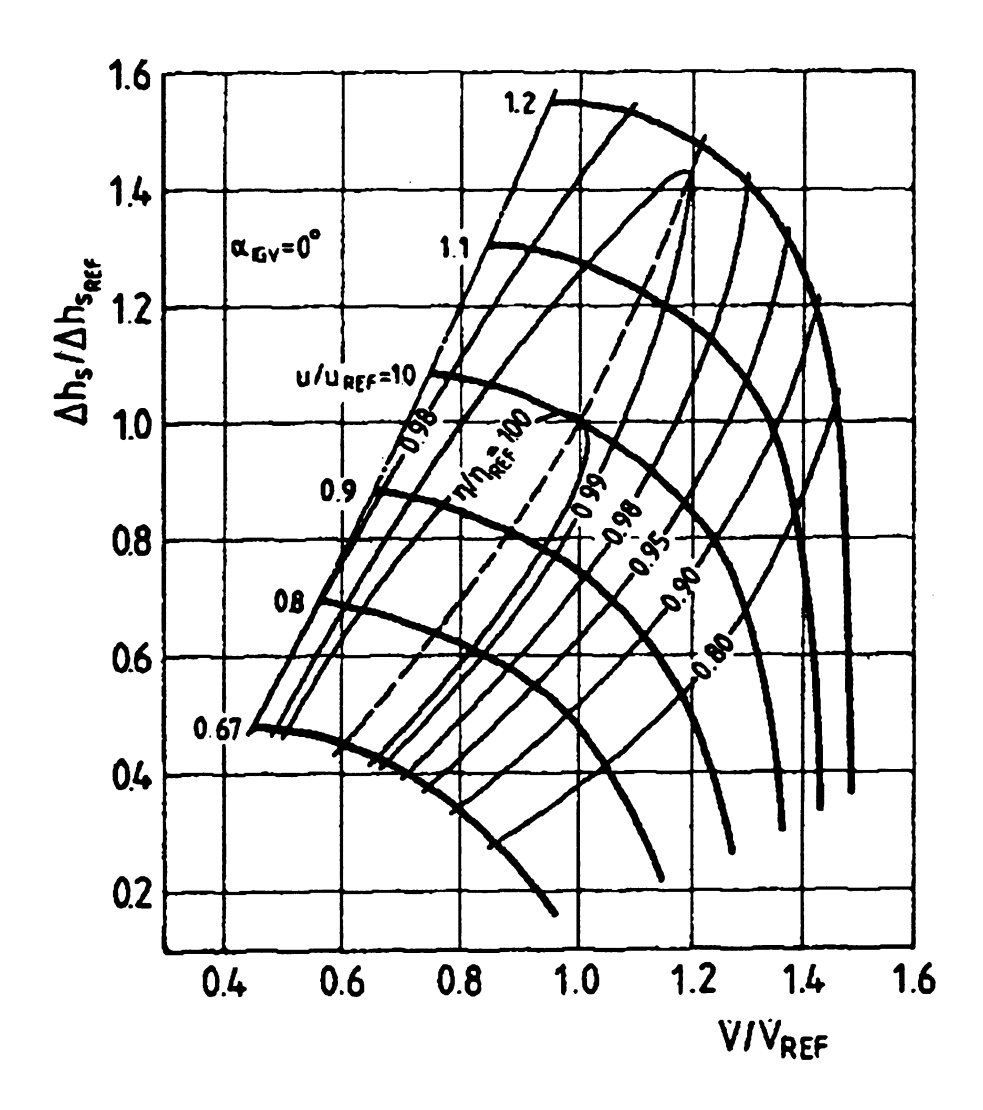


Figure 1.9 Performance map with peripheral speeds using a vaneless diffuser

Variable diffusers:

Yet another alternative to vary the flow range is by variable vaneless or vaned diffusers. If one uses a vaneless diffuser, it is obvious that by changing diffuser width one can easily vary the flow range. However the problem of the vaneless diffusers is the amount of friction that is produced along the endwalls due to the low radial velocity component that is associated with the lower mass flow regime. That is, the flow is very tangential at low mass flows and results in more accumulated friction due to the fact that is simply takes more time for the flow to leave the diffuser. In addition to that, diffuser rotating stall will occur if the flow becomes too tangential.

The vaned diffuser consists of diffusing channels between vanes, where the diffusion process is accomplished in a much shorter flow path (see Figure 1.10) with much higher efficiency than in the vaneless diffuser.

The drawbacks are as follows:

- The maximum mass flow is limited due a throat region.
- At low mass flows, and at certain distances from the impeller tip, there can be a lot of noise and vibration
- At off-design operation incidence is again present and can lead to fully developed stall. That is, no re-attachment of the boundary layer and therefore no pressure rise.

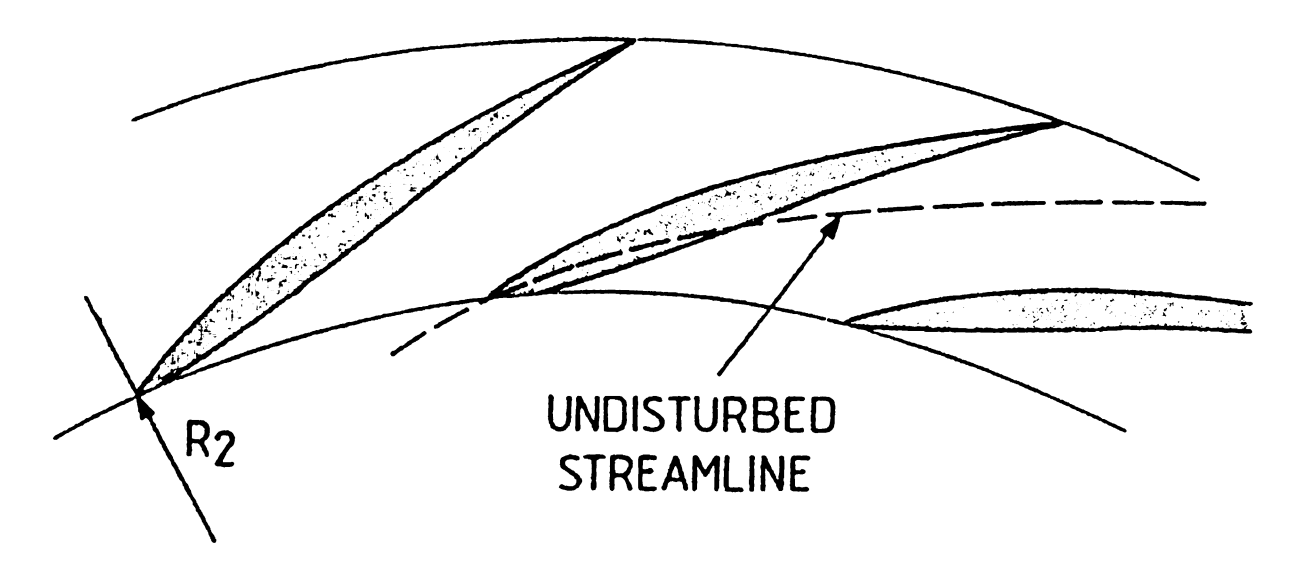


Figure 1.10 Influence of a diffuser vane on the flow in a radial diffuser. [9]

The performance of a compressor with a variable vaned diffuser with no pre-rotation is shown in Figure 1.11. [10]

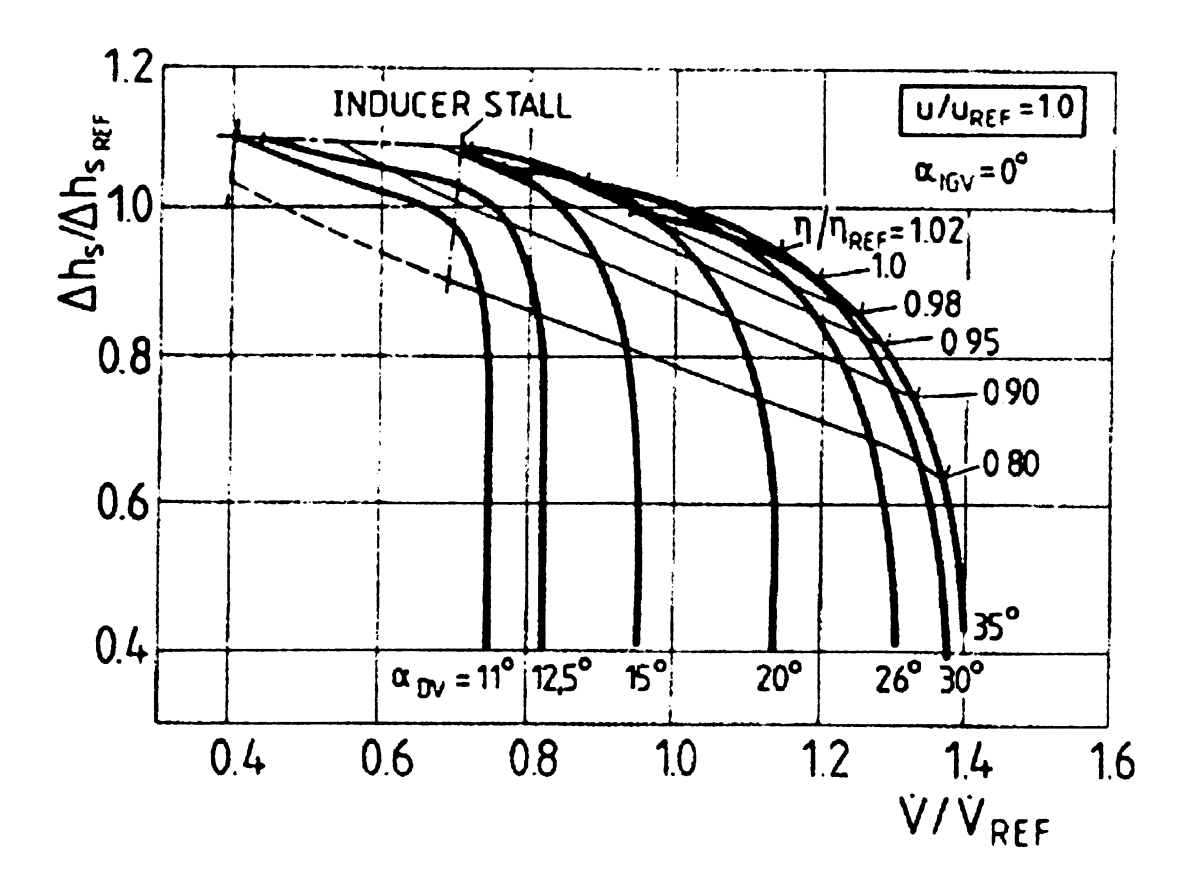


Figure 1.11 Performance map with variable inlet angle of diffuser. Swirl free inflow.

Finally, the IGV was chosen, mainly for cost reasons, as the device to vary the flow range in the compressor in this work. This section leaves with a question. If the IGV already increases the flow range efficiently, then why does one need to consider optimization?

1.4 Need for MultiPoint Optimization

Although IGVs provide high efficiency over a larger mass flow range, a drawback is the separation that occurs at larger pre-rotation angles (lower mass flows). The flow comes into the IGV at a high incidence, which results in high velocity peaks that trigger flow separation. Both phenomena are illustrated in Figures 1.12 and 1.13 respectively. This separated flow zone within the IGV has a lower tangential velocity and thus a lower centrifugal force attempting to maintain radial equilibrium.

Radial Equilibrium:

$$\frac{C_u^2}{R} = \frac{1}{\rho} \frac{\partial P}{\partial R}$$
 [1.6]

The separated flow then mixes with the core flow and because of the higher radial pressure gradient in this region, the lower momentum flow or separated flow is then forced to the hub of the machine. This situation leads to radially non-uniform distributions of total pressure. Thus, one must optimize the impeller to be able to adapt to these very different inlet conditions. Finally, these two effects are seen in Figures 1.14 and 1.15.

Mach number distribution

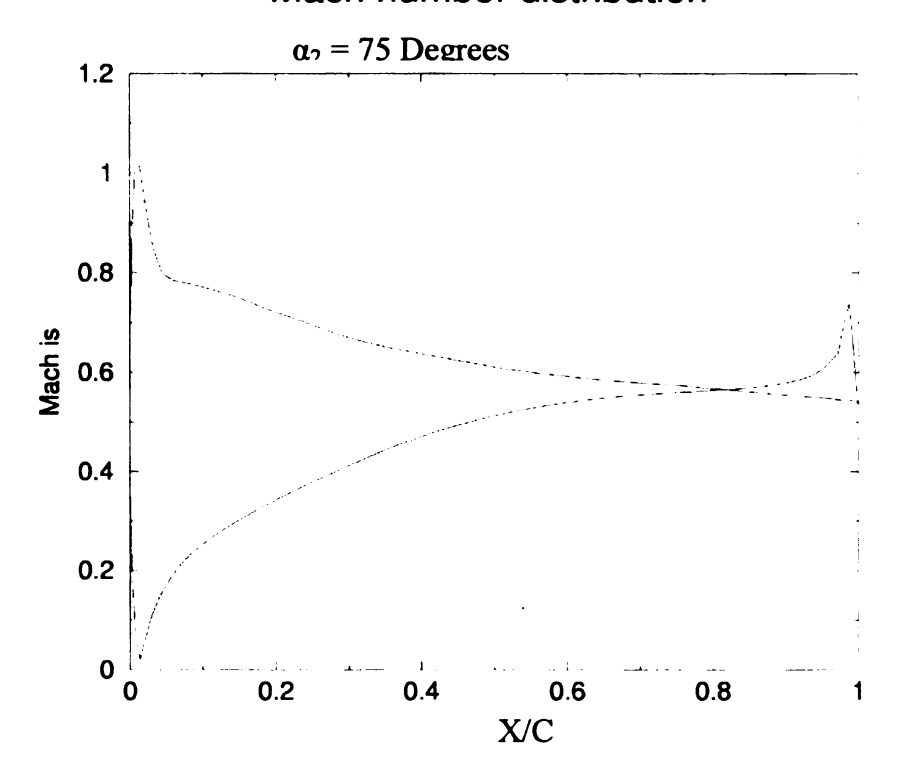


Figure 1.12 Mach number distribution illustrating incidence of IGV. [3]

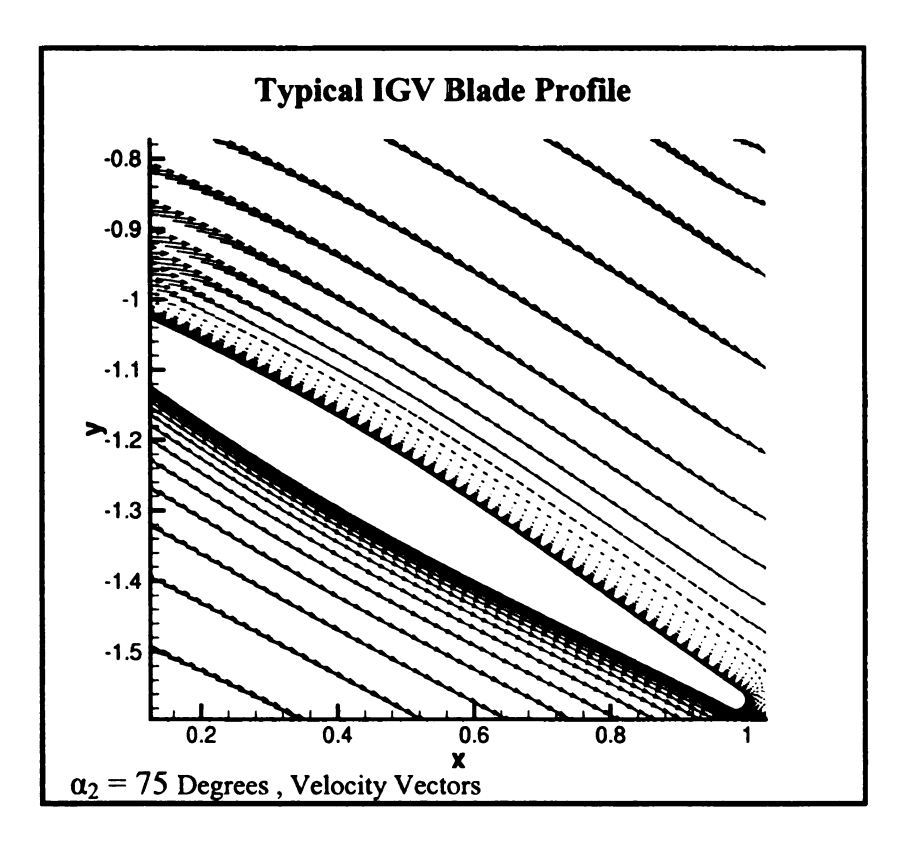


Figure 1.13 Illustration of flow separation of an IGV. [3]

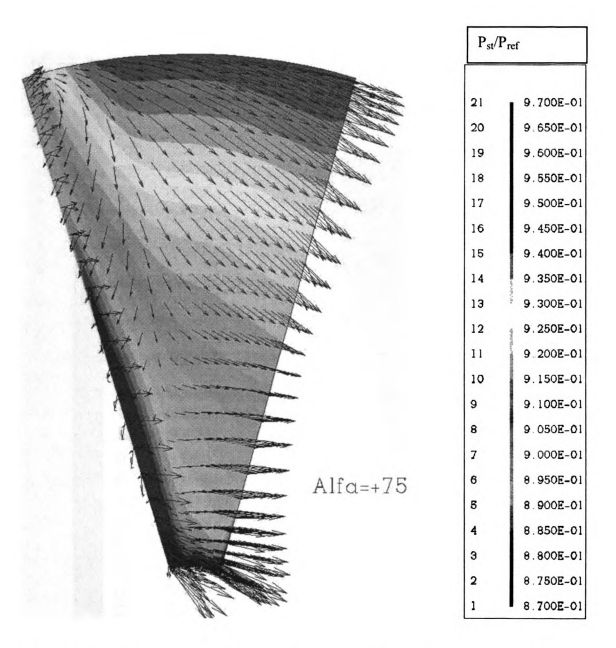


Figure 1.14 Unbalance of Centrifugal and pressure gradient forces and radial shift of separated flow. Suction side.

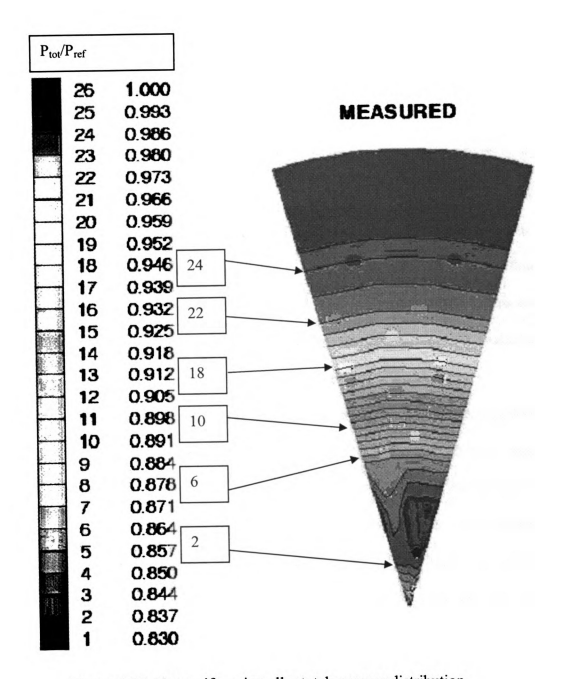


Figure 1.15 Non-uniform impeller total pressure distribution

CHAPTER 2

OPTIMIZATION METHOD

2.1 General Philosophy

The basic principle of the method presented here is to mimic the traditional design procedure in which the designer makes a first optimization by means of an approximate, but fast, geometry generation and analysis method. The evaluation by the approximate model, being very cheap and fast, allows a large number of performance evaluations required by the optimization algorithm to be done with ease.

At the end of this first optimization phase, an accurate Navier-Stokes calculation (high fidelity) is performed to verify the prediction quality of the lower-fidelity model. The optimization, with the simplified model, is then repeated, but not before the fast-evaluation method has been recalibrated using the results of the previous computation. In this way, the design system can be considered self-learning, and the optimum, which is defined by means of the fast evaluation method, should get closer to the one that would be found using the more expensive Navier-Stokes method.

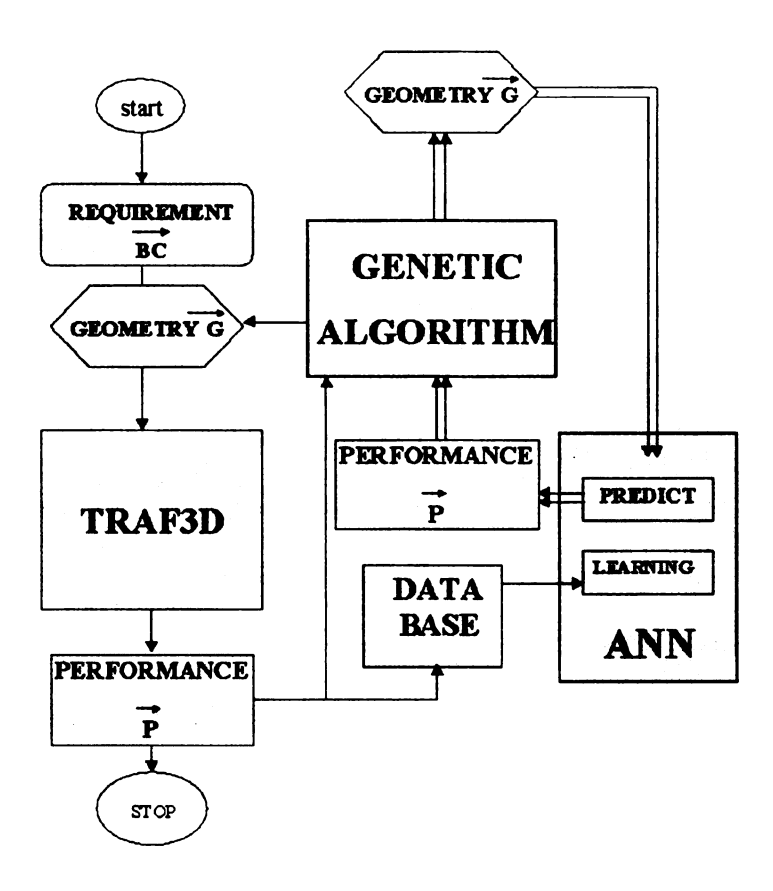


Figure 2.1 Flowchart of optimization system. [2]

The blade design algorithm, of which a flowchart is presented in Figure 2.1, starts from the user-defined aerodynamics and mechanical requirements. They are, depending on the type of optimization conducted (2D, quasi-3D or 3D), inlet and outlet flow angles, outlet static pressure, Reynolds number, mass-flow, efficiency, specific work, maximum/minimum blade cross section and moment of inertia, Mach distribution uniformity, skewness and so on.

The artificial neural network (ANN) is used to build an approximate relation between the geometry (\vec{G}), the boundary conditions (\vec{BC}), and the performance vector (\vec{P}).

This relation can be represented in function form as:

$$\vec{P} = f(\vec{BC}, \vec{G})$$
 [2.1]

The ANN learning process defines this relation using the information stored in a database. The trained ANN is then able to predict the performance of newly encountered geometries using the specified boundary conditions.

The optimizer makes use of a genetic algorithm (GA) whereby the ANN is used to evaluate the performance. The resulting geometry, which is normally optimum according to the ANN predictions, is then verified by means of the Navier-Stokes flow-solver. The geometry and its performance are added to the database as a new sample and the ANN is recalibrated or re-taught.

This iterative optimization cycle is repeated until the performance check confirms that an optimum geometry was found. As the database grows after each iteration, the approximate relation (f in equation 2.1) is expected to become more accurate and the optimizer should finally lead to the real optimum solution.

2.2 Database

The core of the design system is a database containing the input and output results of Navier-Stokes computations performed during past computations. The following information about each sample is stored:

• BC: Flow-field boundary conditions used by the NS solver.

- G: Parameters defining the geometry. Every type of turbomachine (axial, radial, turbine or compressor) will have its own geometry definition and this part of the database has to be adapted accordingly. This will be further explained when we will come to discuss our application.
- P: Aerodynamic performance. The amount of data computed by a two dimensional NS solver can be as large as 800000(4 variables for 200000cell nodes). Due to the ANN intrinsic architecture and to obvious limitations in the database size, their number has to be drastically restricted. This allows a reasonable ANN training and a processing time considerably shorter than the time required for a NS computation. The performance vector usually contains the mass flow, efficiencies, and the Mach number distributions.

The main purpose of the database is to provide information about the impact of the geometrical changes on performance. The more accurate and general this information is, the more accurate may be the ANN and the closer the first optimum geometry, defined by the GA, will be to the real optimum. Hence less iteration loops will be required.

The making of this database is an expensive operation because it requires a large number of 3D Navier-Stokes calculations and one is interested in making the smallest possible database. It is however important that the information contained in the database covers the whole design domain, that it is relevant and with a minimum of redundancy. In other words, that the impact of every design parameter is included at most one time.

Any information missing in the database may introduce an erroneous ANN that could drive the GA into a geometry that is not optimum. This is not a problem because the

Navier-Stokes analysis of that geometry will provide the missing information when it is added to the database. Contrary to this, an incomplete database could result in an erroneous extrapolation by the ANN predicting a low performance in that part of the design space where in reality the performance is high. As a consequence, the corresponding geometry will never be selected by the GA and the real optimum may never be found. This second drawback is more difficult to circumvent because no mechanism is built in to compensate for it and it may continue during the entire optimization. It is therefore import to assure that the initial database covers the whole design domain.

Design of experiment (DOE) refers to the process of planning an experiment such that the appropriate data can be analyzed by statistical methods, resulting in valid conclusions. It is a statistical approach in which logical changes are made to the input variables of a process so that one may discover and identify the reasons for the changes that are observed in the output response. It is used to select the most significant geometries that will be used to construct the database. Figure 2.2, taken from reference [2], demonstrates the loss of information by comparing the ANN predictions, based on different DOE designed databases, with the exact values for the test function displayed below.

$$R(i)=1-0.001(A-D)^3+0.002(C+E)(F-B)-0.06(A-F)^2+(F+C)(E+A)$$
 [2.2]

The DOE constructed databases are also compared to randomly generated databases in Figure 2.2. This is made possible through equation [2.2] and by defining a global error as follows:

$$globalerror = \sum_{i=1}^{n-samples} \left(\frac{R(i) - ANN(i)}{R(i)} \right) 100$$
 [2.3]

Thus, the results show inconsistency of the global error in the random generating case. It also shows that the error is not much smaller from the 64 to the 32 sample databases. Thus, it has been well demonstrated that the DOE technique is sufficient.

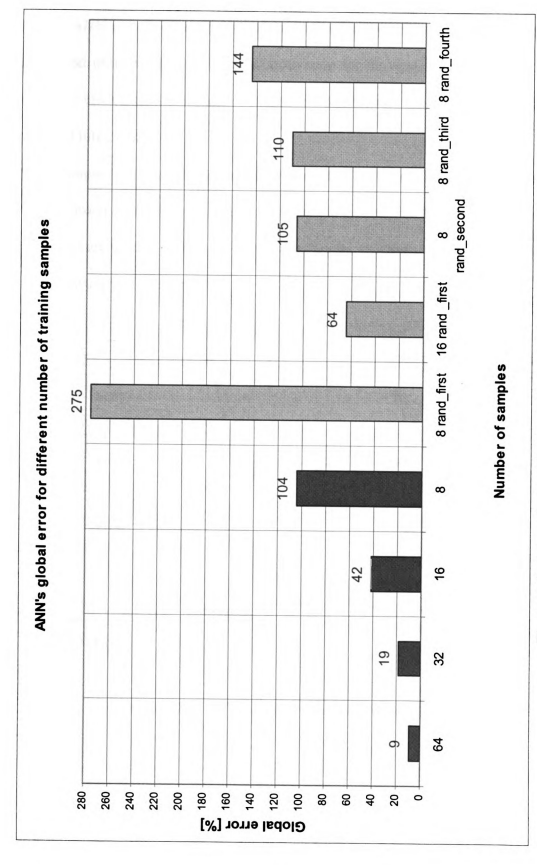


Figure 2.2 Comparison of DOE and Random database generation. [2]

2.3 Artificit

The ANN
inputs and out
computer mod
powerful inter
The input
Navier-Stokes
conditions are
used to quanti



2.3 Artificial Neural Network

The ANN is a function approximation method suitable for functions having multiple inputs and outputs. While the initial motivation for developing an ANN was to create computer models that could mimic certain brain functions, it can also be thought of as a powerful interpolator.

The inputs to the ANN, schematically depicted in Figure 2.3 are the same as for the Navier-Stokes solver. That is, the geometrical parameters and the aerodynamic boundary conditions are used in both tools. The outputs are the aerodynamic parameters that will be used to quantify the performance.

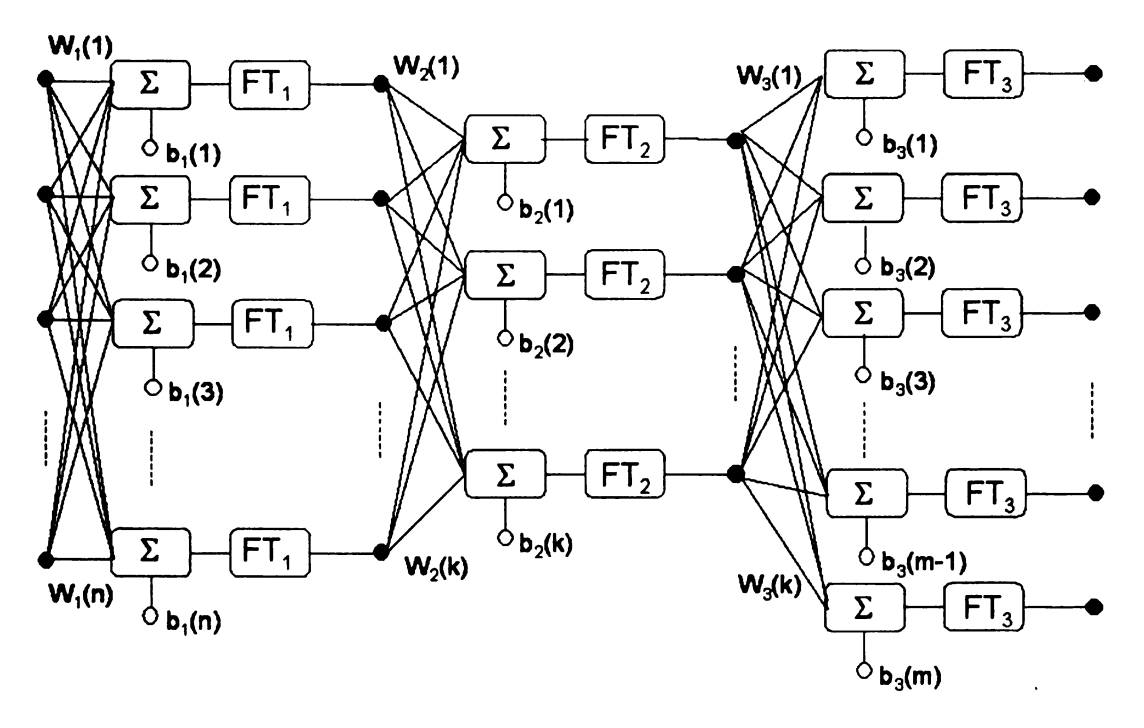


Figure 2.3 A Three-Layer Artificial Neural Network. [2]

A neural network is composed of several layers. The first layer is always the input layer and the last one the output layer. In between is one (or more) hidden layer(s). The processing elements in each layer are called nodes, and they are connected to the nodes of neighboring layers by weight and bias parameters. The first layer has as many nodes as the number of variables of the design problem and the last layer as many as the performance vector.

If each layer is represented by a vector $\vec{a_r}$, and defining the weight matrix W and the bias vector \vec{b} , the input-output mapping of the ANN can be presented in compact matrix form:

$$\overrightarrow{a_r} = F(W_r.\overrightarrow{a_{r-1}} + \overrightarrow{b_r})$$
[2.4]

The transfer function F usually used is a sigmoid function, $F = \frac{1}{1 + e^{-x}}$.

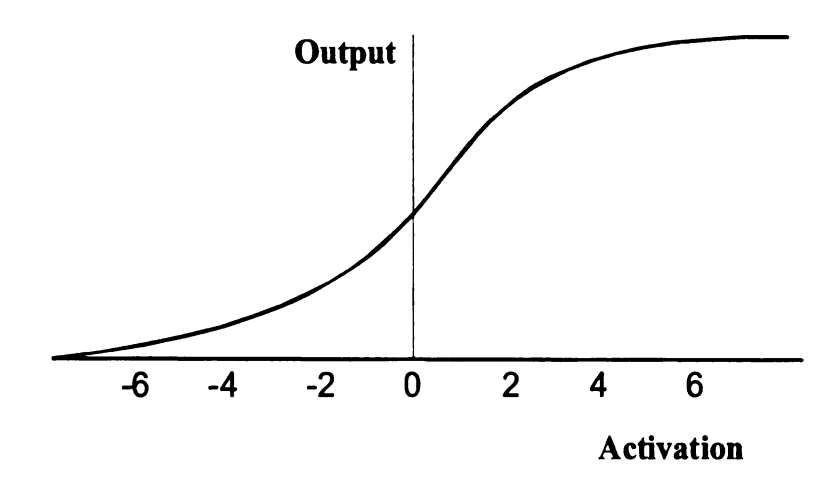


Figure 2.4 Sigmoid Transfer function. [2]

Sigmoid function

Our remaining issue is the number of hidden layers. As the relation becomes more complex, a larger number of layers are needed. The critical number of hidden nodes is defined by [1] as:

$$\boldsymbol{n}_{h} = \frac{\boldsymbol{n}_{training}.\boldsymbol{n}_{out} - \boldsymbol{n}_{out}}{\boldsymbol{n}_{in} + \boldsymbol{n}_{out}}$$

where $n_{training}$ is the number of training samples, n_{in} the number of nodes in the input layer, and n_{out} the number of nodes in the output layer.

All connections are "feed-forward". The optimal values of the connection weights and biases, corresponding to the most accurate prediction for all cases presented, are defined during the ANN learning. This work has used the back-propagation of error algorithm. Before the optimization procedure and the ANN learning are launched, random values are assigned to W and \vec{b} . The output of the first NS calculation is then compared to that of the ANN, and the error is back propagated accordingly, to update the weights in the way that minimizes the mean square evaluated error.

Because of the structure of the transfer function F, all the inputs and outputs of the ANN should be numbers between 0 and 1. To satisfy this criterion, each geometry and performance parameter is scaled. For the optimum sensitivity of the ANN, the upper and lower limits of the outputs should be selected in such a way that the intervals remain as narrow as possible. This is due to the asymptotic behavior of the sigmoid function shown in Figure 2.4.

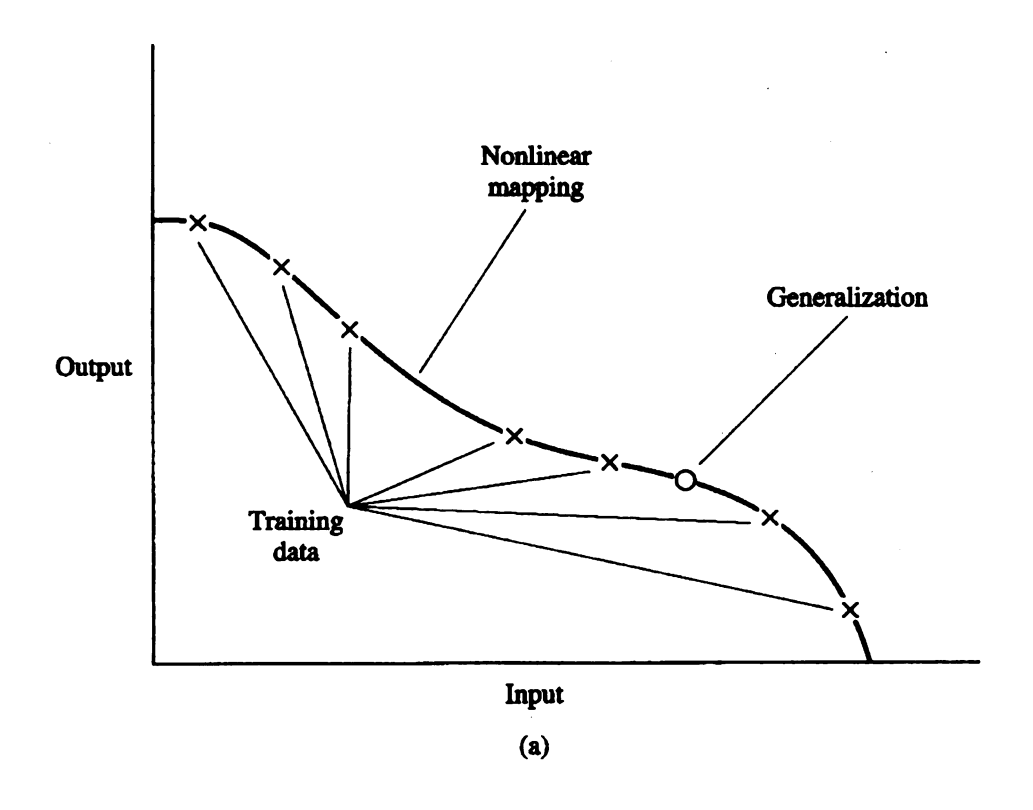
The scaling is performed using the following formula. G_{scaled} is the scale factor, G_{actual} the unscaled variable, while G_{upper} and G_{lower} are the upper and lower variable limits:

$$G_{scaled} = \frac{G_{actual} - G_{lower}}{G_{upper} - G_{lower}}$$
[2.5]

Finally, it is sometimes possible to end up with an overtrained ANN. This means that "f' in equation [2.1] is a polynomial fitted to a high degree. This can lead to situations that, for same input, there are two or more outputs. This is shown Figure 2.5. The steps taken to properly train ANN are beyond the scope of this project and will not be discussed here. The reader should consult reference [2] for more details regarding proper and improper training.

Output

Output



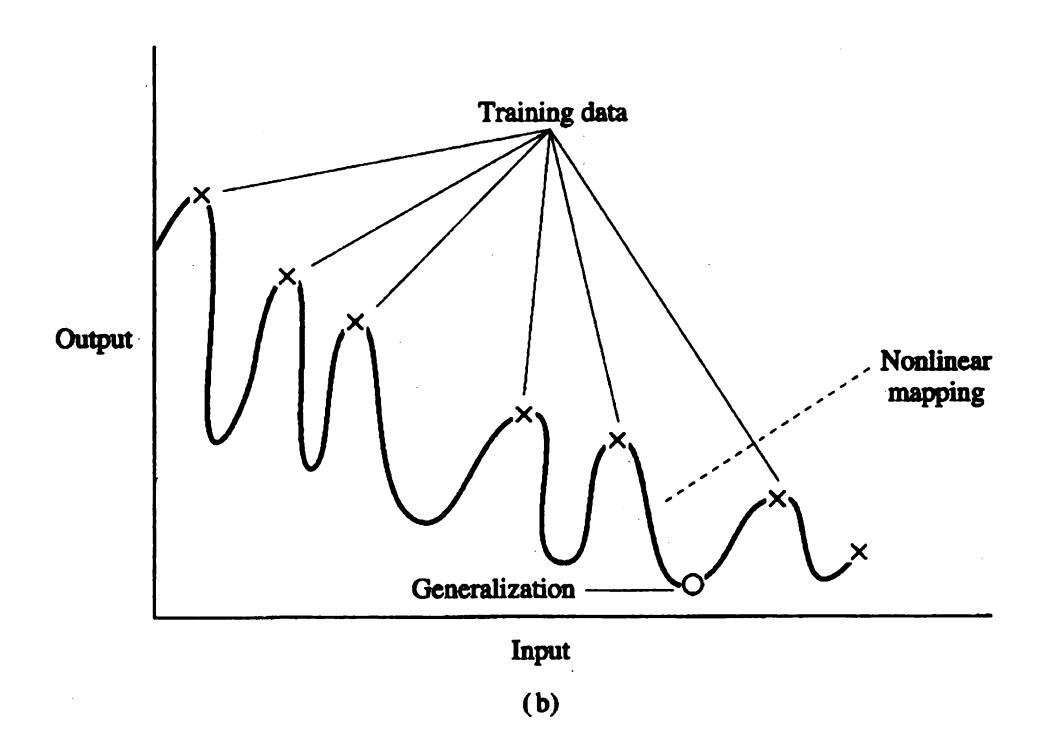


Figure 2.5 Properly trained (a) and improperly trained (b) data

2.4 Genetic Algorithm

The goal of the optimizer is to find the geometry corresponding to the minimum of an objective function using the simplified analysis model $\vec{P} = f(\vec{BC}, \vec{G})$, and knowing that many local optima may exist in the design space for only one global minimum.

The genetic algorithm uses the genetic evolution and Darwin's theory as a model to simulate the design evolution and to reach the best solution. The core of this theory is "the survival of the fittest". Fitness is in general related to the objective function by $Fitness = \frac{1}{Objective Function}$ It is obvious that a design having a lower penalty (minimizing the objective function) will have better fitness and more chance to survive in the optimization procedure.

The GA's terminology is presented in Table 2.1:

Table 2.1 GA's Terminology

Gene	One design Variable
Chromosome	Set of Design Variables
Individual	Blade Shape
Population	Set of Blades
Fitness	Performance Measure of an Individual

We are interested in the fitness of the individual. For this purpose, the algorithm creates a random population. Genetic processes are applied to the population during each iteration. The dynamics of this mechanism is reproduction. After a reproduction, a new

generation of reproduced individuals, takes the place of their parents. This procedure is repeated until a predefined number of generations are reached. The fittest of the last generation and earlier generations is selected and proposed to the NS solver. For each new iteration, beginning with a new and hopefully better approximation of the ANN, a new population is created and a new evolution cycle started. The fitness of the individuals is approximated by the ANN.

Reproduction mechanisms have several subroutines. Selection is one of them. There are different types of selection methods regarding which individuals will survive in the next generation after a reproduction. The tournament selection is usually used. Two random individuals are selected from the population and the fittest is used as one of the parents for the new generation creation. The other individual still survives in the old population, preserving its chances to be selected again. This is done until the required number of individuals for the next generation to be created has been reached. The best individual of the previous generation is also selected and transferred to the next generation.

Recombination is another sub-mechanism of the reproduction process. Recombination means exchange of genes. The mutation is the action under which the gene of an individual is selected with a predefined probability and its value changes to a random one, within the design range. Mutations attempts to prevent the GA from getting trapped in a local minimum of the objective function, by creating some disturbance and increasing the variation of the population.

The operation principle of a standard GA is shown in Figure 2.6. Pairs of individuals (parents) are selected from an initially random population of n designs, each represented

by a binary coded string of length 1. Genetic material is subsequently exchanged between them (crossover) and altered within the child (mutation). This process is repeated to create the n individuals of the new generation. The best geometry of the last generation is the solution of the GA optimization process.

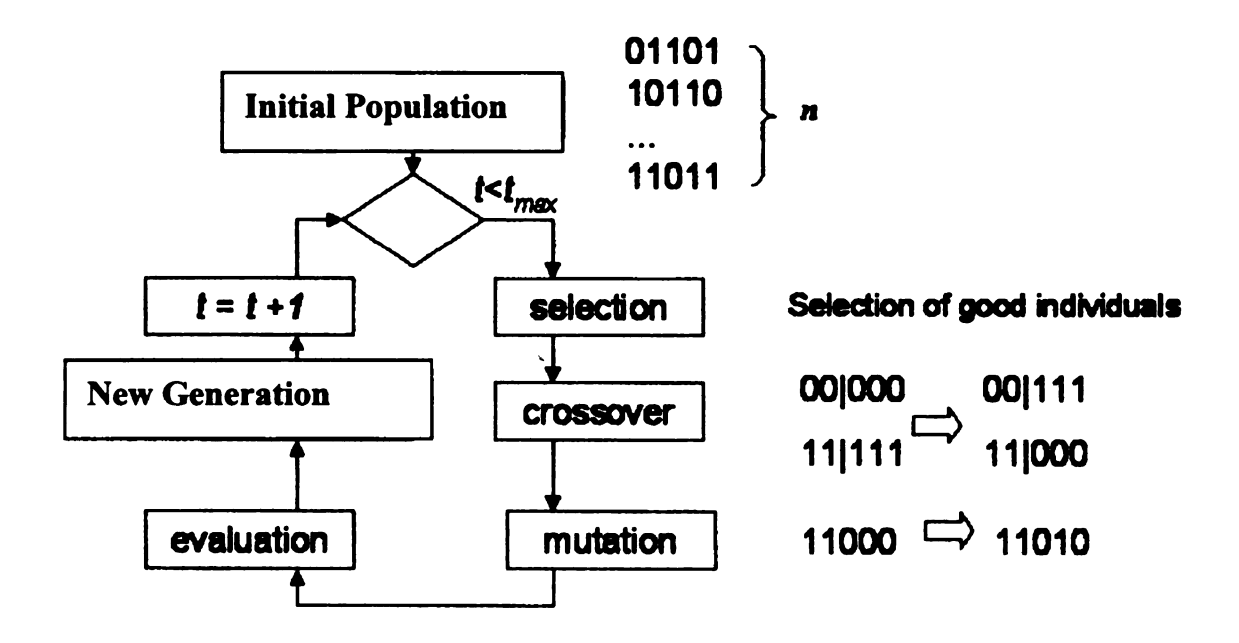


Figure 2.6 Flow Chart of the working principle of a GA. [2]

2.5 Objective Function

A global performance measure is needed for the optimization process, during the ANN and NS calculation evaluations.

High efficiency is only one of the objectives to meet for an aerodynamic shape optimization. A good design should also respect the mechanical and manufacturing constraints, and achieve the required aerodynamic performances (turning, surge margin, good off-design behavior).

This is achieved by the minimization of an objective function (loss coefficient) in several variables subject to several constraints. The general approach to this problem is to

The global

transform

simplest v

penalty ter

 $OF(\vec{P},\vec{G})$

In equa their relativ denoted by

P_{Aerol}

perfo turnir

for tu

≥ P_{Meca} the m

are w

> P_{Geor}

thickn

P_{Side}

overh

transform the original constrained minimization problem into an unconstrained one. The simplest way to do this is to create a pseudo-objective function (OF) by summing up penalty terms which are increasing when the constraints are violated.

The global objective function takes the following form:

$$OF(\vec{P}, \vec{G}, \overrightarrow{BC}) = \omega_a \cdot P_{AeroPerf.} + \omega_m \cdot P_{Meca.} + \omega_g \cdot P_{Geom.} + \omega_s \cdot P_{Side} + \omega_M \cdot P_{Mach}$$
[2.6]

In equation [2.6] the right hand side terms of the equation are the penalty terms and their relative performances can be changed by adjusting the weight factors which are denoted by the symbol ω :

- ➤ P_{AeroPerf.} = penalty on aerodynamic performance, to realize the required performance at the inlet and outlet of the computational domain, (i.e. mass flow, turning, efficiency) and to minimize the losses, i.e. the enthalpy loss coefficient for turbines.
- ➤ P_{Meca.} = penalty for mechanical constraints, to verify if the parameters related to the mechanical integrity of the design, i.e. static and dynamic load of the blade, are within prescribed limits,
- > P_{Geom.}= penalty for geometrical constraints (blade curvature radius, axial chord, thickness...),
- > P_{Side} = penalty for side constraints (acoustic problems, manufacturing problems, overhaul conditions...),

into

cons

➤ P_{Mach} = penalty for non optimum Mach number distribution (to avoid velocity distributions known to be far from optimal, such as those with a high probability of early transition, laminar or turbulent separation, poor off-design performances).

Finally, it is noted that in this work, that only the aerodynamic performance is taken into account. That is, stress, vibrations, heat transfer, and economic calculations are not considered.

3.1

geor

vers

gnd

geon

t

CHAPTER 3

BASELINE GEOMETRY AND TRAF SETTINGS

3.1 Geometric Fitting

Before the optimization system can be utilized, one must start from a reference geometry or baseline geometry. The way in which this was done in this work was to imitate an existing geometry at VKI using Bézier curves to create a parameterized version of the geometry. This parameterization is the input used to create the geometry, grid and stacking of the grid. The definition of the meridional contour using these geometric parameters is illustrated below.

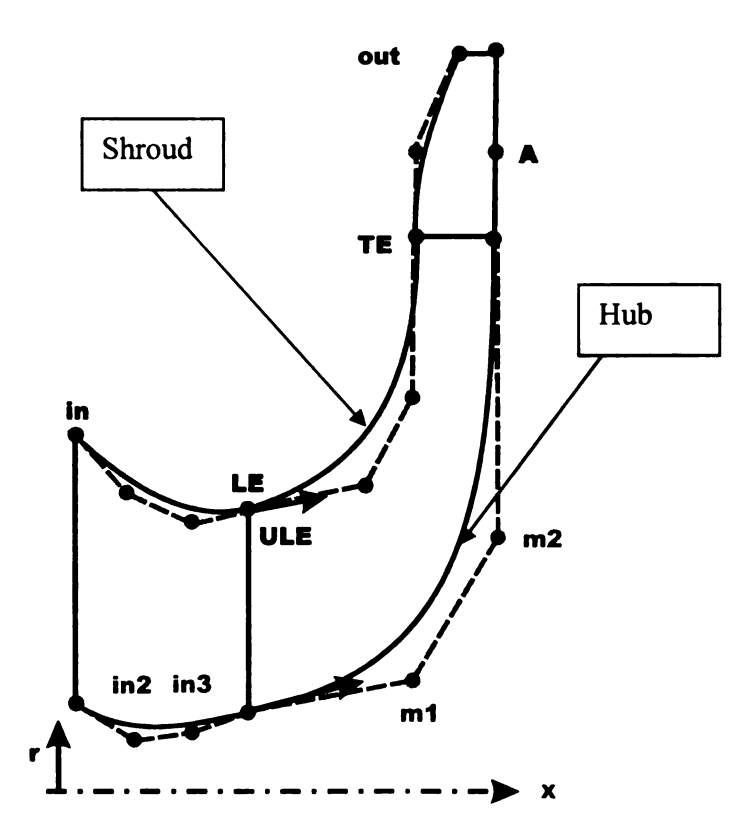


Figure 3.1 Definitions of the meridional contour geometric parameters. [4]

outle

LE) :

filled

inlet To m

are in

blade

blåde

to the

15,77

etpla

points which

mendi

leading

The major stations illustrated above are the inlet, leading edge, trailing edge and outlet which are indicated with black points. The Bézier control points above are the filled circles attached to the dashed lines. The inlet section (between the points in and LE) and the impeller leading edge are parameterized with 3rd order Bézier curves. The inlet section control points are in2 and in3, and the blade control points are m1 and m2. To make the figure more readable the point pairs with the same name at hub and shroud are indicated only at the hub or shroud. The vector ULE, represents the percentage of the blade meridional length where the splitter blade begins, both at hub and shroud. The blade meridional length is the curvilinear distance along the black solid line from the LE to the TE. Although not shown above, one can also vary the metal angle of the blades by varying the above defined points. Finally, one should consult Pierret [1] for a theoretical explanation about Bézier curves.

Using the above definition, a parameterized geometry was created using Bézier points. This was done through a trial and error process that resulted in the final geometry which shall henceforth be known as the baseline geometry. Figure 3.2a shows the meridional contour of the baseline geometry. It clearly identifies the location of the leading and trailing edges of the full blade.

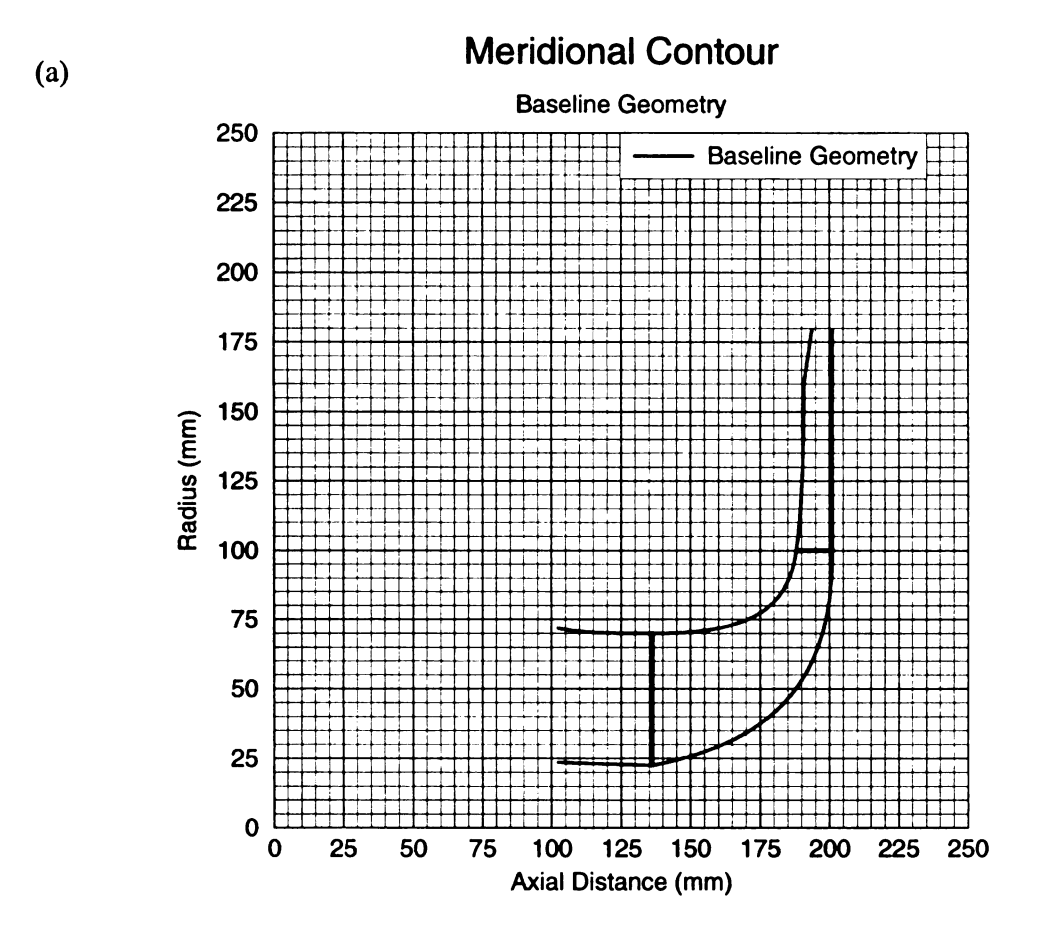


Figure 3.2 Baseline Geometry: (a) Meriodinal contours. (b) Blade profiles

Baseline Blade Profiles

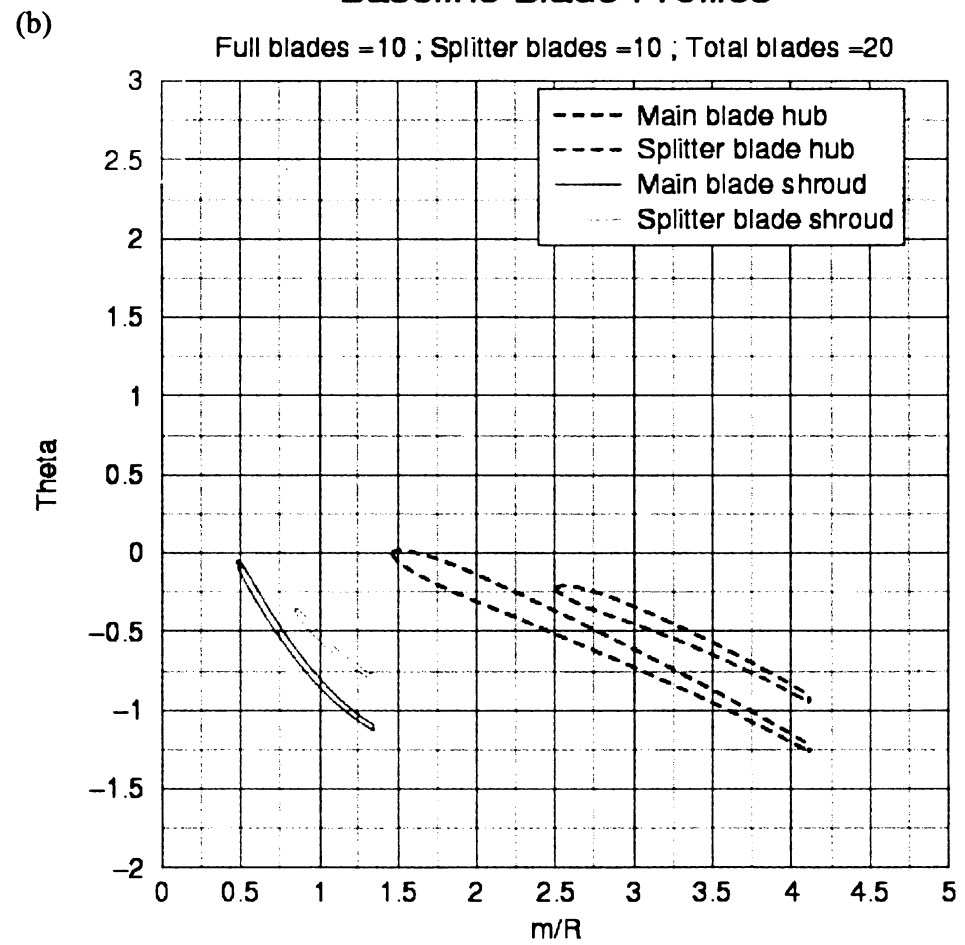


Figure 3.2 (cont'd)

The associated baseline blade profiles are shown 3.2b. In Figure 3.2b the blade profiles were generated using a conformal mapping. This means that the blade angles are preserved. The dashed line profiles represent the hub, with the larger blade obviously being the full blade and the smaller one the splitter blade. The same reasoning applies to the solid lines. That is, the solid lines represent the shroud with the full blade being the larger one and other one being the splitter blade. The blade profiles can also be distinguished by noting that the blade angle is larger at the shroud than at the hub.

lt U

of 101

schi smo

Some characteristics of the above geometry to be noted are listed in Table 3.1 on the next page

Table 3.1 Characteristics of the Baseline Geometry

Geometric Characteristics	
Beta-le-hub	21.70 Degrees
Beta-le-hub-sp	18.00 Degrees
Beta-le-shr	64.73 Degrees
Beta-le-shr-sp	53.00 Degrees
Beta-te	30.00 Degrees
Shroud clearance	0.575 mm
Max Hub Thickness	4 mm
Min Hub Thickness	3 mm
Max Shroud Thickness	3 mm
Min Shroud Thickness	2.5 mm
Percent blade chord length where finishes	25 %
the transition from Max to Min thickness.	
The thickness remains constant from this	
point all the way to the trailing edge.	
Impeller Tip Radius	100 mm

3.2 Fundamentals of the TRAF3D program

The TRAF3D code solves the Reynolds-Averaged Navier-Stokes equations (*RANS*). It was developed in a research project on viscous cascade flow simulation by the University of Florence and NASA [1]. It is able to predict the aerodynamic performance of turbomachinery blades, working on linear or annular cascades, and considering rotating blade passages with tip clearance flow.

These RANS equations are solved using an explicit, steady, four-stage Runge-Kutta scheme, in conjunction with accelerating techniques such as local time stepping, residual smoothing and FAS (Full Approximation Storage) Multigrid. These equations are

discr

The

eval

visco surfa

from

both

fully

trans

33)

upper

A

the s

caleu

Ī

discr num

can o

as po

data, th

comparat

discretized using finite volumes and a cell-centered scheme, with artificial dissipation. The turbulence is simulated using a $Baldwin-Lomax\ two-layer\ mixing\ length\ model$ to evaluate the turbulent viscosity, μ_t , and the turbulent kinetic energy, k, under an eddy-viscosity hypothesis. The transitional criterion of Baldwin-Lomax is adopted on the blade surface while the shear layer on the hub and shroud contours are assumed fully turbulent, from the inlet boundary surface. The transition can also be imposed at a given point on both suction and pressure sides, which is the way we have been proceeding, considering a fully turbulent flow on the blade surface (high Reynolds number). In other words, transition is assumed to start at the leading edge of the blades.

3.3 Meshing approach and parameters

All the meshes were created using an H-type two-block grid, one block devoted to an upper and lower channel. To avoid excessively long computational times, one has to limit the size of the mesh using a reasonable number of cells. This raises the problem of the calculations' grid dependency and of the accuracy of the results that were obtained.

First, one has to note that the use of CFD will <u>never</u> provide exact results. Indeed, the discretization itself, the fact that the turbulence is modeled instead of using direct numerical simulation (DNS), and other assumptions that are made through the process, can only give approximate results. The point is to make these approximations as accurate as possible to provide the designer an idea of what to expect, and to provide information about the flow field. Pierret [1] has shown, comparing experimental and computational data, that the TRAF code gives very good and reliable results for applications that are comparable to ours, even with relatively coarse meshes. The second point is that the

C

TR

code will be used to make comparisons between different geometries. This is important because if one can assure to retain the same, or almost the same, mesh for all the entries, then the studied cases should be entirely comparable, and the grid dependency negligible.

Two identical annular meshes are made, one for the upper and one for lower blade channels. They will be used as the geometric inputs for the NS calculation. The main inputs for the mesh creation are defined in Figure 3.3, Table 3.2, and Table 3.3 (see TRAF Code for Radial Turbomachinery manual for further explanation [5]).

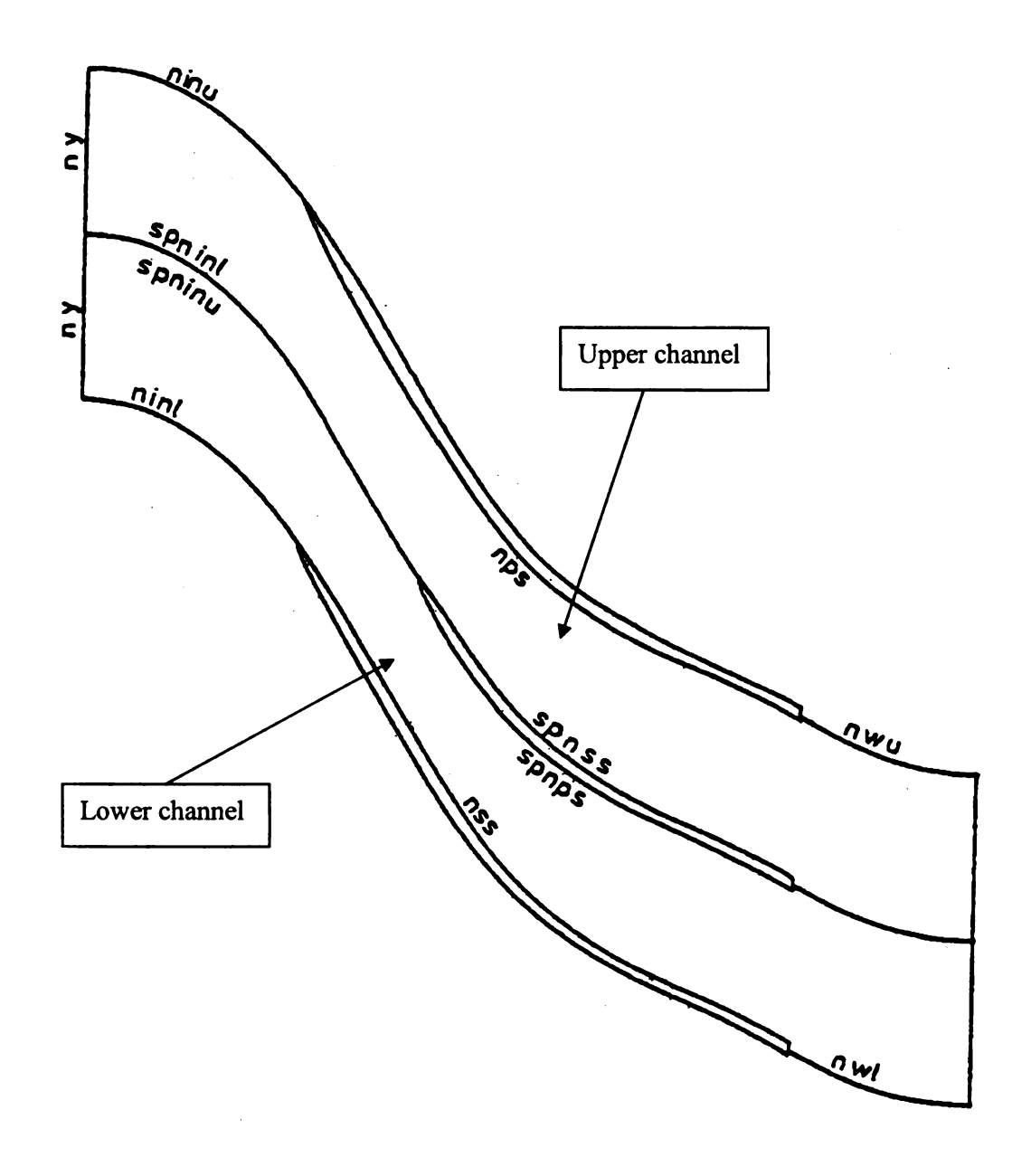


Figure 3.3 Main Grid Parameters. H-type Grid. [5]

Table 3.2 Impeller Mesh Parameters (number of cells)

Parameters	Lower 32				
nwl					
nss	72				
spnps	48				
ninl	24				
ny	36				
spninl	48				
	Upper				
nwu	32				
nps	72				
spnss	48				
ninu	24				
ny	36				
spninu	48				

The parameters near the blade are listed, depicted, and tabulated below: (see TRAF manual for a more detailed treatment [5])

- Lref = impeller tip radius
- d0s=size of first grid on the blade suction side non-dimensionalized by Lref
- d1s= size of last grid on the blade suction side non-dimensionalized by Lref
- d0p=size of first grid on the blade pressure side non-dimensionalized by Lref
- d1p= size of last grid on the blade pressure side non-dimensionalized by Lref
- dsn = distance of the first grid perpendicular to the wall non-dimensionalized by

 Lref
- jfixs = number of cells near leading edge and/or trailing edge with variable length along the suction side of the blade
- jfixp = number of cells near leading edge and/or trailing edge with variable length along the pressure side of the blade

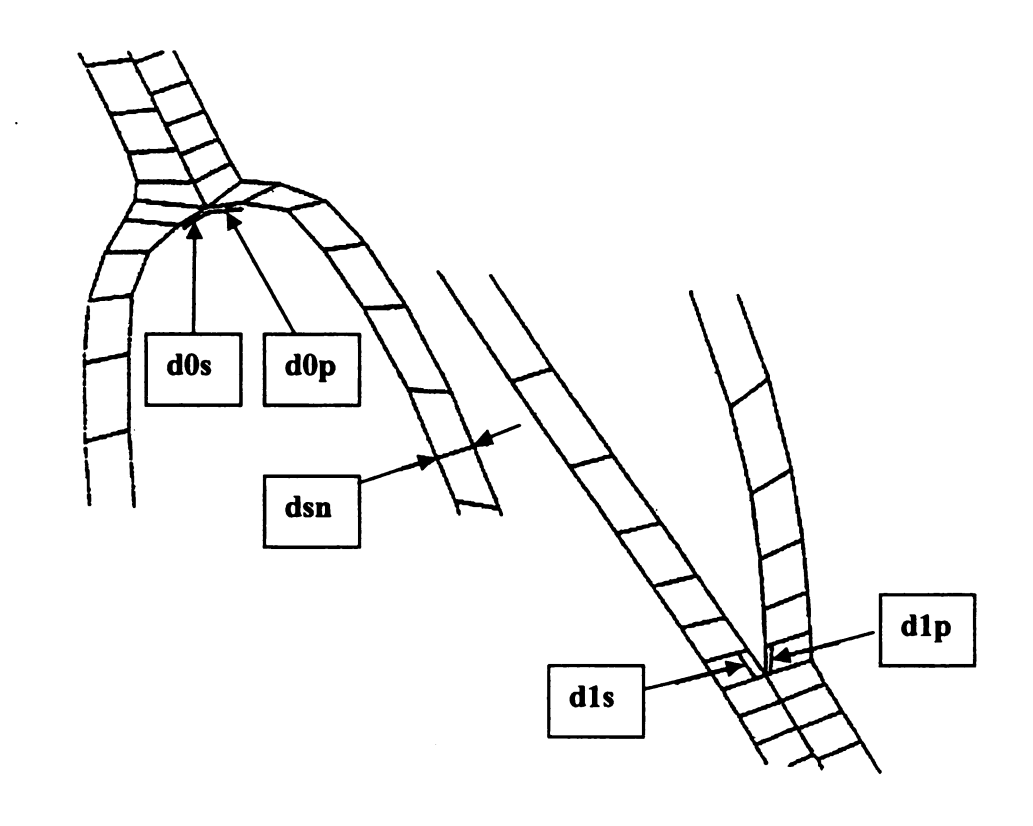


Figure 3.4 Boundary layer mesh parameters. [5]

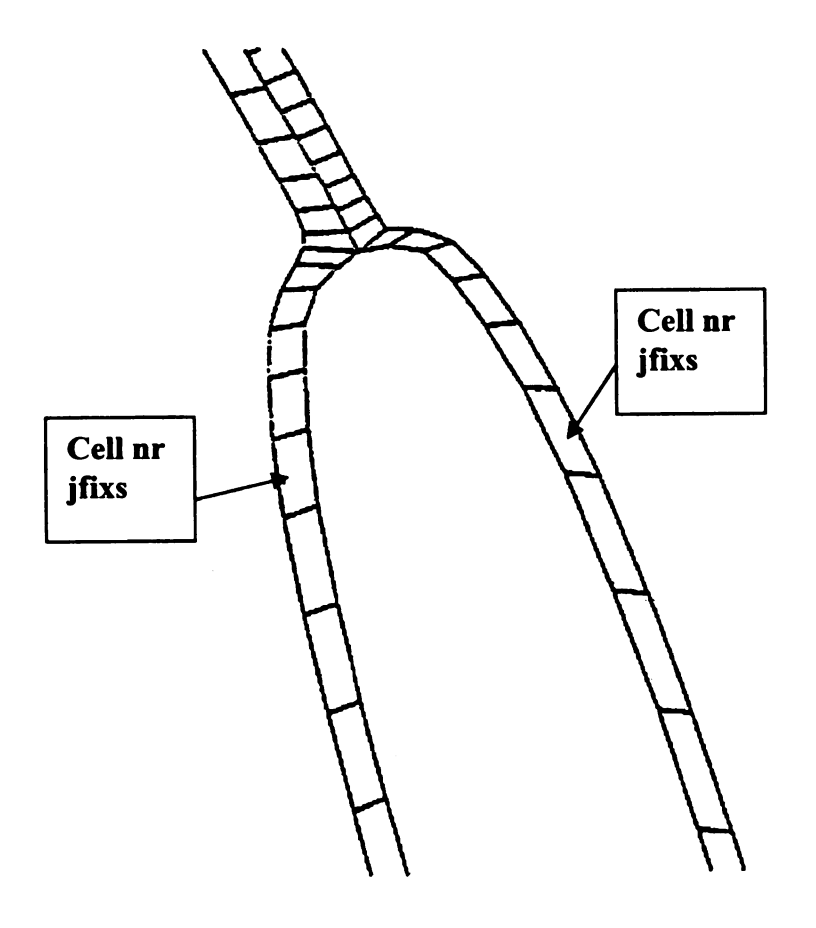


Figure 3.4 (cont'd).

Fin

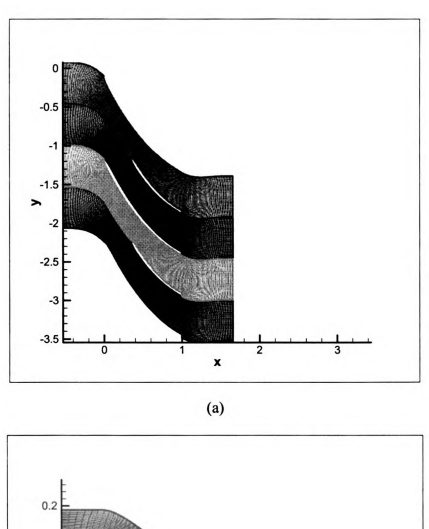
Wit.

Table 3.3 Near wall parameters

Parameters	Full Blade
d0s	0.010
d0p	0.010
d1s	0.010
d1p	0.010
dsn	0.010
jfixs	6
jfixp	6
	Splitter blade
d0s-sp	0.010
d0p-sp	0.010
d1s-sp	0.010
d1p-sp	0.010
dsn-sp	0.010
jfixs-sp	6
jfixp-sp	6

Finally, the stacking procedure for both upper and lower channels is listed below along with typical 2D grids.

- ➤ The number of cells in the spanwise direction is set to 48, with a first and last grid cell size of 5 × 10⁻³ (non-dimensionalized by the reference length).
- > The number of stretched cells near the endwalls is set to 28.
- > The tip clearance is 0.575 mm and 8 cells are used in the clearance



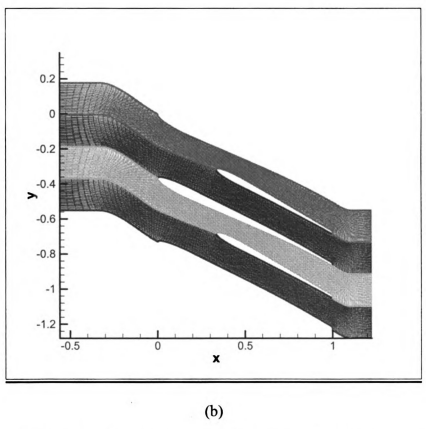


Figure 3.5 Typical Blade to Blade Plane Grids. (a) Shroud (b) Hub

3.4

defi

00.77

3.4

me sett

to 2

100

000

3.4 Navier-Stokes Solver Parameterization

The next step of the work was to set the operating conditions of the flow solver by defining the boundary conditions and the solution parameters to be used for the computations.

3.4.1 Solution parameters

For all our calculations, we used residual smoothing and full-multigrid accelerating methods (the multigrid level was turned to three). Computations have been performed by setting the Baldwin-Lomax coefficients and abscissa for the laminar-turbulent transition to zero, assuming a fully turbulent flow. The total number of iterations was fixed to 700, 100 iterations being spent on the coarse grid (Euler grid) A commonly obtained convergence history is depicted on Figure 3.7:

Typical Convergence History

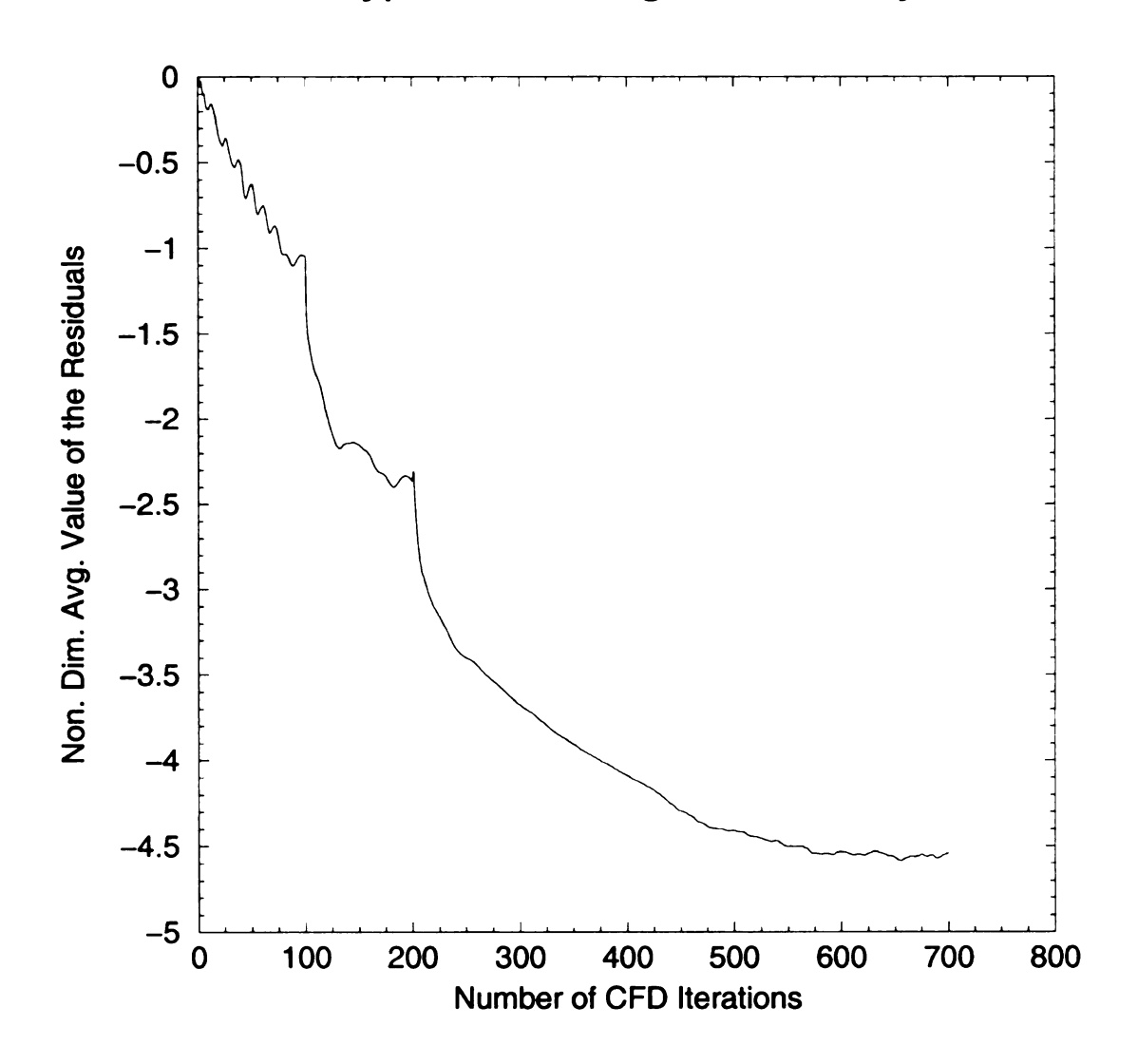


Figure 3.6 Convergence History

3.4.2 Boundary conditions (Lref = Impeller tip radius = constant = 100 mm)

Listed below are the boundary conditions and flow parameters that were used:

- \triangleright Reference pressure, $P_{01} = P_{ref} = 101325 \text{ Pa}$,
- \triangleright Reference temperature, $T_{01} = T_{ref} = 293 \text{ K}$,
- ightharpoonup R = 288 J/kg.K.
- \triangleright $\gamma = 1.4$
- > Reynolds Number, Re = $\frac{\rho_{01}\sqrt{RT_{01}}}{\mu_{01}}L_{ref} = 2389096.25$
- \triangleright Prandtl Number. Pr = 0.7
- ➤ Turbulent Prandtl Number, Pr_t = 0.9
- \triangleright CFL = 4.0
- ➤ Shaft rotational speed, N = 28000 RPM
- Imposed inlet flow measured from axial direction on a blade-to-blade surface (α).
 This value varies over the span. See inlet profiles.
- Imposed inlet flow measured from axial direction on a meridional surface (β=0).
 This value is constant over the span.
- > Imposed pressure ratios were varied to determine the performance map. That is,

$$\frac{P_2}{P_{01}}$$
=1.0, 1.1,1.2, and so on. The chosen design points for the optimizations will

be discussed in those sections.

The current optimization system sets up the above mentioned conditions automatically, so that different Reynolds numbers can be obtained for different impeller

tip radii. However, in the current work, the impeller tip radius was held constant, and thus the parameters that contain the reference length remain constant.

As for the inlet, three inlet profiles corresponding to various IGV setting angles were used. These profiles are presented below in Figure 3.8

(a) Nondimensional span vs. P01/P01ref

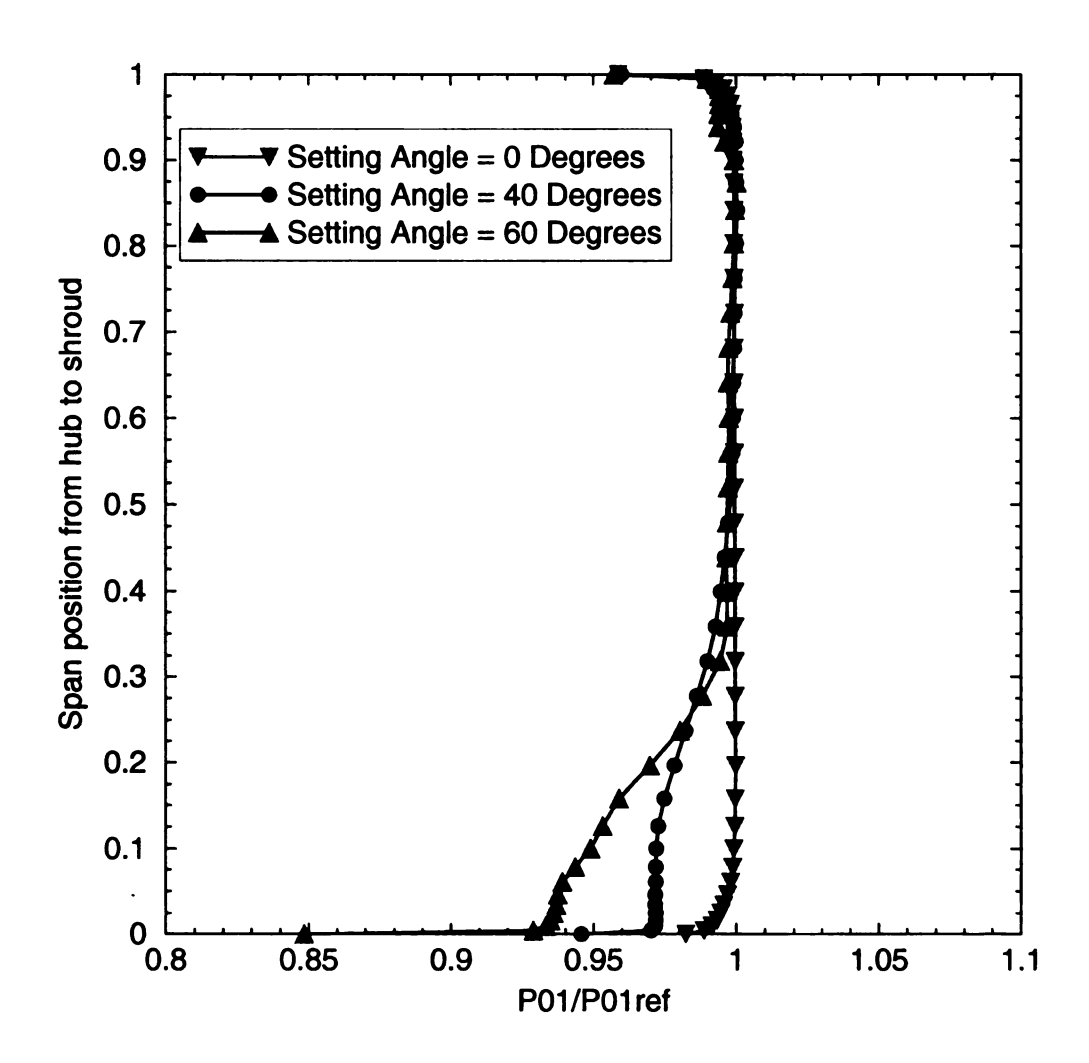


Figure 3.7 Non-Uniform Inlet Profiles. (a). Pressure (b). Flow Angle

(b) Nondimensional span vs. inlet absolute flow angle

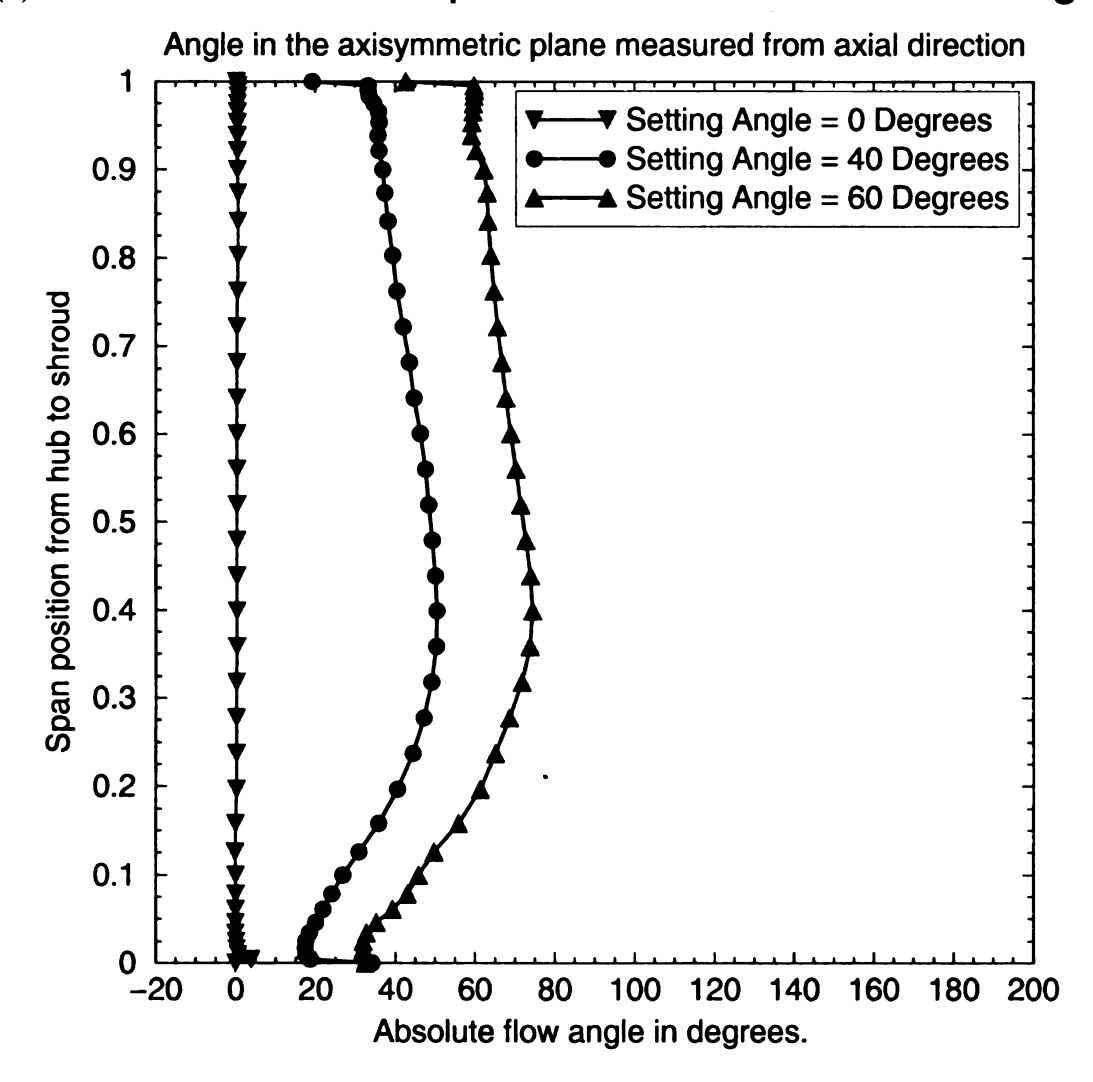


Figure 3.7 (cont'd)

3.4.3 Post-processing parameters

Once the computation is completed, the program uses the flow solution to compute the mass averaged values such as: efficiencies, pressure ratios, mass flows, etc. To do this, one has to set some basic parameters, which are:

- ➤ Position of the impeller inlet-averaging plane: The position of the this plane is set at an axial position of 115 mm as seen in Figure 3.8
- Position of the stage outlet-averaging plane: The position of this plane was chosen at the diffuser exit. This allows a sufficient distance for the mixing at the exit of the impeller to take place.
- The numerical pinch: This pinch is to make sure that one does not get local flow reversal at the exit of the machine because the CFD code will give wrong results if this happens. This is because the code does not know the total temperature, total pressure, and the flow angle of the local return flow at the outlet, which can cause the code to be unstable. Thus, the pinch is just a method of providing stability in the code. The length of the pinch is constant at 20 mm and the exit width of this contraction is always 7.4 mm. This is done so that all geometries will be comparable. That is, the effect of the pinch on performance should be the same for all geometries.

Meridional Contour

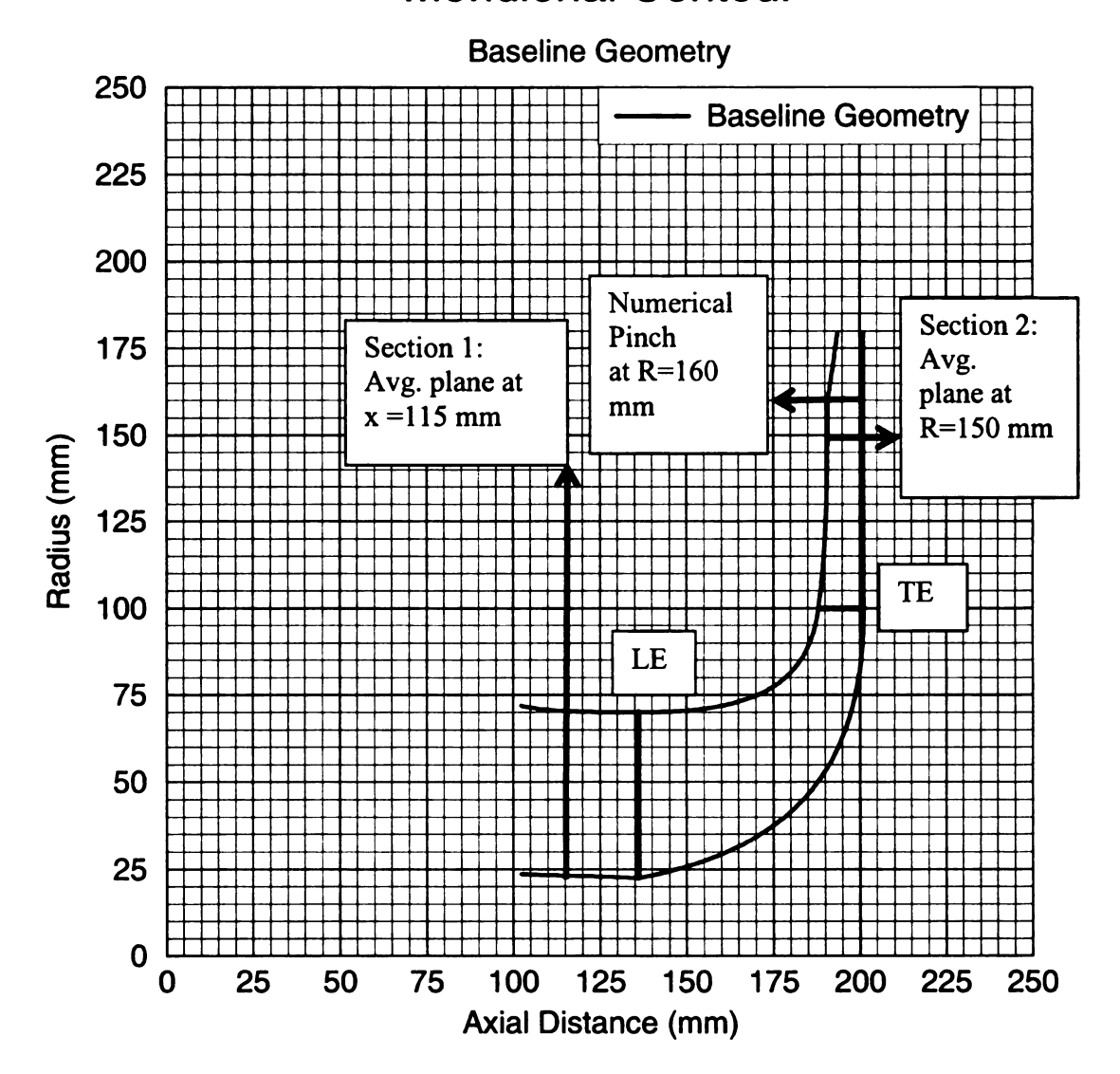


Figure 3.8 Post-Processing Planes and numerical pinch

3.4.4 Baseline Peformance:

(a) Pressure Ratio vs. Mass Flow Rate

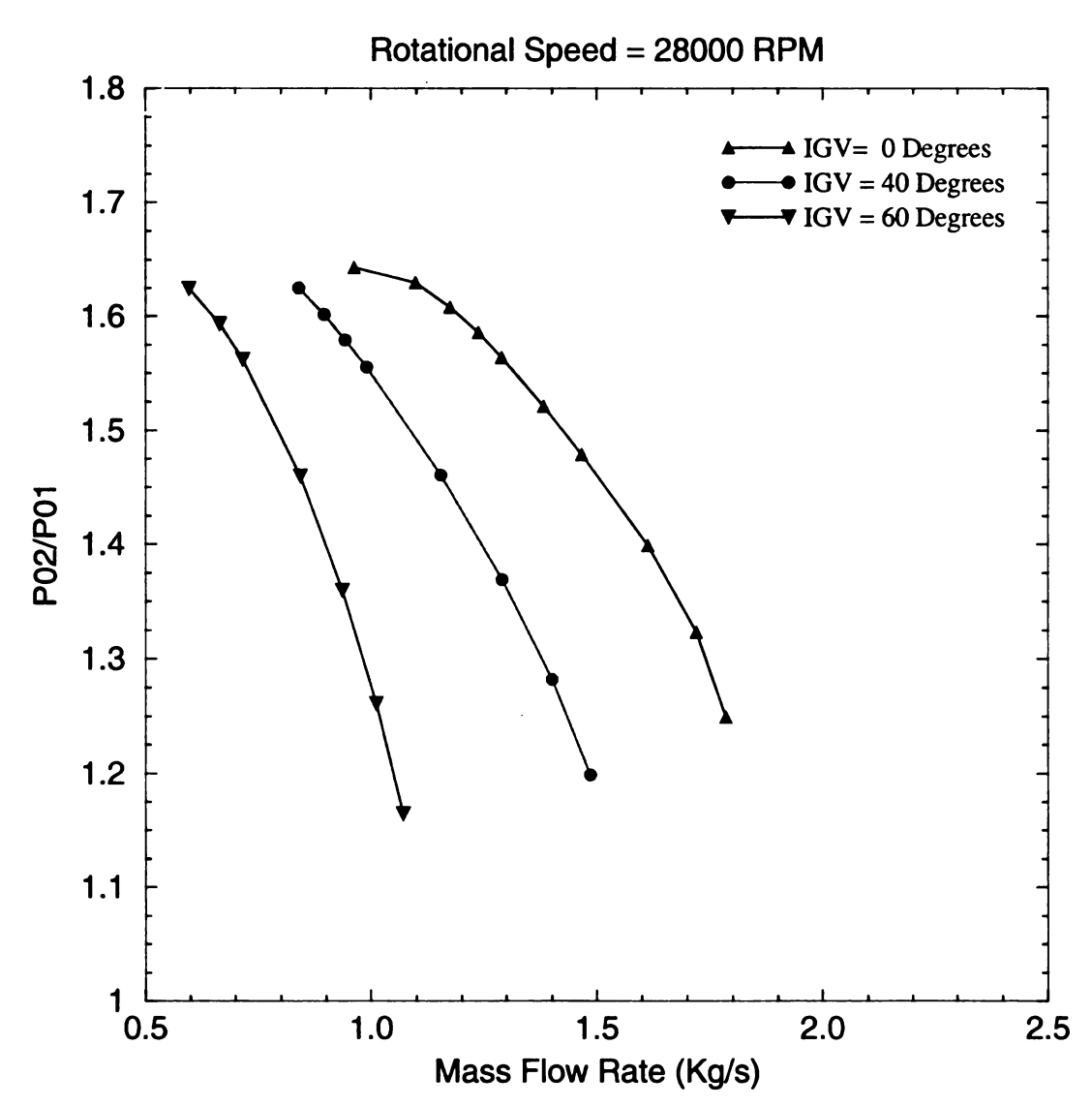


Figure 3.9 Performance Maps. (a) π , (b) η_{ts} , (c) η_{tt}

(b) Total to Static Efficiency vs. Mass flow rate

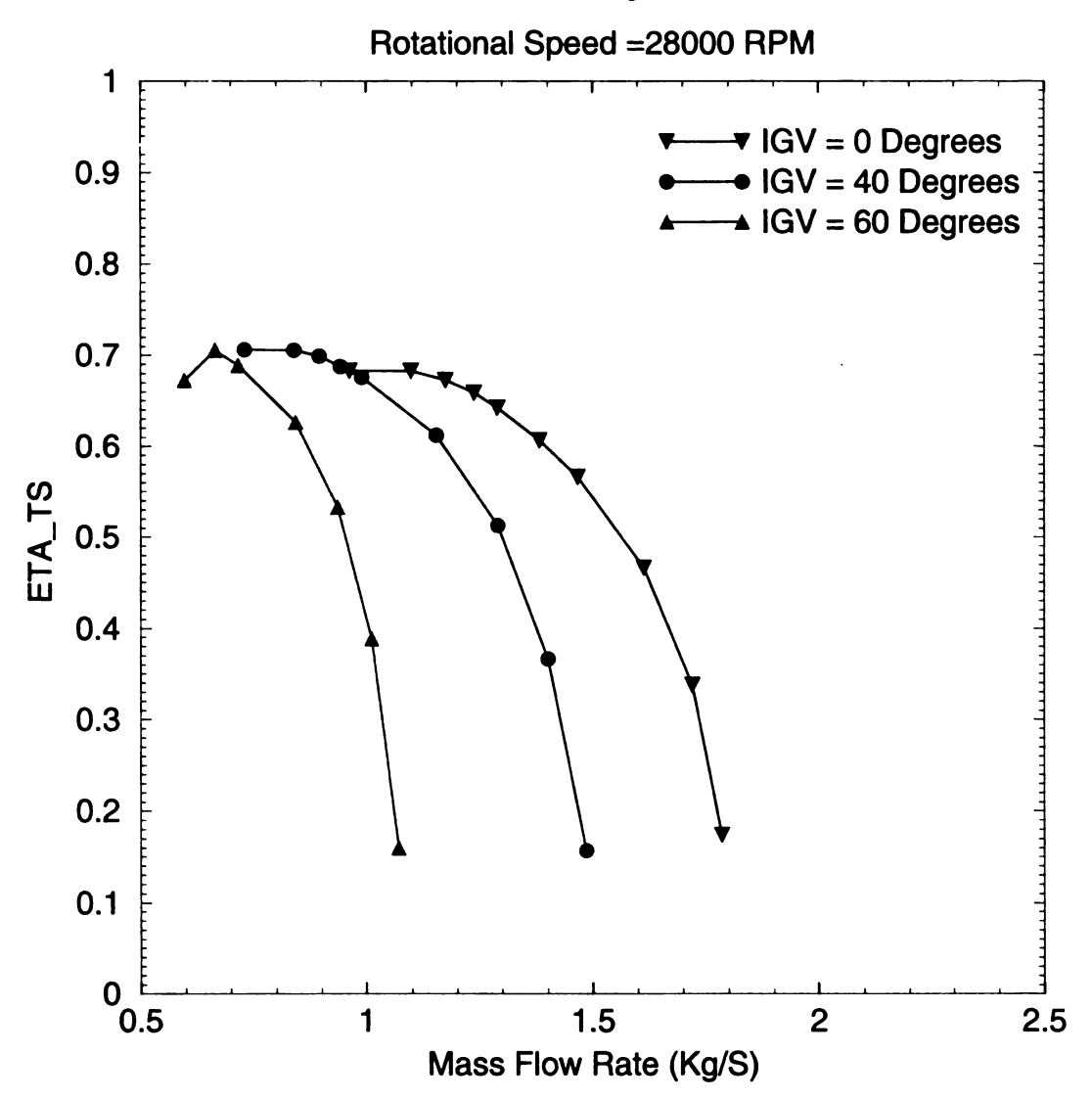


Figure 3.9 (cont'd)

(c) Total to Total Efficiency vs. Mass flow rate

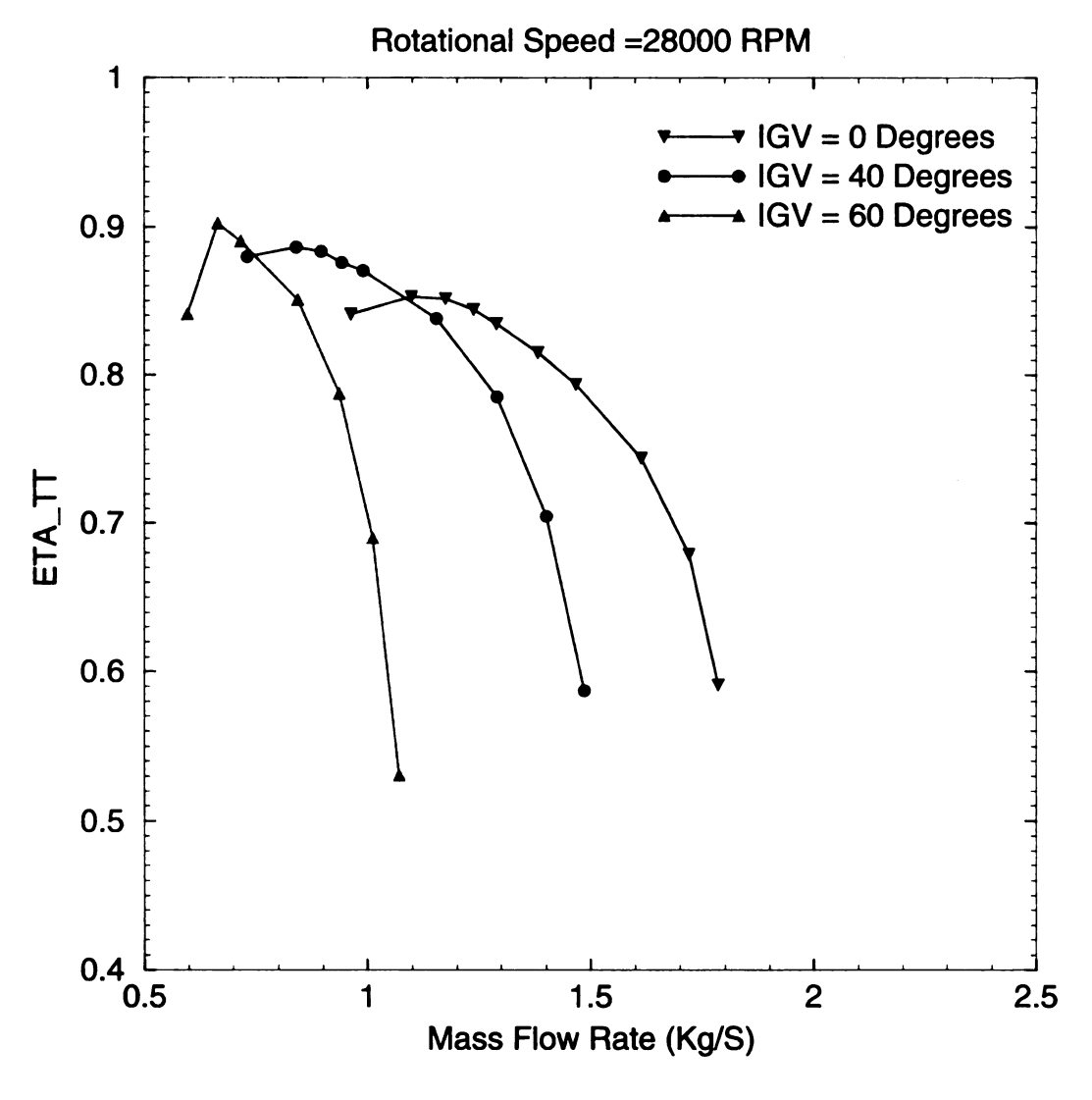


Figure 3.9 (cont'd)

Finally, the Mach number distributions for the three setting angles are displayed below in Figure 3.10.

Baseline Mach number Distribution

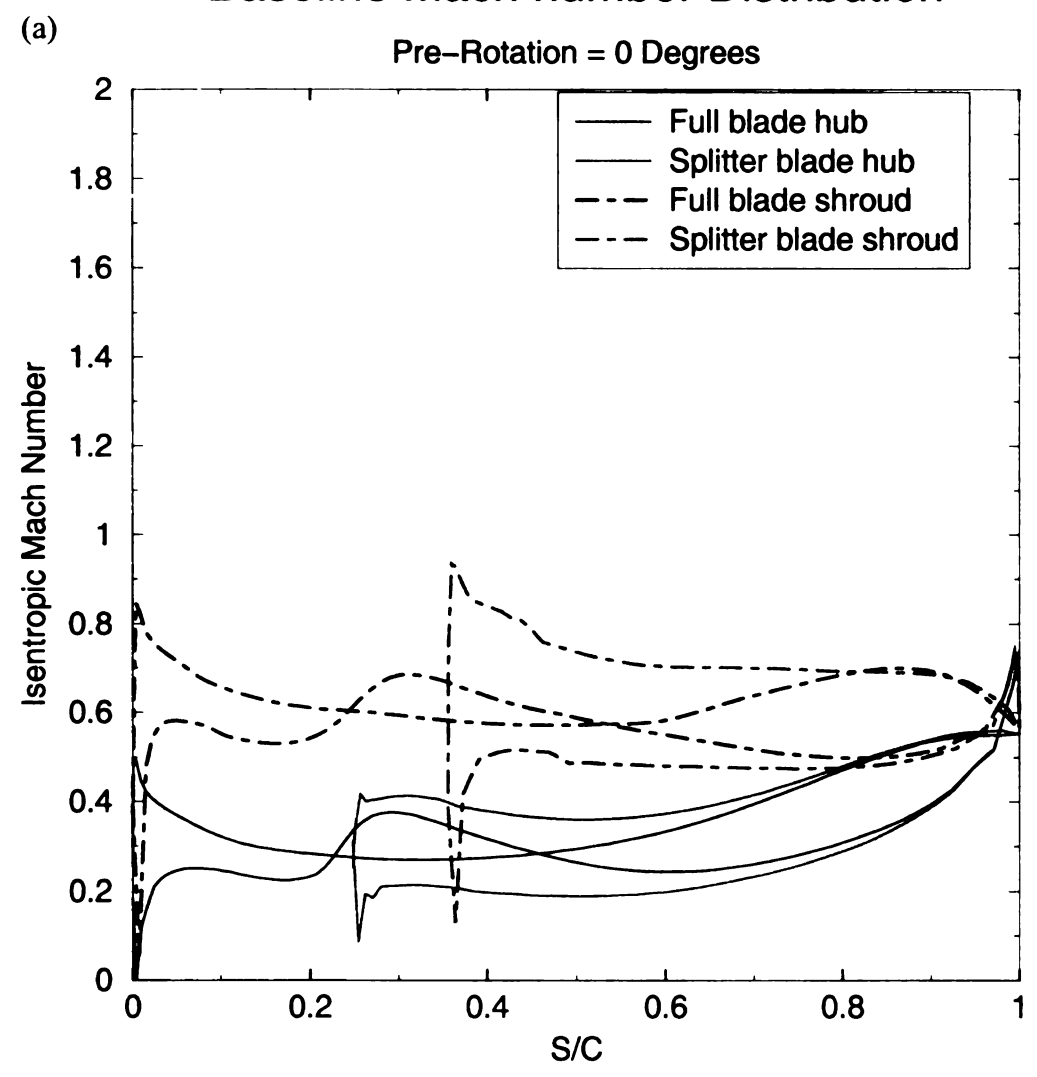


Figure 3.10 Mach Number Distributions at various Pre-Rotations: (a) 0 degrees (b) 40 degrees, (c) 60 degrees

(b) Baseline Mach number Distribution

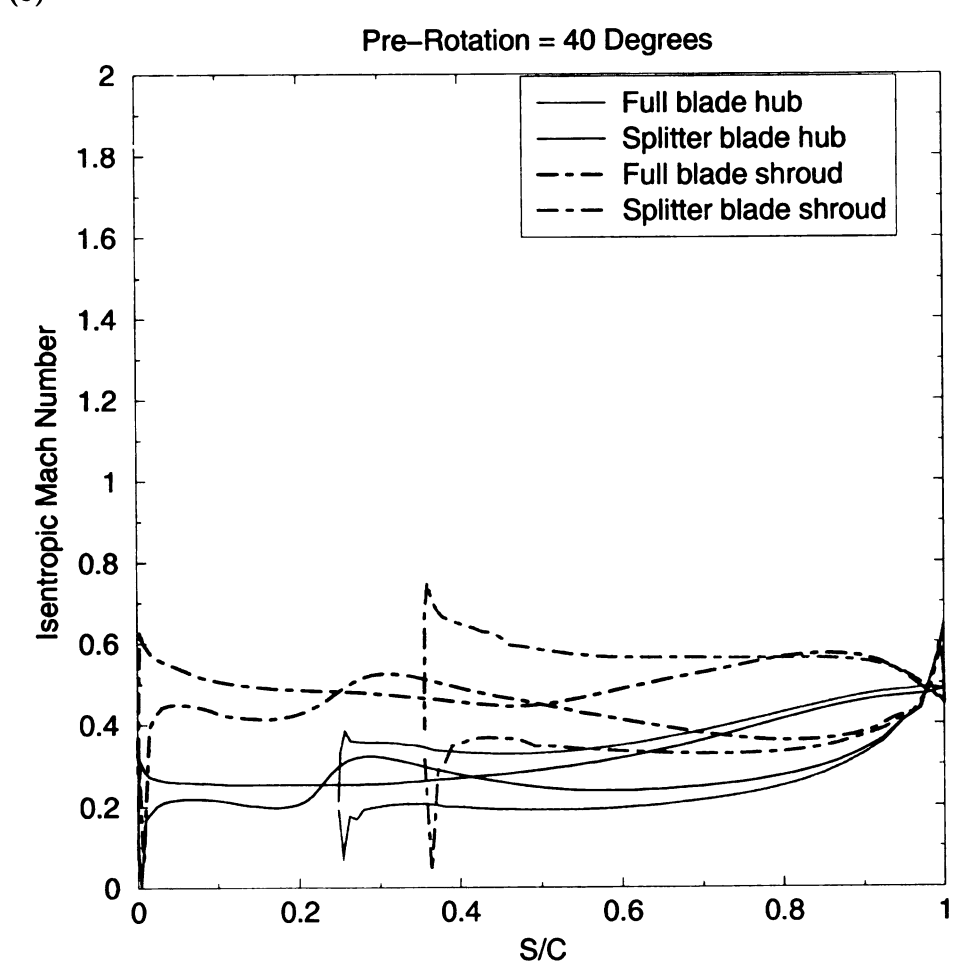


Figure 3.10 (cont'd)

gla like

opti

mac

(c) Baseline Mach number Distribution

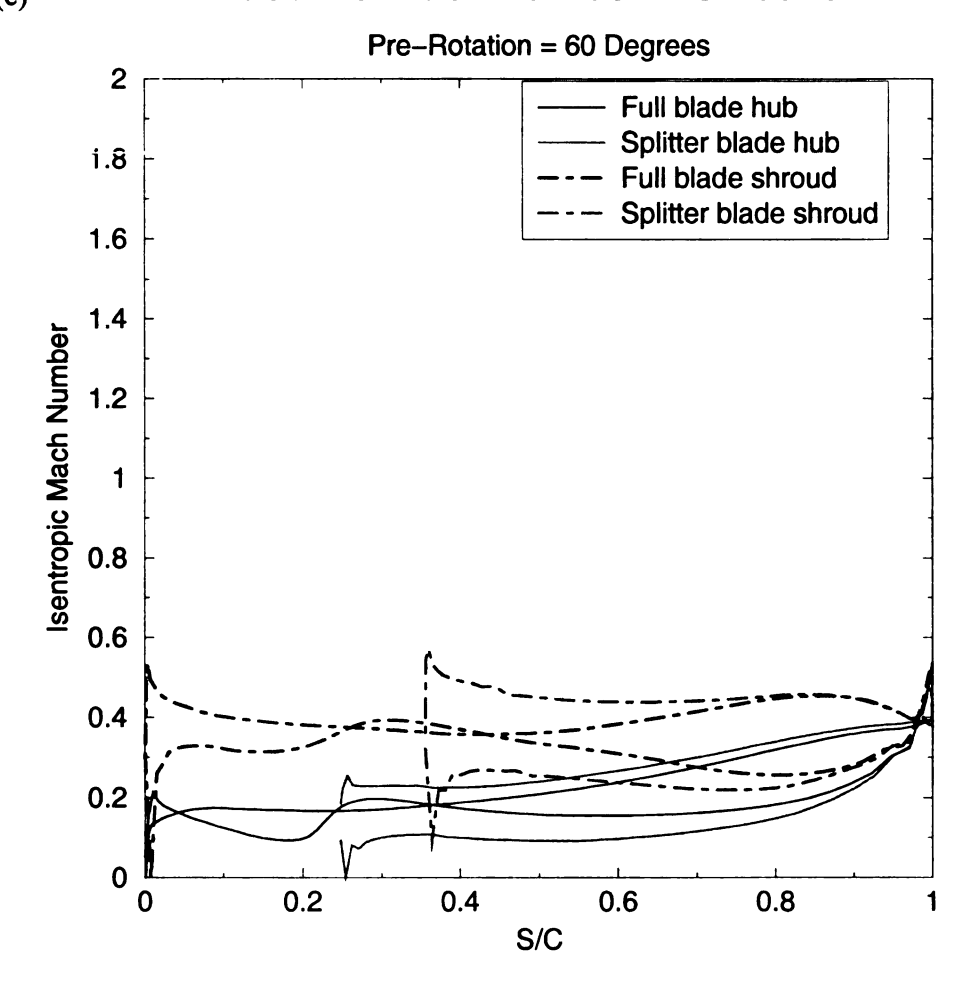


Figure 3.10 (cont'd)

One can obviously see that there is definite room for improvement by simply glancing at these distributions. A designer never likes to see negative loading and would like to eliminate high incidence. In the following chapters, single and multiple point optimizations will be attempted to see if it is possible to improve the performance of this machine.

CHAPTER 4

SINGLE POINT OPTIMIZATION

4.1 Geometry Definition

In order to perform an optimization, one must first parameterize the geometry using Bézier curves. The geometry definition and the resulting baseline geometry can be seen in Figure 4.1. A more detailed description of the definition and how the baseline geometry was obtained was already described in section 3.1, however some figures are repeated here for convenience.

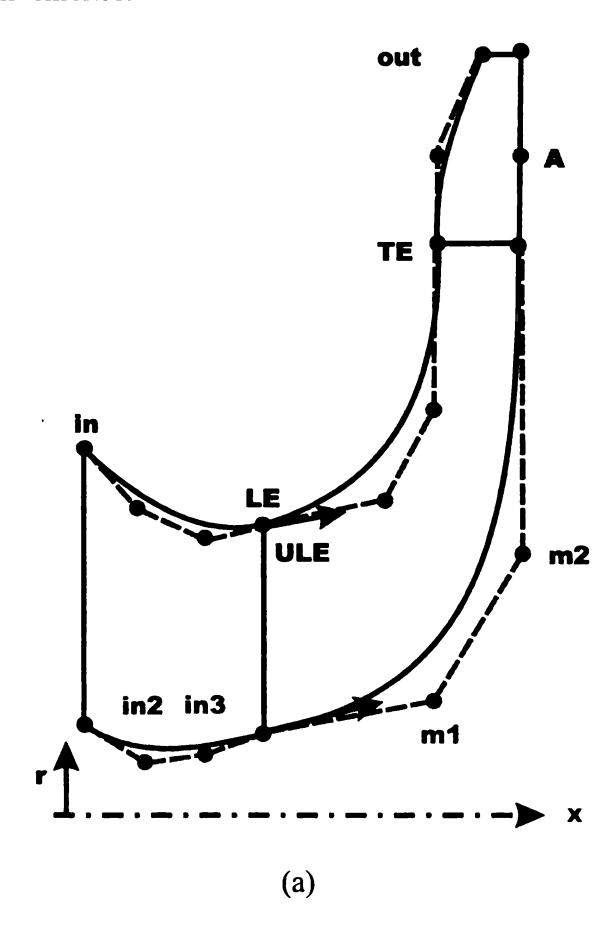
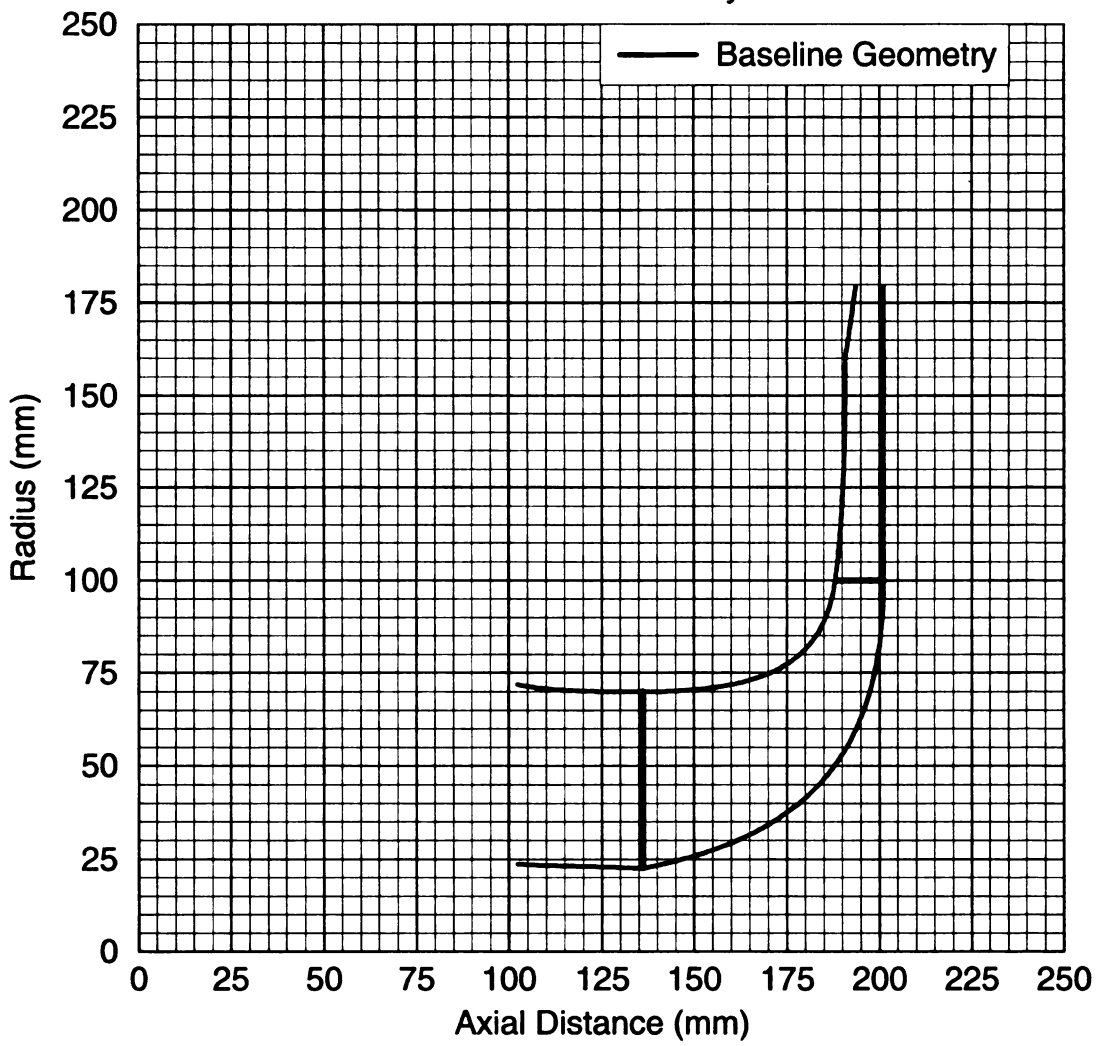


Figure 4.1 Geometry definition and baseline. (a) Geometry Definition, (b) Baseline

Meridional Contour

Baseline Geometry



(b)

Figure 4.1 (cont'd)

From Figure 4.1a and its associated blade profiles, the amount of parameters that can be changed is something like 50. This is not counting a variable tip clearance and a variable thickness distribution along the blades, which would add even more variables. Obviously one must limit the number of variables used both from a computation point of

view and from the fact the designer will have an over whelming amount of material to try and decipher.

From the computational viewpoint, the more variables the designer selects the more computations that have to be stored in the database. Since the Navier-Stokes computational time is approximately 2.5-3.5 hours depending on the machine used, one must limit the computations required. Currently, if the amount of design variables is between 16 and 30, the theory of DOE says that one should use 33 samples or more per operating point. Thus in our case (24 variables), in which three operating points are used, the minimum amount of samples is 99 which leads to 346.5 hours of computational time assuming that the slowest machine is used. Also, if one accounts for the fact that the user and manager of the system is certain to make mistakes or changes along the way, then this is even more costly (5 databases). All of these observations contribute to the fact that the designer should select a limited and physically appropriate design space. It also provides motivation to begin with single point optimization because the designer has to deal with only one third of the computations required for multiple point operation. Although, one would like to avoid making any mistakes, if this happens to occur, it will be less disastrous and more easily circumvented, than for the multi-point case, Finally, for all of the above reasons, the following discussion will be about the single point optimization and the multi-point operation will be deferred until the next chapter.

4.2 Design Space

Now that the design parameters are known, the designer must select the ones that will be variables and to select the range in which they can vary. That is, one must select a feasible design space. Figure 4.2 illustrates the concept of a design space.

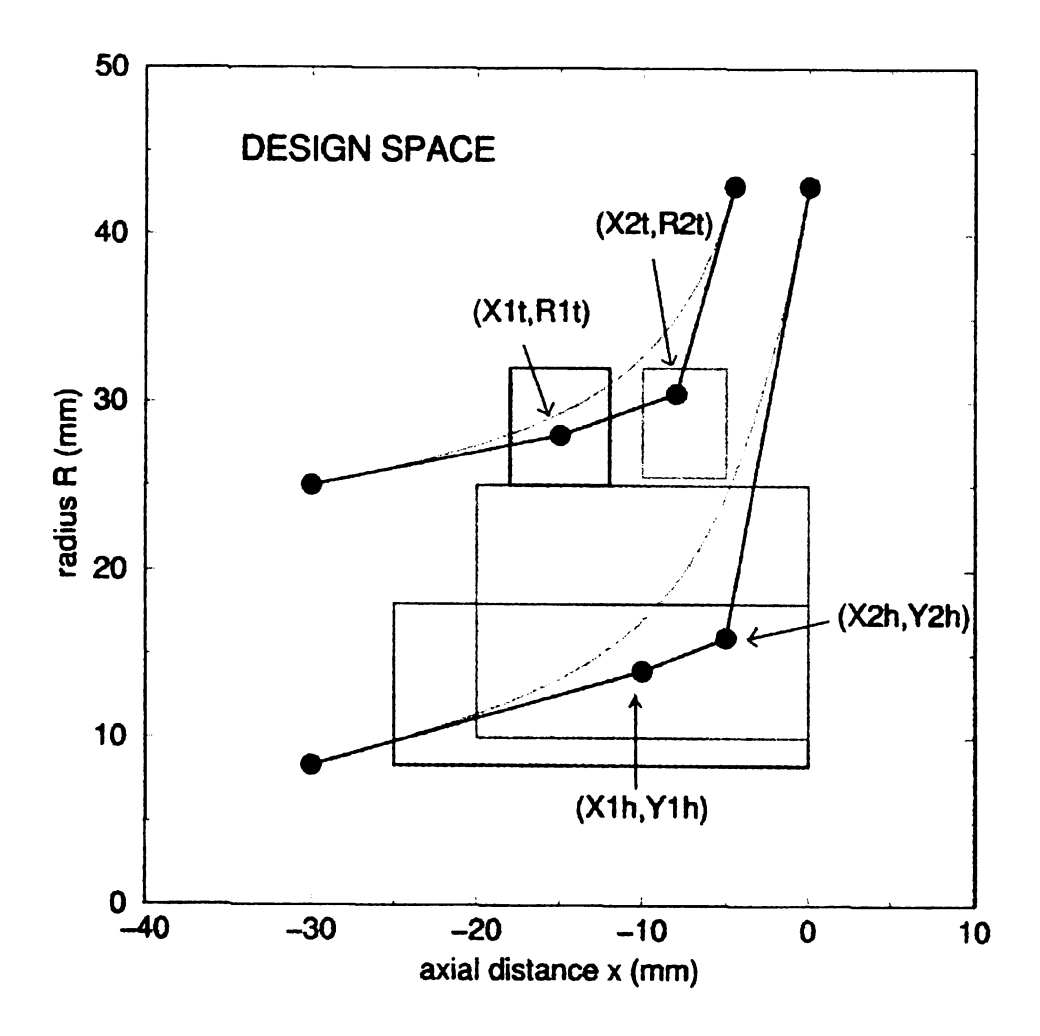


Figure 4.2 Illustration of design space concept

Choosing the design space really requires a vast experience with the particular machine that one wants to optimize. Although one can take the time to try and explain all the variables used in this work, one will just explain a few of them.

The axial position of the shroud trailing edge (xshr-te) was chosen as a variable because it is known that the wheel efficiency depends upon the outlet width. That is, a narrow exit will have a large portion of the span occupied by the boundary layer and less diffusion in the impeller. This means that there will be little or no diffusion and only friction, thus the efficiency will drop. On the other hand, a really wide exit will cause too much diffusion which results in separation with no more diffusion taking place. For a more in depth discussion about wheel efficiency, one should consult VKI course note 134 [7].

Another variable that was selected was the shroud leading edge blade angle. This is because the inducer has an important impact on the impeller performance. A bad inducer will accelerate the fluid and the downstream deceleration will cause an early flow separation at high velocity. The jet velocity will be high and the wake will grow to a large part of the impeller. The mixing downstream of the impeller will involve high losses with a subsequent drop in efficiency. Thus an important design criteria is therefore to minimize the inlet relative Mach number and if possible to keep it subsonic.

It has been shown by C. Rodgers [9] that with higher inlet angles the maximum relative Mach number is lower at a cost of reduced range due to stalling and choking incidence. This can be seen in Figure 4.3. So in the present work, the value of Beta-le-shr was chosen to be between 55 and 65 degrees. Values higher than 65 degrees lead to high blockage due to blade thickness and also to high turning which results in losses in the inducer. Values lower than 55 degrees lead to an increased range but smaller inlet section which results in an increased axial velocity and decreased tangential velocity. This then leads to higher relative tip Mach numbers which results in the impeller having

to do more diffusion which provoques separation and can also lead to shock losses if the Mach number exceeds unity. Also, as illustrated in the following figure, one can show that for a given mass flow and RPM that the minimum relative shroud inlet Mach number is obtained for beta values around 60 degrees.

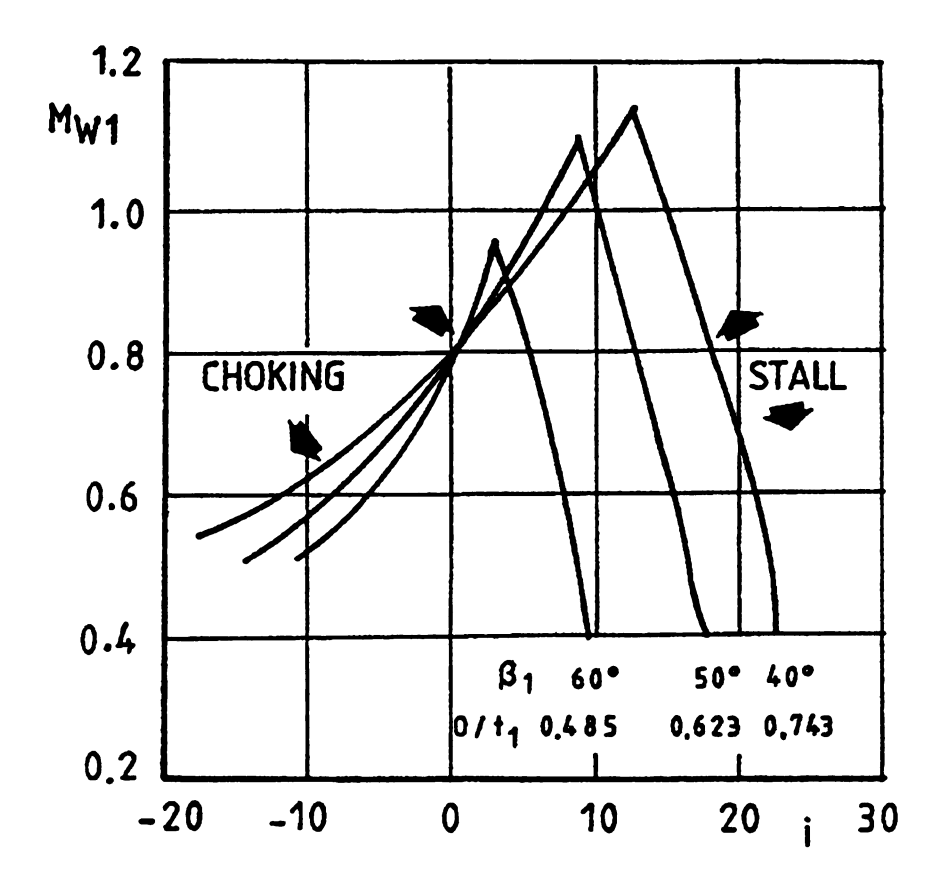


Figure 4.3 Inducer stalling and choking incidence as a function of leading edge angle and inlet Mach number

Another parameter used was the blade number. Obviously, too many blades can lead to too much blockage, while few blades can lead to high loading.

All the variables that were chosen in this work and their corresponding upper and lower limits which define the design space are tabulated in Table 4.1 on the next page. Most of these variables have fixed limits. That is, they are hardwired to a specific value.

Two of the variables have limits that are defined in terms of other limits. For example, xshr-m2 will have limits that are determined by the two other variables near it. That is, xshr_te is the upper limit and xshr_m1 is the lower limit for the variable xshr_m2. This is termed a floating variable because it has variable limits or a variable design space. The other floating variable is Dshr_m1, however it was negated by a constraint that was implemented. This will be shown shortly.

 Table 4.1 Geometric Variables

Geometric Variables	Lower Limit	Upper Limit
	(Meters)	(Meters)
Meridional Contour		
Xhub-le	0.130	0.140
Xhub-m1	0.150	0.170
Dhub-m1	0.040	0.060
Dhub-m2	0.090	0.160
Xshr-m1	0.150	0.170
Xshr-m2	0	1
Xhshr-te	0.175	0.190
Dshr-le	0.130	0.150
Dshr-m1	0	1
Dshr-m2	0.160	0.180
Blade angles	(Degrees)	(Degrees)
Beta-le-hub	20	30
Beta-m1-hub	20	30
Beta-m2-hub	20	30
Beta-le-shr	55	65
Beta-m1-shr	50	59
Beta-m2-shr	30	50
Beta-le-hub-sp	20	30
Beta-m1-hub-sp	20	30
Beta-m2-hub-sp	20	30
Beta-le-shr-sp	55	65
Beta-m1-shr-sp	50	60
Beta-m2-shr-sp	20	50
Splitter position		
ULEtip	0.2	0.3
Number of Full Blades	7	11

In addition to the above variables, one can preserve the shape of certain areas if it looks good to the designer. This can be done by using Bezier curves that are chained.

That is, one can preserve the shape of one area of the contour (inlet) while letting others vary. The following geometric constraints have been implemented:

- 1. Xshr le = Xhub le
- 2. Dshr_te = Dhub_te
- 3. Dshr m1 = Dshr le
- 4. Beta_te hub_sp = Beta_te_hub
- 5. Beta te shr sp = Beta te shr
- 6. Dshr in2 = Dshr le . Axial Shroud at inlet
- 7. Dshr_in3 = Dshr_le. Axial Shroud at inlet

8.
$$\frac{xhub_out - xshr_out}{xhub_te - xshr_te} = \frac{b3}{b2} = 0.7884$$
. Preserves diffuser area ratio

One can see that even though Dshr_m1 has variable limits, it will always float to Dshr_le because of constraint number 3. Thus one can say that there are really only 23 variables instead of 24. This was done to preserve the shape of the inlet.

Another particular aspect of this optimization is that the splitter blade is constrained to be at constant axial position(x). That is xhub_le_sp = xshr_le_sp. The reason for this is because the impeller has shroud clearance which results in a lack of support of the splitter blade. The fact that the splitter is at constant axial position(x) eliminates the bending problems that are associated with non-axially aligned splitters (xhub_le_sp > xshr_le_sp). In Figure 4.4 it is demonstrated that the splitter is at constant axial position(x). That is,

the splitter leading edge line indicated in Figure 4.4 is completely vertical. All geometries in the database and the ones produced during the optimization process have this characteristic. Perhaps the use of the word constant can be misleading. The splitter blade in this optimization can still move left or right, and it does so in such a way that the axial position of the leading edge at hub and shroud are the same.

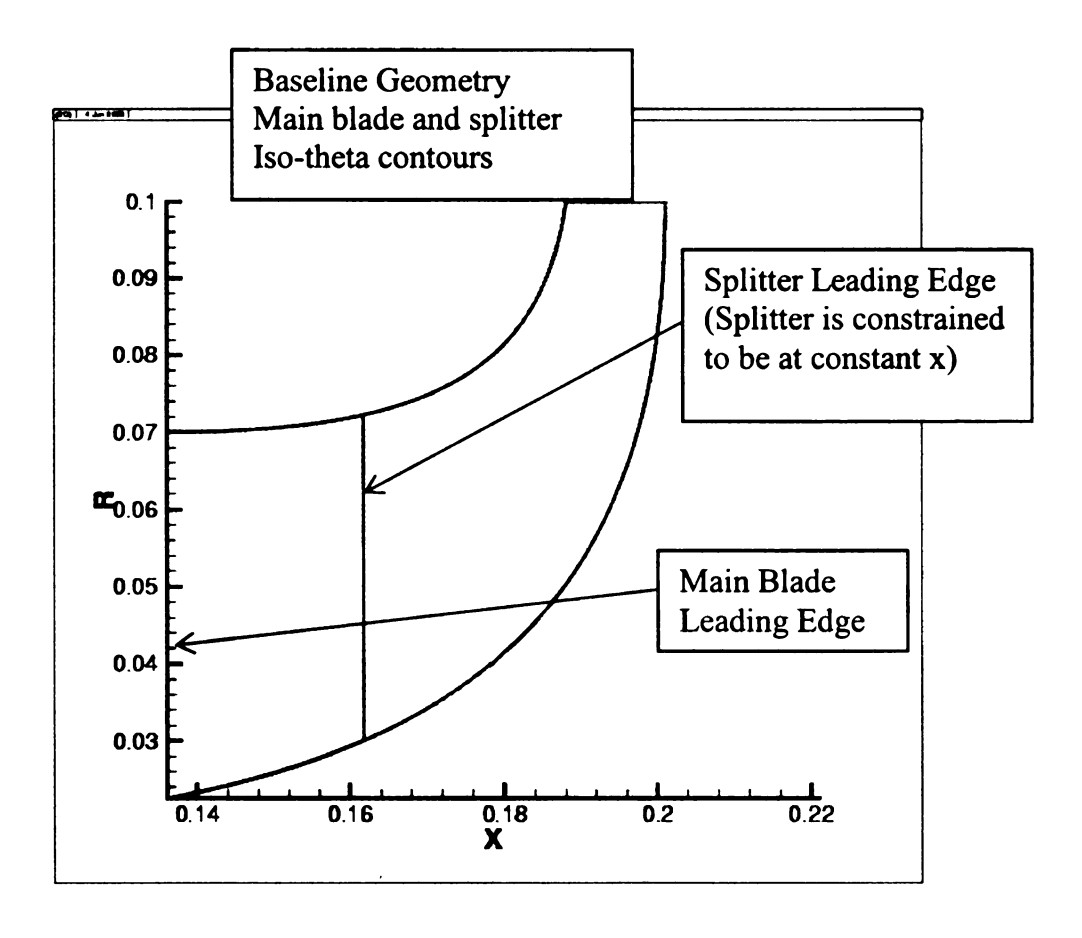
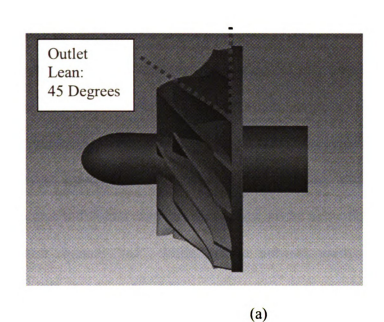
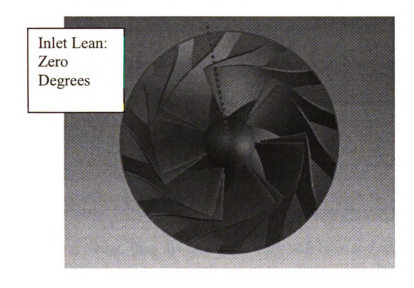


Figure 4.4 Main Blade and splitter blade contours

One final thing that needs to be mentioned before moving to the next section is that inlet and outlet lean plays a role in the design process. A large inlet lean results in very high bending stresses. Thus the inlet lean was constrained to be between \pm 8 degrees. With the negative meaning that the blade is leaned in the opposite direction of rotation. The outlet

lean is linked to the inlet lean and it is attempted to keep it below 45 degrees. Anything that is larger than 45 degrees will amount to high friction. The definition of lean can be seen in Figure 4.5





(b) Figure 4.5 Definition of (a) outlet lean (b) inlet lean

Finally, some of the constants in the optimization are the Impeller tip radius, and the blade thickness distribution, both of which were defined in section 3.1

4.3 ANNs Utilized

During the optimization process, certain characteristics of the performance of the impeller are predicted by multiple artificial neural networks for each operating point. For a single point prediction, seven neural networks were used to predict the performance of a given geometry using the above mentioned geometric variables and boundary conditions as inputs. Given the 24 geometric variables, plus BC's as inputs, the neural networks give individual outputs. That is, one of the networks is devoted to the mass flow in a splitter channel "m1", while another network predicts the mass flow in splitter channel "m2" of the machine. Figure 4.6 depicts the mass flows in the separate channels in a clear way. Figure 4.7 indicates that 4 of the networks are dedicated to predicting a total of 160 Mach numbers. This results in networks 4 to 7 predicting 40 Mach numbers per blade profile. This breaks down further to 20 Mach numbers on suction side and pressure sides. Also since there are four blade profiles, that is, hub/shroud main blade and hub/shroud splitter blade, this leads to the grand total of 160 Mach numbers. Also, one of the networks predicts the total to static efficiency.

The reason for using such an implementation is that if just one ANN is used to predict everything, than the neural network will have too much information, and may try to predict all of the quantities with the same accuracy. That is mass flow, efficiency, and the mach numbers at each point are all equally important. This means, that there will be many unknowns that have to be found within the hidden layers. Thus, a way to

circumvent this is to have more networks. In this work 7 neural networks are used per operating point, which means that 21 neural networks were used for the multiple point optimization discussed in the next chapter. Finally a simple, yet not technical way of saying the same thing, is that "Two heads are better than one", or in our case "7 to 21 heads are better than one". One should consult reference [2] for a more in depth discussion.

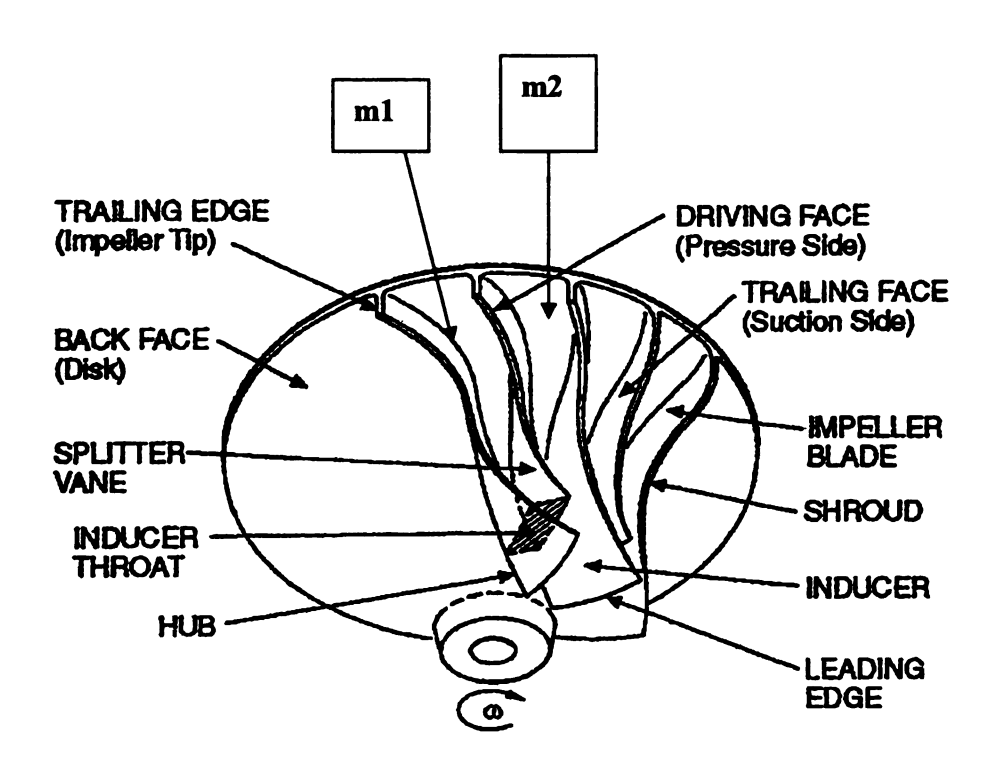


Figure 4.6 Illustration of Splitter channels

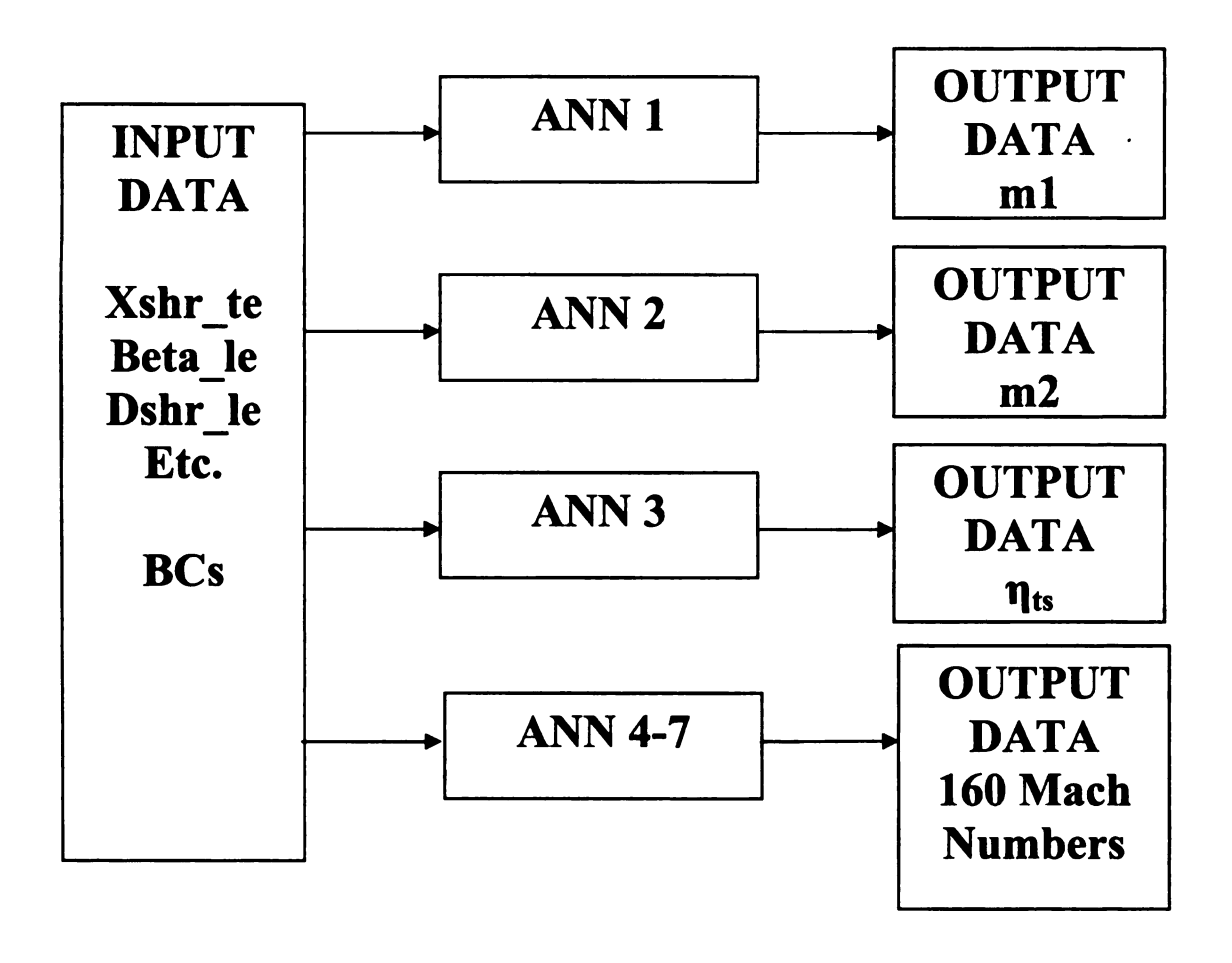


Figure 4.7 Neural Network Structure

4.4 Objective Function and GA Settings

4.4.1 Objective Function

Once the ANN has predicted the performance of an individual, this performance is then converted to an objective function with which the genetic algorithm will minimize. The Genetic algorithm mimics biological evolution and thus is a statistical or non-deterministic process. The purpose is that blades will reproduce other better geometries and the poor geometries will tend to die out. This is why the term survival of the fittest is usually used. A somewhat in depth treatment of the operational principle of the GA was

given in section 2.3, consequently, we will progress to the specifics that apply to our design case.

The objective function used by the genetic algorithm is displayed below:

$$OF = W_{massflow} P_{mass_diff} P_{mass_diff} P_{mass_diff} + W_{\eta_{ts}} P_{\eta_{ts}} + W_{lu} P_{lu} + W_{nl} P_{nl}$$

$$[4.1]$$

This function is a weighted sum of various penalties used to quantify the performance. A higher value of the objective function implies a lower performance impeller, while a lower value represents good impeller performance. In the above equation, the first term represents the penalty for the mass flow in the machine. It is desired to keep the mass flow within a certain tolerance of the required mass flow. The penalty for the mass flow of the machine can be seen in equation [4.2]

$$P_{massflow} = \frac{\max\left\{\dot{m}_{req} - \dot{m} \middle| - \dot{m}_{threshold}, 0\right\}}{\dot{m}_{ref}}$$
[4.2]

In this equation there is a percentage tolerance on the reference flow, for which there is no penalty, which is taken as 1 % of the reference mass flow. The reference mass flow is 1.3 Kg/sec for both single and multiple point optimizations.

The second term on the right hand side accounts for the difference in mass flow in between the separate channels which are created by the splitter blade. Recall Figure 4.6 for visualization of the channels and for illustration of the corresponding mass flows denoted by m_1 and m_2 . A designer does not want 90% of the mass flow in one channel and then the 10% in the other. As we require constant pitch at the exit for both full and splitter blades. Having widely different mass flow in the separate channels would lead to non-periodic outflow. Thus the following mass difference penalty was implemented to account for it.

$$P_{mass_diff} = \left[\frac{m_1 - m_2}{m_1 + m_2} \right]^2$$
 [4.3]

The next term is the obvious one. That is, the designer wants the efficiency to be high. With the current optimization system, one can choose either to optimize total-static or total-total efficiency. The total to static efficiency was chosen because the flow is not directed into another stage, but is pumped to another component. If one sticks to the application of air-conditioners, the fluid is pumped to the condenser as discussed before, and does not enter another compressor before going there. The total to static efficiency penalty is as follows:

$$P_{\eta_{ts}} = \left| \eta_{ts} - \eta_{ts \, req} \right|$$

The fourth term in equation [4.1], is the loading unbalance penalty. That is, a designer does not want most of the load on the splitter or main blade. If this occurs this can be a source of separation for the highly loaded blade if too much acceleration precedes the deceleration. It can also cause really high forces acting on individual blades. The loading unbalance penalty can be expressed with just a few equations.

$$Area_{fb} = M_{ss_fb} - M_{ps_fb}$$
4.5]

$$Area_sb = M_{ss_sb} - M_{ps_sb}$$
[4.6]

$$P_{lu} = \sum_{LE}^{TE} \frac{\left| Area_fb - Area_sb \right|}{\left(\frac{Area_fb + Area_sb}{2} \right)}$$
[4.7]

The final penalty that was implemented was the negative loading penalty. A designer certainly does not want his/her impeller behaving like a turbine. Thus, the following penalty was employed.

$$P_{nl} = \max[(Mps - Mss).dm,0]$$
[4.8]

Perhaps the loading unbalance and negative loading penalties can be better illustrated through the use of a Mach number distribution displayed on the next page.

Baseline Mach number Distribution

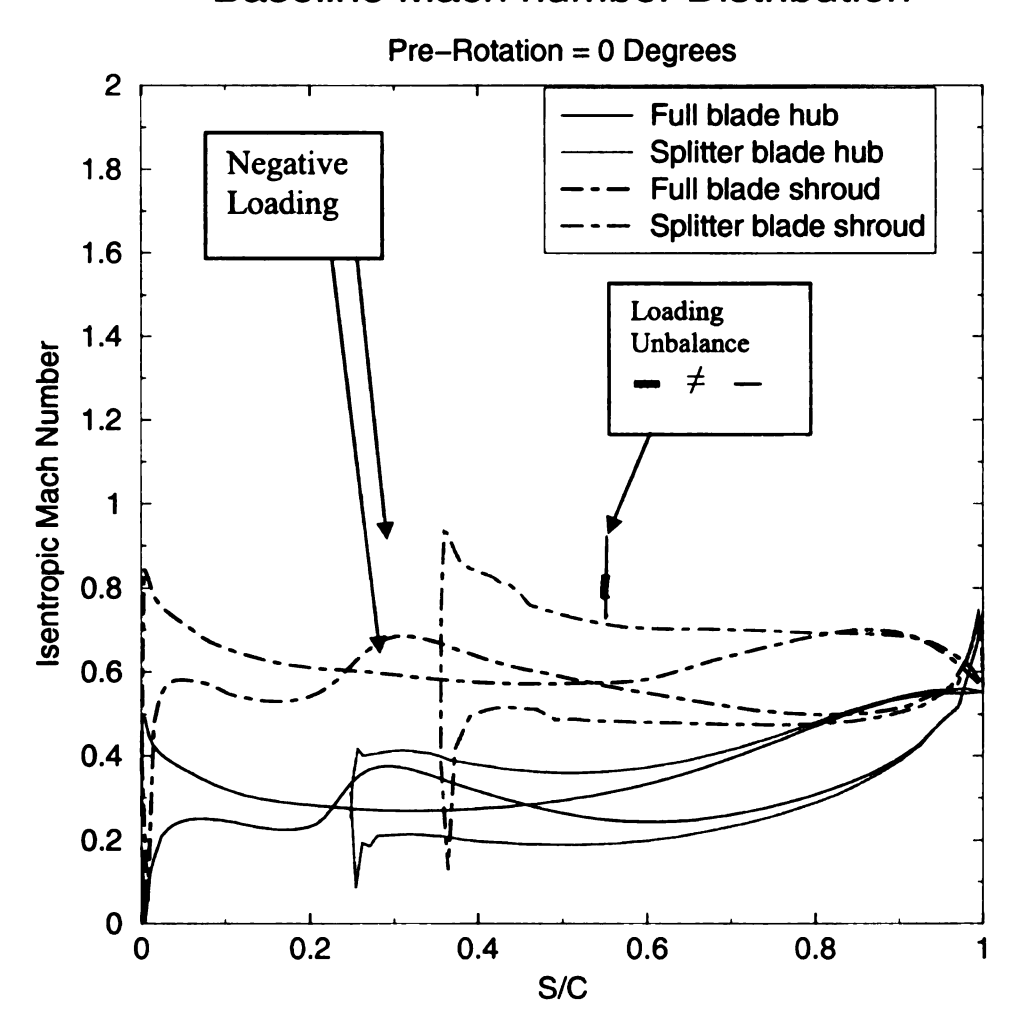


Figure 4.8 Mach number distribution demonstrating unwanted features

Associated with each of these penalties is a corresponding weight. The weights are applied to achieve a desired penalty. That is, if one wants a higher efficiency, the more weight he/she should put on this penalty. For the single point optimization, approximately the same order of magnitude was given to the mass and efficiency penalty, with the negative loading and unbalance penalties being just a little higher. This can be seen in the

figures containing the database penalties in the next section, which is devoted to the convergence history. Finally, the choosing of the weights is rather subjective and it is unknown to the author if there is an optimum choice of these weights. In any event, the weights used in this work are tabulated in Table 4.2 on the next page.

Table 4.2 Weights used in Single point Optimization

Penalty	Weight		
Mass Flow	700		
Mass Difference	100000		
Total to static Efficiency	400		
Loading unbalance at hub	100		
Loading unbalance at shroud	100		
Negative loading at hub	3300		
Negative loading at shroud	3300		

4.4.2 GA Settings

Before performing the optimization one must select the GA and ANN settings.

Through the advice of the system manager and literature[2], the following parameters were used

Table 4.3 GA and ANN Parameters

Parameter	Settings
GA	2/4/19
irestrt	1
npopsiz	50
pmutate	1%
maxgen	100
pcross	75%
ielite	1
itourny	1
pcreep	5%
iunifrm	0
nchild	2
ANN	
TRAINING	80%
NANN	7

Where the parameters in the table are defined as follows (see reference [4]):

GA:

- irestrt = 0 for a new GA run; 1 for a restart continuation of a GA run
- npopsiz = The population size of a GA run
- pmutate = Jump mutation probability
- maxgen = The maximum number of generations to be run by the GA
- pcross = Cross over probability
- ielite = 1; Implies that the best individual is replicated into the next generation
- itourny = 1; Implies tournament selection
- pcreep = Creep mutation probability
- iunifrm = 0; Implies single point crossover
- nchild = 2 children are produced per pair of parents

ANN:

• TRAINING = 80 % of all the samples are used for training of the ANN

• NANN = Number of neural networks per operating point.

The working principle of the GA was already explained. However the following figure should give a basic knowledge of the principle and to make connections to the values listed in Table 4.3 above.

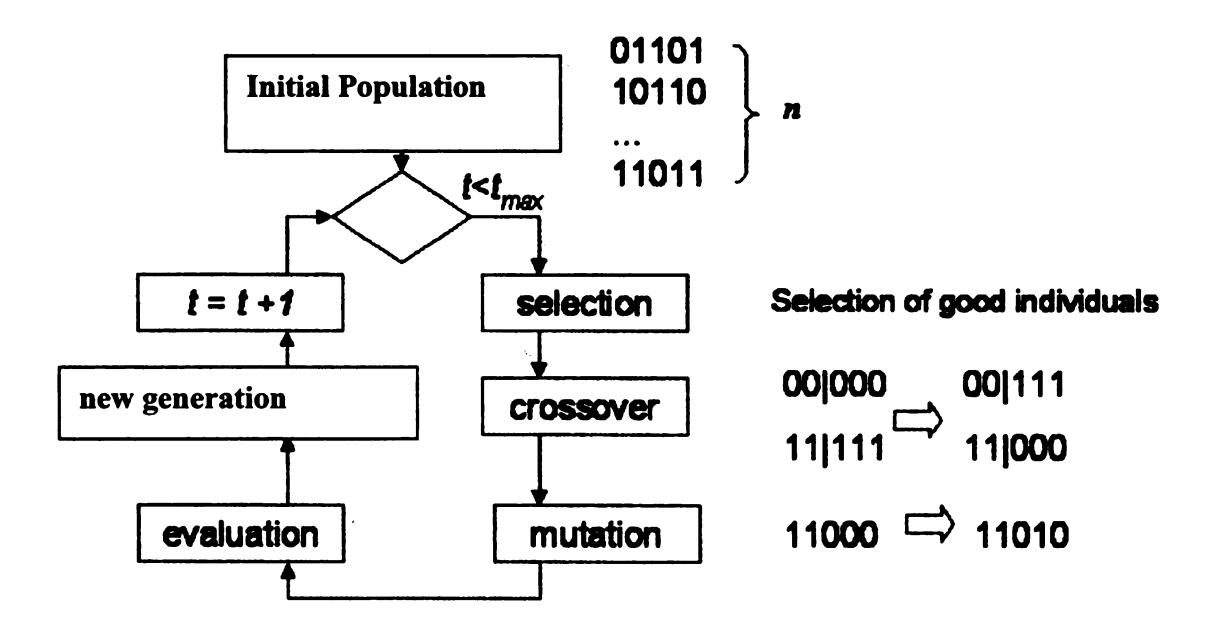


Figure 4.9 General Working Principle of the Genetic Algorithm. [2]

4.5 Presentation of the Optimization

In this section one will discuss the database creation, the convergence history, and finally compare a few of geometries which were obtained during the optimization. However, one must first mention the operating point that was chosen.

The operating point was chosen near the high efficiency plateau shown in Figure 4.10. A designer should optimize at a point with sufficient surge margin.

Total to Static Efficiency vs. Mass flow rate

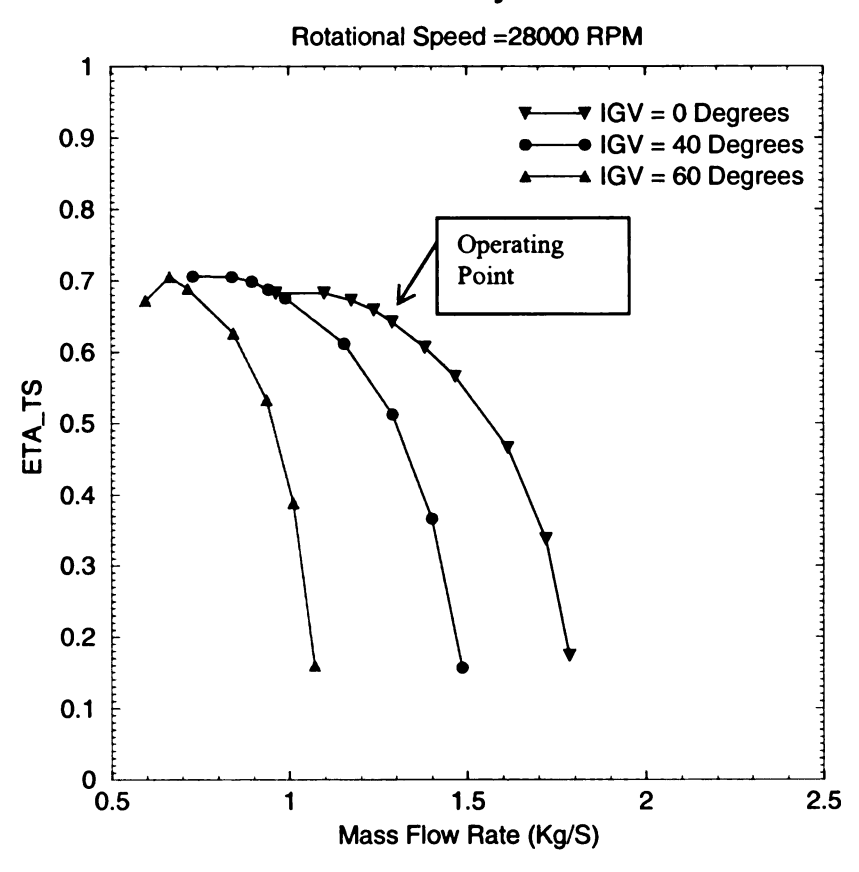


Figure 4.10 The operating point chosen. $P2/P01_{imposed} = 1.4$

Pressure Ratio vs. Mass Flow Rate

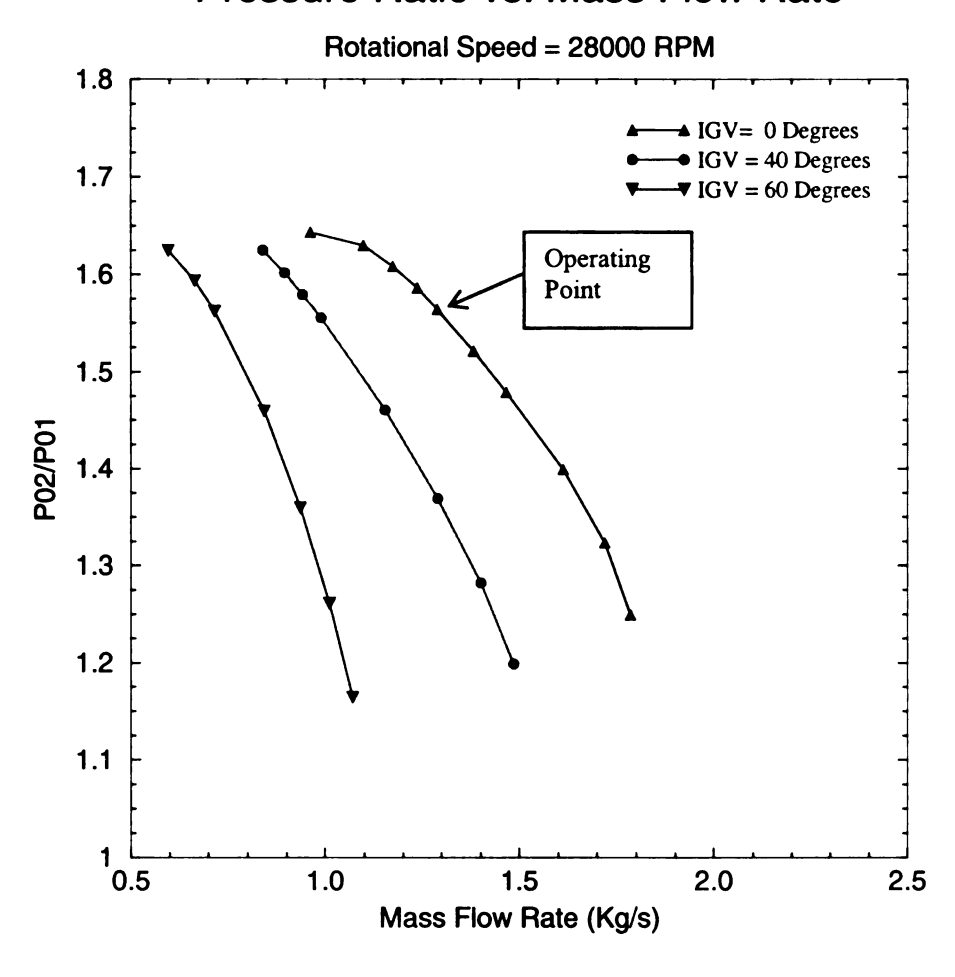


Figure 4.10 (cont'd)

The mass flow required for the operating point was chosen to be 1.3 Kg/sec. The efficiency requirement on total-static efficiency was set at 90%. The reason being is that one does not expect to improve the efficiency by more than 25 points. That is, going from 63% to 90% seems a little unreachable, and it has been observed by the system manager that is it better to put a value that is within expectation, rather than to just put 100%. However, 90% seems a little high also.

4.5.1 Database

As explained before in chapter 2, the knowledge of the ANN and GA comes from a reference database. The database contains 34 Navier-Stokes calculations, coming from different geometries representing the design space within the previously defined limits. The selection of the geometries can be realized in two different ways, either randomly, or using the design of experiment method, DOE technique. It can be used in a wide variety of applications when some parametric analyses are needed. Its aim is to construct a more representative and systematic database, performing a statistical survey of the design parameters. This approach was used for 32 of the samples. Indeed, it presents the disadvantage of considering only two extreme values (25% and 75% over the lower limit) of the parameter's range so that in the end not much is known about the center of the design space. This is why a central point case is run in which the variables are forced to be at 50% over their lower limit. Cases 1-32 were given by the DOE, while the other samples that were included were the baseline geometry and the central point run as can be seen in Table 4.4 below.

Table 4.4 Database Navier-Stokes Results

DB Sample #	Mass flow	ETA_TT	ETA_TS	P02/P01	P2/P01	Inlet Lean (Deg)	Outlet Lean (Deg)
1	1.456	0.865	0.680	1.599	1.453	-21.766	507 St 45:000
2	1.102	0.717	0.575	1.564	1.437	-13.496	45.000
3	1.311	0.832	0.660	1.574	1.440	-9.928	45.000
4	1.370	0.820	0.675	1.603	1.481	-12.970	45.000
5	1.437	0.826	0.678	1.612	1.486	-6.092	45.000
6	1.350	0.821	0.643	1.585	1.442	-6.751	45.000
7	1.177	0.761	0.617	1.575	1.452	-15.328	45.000
8	1.382	0.852	0.674	1.587	1.448	-5.001	45.000
9	1.187	0.799	0.636	1.563	1.433	-10.028	45.000
10	1.117	0.727	0.585	1.559	1.435	-2.540	45.000
11	1.402	0.851	0.672	1.582	1.443	0.000	42.882
12	1.228	0.729	0.582	1.571	1.441	-2.355	45.000
13	1.037	0.680	0.541	1.542	1.417	-8.831	45.000
14	1.213	0.795	0.631	1.556	1.426	-9.086	45.000
15	1.298	0.791	0.645	1.589	1.465	-20.146	45.000
16	1.413	0.839	0.656	1.600	1.452	-10.480	45.000
17	1.305	0.841	0.670	1.575	1.443	-14.990	45.000
18	1.017	0.697	0.556	1.554	1.428	-17.209	45.000
19	1.313	0.832	0.662	1.568	1.436	-13.680	45.000
20	1430	0.840	C.0.693	1,606	1.486	25.641	45'000
21	1.516	0.836	0.680	1.637	1.501	0.000	14.790
22	1.322	0.818	0.644	1.575	1.437	0.000	43.814
23	1.221	0.777	0.632	1.581	1.458	-6.349	45.000
24	362	0.848		1.580	1.444	-8-86)	25000
25	1.245	0.802	0.634	1.566	1.432	0.000	34.625
26	0.976	0.682	0.542	1.544	1.418	-0.260	45.000
27	1.442	0.842	0.658	1.583	1.439	0.000	27.734
28	1.079	0.698	0.557	1.547	1.423	-8.991	45.000
29	1.295	0.768	0.617	1.595	1.462	0.000	0.649
30	1.323	0.810	0.635	1.565	1.428	0.000	30.363
31	1.252	0.776	0.631	1.574	1.452	-4.616	45.000
32	1.248	0.810	0.642	1.573	1.438	-6.748	45.000
Central	1.371	0.821	0.664	1.596	1.466	-6.854	45.000
Baseline	1.257	0.824	0.635	1.562	1.417	-4.336	45.000

If one surveys the table, one would probably argue that database sample 1 has the highest total-total efficiency and thus why pursue the optimization? Well, the reason is that this geometry exceeds the lean limit (± 8 degrees) and thus will have high bending stresses. Also if one looks at the Mach number distribution (Figure 4.11), it can be easily seen in the following figure that it is plagued by negative loading (full blade hub) and

also by loading unbalance at the shroud. Plus, one could also say that there is a little bit too much incidence on the splitter blade amongst other things.

The reader should keep in mind that the number of blades in Figure 4.11 is really just the number of full blades and one must double this to get the total number of blades. Also, that the value of P_2/P_{01} is an imposed pressure, or boundary condition.

DB Sample 1, 8 Blades P2/P01=1.400000; Pre-Rotation = 0 Degrees 2 Full blade hub Splitter blade hub 1.8 Full blade shroud Splitter blade shroud 1.6 1.4 Isentropic Mach Number 1.2 1 8.0 0.6 0.4 0.2 0 0 0.2 0.4 0.6 8.0 1 S/C

Figure 4.11 Mach Number Distribution Database sample 1

Continuing with our survey, one might say, well number 20 has the highest total-static efficiency. Also again, the lean is exceeded. One must also pay attention to the fact that the design requires that the mass flow be at or near 1.3 Kg/sec when making these

comparisons. The Mach number distribution for sample 20 (Figure 4.12) has negative loading at the splitter blade hub and shroud.

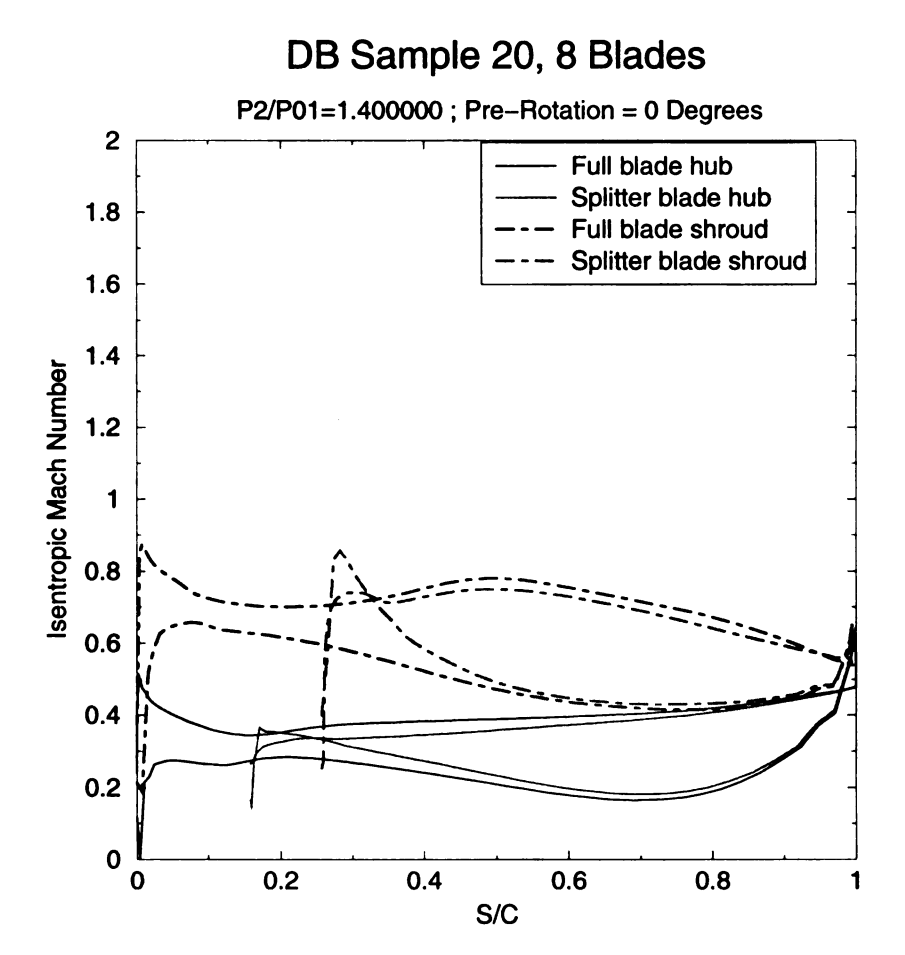


Figure 4.12 Mach number distribution of Database sample 20

Continuing with this process of analyzing the Table 4.4 and the Mach number distributions, the best database sample in the authors opinion is number 24(Figure 4.13). Well, in terms of negative loading, it is better. There is still too much incidence at the full blade shroud and still loading unbalance. The mass flow is around 1.3 Kg/Sec and the lean is just a touch over the limit (-8.861 Degrees). The total-static efficiency is 4 points

higher than the baseline, while the total-total efficiency is 3 points higher. However, it should be possible to obtain even more efficiency improvement than this.

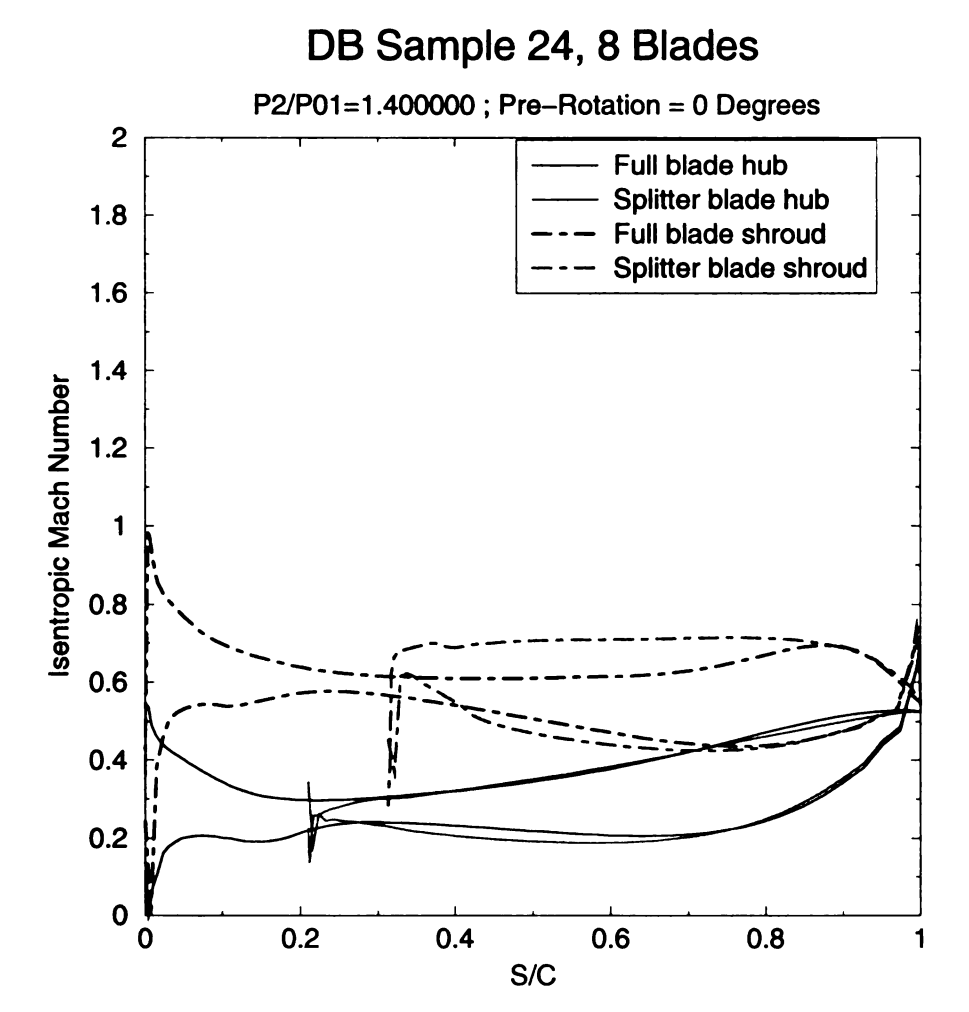


Figure 4.13 Mach number distribution of Database sample 24

Finally, none of the samples in the database has the optimum combination of parameters. This is why we will now progress to the results of the optimization in hopes that the system can find the optimum.

4.5.2 Convergence History

In theory, the NS and ANN penalties should overlap each other in order to say that the system has found the optimum geometry, or converged. One can see in Figure 4.14 that the NS and ANN penalties slowly start to come together. A possible reason why the lines do not come fully together could be that other penalties are offsetting each other. For instance, in Figure 4.15 the ANN and NS actually come completely together because it is only one penalty, instead of the sum of all the penalties.

Figure 4.14b shows that between iterations 50-58 the geometries are quite similar. One possible explanation for this could be that the solution is converged and thus there is not anything better in the design space. Another possible explanation is that since the GA always starts from the previous solution, it eventually gets saturated with the similar geometries, which leads to offspring that are very similar. The penalties still vary slightly due to the fact that mutations are taking place. At the around iteration 60 the penalty starts to increase, probably because the mutations are producing worse geometries. The penalty continues to increase up to Iteration 62, where finally a particular geometry is produced that gives a negative temperature. The author tried to rerun the program again without restarting the GA from scratch, however, the same result was obtained. That is, a negative temperature. The only way to begin the optimization process again was to restart the GA from scratch. That is, a new randomly created population of 50 members is introduced into the GA. This leads to an increased penalty at Iteration 63 because the geometries are randomly generated at the beginning of the GA process. Finally, the penalty starts to decrease again as the GA is reconfigured to start from the previous solution and the penalties appear to be converging again.

As can be see in Figure 4.14b, Iteration 12 had the lowest total penalty and will be one of the geometries that will be analyzed in the next section. "Why can it be that the penalty is already so low at Iteration 12?", one might ask. Well, the reason is that it can happen because of chance. That is, the system is statistical, or non-deterministic, which means that sometimes the system can be lucky.

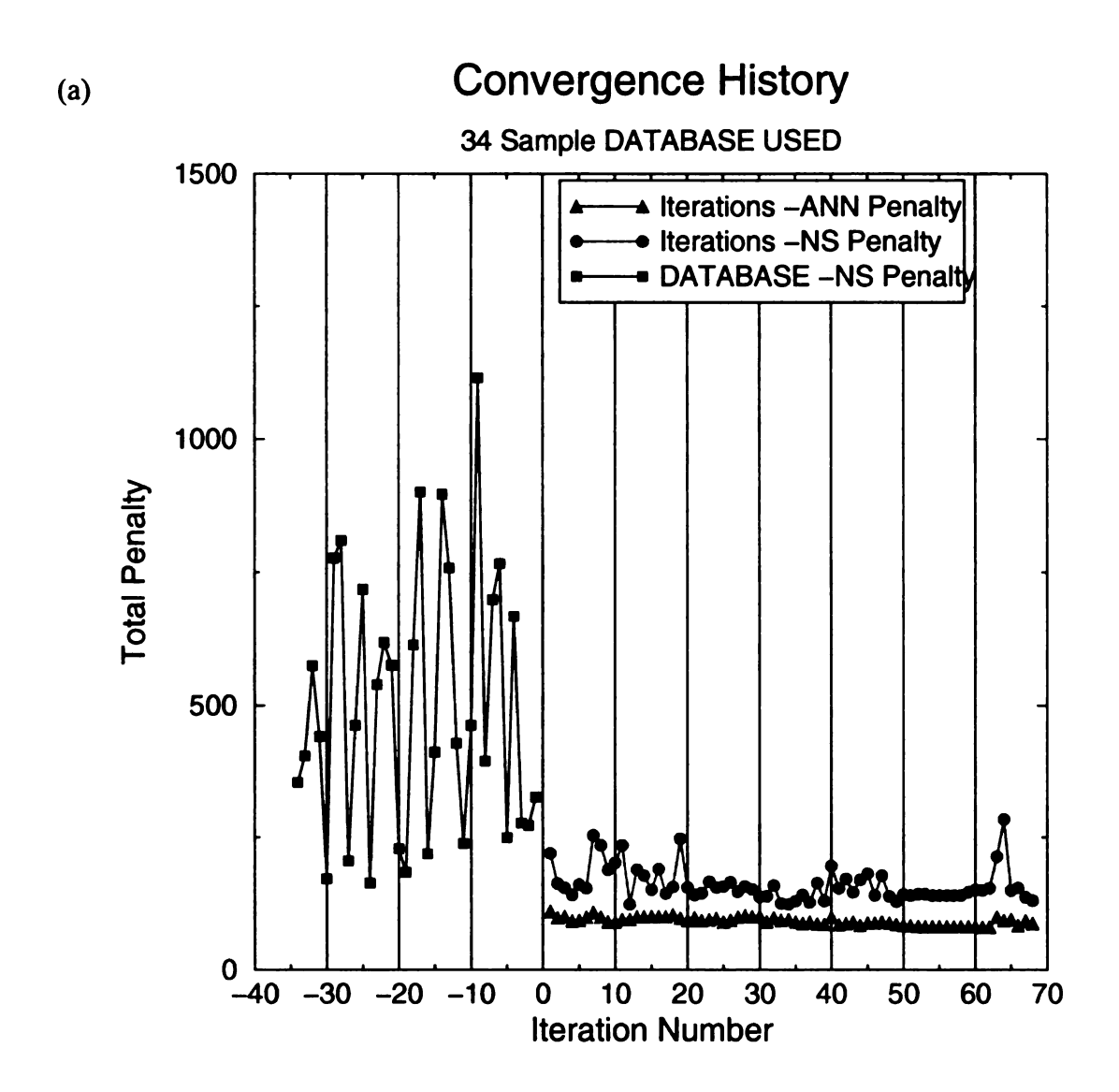


Figure 4.14 Total Penalty. (a) With database. (b) Without database

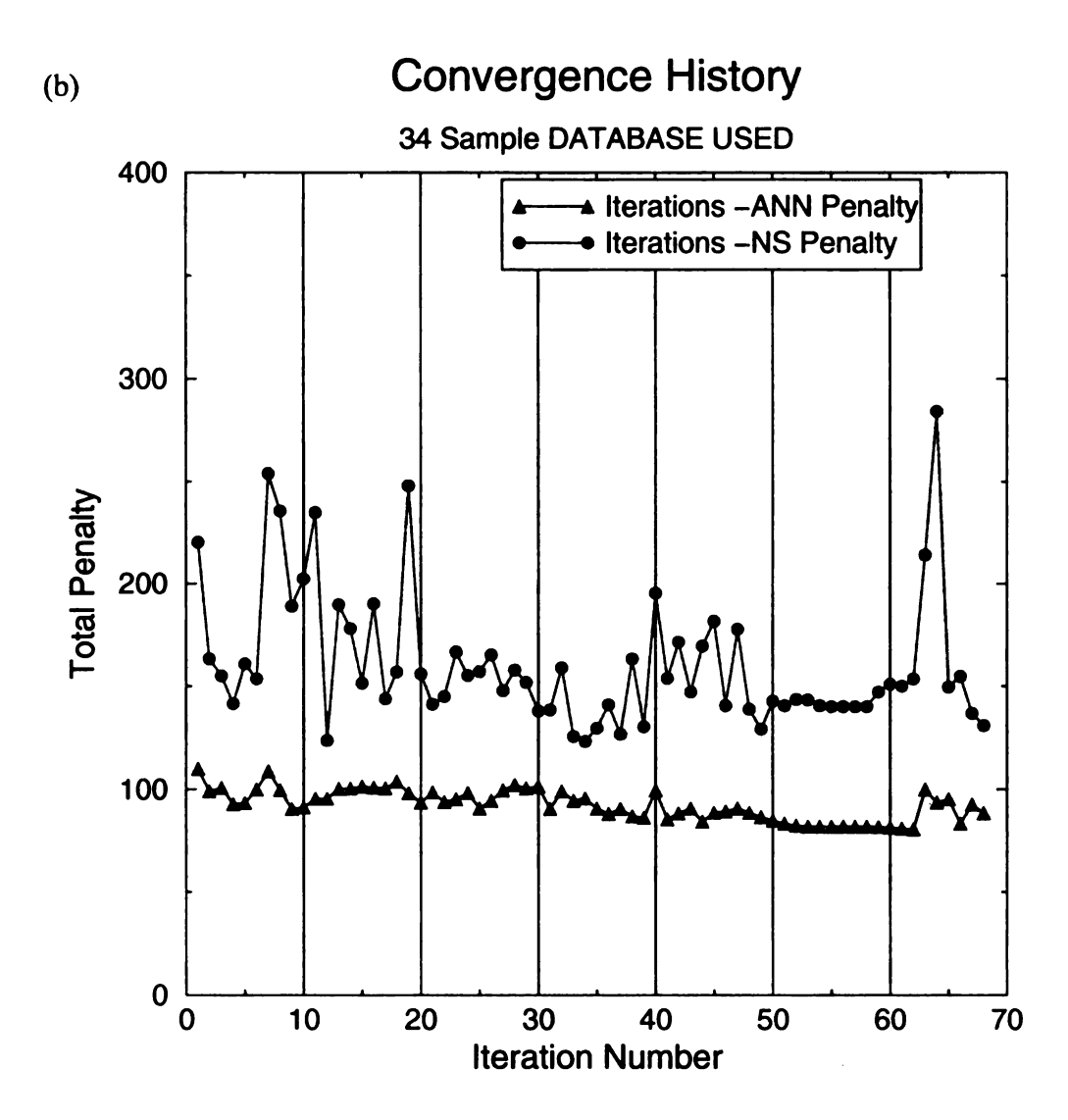


Figure 4.14 (cont'd)

In Figure 4.15 one can see that the ANN and NS come together at around Iteration 50. It appears that Iteration 13 has the best total-static efficiency and will also be analyzed in the next section.

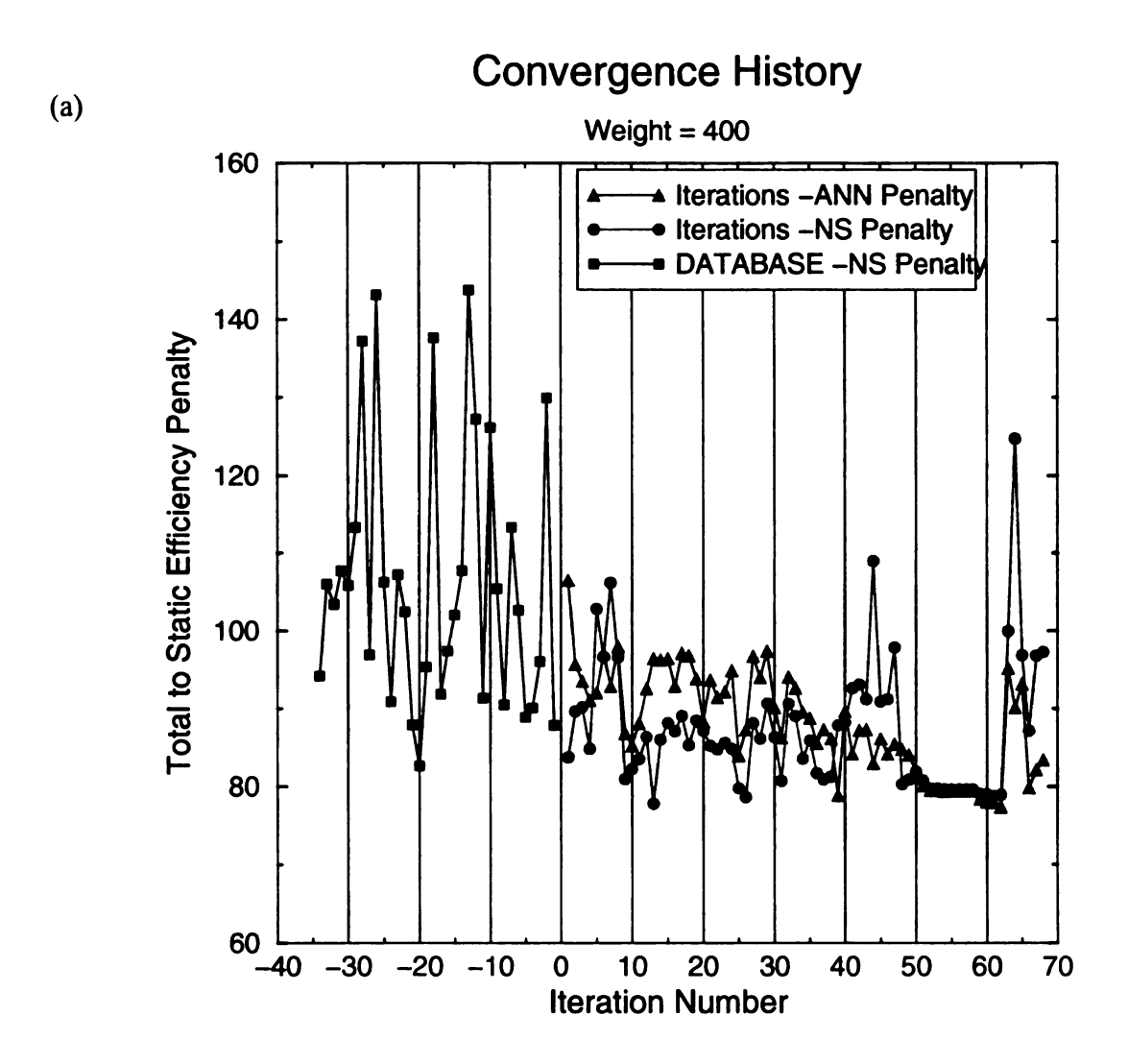


Figure 4.15 Total-Static Efficiency Penalty. (a) With database (b) Without database

Convergence History

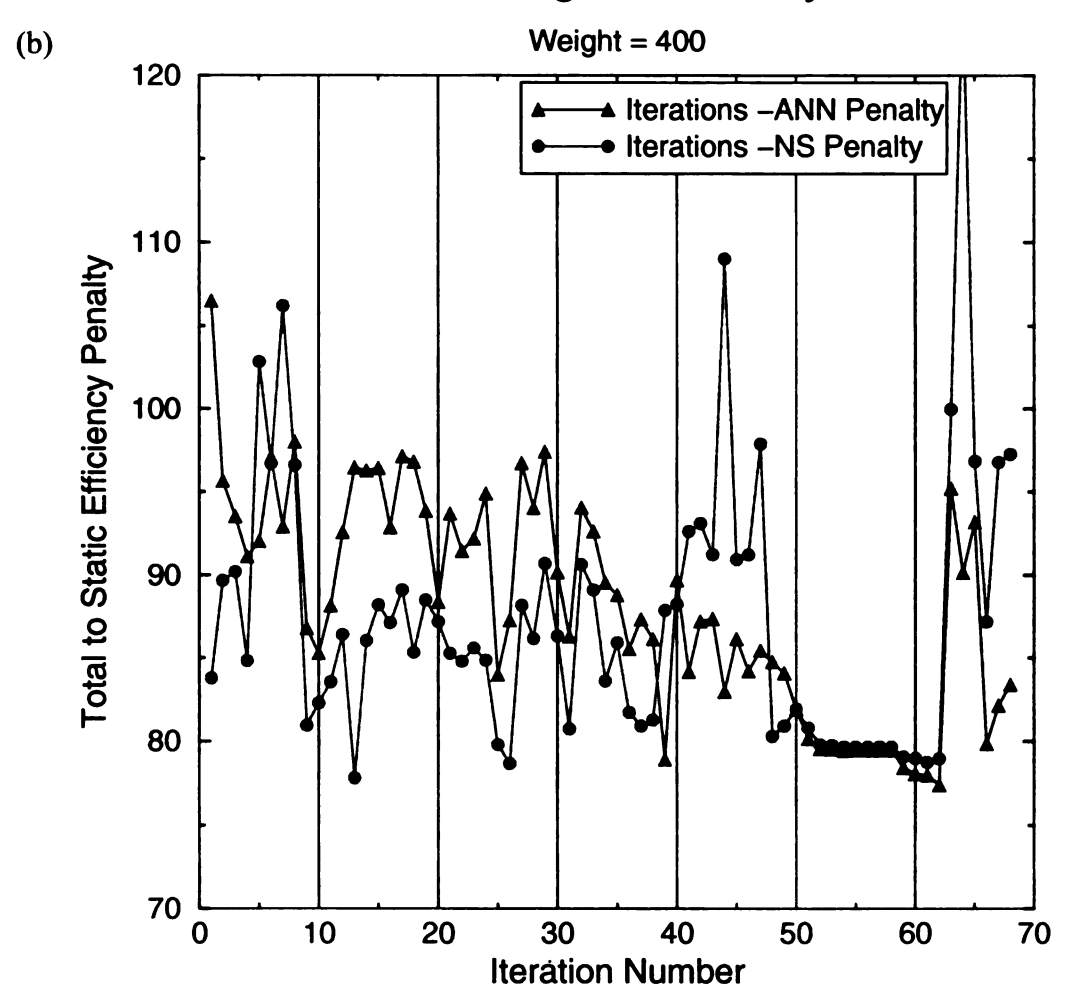


Figure 4.15 (cont'd)

Finally, for the sake of completeness, the rest of the convergence history will be listed because similar trends can be observed in each of them.

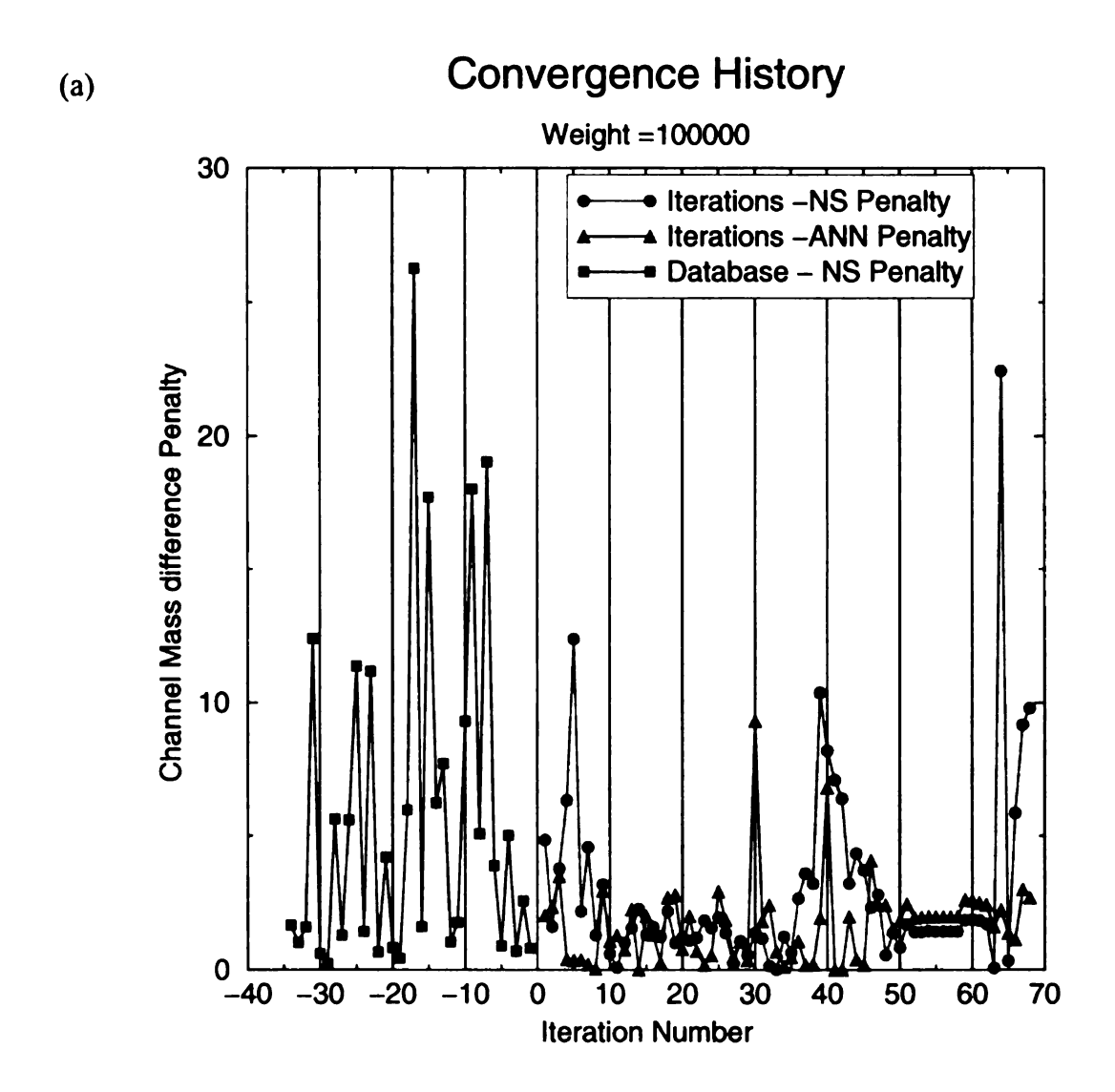


Figure 4.16 Channel mass difference Penalty. (a) With database (b) Without database

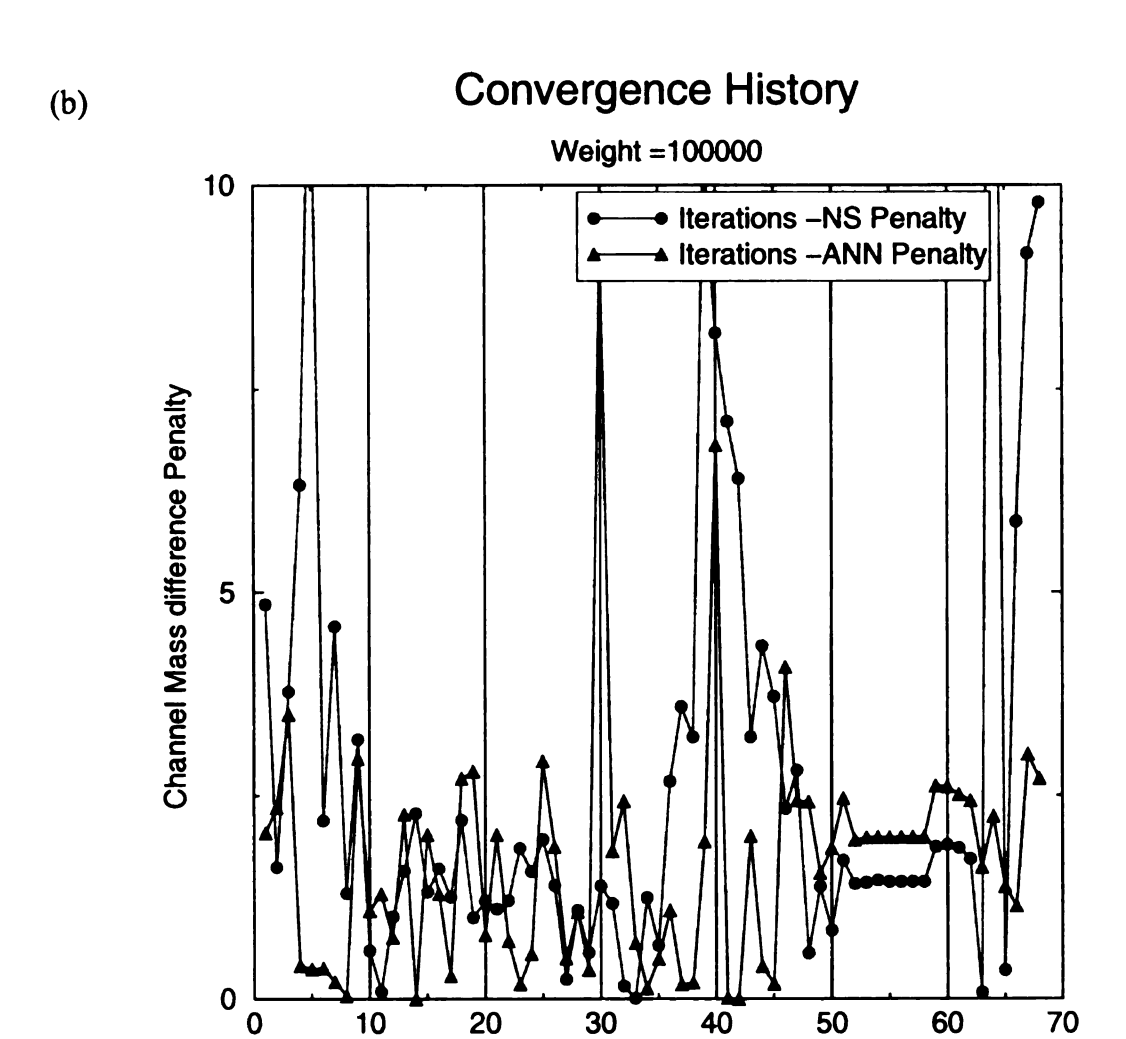


Figure 4.16 (cont'd)

Iteration Number

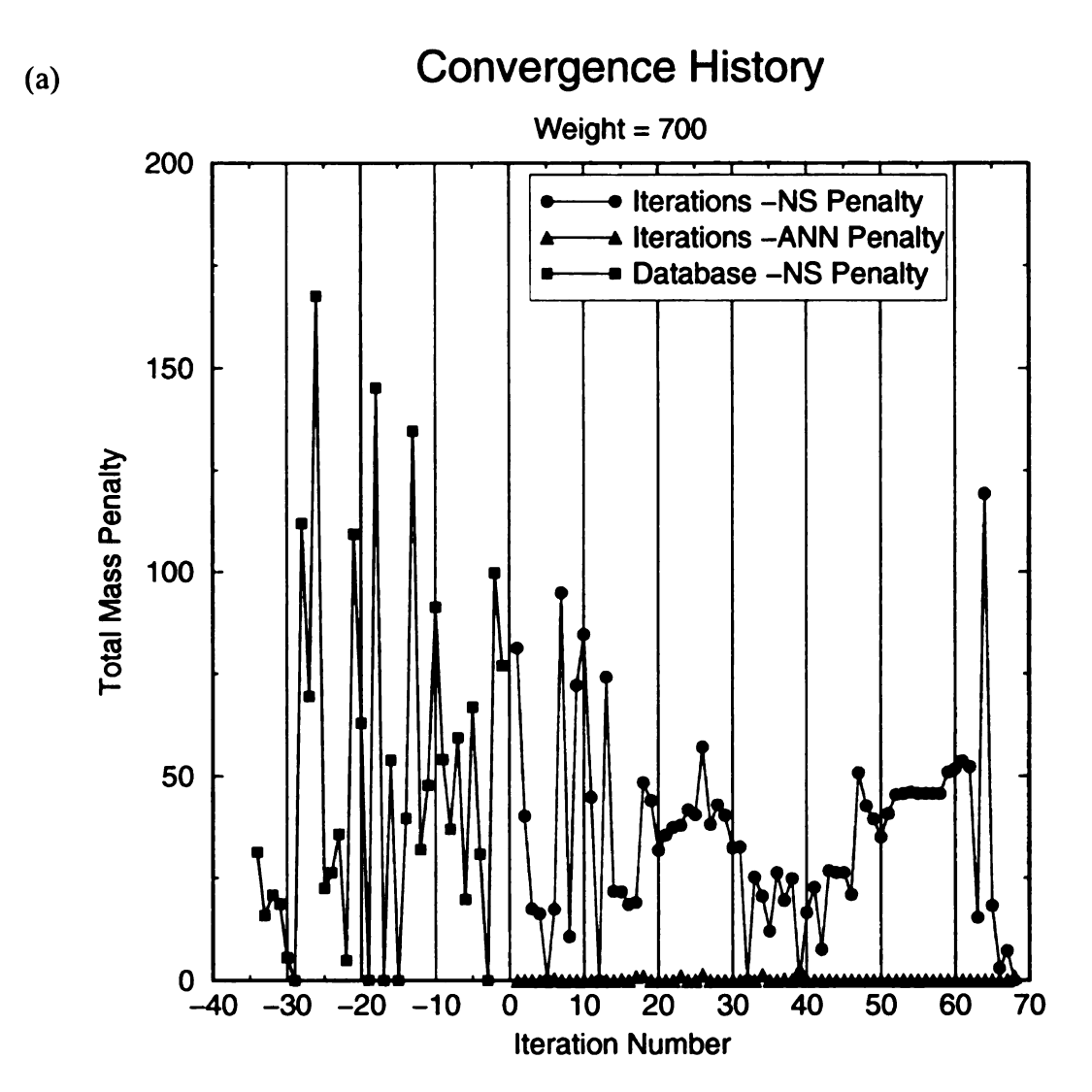


Figure 4.17 Mass Penalty. (a) With database (b) Without database

Convergence History

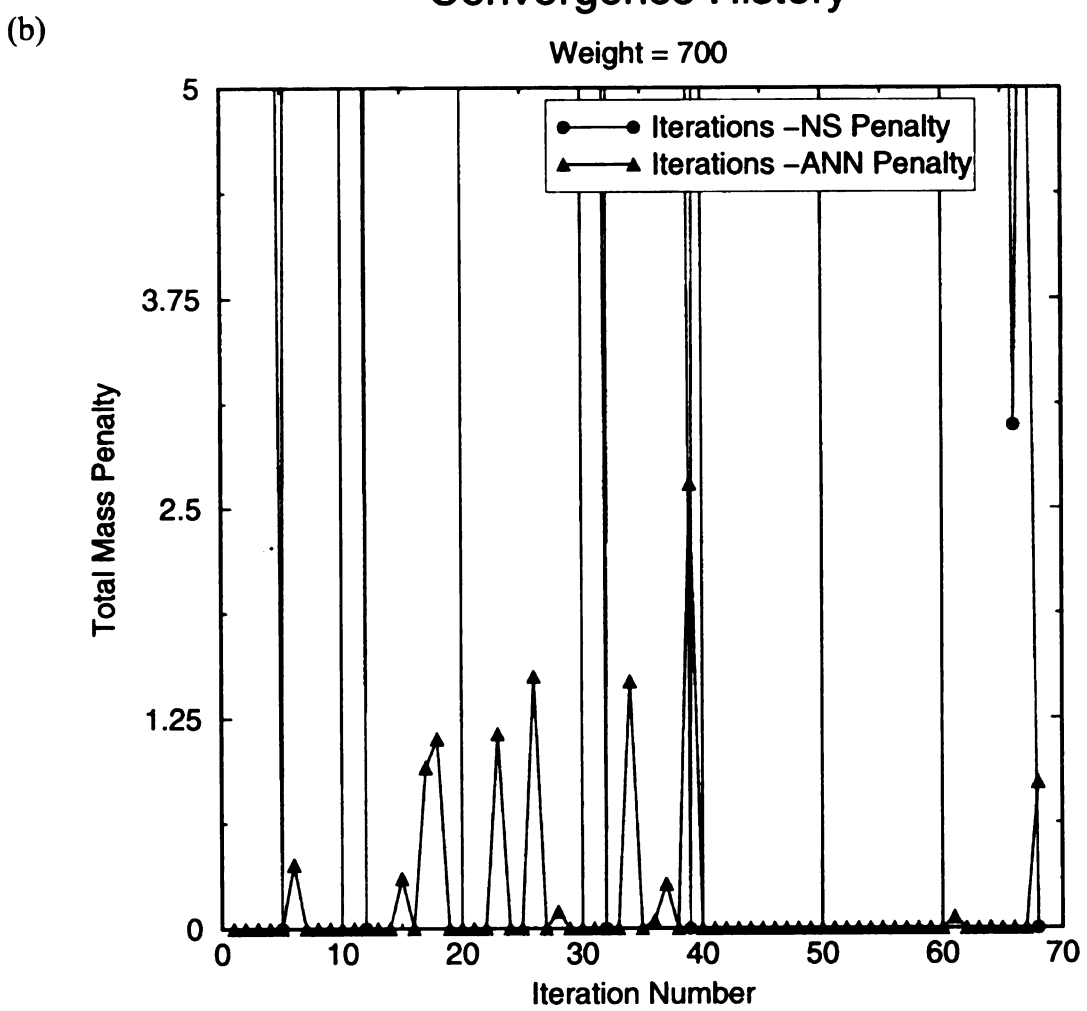


Figure 4.17 (cont'd)

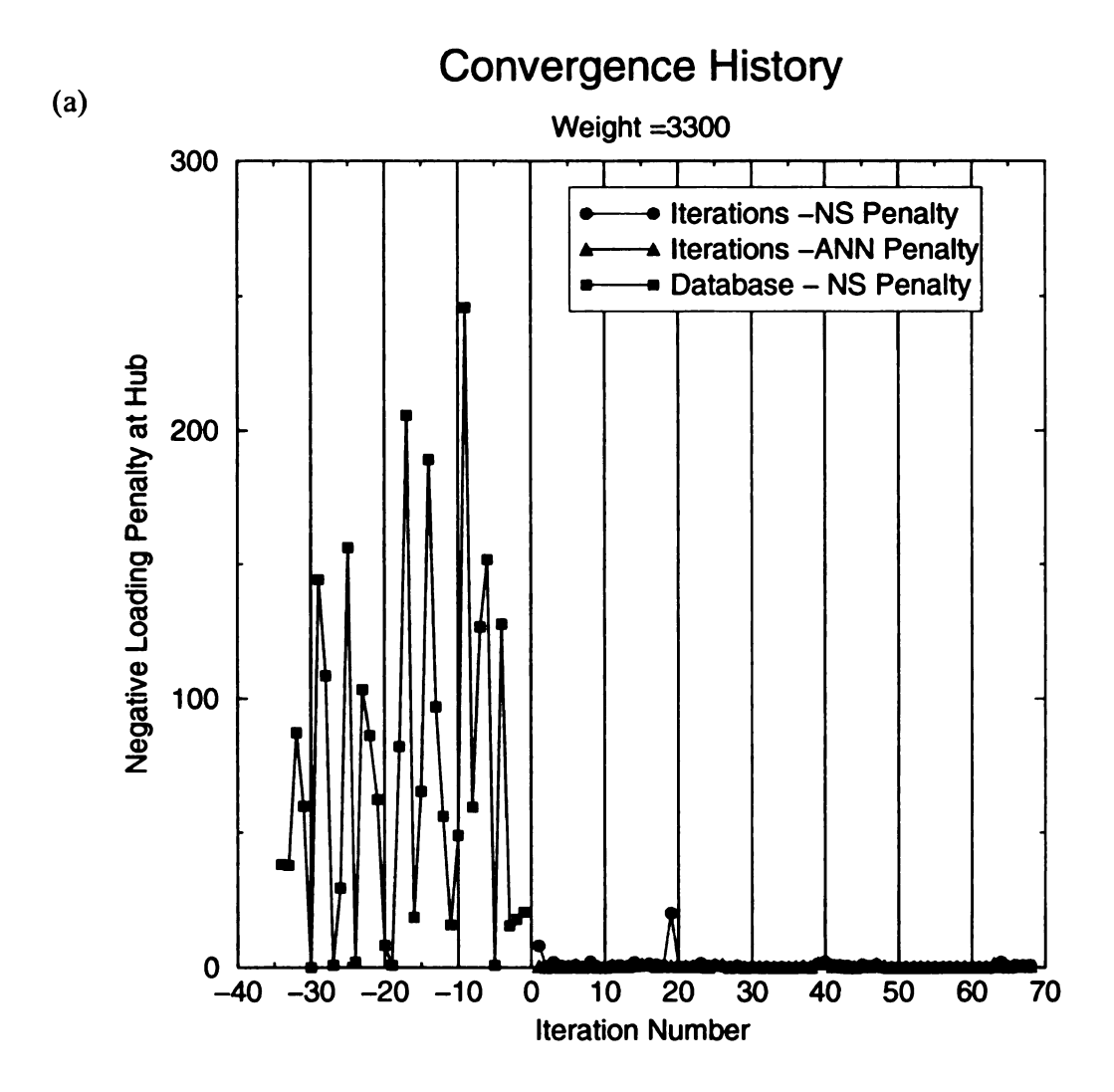


Figure 4.18 Negative Loading Penalty. (a) With database (b) Without database



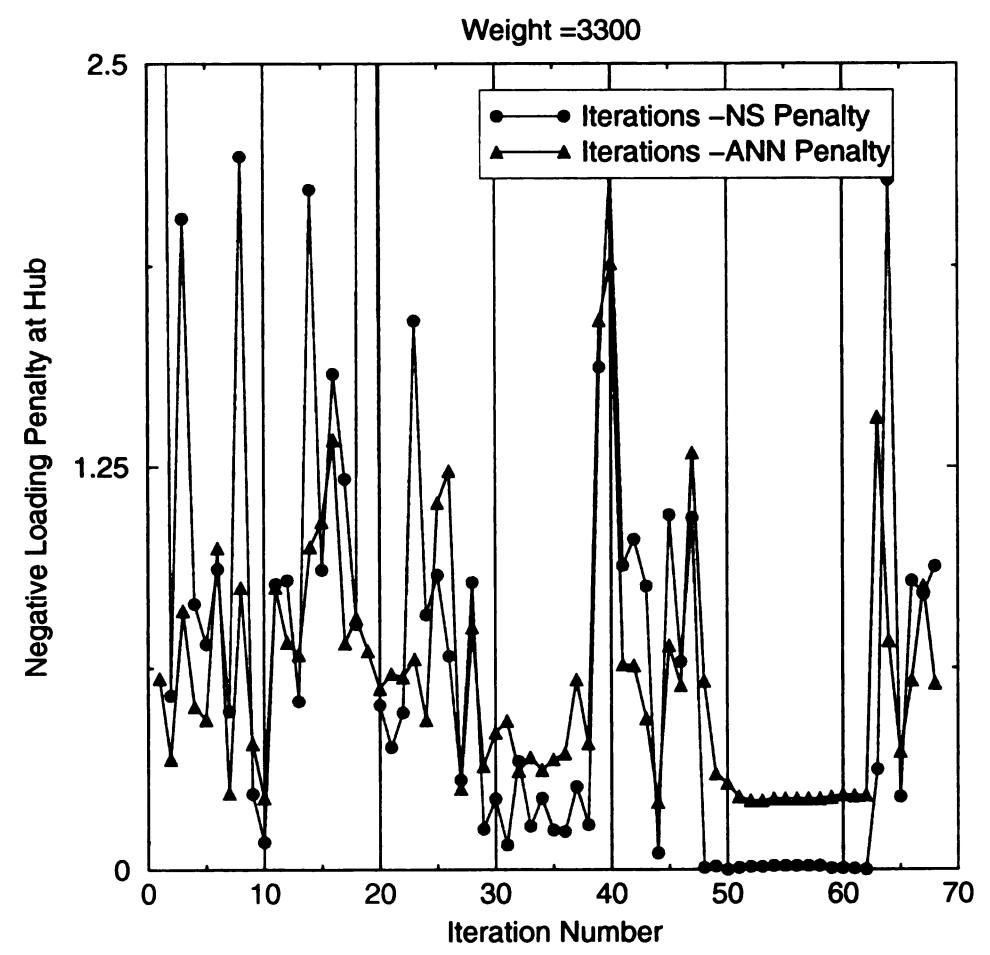


Figure 4.18 (cont'd)



(a)

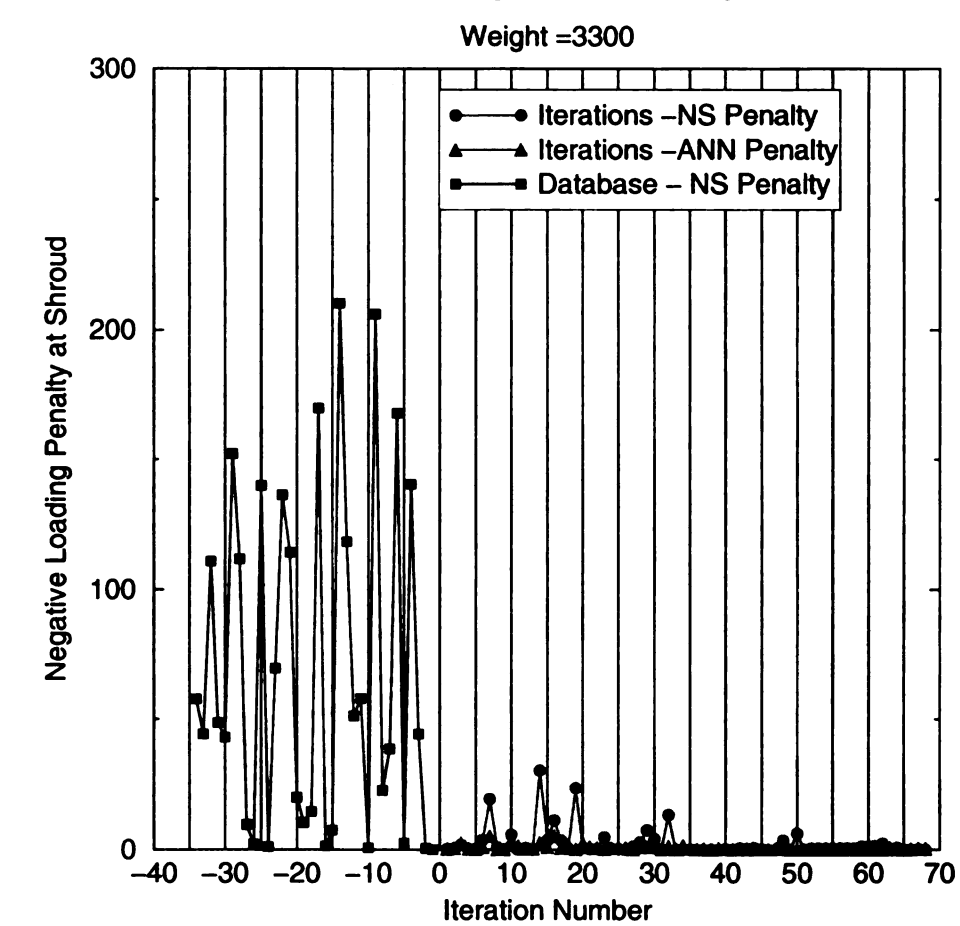


Figure 4.19 Negative Loading Penalty. (a) With database (b) Without database



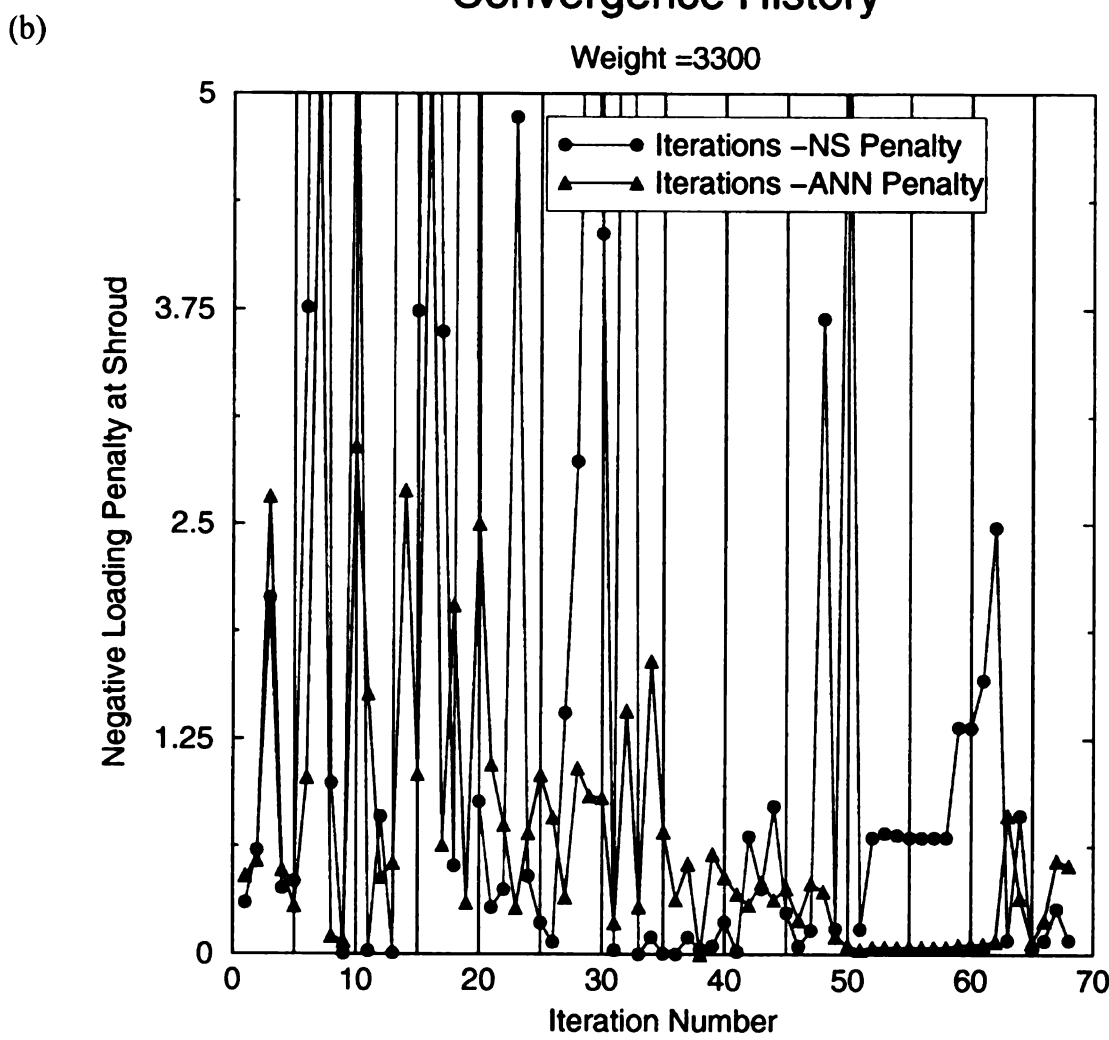
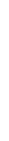


Figure 4.19 (cont'd)



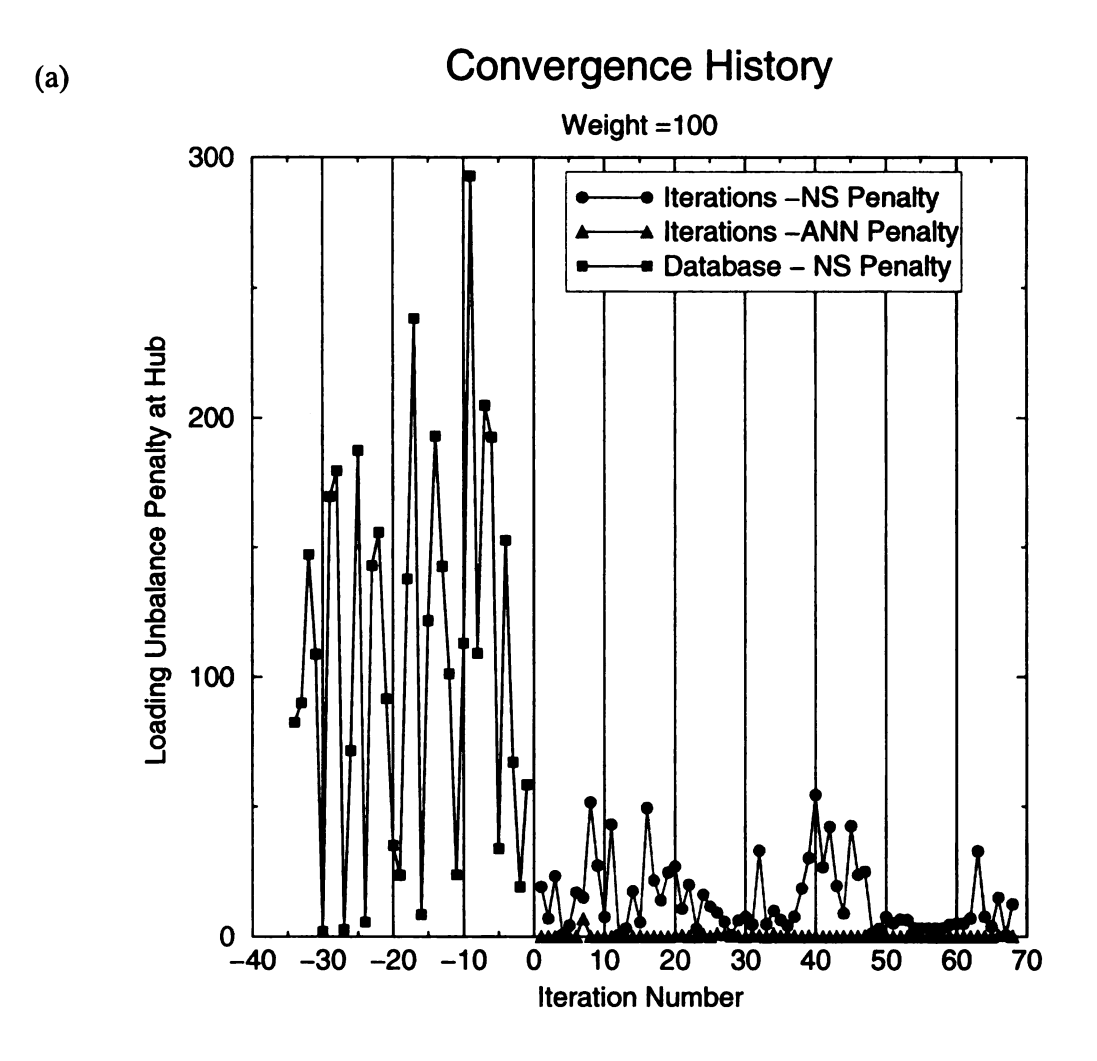


Figure 4.20 Loading Unbalance Penalty. (a) With database (b) Without database

Convergence History

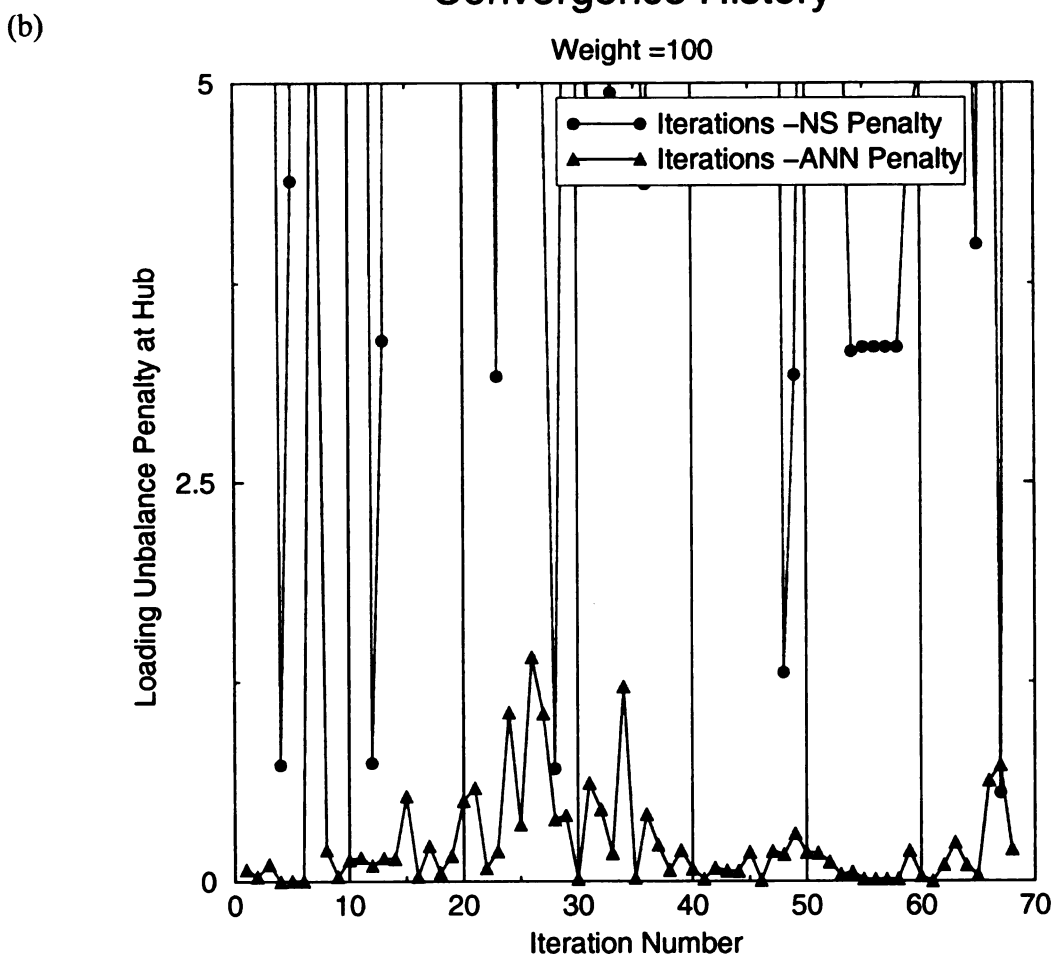


Figure 4.20 (cont'd)

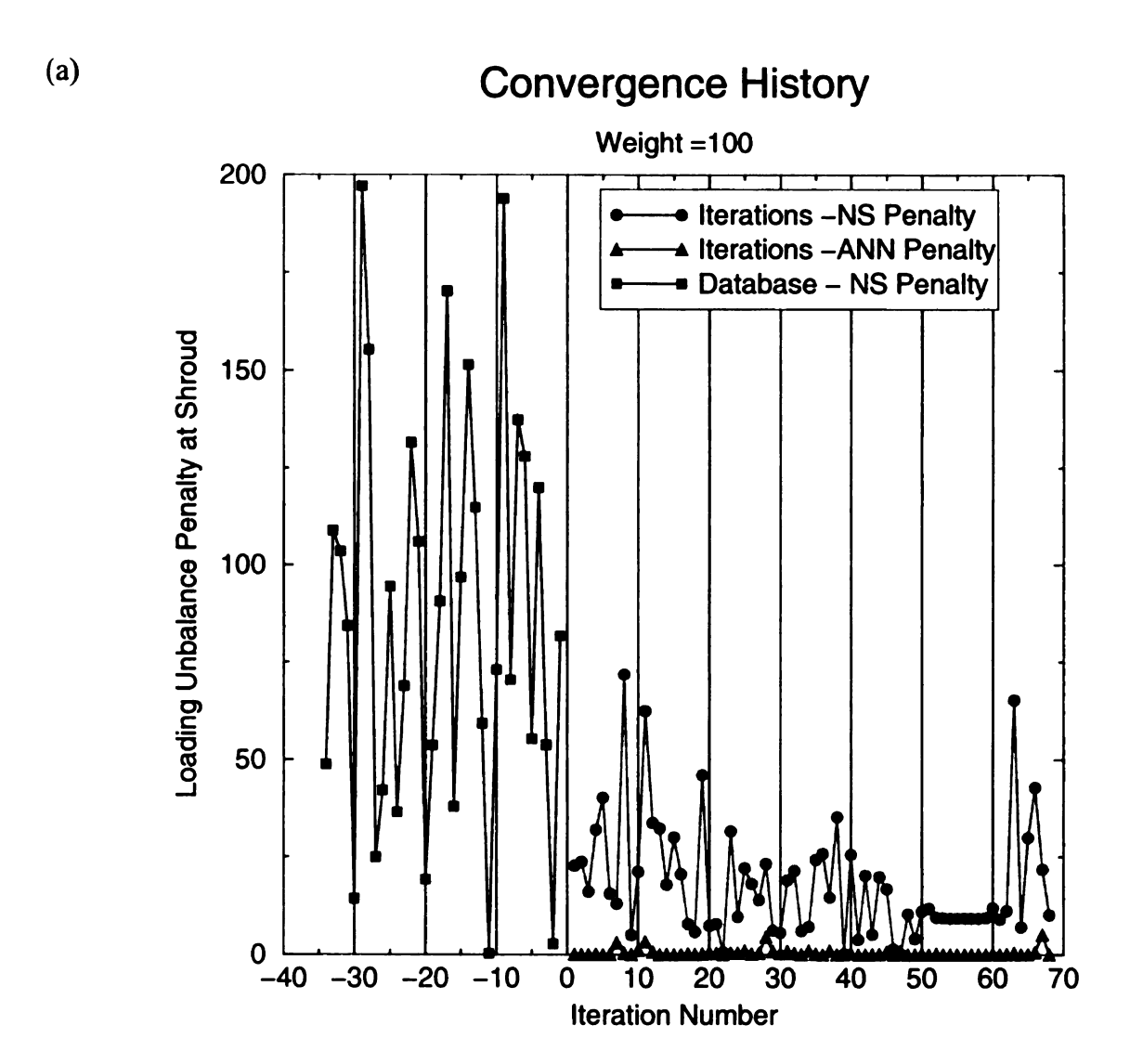


Figure 4.21 Loading Unbalance Penalty. (a) With database (b) Without database

Convergence History

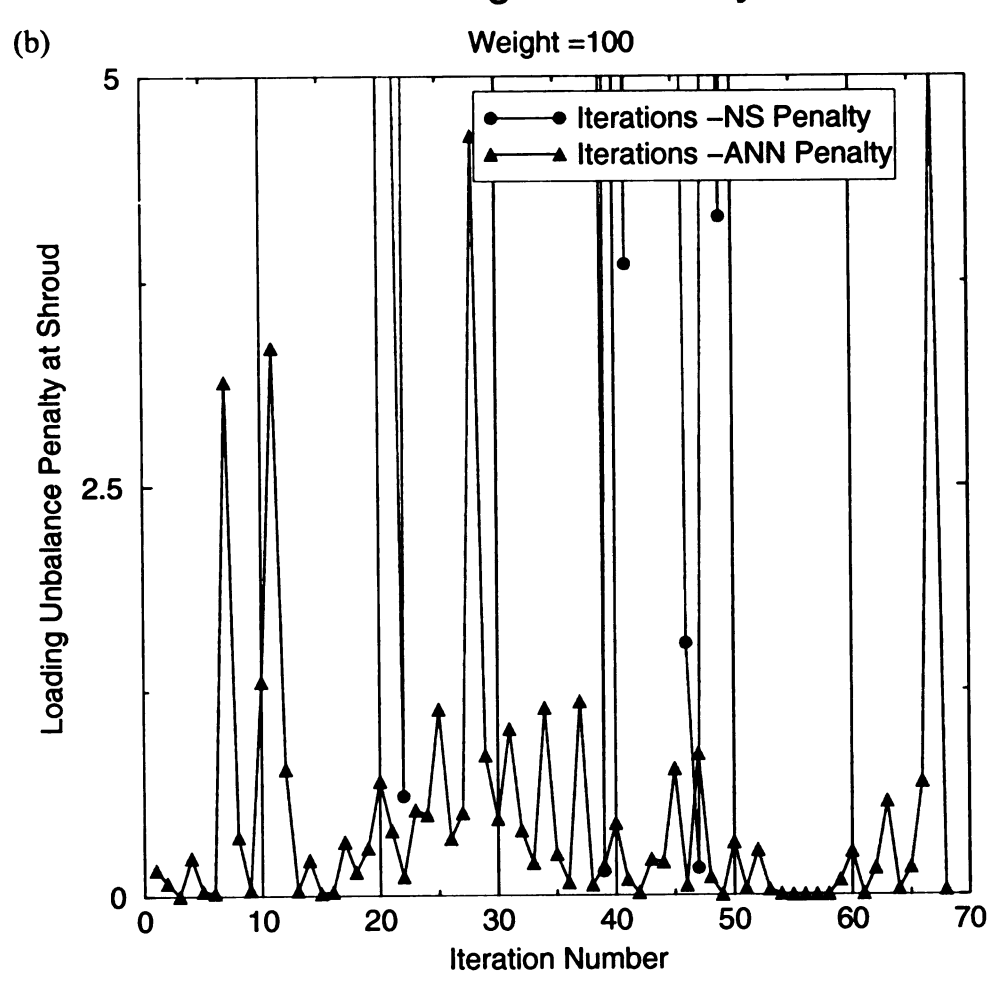


Figure 4.21 (cont'd)

4.5.3 Analysis of Optimized Geometries

If a designer is to select the most important criteria by which to make a selection from a large amount of geometries, it would obviously be the efficiency. In this section, we will compare a few geometries that were produced during the optimization process with the aid of Figure 4.22 and Table 4.5

Figure 4.22 shows the value of the total-total and total-static efficiency versus the number of iterations. The negative Iterations represent the NS efficiencies of the database, while the positive values represent the efficiencies obtained during the optimization process. Indeed, this figure resembles the convergence history, but in a way that has more physical meaning to the designer. That is, it is easier to understand efficiencies rather than penalties.

Figure 4.22 demonstrates that both the total-total and total-static efficiency increase as the optimization unfolds. Looking at the total-total efficiency, it is clearly shown that database sample number 1 (-1 iteration) has the highest value in the database of 86.5%. However, with the aid of Table 4.4 in section 4.5.1, one can see that the inlet lean is -21.76 degrees, which exceeds the ±8 degree limit. If one examines the Iterations, it is evident that, Iteration 39 has the highest total-total efficiency (87.3%), with a relatively high total-static efficiency (68%). This sample has a lower value of total-static efficiency than other geometries because it has a narrow channel (Fig. 4.23e), when compared to other geometries that have wider channels. Recall that the performance is evaluated at the diffuser exit and thus it explains why the total-static efficiency is lower because of the fact that the boundary layer occupies a large percentage of the span in narrow channels.

Efficiences vs. Iterations

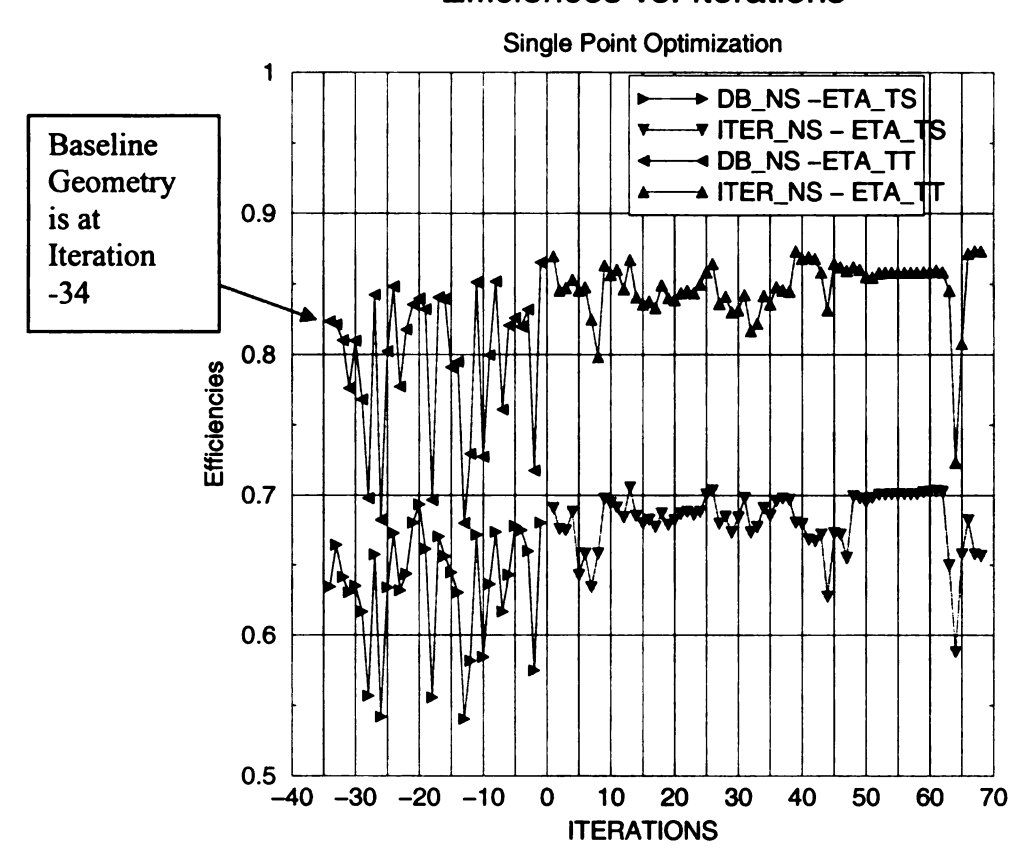


Figure 4.22 Comparison of efficiencies (T-S and T-T) of the database and iterations

Iteration 39 also has an acceptable inlet/outlet lean and mass flow (1.31 Kg/Sec) which are listed in Table 4.5. Recall that the desired mass flow is 1.3 Kg/sec. The Mach number distribution (Figure 4.23f) for this sample illustrates that the machine will make pressure rise because there is a deceleration on the shroud at both the full and splitter blades. There is no loading unbalance and negative loading, which is good. However, there is still a slight velocity peak at the shroud full blade and splitter blade.

Iteration 12 has the lowest total penalty as already demonstrated in Figure 4.14. The total-total efficiency is 84.6 % and the total-static efficiency is 68.4 %. One can say that the total-total efficiency is lower because there is slight loading unbalance (Fig 4.23b)

and also because of the fact that there is almost no loading on the main blade shroud at approximately S/C=0.25. However, it has a medium size exit width, which possibly explains why it has approximately the same total-static efficiency at Iteration 39. The mass flow is 1.305 Kg/sec and is close to the desired value. The mass flows of Iterations 39 and 12 are approximately the same because even though Iteration 39's exit width is more narrow than Iteration 12 (fig. 4.23a), the impeller inlet width is larger in 39(fig. 4.23e) and smaller in 12, which provides the reason for similar mass flows. When looking at the Mach number distribution (Fig. 4.23 b) more carefully, it can be observed that the high velocity peaks are rounded off which is good in terms of preventing separation. Finally, the inlet and outlet lean of the impeller are within acceptable limits as shown in Table 4.5

Figure 4.22 demonstrates that Iteration 13 has the highest total-static efficiency. It also has the widest exit width (Fig 4.23c) of the three Iterations which provides the reason to why it has the highest total-static efficiency. The mass flow is 1.451 Kg/Sec, which is due to the fact that is has larger exit width, but the same impeller inlet width as the baseline. That is, the outlet width changes, while the impeller inlet height remained the same as the baseline. Looking at the Mach number distribution (Fig 4.23d), it is evident that the velocity peaks have been eliminated, however now it appears there is not a lot of diffusion present at the full blade shroud. Perhaps the diffuser makes up for it, since of the three samples the total pressure ratio is a litter bit higher than the other Iterations discussed. This can be seen in Table 4.5. Finally, there is no negative loading and no loading unbalance, although the loading of the main blade shroud between 0 and 40 % of the blade length (S/C) is a little on the low side.

Finally, all the above mentioned geometries are much better than the baseline. The baseline Mach number distribution is repeated in Figure 4.24 in order to show the improvement. Also geometries at the later Iterations (68) have not been considered here because they are similar to Iteration 39. Also, the author wanted to avoid choosing a geometry from the last few Iterations because it is unknown as to exactly what is happening in between Iterations 50-60. In any event, Figure 4.22 shows that these geometries are not any better than the ones that have been considered above.

 Table 4.5 Navier-Stokes calculations of Optimized Geometries

	Table 4.5	1 14 1 101				1 Optimized O	00111011100
Iteration #	Mass flow (Kg/S)	ETA TT	ETA TS	P02/P01	P2/P01	Inlet Lean (Degrees)	Outlet Lean (Degrees)
1	1.464	0.870	0.691	1.601	1.460	0.000	38.233
2		0.845	0.676	1.585	1.452	-6.344	45.000
3		0.847	0.674	1.577	1.444	-7.193	45.000
4		0.853	0.688	1.577	1.450	-6.304	45.000
5		0.845	0.643	1.559	1.409	0.000	17.256
6	1.255	0.848	0.658	1.555	1.415	-3.695	45.000
7	1.111	0.825	0.634	1.529	1.392	-2.791	45.000
8	1.333	0.798	0.658	1.590	1.472	0.000	42.812
9		0.863	0.698	1.592	1.463	0.000	39.927
10	1.470	0.857	0.694	1.603	1.473	-3.569	45.000
11					1.451		
- 13	1.396	0.860	0.691	1.581		-7.607	45.000
			-		17.4		MANAGE SANGE
13	mark the same				2470m	nemerical Management	
14	1.354	0.841	0.685	1.586	1.463	-5 .529	45.000
15	1.353	0.836	0.679	1.588	1.463	-5.680	45.000
16	1.347	0.838	0.682	1.587	1.463	-7.279	45.000
17.	1.348	0.833	0.677	1.589	1.464	-6.591	45.000
18	1.403	0.849	0.687	1.591	1.463	-7.461	45.000
19	1.395	0.840	0.679	1.598	1.467	-6.548	45.000
	1.372	0.839			1.462		
20			0.682	1.587		-2.157	45.000
21	1.379	0.844	0.687	1.588	1.464	-4.836	45.000
22	1.383	0.845	0.688	1.588	1.464	-6.378	45.000
23	1.383	0.844	0.686	1.589	1.464	0.000	43.832
24	1.390	0.850	0.688	1.589	1.462	-4.585	45.000
25	1.388	0.858	0.700	1.583	1.461	0.000	44.944
26	1.419	0.864	0.703	1.586	1.462	-5.725	45.000
27	1.384	0.836	0.680	1.591	1.465	-4.394	45.000
28	1.393	0.841	0.685	1.592	1.467	-7.338	45.000
29	1.388	0.830	0.673	1.593	1.465	-7.043	45.000
30	1.373	0.831	0.684	1.591	1.472	-7.839	45.000
	1.3/3		0.698	1.588	1.472		45.000
24	4.274			1 1288	14/3	-3.523	45 000
31	1.374	0.842					
32	1.311	0.817	0.673	1.584	1.467	-0.727	45.000
32 33	1.311 1.360	0.817 0.822	0.673 0.677	1.584 1.594	1.467 1.475	-0.727 -4.850	45.000 45.000
32	1.311	0.817	0.673	1.584	1.467	-0.727	45.000
32 33	1.311 1.360	0.817 0.822	0.673 0.677	1.584 1.594	1.467 1.475	-0.727 -4.850	45.000 45.000
32 33 34 35	1.311 1.360 1.351 1.335	0.817 0.822 0.842 0.836	0.673 0.677 0.691 0.685	1.584 1.594 1.581 1.578	1.467 1.475 1.463 1.460	-0.727 -4.850 -7.499 -0.733	45.000 45.000 45.000 45.000
32 33 34 35 36	1.311 1.360 1.351 1.335 1.362	0.817 0.822 0.842 0.836 0.848	0.673 0.677 0.691 0.685 0.696	1.584 1.594 1.581 1.578 1.580	1.467 1.475 1.463 1.460 1.462	-0.727 -4.850 -7.499 -0.733 0.000	45.000 45.000 45.000 45.000 42.908
32 33 34 35 36 37	1.311 1.360 1.351 1.335 1.362 1.349	0.817 0.822 0.842 0.836 0.848 0.846	0.673 0.677 0.691 0.685 0.696 0.698	1.584 1.594 1.581 1.578 1.580 1.581	1.467 1.475 1.463 1.460 1.462 1.465	-0.727 -4.850 -7.499 -0.733 0.000 -2.525	45.000 45.000 45.000 45.000 42.908 45.000
32 33 34 35 36 37 38	1.311 1.360 1.351 1.335 1.362 1.349 1.359	0.817 0.822 0.842 0.836 0.848 0.846	0.673 0.677 0.691 0.685 0.696 0.698 0.697	1.584 1.594 1.581 1.578 1.580 1.581 1.585	1.467 1.475 1.463 1.460 1.462 1.465 1.468	-0.727 -4.850 -7.499 -0.733 0.000 -2.525 -6.308	45.000 45.000 45.000 45.000 42.908 45.000 45.000
32 33 34 35 36 37 38 39	1.311 1.360 1.351 1.335 1.362 1.349 1.359	0.817 0.822 0.842 0.836 0.848 0.846 0.845	0.673 0.677 0.691 0.685 0.696 0.698	1.584 1.594 1.581 1.578 1.580 1.581 1.585	1.467 1.475 1.463 1.460 1.462 1.465 1.468	-0.727 -4.850 -7.499 -0.733 0.000 -2.525 -6.308	45.000 45.000 45.000 45.000 42.908 45.000 45.000
32 33 34 35 36 37 38 39	1.311 1.360 1.351 1.335 1.362 1.349 1.359	0.817 0.822 0.842 0.836 0.848 0.846 0.845	0.673 0.677 0.691 0.685 0.696 0.698 0.697	1.584 1.594 1.581 1.578 1.580 1.581 1.585	1.467 1.475 1.463 1.460 1.462 1.465 1.468	-0.727 -4.850 -7.499 -0.733 0.000 -2.525 -6.308	45.000 45.000 45.000 45.000 42.908 45.000 45.000
32 33 34 35 36 37 38 39 40	1.311 1.360 1.351 1.335 1.362 1.349 1.359	0.817 0.822 0.842 0.836 0.848 0.846 0.845	0.673 0.677 0.691 0.685 0.696 0.698 0.697	1.584 1.594 1.581 1.578 1.580 1.581 1.585	1.467 1.475 1.463 1.460 1.462 1.465 1.468	-0.727 -4.850 -7.499 -0.733 0.000 -2.525 -6.308	45.000 45.000 45.000 45.000 42.908 45.000 45.000
32 33 34 35 36 37 38 39 40 41	1.311 1.360 1.351 1.335 1.362 1.349 1.359 1.256 1.245	0.817 0.822 0.842 0.836 0.848 0.846 0.845 0.868 0.869	0.673 0.677 0.691 0.685 0.696 0.698 0.697 0.679 0.668	1.584 1.594 1.581 1.578 1.580 1.581 1.585 1.549 1.545 1.550	1.467 1.475 1.463 1.460 1.462 1.465 1.468 1.415 1.415 1.404	-0.727 -4.850 -7.499 -0.733 0.000 -2.525 -6.308 -4.155 -4.942 -6.305	45.000 45.000 45.000 45.000 42.908 45.000 45.000 45.000 45.000 45.000
32 33 34 35 36 37 38 39 40 41 42	1.311 1.360 1.351 1.335 1.362 1.349 1.359 1.256 1.245 1.273 1.237	0.817 0.822 0.842 0.836 0.848 0.846 0.845 0.868 0.869 0.868	0.673 0.677 0.691 0.685 0.696 0.698 0.697 0.679 0.668 0.667	1.584 1.594 1.581 1.578 1.580 1.581 1.585 1.585 1.549 1.545 1.550 1.545	1.467 1.475 1.463 1.460 1.462 1.465 1.468 1.415 1.415 1.404 1.407	-0.727 -4.850 -7.499 -0.733 0.000 -2.525 -6.308 -4.155 -4.942 -6.305 -4.878	45.000 45.000 45.000 45.000 42.908 45.000 45.000 45.000 45.000 45.000 45.000
32 33 34 35 36 37 38 39 40 41 42 43	1.311 1.360 1.351 1.335 1.362 1.349 1.359 1.256 1.245 1.273 1.237	0.817 0.822 0.842 0.836 0.848 0.846 0.845 0.869 0.868 0.869 0.868 0.858	0.673 0.677 0.691 0.685 0.696 0.698 0.697 0.679 0.668 0.667 0.672	1.584 1.594 1.581 1.578 1.580 1.581 1.585 1.545 1.545 1.545 1.550 1.545	1.467 1.475 1.463 1.460 1.462 1.465 1.468 1.415 1.404 1.407 1.413 1.402	-0.727 -4.850 -7.499 -0.733 0.000 -2.525 -6.308 -4.155 -4.942 -6.305 -4.878 0.000	45.000 45.000 45.000 45.000 42.908 45.000 45.000 45.000 45.000 45.000 45.000 45.000 45.000
32 33 34 35 36 37 38 39 40 41 42 43 43	1.311 1.360 1.351 1.335 1.362 1.349 1.359 1.256 1.245 1.273 1.237 1.362 1.238	0.817 0.822 0.842 0.836 0.848 0.846 0.845 23 0.869 0.869 0.868 0.858 0.831	0.673 0.677 0.691 0.685 0.696 0.698 0.697 0.672 0.667 0.672 0.627 0.673	1.584 1.594 1.581 1.578 1.580 1.581 1.585 1.585 1.545 1.545 1.550 1.545 1.555 1.546	1.467 1.475 1.463 1.460 1.462 1.465 1.468 1.415 1.404 1.407 1.413 1.402 1.410	-0.727 -4.850 -7.499 -0.733 0.000 -2.525 -6.308 -4.155 -4.942 -6.305 -4.878 0.000 -7.610	45.000 45.000 45.000 45.000 42.908 45.000 45.000 45.000 45.000 45.000 45.000 45.000 45.000
32 33 34 35 36 37 38 39 40 41 42 43 44 45	1.311 1.360 1.351 1.335 1.362 1.349 1.359 1.256 1.245 1.273 1.237 1.362 1.238 1.248	0.817 0.822 0.842 0.836 0.848 0.846 0.845 22 0.868 0.869 0.868 0.858 0.831 0.864	0.673 0.677 0.691 0.685 0.696 0.698 0.697 0.679 0.668 0.667 0.672 0.672 0.673 0.672	1.584 1.594 1.581 1.578 1.580 1.581 1.585 1.549 1.545 1.545 1.550 1.545 1.555 1.546	1.467 1.475 1.463 1.460 1.462 1.465 1.468 1.415 1.404 1.407 1.413 1.402 1.410	-0.727 -4.850 -7.499 -0.733 0.000 -2.525 -6.308 -4.155 -4.942 -6.305 -4.878 0.000 -7.610 -5.634	45.000 45.000 45.000 45.000 42.908 45.000 45.000 45.000 45.000 45.000 45.000 45.000 45.000 45.000
32 33 34 35 36 37 38 39 40 41 42 43 43	1.311 1.360 1.351 1.335 1.362 1.349 1.359 1.256 1.245 1.273 1.237 1.362 1.238	0.817 0.822 0.842 0.836 0.848 0.846 0.845 23 0.869 0.869 0.868 0.858 0.831	0.673 0.677 0.691 0.685 0.696 0.698 0.697 0.672 0.667 0.672 0.627 0.673	1.584 1.594 1.581 1.578 1.580 1.581 1.585 1.585 1.545 1.545 1.550 1.545 1.555 1.546	1.467 1.475 1.463 1.460 1.462 1.465 1.468 1.415 1.404 1.407 1.413 1.402 1.410	-0.727 -4.850 -7.499 -0.733 0.000 -2.525 -6.308 -4.155 -4.942 -6.305 -4.878 0.000 -7.610	45.000 45.000 45.000 45.000 42.908 45.000 45.000 45.000 45.000 45.000 45.000 45.000 45.000
32 33 34 35 36 37 38 39 40 41 42 43 44 45	1.311 1.360 1.351 1.335 1.362 1.349 1.359 1.256 1.245 1.273 1.237 1.362 1.238 1.248	0.817 0.822 0.842 0.836 0.848 0.846 0.845 22 0.868 0.869 0.868 0.858 0.831 0.864	0.673 0.677 0.691 0.685 0.696 0.698 0.697 0.679 0.668 0.667 0.672 0.672 0.673 0.672	1.584 1.594 1.581 1.578 1.580 1.581 1.585 1.549 1.545 1.545 1.550 1.545 1.555 1.546	1.467 1.475 1.463 1.460 1.462 1.465 1.468 1.415 1.404 1.407 1.413 1.402 1.410	-0.727 -4.850 -7.499 -0.733 0.000 -2.525 -6.308 -4.155 -4.942 -6.305 -4.878 0.000 -7.610 -5.634	45.000 45.000 45.000 45.000 42.908 45.000 45.000 45.000 45.000 45.000 45.000 45.000 45.000 45.000
32 33 34 35 36 37 38 39 40 41 42 43 44 45 46	1.311 1.360 1.351 1.335 1.362 1.349 1.359 1.256 1.245 1.273 1.237 1.362 1.238 1.248 1.193	0.817 0.822 0.842 0.836 0.848 0.846 0.845 23 0.869 0.869 0.868 0.858 0.831 0.864 0.862	0.673 0.677 0.691 0.685 0.696 0.698 0.697 0.679 0.668 0.667 0.672 0.672 0.673 0.672	1.584 1.594 1.581 1.578 1.580 1.581 1.585 1.585 1.545 1.545 1.545 1.555 1.546 1.548 1.538	1.467 1.475 1.463 1.460 1.462 1.465 1.468 1.415 1.404 1.407 1.413 1.402 1.410 1.412	-0.727 -4.850 -7.499 -0.733 0.000 -2.525 -6.308 -4.155 -4.942 -6.305 -4.878 0.000 -7.610 -5.634	45.000 45.000 45.000 45.000 42.908 45.000 45.000 45.000 45.000 45.000 45.000 45.000 45.000 45.000 45.000
32 33 34 35 36 37 38 39 40 41 42 43 44 45 46 47 48	1.311 1.360 1.351 1.335 1.362 1.349 1.359 1.256 1.245 1.273 1.237 1.362 1.238 1.248 1.193 1.392 1.386	0.817 0.822 0.842 0.836 0.848 0.846 0.869 0.868 0.858 0.858 0.858 0.858 0.858 0.858 0.864 0.862 0.862	0.673 0.677 0.691 0.685 0.696 0.698 0.697 0.679 0.668 0.667 0.672 0.627 0.673 0.672 0.655 0.699	1.584 1.594 1.581 1.578 1.580 1.585 1.549 1.545 1.545 1.550 1.545 1.555 1.546 1.548 1.538 1.579	1.467 1.475 1.463 1.460 1.462 1.465 1.465 1.415 1.404 1.407 1.413 1.402 1.410 1.412 1.395 1.455 1.454	-0.727 -4.850 -7.499 -0.733 0.000 -2.525 -6.308 -4.155 -4.942 -6.305 -4.878 0.000 -7.610 -5.634 -7.724 -0.629 -4.628	45.000 45.000 45.000 45.000 42.908 45.000 45.000 45.000 45.000 45.000 45.000 45.000 45.000 45.000 45.000 45.000
32 33 34 35 36 37 38 39 40 41 42 43 44 45 46 47 48 49	1.311 1.360 1.351 1.335 1.362 1.349 1.359 1.256 1.245 1.273 1.237 1.362 1.238 1.248 1.193 1.392 1.386 1.378	0.817 0.822 0.842 0.836 0.848 0.846 0.869 0.868 0.858 0.831 0.864 0.862 0.862 0.862 0.860 0.855	0.673 0.677 0.691 0.685 0.696 0.698 0.697 0.679 0.668 0.667 0.672 0.673 0.672 0.655 0.699	1.584 1.594 1.581 1.581 1.585 1.585 1.545 1.545 1.550 1.545 1.555 1.546 1.548 1.579 1.578	1.467 1.475 1.463 1.460 1.462 1.465 1.468 1.415 1.404 1.407 1.413 1.402 1.410 1.412 1.395 1.455 1.454 1.455	-0.727 -4.850 -7.499 -0.733 0.000 -2.525 -6.308 -4.155 -4.942 -6.305 -4.878 0.000 -7.610 -5.634 -7.724 -0.629 -4.628 -2.621	45.000 45.000 45.000 45.000 42.908 45.000 45.000 45.000 45.000 45.000 45.000 45.000 45.000 45.000 45.000 45.000
32 33 34 35 36 37 38 39 40 41 42 43 44 45 46 47 48 49 50	1.311 1.360 1.351 1.335 1.362 1.349 1.359 1.256 1.245 1.273 1.237 1.362 1.238 1.248 1.193 1.392 1.386 1.378 1.389	0.817 0.822 0.842 0.836 0.848 0.846 0.869 0.868 0.858 0.831 0.864 0.862 0.862 0.862 0.855 0.862	0.673 0.677 0.691 0.685 0.696 0.698 0.697 0.679 0.668 0.667 0.672 0.627 0.673 0.672 0.699 0.698	1.584 1.594 1.581 1.581 1.585 1.585 1.545 1.545 1.545 1.545 1.546 1.548 1.538 1.579 1.578	1.467 1.475 1.463 1.460 1.462 1.465 1.468 1.415 1.404 1.407 1.413 1.402 1.410 1.412 1.395 1.455 1.454 1.455	-0.727 -4.850 -7.499 -0.733 0.000 -2.525 -6.308 -4.155 -4.942 -6.305 -4.878 0.000 -7.610 -5.634 -7.724 -0.629 -4.628 -2.621 -5.372	45.000 45.000 45.000 45.000 42.908 45.000 45.000 45.000 45.000 45.000 45.000 45.000 45.000 45.000 45.000 45.000 45.000 45.000
32 33 34 35 36 37 38 40 41 42 43 44 45 46 47 48 49 50 50	1.311 1.360 1.351 1.335 1.362 1.349 1.359 1.256 1.245 1.273 1.237 1.362 1.238 1.248 1.193 1.392 1.386 1.378 1.389 1.397	0.817 0.822 0.842 0.836 0.848 0.846 0.869 0.868 0.858 0.831 0.864 0.862 0.859 0.862 0.855 0.854	0.673 0.677 0.691 0.685 0.696 0.698 0.697 0.679 0.668 0.667 0.672 0.672 0.673 0.672 0.699 0.698 0.698	1.584 1.594 1.581 1.581 1.585 1.585 1.545 1.545 1.545 1.545 1.546 1.548 1.538 1.579 1.579 1.578 1.577	1.467 1.475 1.463 1.460 1.462 1.465 1.468 1.415 1.404 1.407 1.413 1.402 1.410 1.412 1.395 1.455 1.455 1.454 1.455	-0.727 -4.850 -7.499 -0.733 0.000 -2.525 -6.308 -4.155 -4.942 -6.305 -4.878 0.000 -7.610 -5.634 -7.724 -0.629 -4.628 -2.621 -5.372 -4.784	45.000 45.000 45.000 45.000 42.908 45.000 45.000 45.000 45.000 45.000 45.000 45.000 45.000 45.000 45.000 45.000 45.000 45.000 45.000
32 33 34 35 36 37 38 39 40 41 42 43 44 45 46 47 48 50 51 52 53	1.311 1.360 1.351 1.335 1.362 1.349 1.359 1.256 1.245 1.273 1.237 1.362 1.238 1.248 1.193 1.392 1.386 1.378 1.389 1.397 1.398	0.817 0.822 0.842 0.836 0.848 0.845 0.869 0.868 0.858 0.858 0.859 0.862 0.862 0.859 0.862 0.855 0.855 0.855	0.673 0.677 0.691 0.685 0.696 0.698 0.679 0.679 0.668 0.667 0.672 0.672 0.673 0.672 0.655 0.699 0.698 0.698 0.698	1.584 1.594 1.581 1.578 1.580 1.581 1.585 1.585 1.545 1.545 1.545 1.546 1.548 1.538 1.579 1.577 1.578 1.577 1.582	1.467 1.475 1.463 1.460 1.462 1.465 1.468 1.415 1.404 1.407 1.413 1.402 1.410 1.412 1.395 1.455 1.455 1.461 1.461	-0.727 -4.850 -7.499 -0.733 0.000 -2.525 -6.308 -4.155 -4.942 -6.305 -4.878 0.000 -7.610 -5.634 -7.724 -0.629 -4.628 -2.621 -5.372 -4.784 -4.750	45.000 45.000 45.000 45.000 42.908 45.000 45.000 45.000 45.000 45.000 45.000 45.000 45.000 45.000 45.000 45.000 45.000 45.000 45.000 45.000 45.000
32 33 34 35 36 37 38 39 40 41 42 43 44 45 46 47 48 49 50 51 51 52 53	1.311 1.360 1.351 1.335 1.362 1.349 1.359 1.256 1.245 1.273 1.237 1.362 1.238 1.248 1.193 1.392 1.386 1.378 1.389 1.397 1.398	0.817 0.822 0.842 0.836 0.848 0.846 0.845 0.868 0.869 0.868 0.858 0.858 0.862 0.862 0.862 0.862 0.855 0.858 0.858	0.673 0.677 0.691 0.685 0.696 0.698 0.697 0.679 0.668 0.667 0.672 0.672 0.673 0.672 0.655 0.699 0.698 0.698 0.701 0.701	1.584 1.594 1.581 1.578 1.580 1.581 1.585 1.585 1.545 1.545 1.545 1.546 1.548 1.538 1.579 1.577 1.578 1.577 1.582 1.583 1.583	1.467 1.475 1.463 1.460 1.462 1.465 1.468 1.415 1.415 1.404 1.407 1.413 1.402 1.410 1.412 1.395 1.455 1.454 1.455 1.461 1.461	-0.727 -4.850 -7.499 -0.733 0.000 -2.525 -6.308 -4.155 -4.942 -6.305 -4.878 0.000 -7.610 -5.634 -7.724 -0.629 -4.628 -2.621 -5.372 -4.784 -4.750 -5.049	45.000 45.000
32 33 34 35 36 37 38 39 40 41 42 43 44 45 46 47 48 49 50 51 51 52 53	1.311 1.360 1.351 1.335 1.362 1.349 1.359 1.256 1.245 1.273 1.237 1.362 1.238 1.248 1.193 1.392 1.386 1.378 1.389 1.397 1.398 1.398 1.398	0.817 0.822 0.842 0.836 0.848 0.846 0.845 0.868 0.869 0.868 0.858 0.858 0.862 0.862 0.862 0.862 0.862 0.863 0.864 0.862 0.868 0.858 0.	0.673 0.677 0.691 0.685 0.696 0.698 0.697 0.672 0.672 0.672 0.673 0.672 0.655 0.699 0.698 0.698 0.701 0.701	1.584 1.594 1.581 1.578 1.580 1.581 1.585 1.585 1.545 1.545 1.545 1.546 1.548 1.579 1.578 1.578 1.578 1.578 1.578 1.583 1.583	1.467 1.475 1.463 1.460 1.462 1.465 1.468 1.415 1.404 1.407 1.413 1.402 1.410 1.412 1.395 1.455 1.455 1.454 1.455 1.461 1.461	-0.727 -4.850 -7.499 -0.733 0.000 -2.525 -6.308 -4.155 -4.942 -6.305 -4.878 0.000 -7.610 -5.634 -7.724 -0.629 -4.628 -2.621 -5.372 -4.784 -4.750 -5.049 -4.995	45.000 45.000
32 33 34 35 36 37 38 39 40 41 42 43 44 45 46 47 48 49 50 51 51 52 53 53	1.311 1.360 1.351 1.335 1.362 1.349 1.359 1.256 1.245 1.273 1.237 1.362 1.238 1.248 1.193 1.392 1.386 1.378 1.389 1.397 1.398 1.398 1.398	0.817 0.822 0.842 0.836 0.848 0.846 0.845 0.868 0.869 0.868 0.858 0.851 0.864 0.862 0.859 0.862 0.855 0.854 0.858 0.858	0.673 0.677 0.691 0.685 0.696 0.698 0.697 0.668 0.667 0.672 0.672 0.673 0.672 0.698 0.698 0.695 0.698 0.701 0.701 0.701	1.584 1.594 1.581 1.578 1.580 1.585 1.545 1.545 1.545 1.545 1.555 1.546 1.548 1.579 1.578 1.577 1.582 1.583 1.583 1.583	1.467 1.475 1.463 1.460 1.462 1.465 1.415 1.404 1.407 1.413 1.402 1.410 1.412 1.395 1.455 1.454 1.455 1.461 1.461 1.461 1.461	-0.727 -4.850 -7.499 -0.733 0.000 -2.525 -6.308 -4.155 -4.942 -6.305 -4.878 0.000 -7.610 -5.634 -7.724 -0.629 -4.628 -2.621 -5.372 -4.784 -4.750 -5.049 -4.995 -4.995	45.000 45.000
32 33 34 35 36 37 38 39 40 41 42 43 44 45 46 47 48 49 50 51 51 52 53	1.311 1.360 1.351 1.335 1.362 1.349 1.359 1.256 1.245 1.273 1.237 1.362 1.238 1.238 1.193 1.392 1.386 1.378 1.389 1.397 1.398 1.398 1.398 1.398	0.817 0.822 0.842 0.836 0.848 0.846 0.845 0.868 0.869 0.868 0.858 0.858 0.859 0.862 0.862 0.859 0.855 0.854 0.858 0.858 0.858 0.858	0.673 0.677 0.691 0.685 0.696 0.698 0.697 0.668 0.667 0.672 0.655 0.699 0.698 0.701 0.701 0.701 0.701	1.584 1.594 1.581 1.578 1.580 1.585 1.585 1.545 1.545 1.550 1.545 1.555 1.546 1.548 1.579 1.578 1.577 1.582 1.583 1.583 1.583 1.583 1.583	1.467 1.475 1.463 1.460 1.462 1.465 1.468 1.415 1.404 1.407 1.413 1.402 1.410 1.412 1.395 1.455 1.455 1.454 1.455 1.461 1.461	-0.727 -4.850 -7.499 -0.733 0.000 -2.525 -6.308 -4.155 -4.942 -6.305 -4.878 0.000 -7.610 -5.634 -7.724 -0.629 -4.628 -2.621 -5.372 -4.784 -4.750 -5.049 -4.995	45.000 45.000
32 33 34 35 36 37 38 39 40 41 42 43 44 45 46 47 48 49 50 51 51 52 53 54 55	1.311 1.360 1.351 1.335 1.362 1.349 1.359 1.256 1.245 1.273 1.237 1.362 1.238 1.248 1.193 1.392 1.386 1.378 1.389 1.397 1.398 1.398 1.398	0.817 0.822 0.842 0.836 0.848 0.846 0.845 0.868 0.869 0.868 0.858 0.851 0.864 0.862 0.859 0.862 0.855 0.854 0.858 0.858	0.673 0.677 0.691 0.685 0.696 0.698 0.697 0.668 0.667 0.672 0.672 0.673 0.672 0.698 0.698 0.695 0.698 0.701 0.701 0.701	1.584 1.594 1.581 1.578 1.580 1.585 1.545 1.545 1.545 1.545 1.555 1.546 1.548 1.579 1.578 1.577 1.582 1.583 1.583 1.583	1.467 1.475 1.463 1.460 1.462 1.465 1.415 1.404 1.407 1.413 1.402 1.410 1.412 1.395 1.455 1.454 1.455 1.461 1.461 1.461 1.461	-0.727 -4.850 -7.499 -0.733 0.000 -2.525 -6.308 -4.155 -4.942 -6.305 -4.878 0.000 -7.610 -5.634 -7.724 -0.629 -4.628 -2.621 -5.372 -4.784 -4.750 -5.049 -4.995 -4.995	45.000 45.000
32 33 34 35 36 37 38 39 40 41 42 43 44 45 50 51 52 53 54 55 56	1.311 1.360 1.351 1.335 1.362 1.349 1.359 1.256 1.245 1.273 1.237 1.362 1.238 1.238 1.193 1.392 1.386 1.378 1.389 1.397 1.398 1.398 1.398 1.398	0.817 0.822 0.842 0.836 0.848 0.846 0.845 0.868 0.869 0.868 0.858 0.858 0.859 0.862 0.862 0.859 0.855 0.854 0.858 0.858 0.858 0.858	0.673 0.677 0.691 0.685 0.696 0.698 0.697 0.668 0.667 0.672 0.655 0.699 0.698 0.701 0.701 0.701 0.701	1.584 1.594 1.581 1.578 1.580 1.585 1.585 1.545 1.545 1.550 1.545 1.555 1.546 1.548 1.579 1.578 1.577 1.582 1.583 1.583 1.583 1.583 1.583	1.467 1.475 1.463 1.460 1.462 1.465 1.465 1.415 1.404 1.407 1.413 1.402 1.410 1.412 1.395 1.455 1.454 1.455 1.461 1.461 1.461 1.461 1.461 1.461	-0.727 -4.850 -7.499 -0.733 0.000 -2.525 -6.308 -4.155 -4.942 -6.305 -4.878 0.000 -7.610 -5.634 -7.724 -0.629 -4.628 -2.621 -5.372 -4.784 -4.750 -5.049 -4.995 -4.995	45.000 45.000
32 33 34 35 36 37 38 39 40 41 42 43 44 45 46 47 48 49 50 51 52 53 54 55 56 57 58	1.311 1.360 1.351 1.335 1.362 1.349 1.359 1.256 1.245 1.273 1.237 1.362 1.238 1.248 1.193 1.392 1.386 1.378 1.389 1.397 1.398 1.398 1.398 1.398 1.398 1.398 1.398 1.398	0.817 0.822 0.842 0.836 0.848 0.846 0.845 0.868 0.869 0.868 0.858 0.851 0.864 0.862 0.859 0.862 0.855 0.854 0.858 0.858	0.673 0.677 0.691 0.685 0.696 0.698 0.697 0.668 0.667 0.672 0.672 0.655 0.699 0.698 0.701 0.701 0.701 0.701 0.701	1.584 1.594 1.581 1.581 1.585 1.585 1.585 1.545 1.545 1.545 1.555 1.546 1.548 1.577 1.578 1.577 1.582 1.583 1.583 1.583 1.583 1.583 1.583 1.583 1.583	1.467 1.475 1.463 1.460 1.462 1.465 1.468 1.415 1.404 1.407 1.413 1.402 1.410 1.412 1.395 1.455 1.455 1.461 1.461 1.461 1.461 1.461 1.461 1.461 1.461 1.461	-0.727 -4.850 -7.499 -0.733 0.000 -2.525 -6.308 -4.155 -4.942 -6.305 -4.878 0.000 -7.610 -5.634 -7.724 -0.629 -4.628 -2.621 -5.372 -4.784 -4.750 -5.049 -4.995 -4.995 -4.995 -4.995	45.000 45.000
32 33 34 35 36 37 38 39 40 41 42 43 44 45 46 47 48 49 50 51 52 53 54 55 56 57 58 59 60	1.311 1.360 1.351 1.335 1.362 1.349 1.359 1.256 1.245 1.273 1.237 1.362 1.238 1.248 1.193 1.392 1.386 1.378 1.389 1.397 1.398 1.398 1.398 1.398 1.398 1.398 1.398 1.398 1.398 1.398	0.817 0.822 0.842 0.836 0.848 0.846 0.845 0.868 0.869 0.868 0.858 0.831 0.864 0.862 0.862 0.855 0.854 0.858 0.858 0.858 0.858 0.858 0.858 0.858	0.673 0.677 0.691 0.685 0.696 0.698 0.697 0.679 0.668 0.667 0.672 0.627 0.673 0.672 0.699 0.698 0.698 0.701 0.701 0.701 0.701 0.701 0.701 0.701 0.701 0.701 0.701 0.701 0.701 0.701	1.584 1.594 1.581 1.581 1.585 1.585 1.585 1.545 1.545 1.545 1.545 1.546 1.548 1.538 1.577 1.582 1.583 1.583 1.583 1.583 1.583 1.583 1.583 1.583 1.583 1.583 1.583 1.583 1.583 1.583 1.583	1.467 1.475 1.463 1.460 1.462 1.468 1.468 1.415 1.404 1.407 1.413 1.402 1.410 1.412 1.395 1.455 1.455 1.454 1.461 1.461 1.461 1.461 1.461 1.461 1.461 1.461 1.461 1.461 1.461 1.461 1.461 1.461 1.461 1.461 1.461 1.461 1.464 1.465	-0.727 -4.850 -7.499 -0.733 0.000 -2.525 -6.308 -4.155 -4.942 -6.305 -4.878 0.000 -7.610 -5.634 -7.724 -0.629 -4.628 -2.621 -5.372 -4.784 -4.750 -5.049 -4.995 -4.995 -4.995 -4.995 -5.703	45.000 45.000
32 33 34 35 36 37 38 39 40 41 42 43 44 45 46 47 48 49 50 51 52 53 54 55 56 57 58 59 60 61	1.311 1.360 1.351 1.335 1.362 1.349 1.359 1.256 1.245 1.273 1.237 1.362 1.238 1.248 1.193 1.392 1.386 1.378 1.389 1.398 1.398 1.398 1.398 1.398 1.398 1.398 1.398 1.398 1.398 1.398 1.407 1.409 1.413	0.817 0.822 0.842 0.836 0.848 0.846 0.845 0.868 0.869 0.868 0.858 0.831 0.864 0.862 0.855 0.854 0.858 0.858 0.858 0.858 0.858 0.858 0.858 0.858 0.858 0.858	0.673 0.677 0.691 0.685 0.696 0.698 0.697 0.679 0.668 0.667 0.672 0.627 0.673 0.672 0.699 0.698 0.695 0.698 0.701 0.701 0.701 0.701 0.701 0.701 0.701 0.701 0.701 0.701 0.701 0.701 0.701 0.701 0.701 0.701 0.701 0.701 0.701	1.584 1.594 1.581 1.581 1.585 1.585 1.585 1.545 1.545 1.545 1.546 1.548 1.548 1.577 1.578 1.577 1.582 1.583 1.583 1.583 1.583 1.583 1.583 1.583 1.583 1.583 1.583 1.583 1.583 1.583 1.583 1.583 1.583 1.583 1.583 1.583 1.586 1.586 1.586	1.467 1.475 1.463 1.460 1.462 1.465 1.468 1.415 1.404 1.407 1.413 1.402 1.410 1.412 1.395 1.455 1.455 1.455 1.461 1.461 1.461 1.461 1.461 1.461 1.461 1.461 1.461 1.461 1.461 1.461 1.461 1.461 1.461 1.461 1.461 1.465 1.465	-0.727 -4.850 -7.499 -0.733 0.000 -2.525 -6.308 -4.155 -4.942 -6.305 -4.878 0.000 -7.610 -5.634 -7.724 -0.629 -4.628 -2.621 -5.372 -4.784 -4.750 -5.049 -4.995 -4.995 -4.995 -4.995 -4.995 -5.703 -5.587	45.000 45.000
32 33 34 35 36 37 38 39 40 41 42 43 44 45 46 47 48 49 50 51 52 53 54 55 56 57 58 59 60 61 62	1.311 1.360 1.351 1.362 1.349 1.359 1.256 1.245 1.273 1.237 1.362 1.238 1.248 1.193 1.392 1.386 1.378 1.398 1.398 1.398 1.398 1.398 1.398 1.398 1.398 1.398 1.398 1.398 1.398 1.407 1.409 1.413 1.410	0.817 0.822 0.842 0.836 0.848 0.846 0.845 0.868 0.869 0.868 0.858 0.831 0.864 0.862 0.862 0.862 0.862 0.858 0.858 0.858 0.858 0.858 0.858 0.858 0.858 0.858 0.858 0.858 0.858 0.858	0.673 0.677 0.691 0.685 0.696 0.698 0.697 0.679 0.668 0.667 0.672 0.627 0.673 0.672 0.699 0.698 0.699 0.698 0.701 0.701 0.701 0.701 0.701 0.701 0.701 0.701 0.701 0.701 0.702 0.703 0.703	1.584 1.594 1.581 1.578 1.580 1.581 1.585 1.585 1.545 1.545 1.545 1.546 1.548 1.538 1.577 1.578 1.577 1.582 1.583 1.586	1.467 1.475 1.463 1.460 1.462 1.465 1.468 1.415 1.404 1.407 1.413 1.402 1.410 1.412 1.395 1.455 1.455 1.455 1.461 1.461 1.461 1.461 1.461 1.461 1.461 1.461 1.461 1.461 1.461 1.461 1.461 1.461 1.461 1.461 1.461 1.461 1.465 1.465 1.465	-0.727 -4.850 -7.499 -0.733 0.000 -2.525 -6.308 -4.155 -4.942 -6.305 -4.878 0.000 -7.610 -5.634 -7.724 -0.629 -4.628 -2.621 -5.372 -4.784 -4.750 -5.049 -4.995 -4.995 -4.995 -4.995 -4.995 -5.703 -5.587 -4.417	45.000 45.000
32 33 34 35 36 37 38 39 40 41 42 43 44 45 46 47 48 49 50 51 52 53 54 55 56 57 58 60 61 62 63	1.311 1.360 1.351 1.362 1.349 1.359 1.256 1.245 1.273 1.237 1.362 1.238 1.248 1.193 1.392 1.386 1.378 1.389 1.398 1.398 1.398 1.398 1.398 1.398 1.398 1.398 1.407 1.409 1.413 1.410 1.342	0.817 0.822 0.842 0.836 0.848 0.846 0.845 0.868 0.869 0.868 0.858 0.831 0.864 0.862 0.859 0.862 0.860 0.855 0.858 0.858 0.858 0.858 0.858 0.858 0.858 0.858 0.858 0.858 0.858 0.858 0.858 0.858 0.858 0.858 0.858 0.858 0.858	0.673 0.677 0.691 0.685 0.696 0.698 0.697 0.668 0.667 0.672 0.672 0.673 0.672 0.655 0.699 0.698 0.695 0.698 0.701 0.701 0.701 0.701 0.701 0.701 0.701 0.701 0.701 0.701 0.701 0.701 0.701 0.703 0.703 0.703	1.584 1.594 1.581 1.578 1.580 1.581 1.585 1.545 1.545 1.545 1.545 1.545 1.546 1.548 1.579 1.578 1.577 1.582 1.583 1.586	1.467 1.475 1.463 1.460 1.462 1.465 1.468 1.415 1.404 1.407 1.413 1.402 1.410 1.412 1.395 1.455 1.454 1.455 1.461 1.461 1.461 1.461 1.461 1.461 1.461 1.461 1.465 1.465 1.465	-0.727 -4.850 -7.499 -0.733 0.000 -2.525 -6.308 -4.155 -4.942 -6.305 -4.878 0.000 -7.610 -5.634 -7.724 -0.629 -4.628 -2.621 -5.372 -4.784 -4.750 -5.049 -4.995 -4.995 -4.995 -4.995 -4.995 -4.995 -5.703 -5.587 -4.417 0.000	45.000 45.000 45.000 45.000 42.908 45.000
32 33 34 35 36 37 38 39 40 41 42 43 44 45 50 51 52 53 54 55 56 57 58 59 60 61 62 63 64	1.311 1.360 1.351 1.362 1.349 1.359 1.256 1.245 1.273 1.237 1.362 1.238 1.248 1.193 1.392 1.386 1.378 1.398 1.398 1.398 1.398 1.398 1.398 1.398 1.398 1.398 1.398 1.407 1.409 1.413 1.410 1.342 1.066	0.817 0.822 0.842 0.836 0.848 0.846 0.845 0.868 0.869 0.868 0.858 0.851 0.864 0.855 0.855 0.855 0.855 0.858	0.673 0.677 0.691 0.685 0.696 0.698 0.697 0.668 0.667 0.672 0.627 0.673 0.672 0.655 0.699 0.698 0.701 0.701 0.701 0.701 0.701 0.701 0.701 0.701 0.701 0.701 0.701 0.701 0.701 0.703 0.650 0.588	1.584 1.594 1.581 1.578 1.580 1.581 1.585 1.545 1.545 1.545 1.545 1.555 1.546 1.548 1.577 1.582 1.577 1.583 1.586	1.467 1.475 1.463 1.460 1.462 1.465 1.465 1.415 1.404 1.407 1.413 1.402 1.410 1.412 1.395 1.455 1.454 1.455 1.461 1.461 1.461 1.461 1.461 1.461 1.461 1.465 1.465 1.465 1.465	-0.727 -4.850 -7.499 -0.733 0.000 -2.525 -6.308 -4.155 -4.942 -6.305 -4.878 0.000 -7.610 -5.634 -7.724 -0.629 -4.628 -2.621 -5.372 -4.784 -4.750 -5.049 -4.995 -4.995 -4.995 -4.995 -4.995 -4.995 -4.995 -5.703 -5.587 -4.417 0.000 -1.021	45.000 45.000 45.000 45.000 42.008 45.000
32 33 34 35 36 37 38 39 40 41 42 43 44 45 50 51 52 53 54 55 56 57 58 59 60 61 62 63 64 65	1.311 1.360 1.351 1.362 1.349 1.359 1.256 1.245 1.273 1.237 1.362 1.238 1.248 1.193 1.392 1.386 1.378 1.399 1.397 1.398	0.817 0.822 0.842 0.836 0.848 0.846 0.845 0.868 0.869 0.868 0.858 0.858 0.859 0.862 0.860 0.855 0.854 0.858	0.673 0.677 0.691 0.685 0.696 0.698 0.697 0.668 0.667 0.672 0.655 0.699 0.698 0.701 0.701 0.701 0.701 0.701 0.701 0.701 0.701 0.702 0.703 0.703 0.650 0.588 0.658	1.584 1.594 1.581 1.578 1.580 1.581 1.585 1.585 1.545 1.545 1.550 1.545 1.555 1.546 1.548 1.579 1.578 1.577 1.582 1.583 1.583 1.583 1.583 1.583 1.583 1.583 1.583 1.586 1.586 1.586 1.587 1.576 1.576 1.576 1.590	1.467 1.475 1.463 1.460 1.462 1.465 1.468 1.415 1.404 1.407 1.413 1.402 1.410 1.412 1.395 1.455 1.454 1.455 1.461 1.461 1.461 1.461 1.461 1.461 1.461 1.461 1.465 1.465 1.465 1.465 1.422 1.466	-0.727 -4.850 -7.499 -0.733 0.000 -2.525 -6.308 -4.155 -4.942 -6.305 -4.878 0.000 -7.610 -5.634 -7.724 -0.629 -4.628 -2.621 -5.372 -4.784 -4.750 -5.049 -4.995 -4.995 -4.995 -4.995 -4.995 -4.995 -4.995 -5.703 -5.587 -4.417 0.000 -1.021 -3.409	45.000 45.000
32 33 34 35 36 37 38 39 40 41 42 43 44 45 50 51 52 53 54 55 56 57 58 60 61 62 63 64 65 66	1.311 1.360 1.351 1.362 1.351 1.335 1.362 1.349 1.359 1.256 1.245 1.273 1.237 1.362 1.238 1.248 1.193 1.392 1.386 1.378 1.389 1.397 1.398	0.817 0.822 0.842 0.836 0.848 0.846 0.845 0.868 0.869 0.868 0.858 0.831 0.864 0.862 0.859 0.862 0.854 0.858	0.673 0.677 0.691 0.685 0.696 0.698 0.697 0.668 0.667 0.672 0.627 0.672 0.655 0.699 0.698 0.701 0.701 0.701 0.701 0.701 0.701 0.701 0.701 0.701 0.701 0.701 0.701 0.702 0.703 0.703 0.703 0.658 0.658	1.584 1.594 1.581 1.578 1.580 1.581 1.585 1.585 1.545 1.545 1.550 1.545 1.555 1.546 1.548 1.579 1.577 1.582 1.583 1.583 1.583 1.583 1.583 1.583 1.583 1.583 1.586 1.586 1.587 1.576 1.576 1.576 1.576 1.576 1.590 1.559	1.467 1.475 1.463 1.460 1.462 1.465 1.468 1.415 1.404 1.407 1.413 1.402 1.410 1.412 1.395 1.455 1.454 1.455 1.461 1.461 1.461 1.461 1.461 1.461 1.461 1.461 1.465 1.465 1.465 1.465 1.422 1.466 1.422	-0.727 -4.850 -7.499 -0.733 0.000 -2.525 -6.308 -4.155 -4.942 -6.305 -4.878 0.000 -7.610 -5.634 -7.724 -0.629 -4.628 -2.621 -5.372 -4.784 -4.750 -5.049 -4.995 -4.995 -4.995 -4.995 -4.995 -4.995 -5.703 -5.587 -4.417 0.000 -1.021 -3.409 -6.870	45.000 45.000
32 33 34 35 36 37 38 39 40 41 42 43 44 45 46 47 48 49 50 51 52 53 54 55 56 57 58 60 61 62 63 64 65 66 67	1.311 1.360 1.351 1.360 1.351 1.335 1.362 1.349 1.359 1.256 1.245 1.273 1.237 1.362 1.238 1.248 1.193 1.392 1.386 1.378 1.389 1.397 1.398	0.817 0.822 0.842 0.836 0.848 0.846 0.845 0.868 0.869 0.868 0.858 0.858 0.859 0.862 0.860 0.855 0.854 0.858	0.673 0.677 0.691 0.685 0.696 0.698 0.697 0.668 0.667 0.672 0.655 0.699 0.698 0.701 0.701 0.701 0.701 0.701 0.701 0.701 0.701 0.702 0.703 0.703 0.650 0.588 0.658	1.584 1.594 1.581 1.581 1.580 1.581 1.585 1.585 1.545 1.545 1.555 1.546 1.548 1.577 1.578 1.577 1.582 1.583 1.583 1.583 1.583 1.583 1.583 1.583 1.583 1.583 1.586 1.586 1.586 1.586 1.587 1.576 1.576 1.590 1.559 1.548	1.467 1.475 1.463 1.460 1.462 1.465 1.468 1.415 1.404 1.407 1.413 1.402 1.410 1.412 1.395 1.455 1.461 1.461 1.461 1.461 1.461 1.461 1.461 1.461 1.461 1.465 1.465 1.465 1.465 1.465 1.466 1.422 1.397	-0.727 -4.850 -7.499 -0.733 0.000 -2.525 -6.308 -4.155 -4.942 -6.305 -4.878 0.000 -7.610 -5.634 -7.724 -0.629 -4.628 -2.621 -5.372 -4.784 -4.750 -5.049 -4.995 -4.995 -4.995 -4.995 -4.995 -4.995 -4.995 -5.703 -5.587 -4.417 0.000 -1.021 -3.409	45.000 45.000
32 33 34 35 36 37 38 39 40 41 42 43 44 45 50 51 52 53 54 55 56 57 58 60 61 62 63 64 65 66	1.311 1.360 1.351 1.360 1.351 1.335 1.362 1.349 1.359 1.256 1.245 1.273 1.237 1.362 1.238 1.248 1.193 1.392 1.386 1.378 1.399 1.397 1.398	0.817 0.822 0.842 0.836 0.848 0.846 0.845 0.868 0.869 0.868 0.858 0.831 0.864 0.862 0.859 0.862 0.854 0.858	0.673 0.677 0.691 0.685 0.696 0.698 0.697 0.668 0.667 0.672 0.627 0.672 0.655 0.699 0.698 0.701 0.701 0.701 0.701 0.701 0.701 0.701 0.701 0.701 0.701 0.701 0.701 0.702 0.703 0.703 0.703 0.658 0.658	1.584 1.594 1.581 1.578 1.580 1.581 1.585 1.585 1.545 1.545 1.550 1.545 1.555 1.546 1.548 1.579 1.577 1.582 1.583 1.583 1.583 1.583 1.583 1.583 1.583 1.583 1.586 1.586 1.587 1.576 1.576 1.576 1.576 1.576 1.590 1.559	1.467 1.475 1.463 1.460 1.462 1.465 1.468 1.415 1.404 1.407 1.413 1.402 1.410 1.412 1.395 1.455 1.454 1.455 1.461 1.461 1.461 1.461 1.461 1.461 1.461 1.461 1.465 1.465 1.465 1.465 1.422 1.466 1.422	-0.727 -4.850 -7.499 -0.733 0.000 -2.525 -6.308 -4.155 -4.942 -6.305 -4.878 0.000 -7.610 -5.634 -7.724 -0.629 -4.628 -2.621 -5.372 -4.784 -4.750 -5.049 -4.995 -4.995 -4.995 -4.995 -4.995 -4.995 -5.703 -5.587 -4.417 0.000 -1.021 -3.409 -6.870	45.000 45.000

Meridional Contours

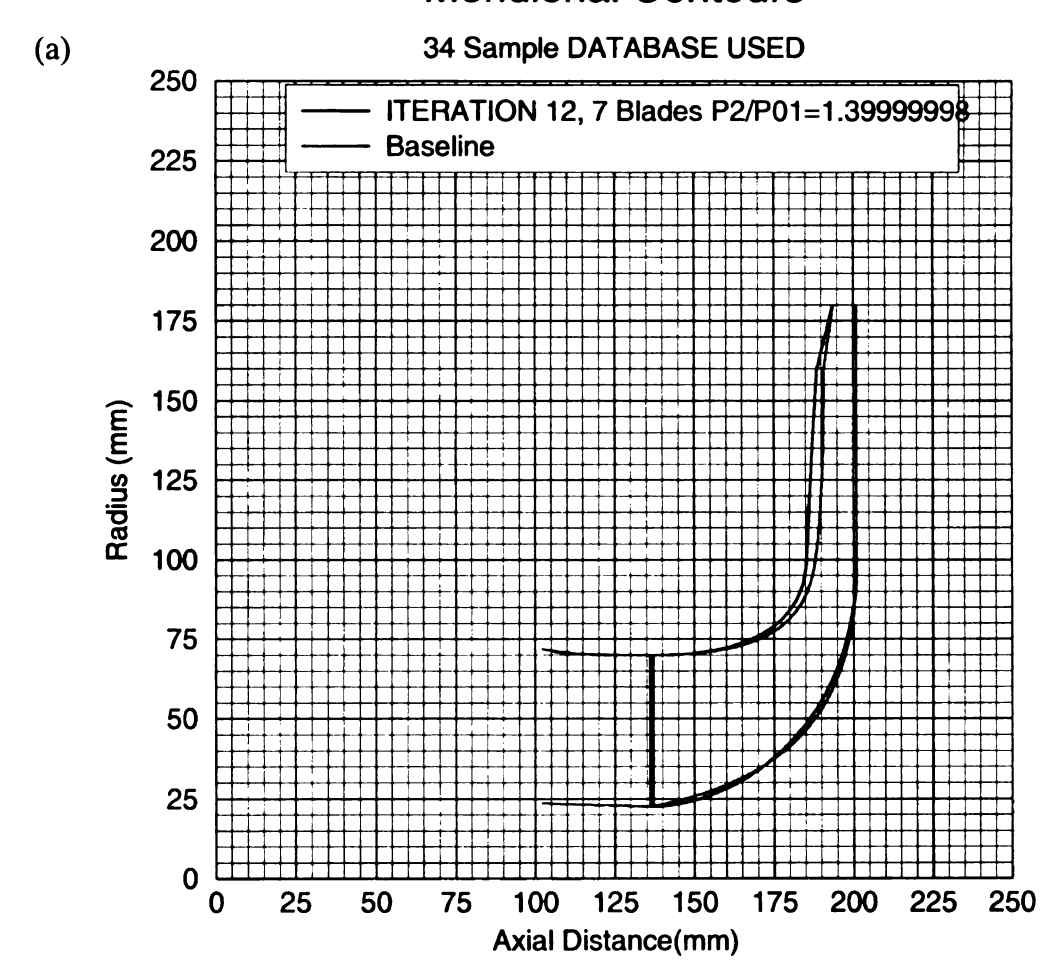


Figure 4.23 Meridional Contours (left) and Mach distributions (right) of Iterations

(b) ITERATION 12, 7 Blades

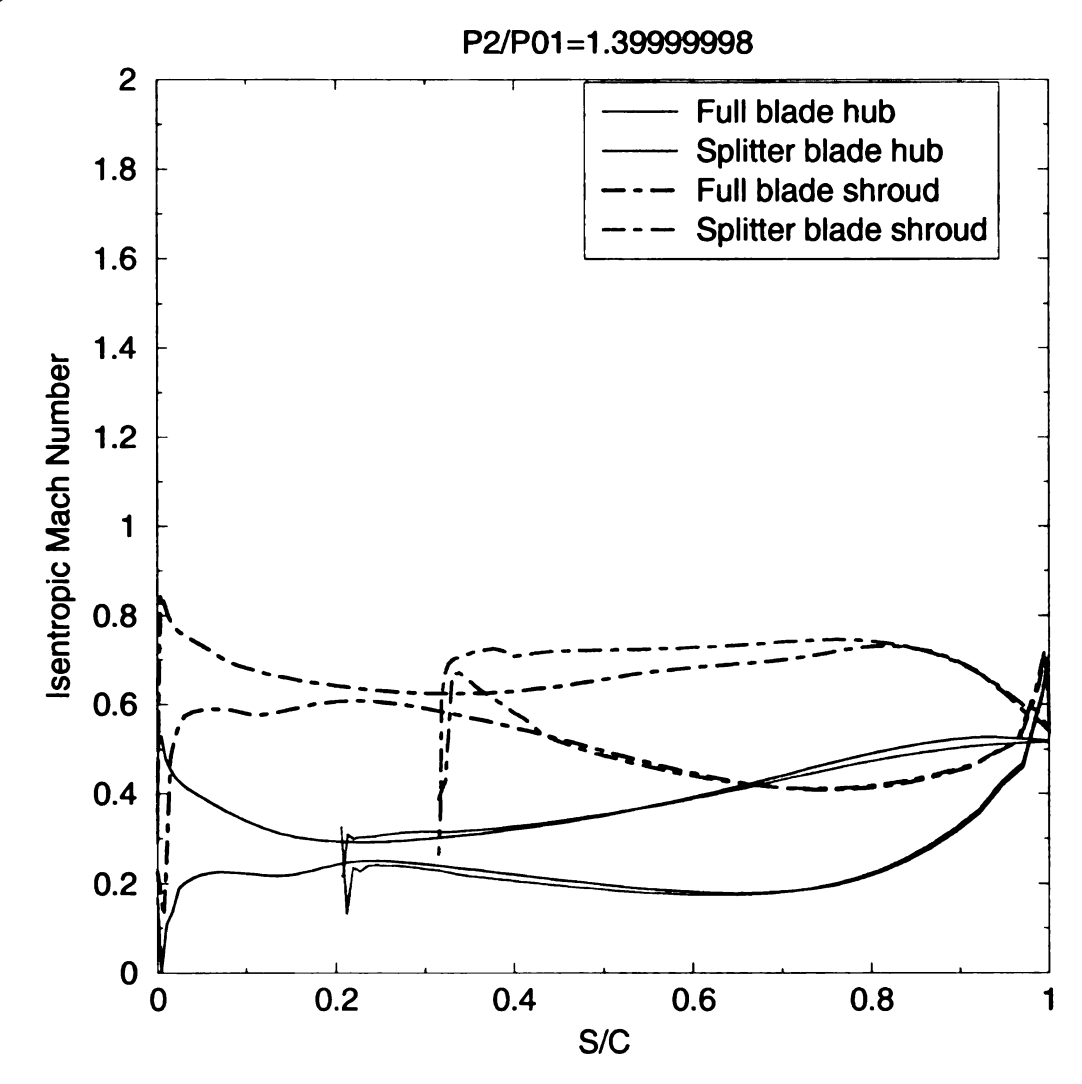


Figure 4.23 (cont'd)

Meridional Contours

34 Sample DATABASE USED

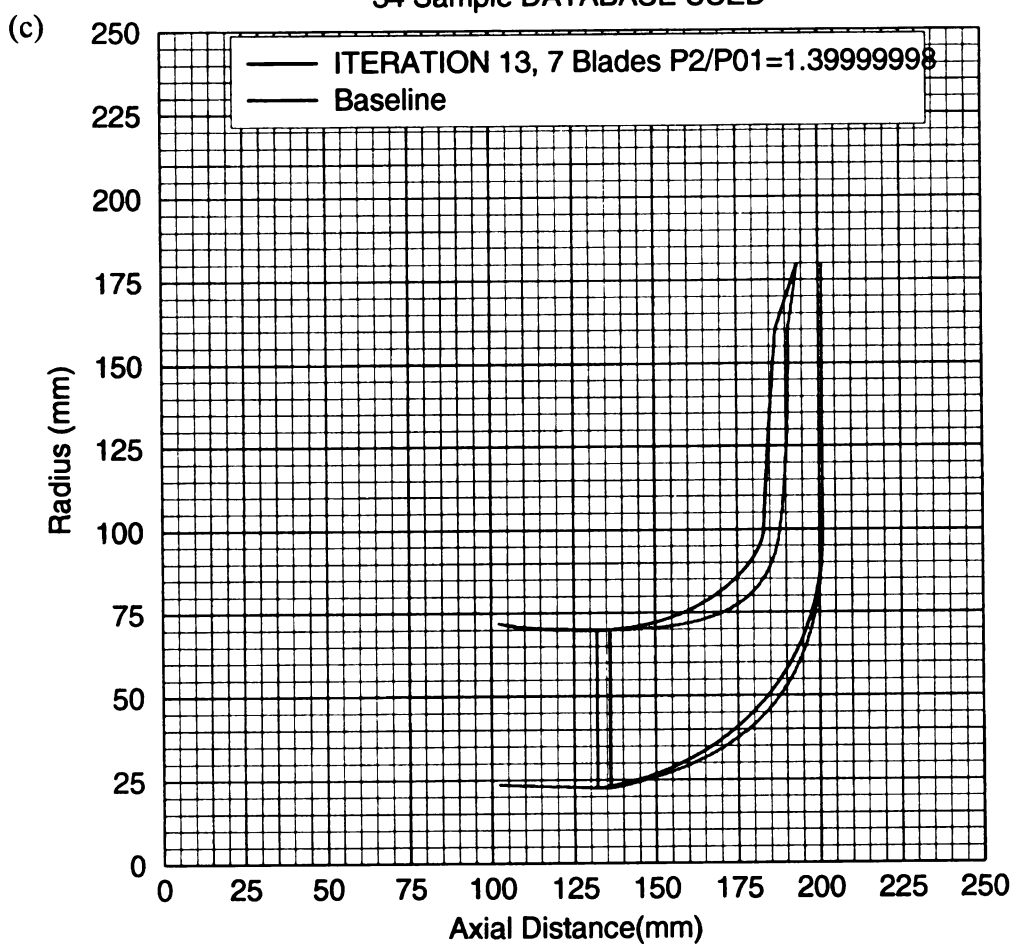


Figure 4.23 (cont'd)

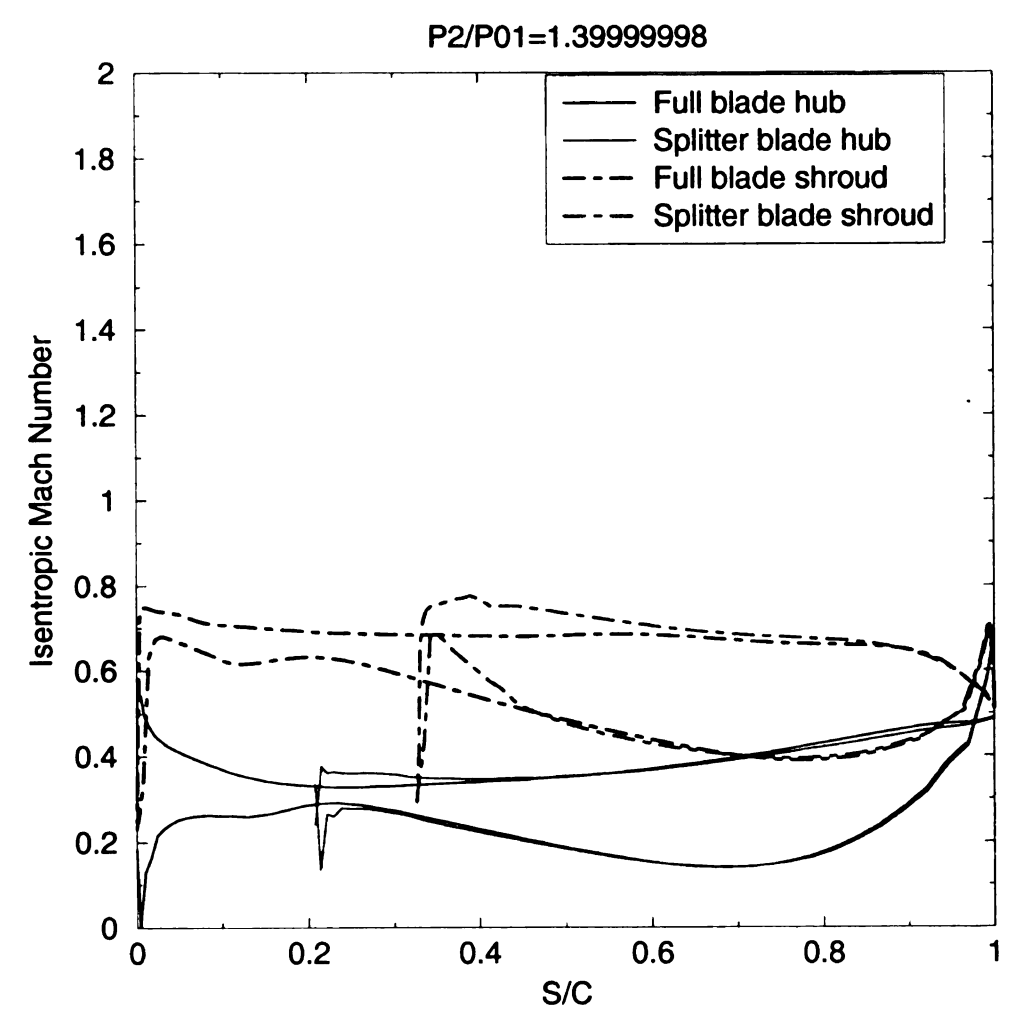


Figure 4.23 (cont'd)

(e) Meridional Contours



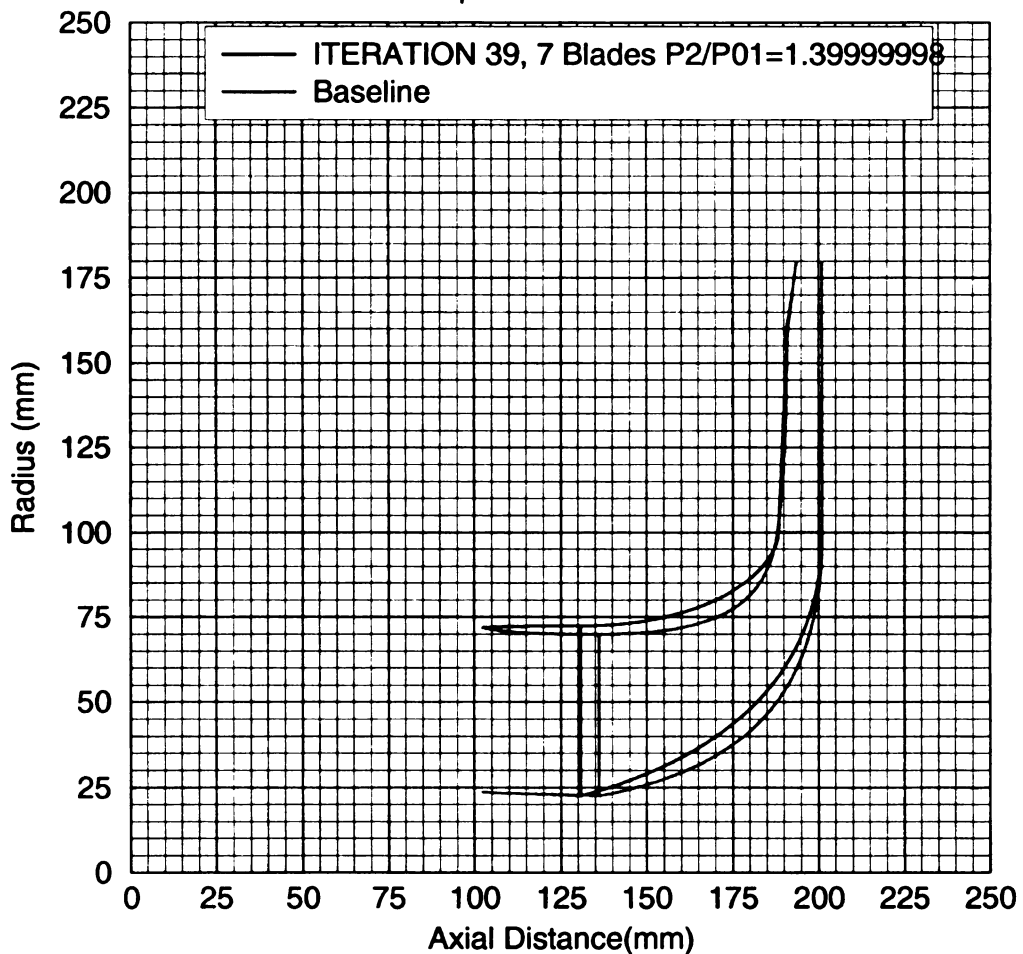


Figure 4.23 (cont'd)

ITERATION 39, 7 Blades

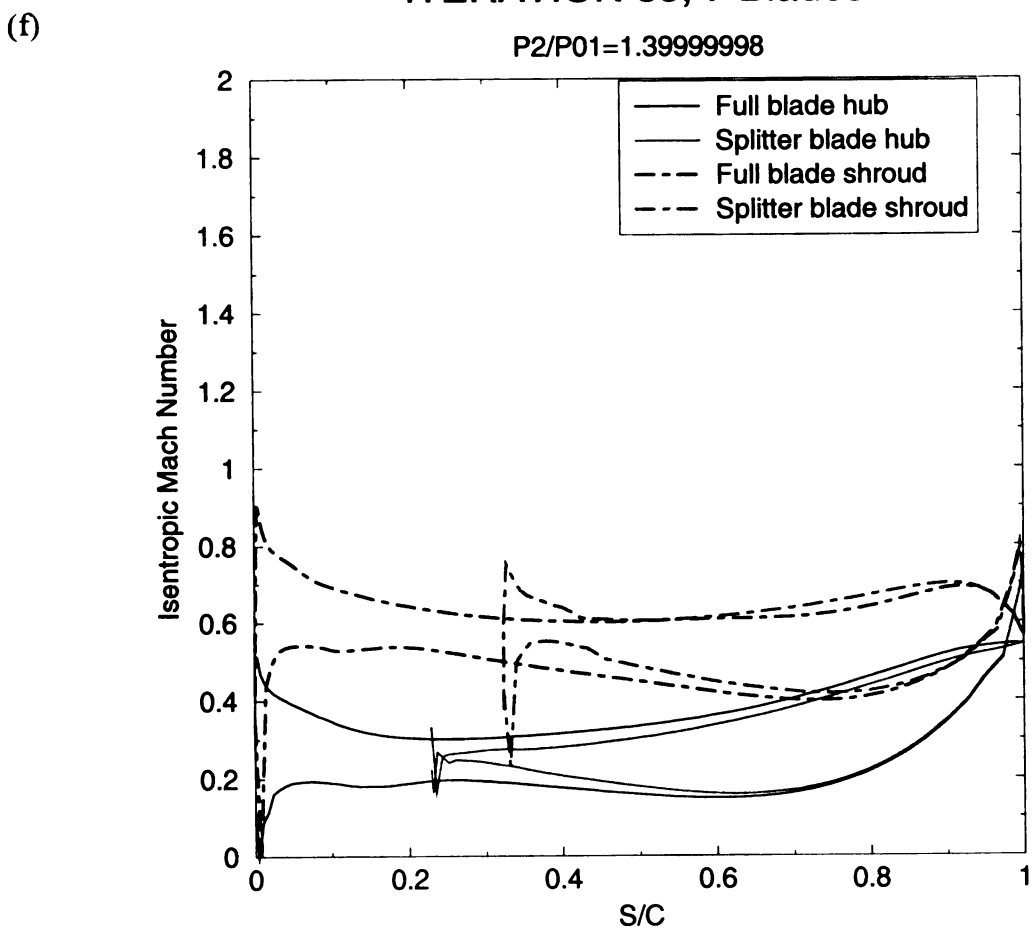


Figure 4.23 (cont'd)

Baseline Mach number Distribution

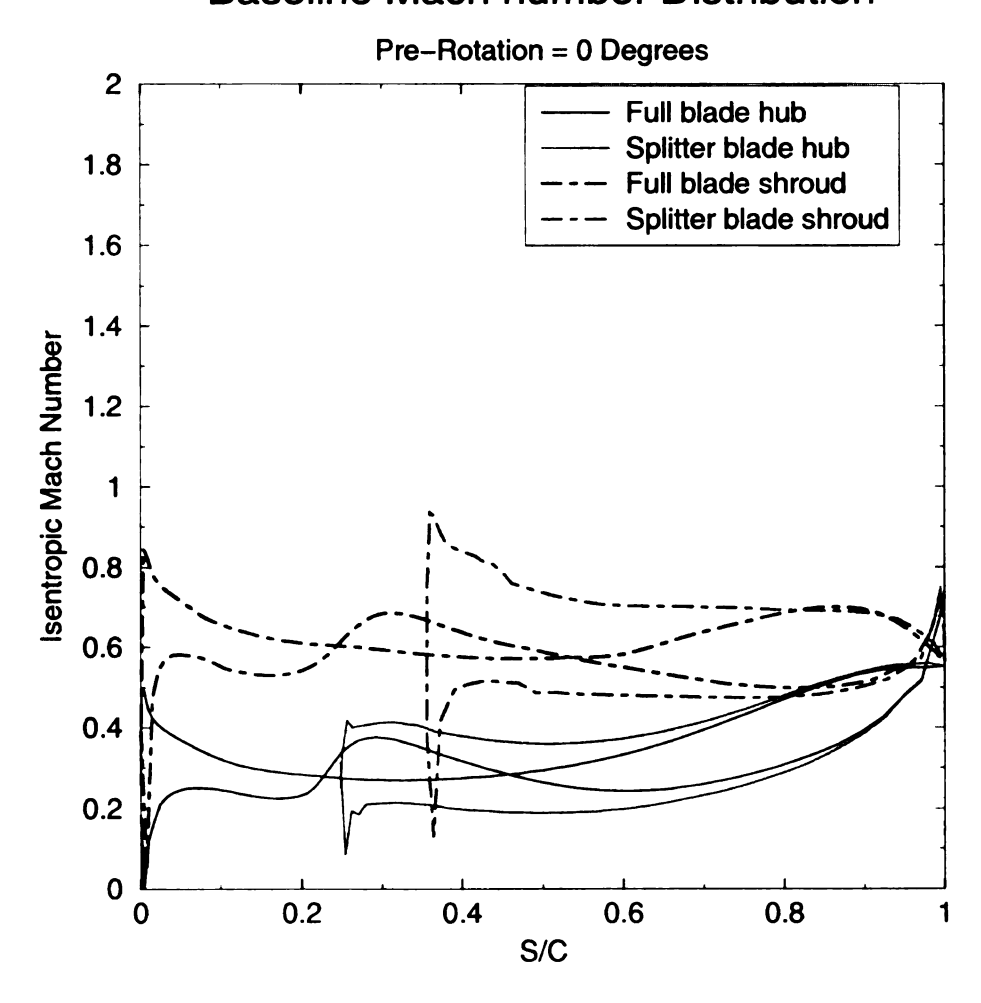


Figure 4.24 Baseline Mach number distribution. Illustrates the improvement.

4.6 Peformance of Optimum Geometry and Conclusion

All of the geometries that have been analyzed are rather good, when compared to the baseline. So the question is, how does one select the best one? It is quite difficult to say that there is the ultimate optimum geometry that is by far better than any other one. In fact, there are many suitable candidates for the operation of an air conditioner and other applications. So, the way in which the author chose the optimum was to take the one with the maximum total-static efficiency, because that is the quantity that we are trying to optimize using the system. Thus, using this criteria, the one that was chosen is Iteration

13. The mass flow is 1.451 Kg/sec which is 11.6 % more mass flow than the desired 1.3 Kg/sec. However, it is not likely that this machine will go directly to the market, and that the mass flow is really strictly required to be 1.3 Kg/sec. Perhaps, Iteration 39 was the wiser choice, if one considers mass flow and η_{TT} . Nevertheless, the author made the decision and thus single point optimum is Iteration 13. The performance map of this machine is displayed in Figure 4.25

Table 4.6 Characteristics of Single Point Optimum

Geometric Characteristics	
Beta-le-hub	21.70 Degrees
Beta-le-hub-sp	20.87 Degrees
Beta-le-shr	64.73 Degrees
Beta-le-shr-sp	64.60 Degrees
Beta-te	30.00 Degrees
Shroud clearance	0.575 mm
Max Hub Thickness	4 mm
Min Hub Thickness	3 mm
Max Shroud Thickness	3 mm
Min Shroud Thickness	2.5 mm
Percent blade chord length where finishes	25 %
the transition from Max to Min thickness.	
Thickness remains constant from this	
point all the way the trailing edge.	
Impeller Tip Radius	100 mm

(a) Pressure Ratio vs. Mass Flow Rate

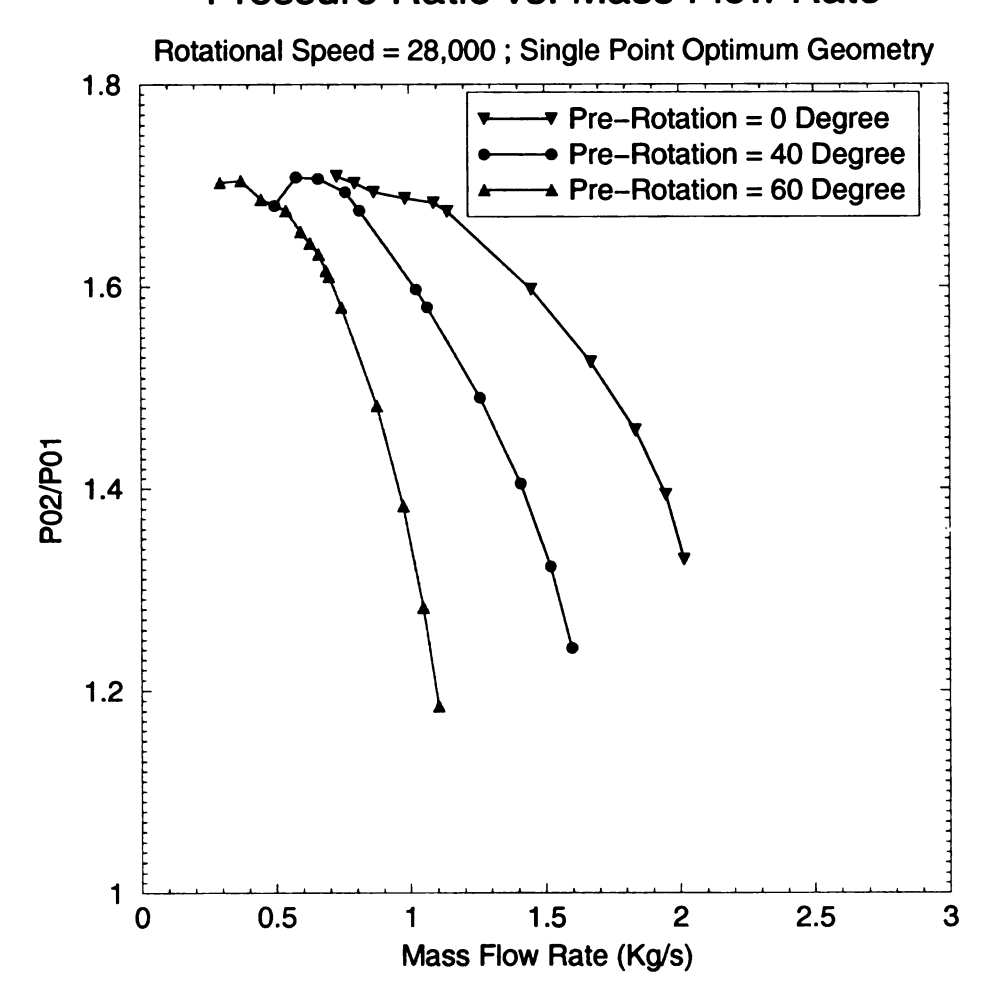


Figure 4.25 Performance Maps. (a) π (b) η_{ts} (c) η_{tt}

Total to Static Efficiency vs. Mass flow rate

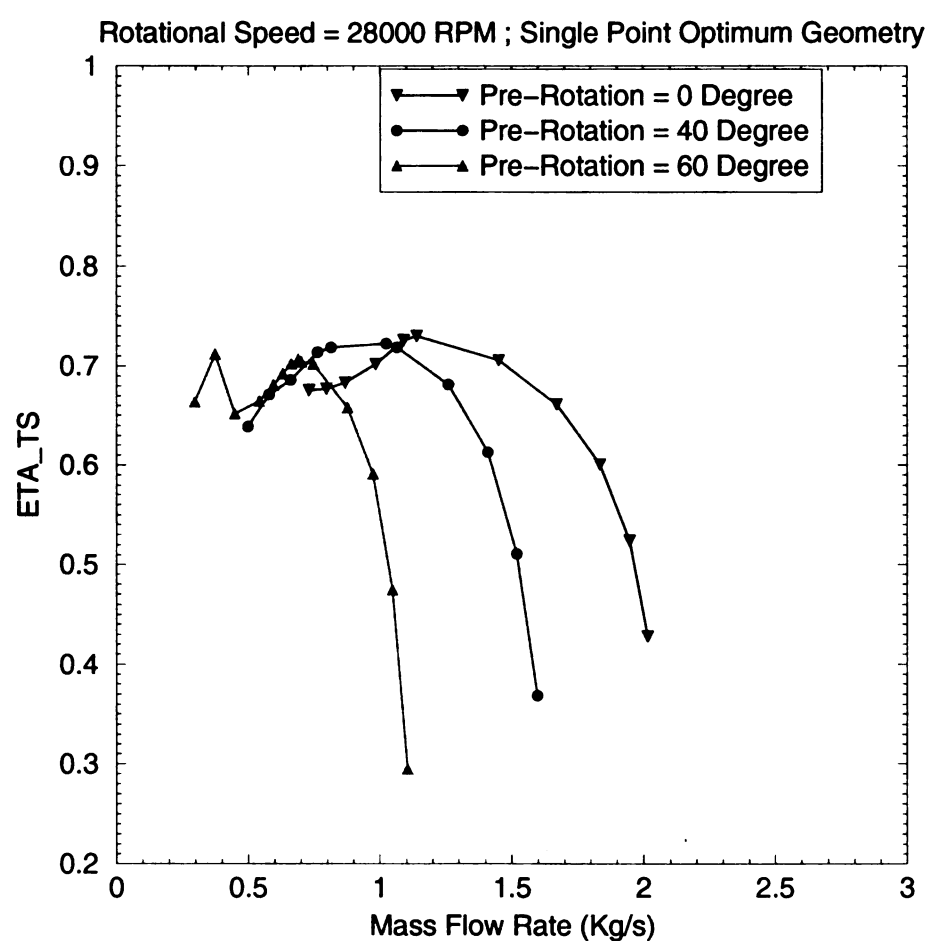


Figure 4.25 (cont'd)

Total to Total Efficiency vs. Mass flow rate

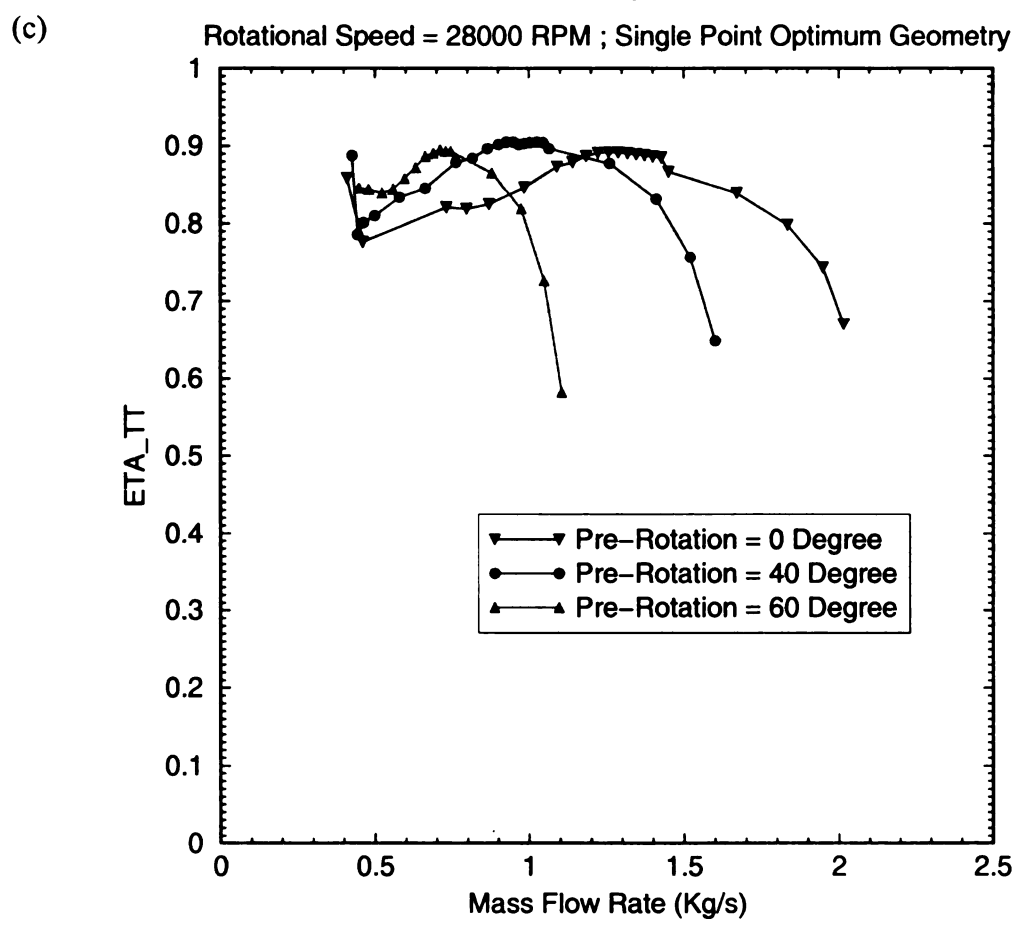


Figure 4.25 (cont'd)

Finally, the Mach number distributions of the single point optimum at various Prerotations demonstrate an improvement over the baseline. However there is a problem at 60 degrees Pre-Rotation. That is, there is some negative loading on the full blade hub and even worse, there is separation at the splitter blade hub, which is shown in Figure 4.26c. Thus, the geometry that gives an improvement by 7(63.5% to 70%) points of total-static efficiency for a pre-rotation of 0 degrees, however, will not be suitable for all three

operating points. Finally, this gives motivation to pursue the multi-point optimization in the next chapter.

(a)

Single Point Optimum 7 Blades

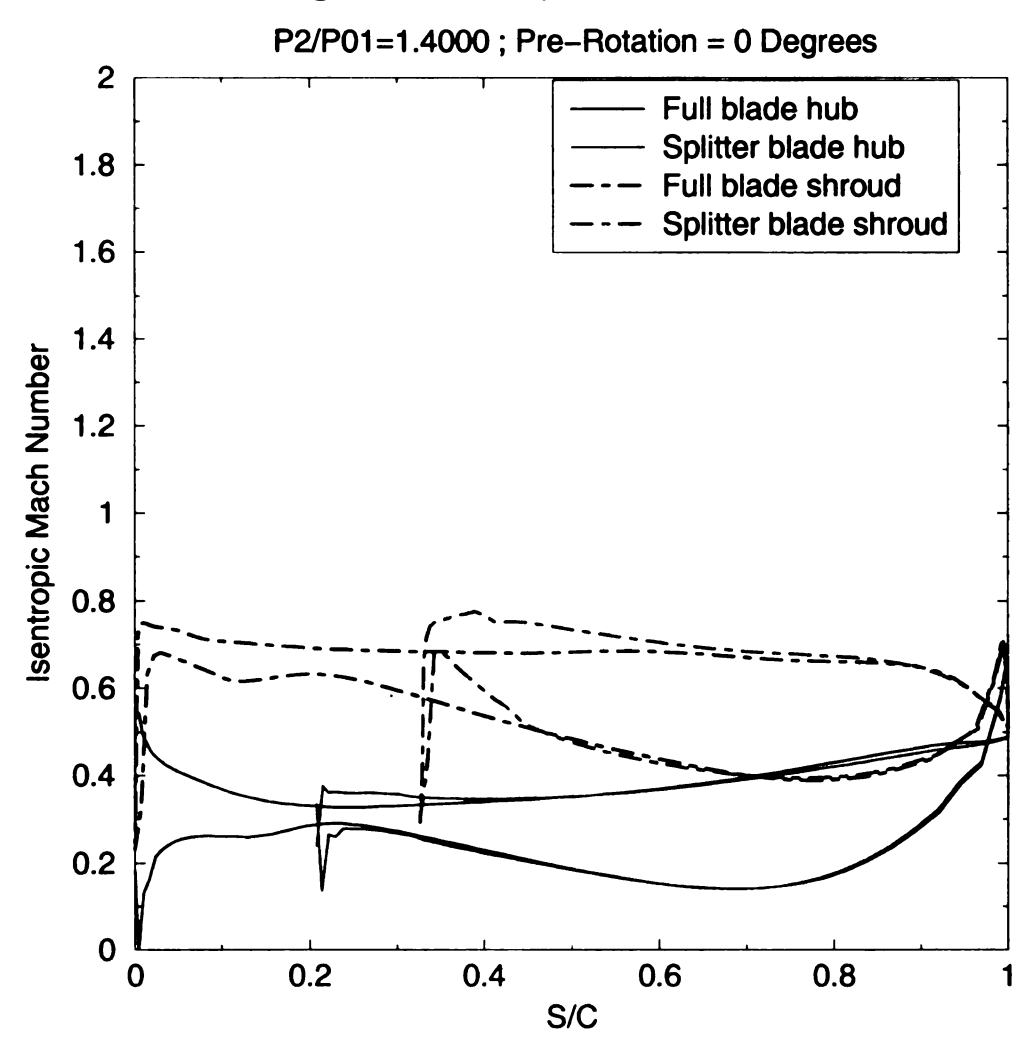


Figure 4.26 Mach Number Distributions at various Pre-Rotations: (a) 0 degrees (b) 40 degrees, (c) 60 degees

(b) Single Point Optimum, 7 Blades

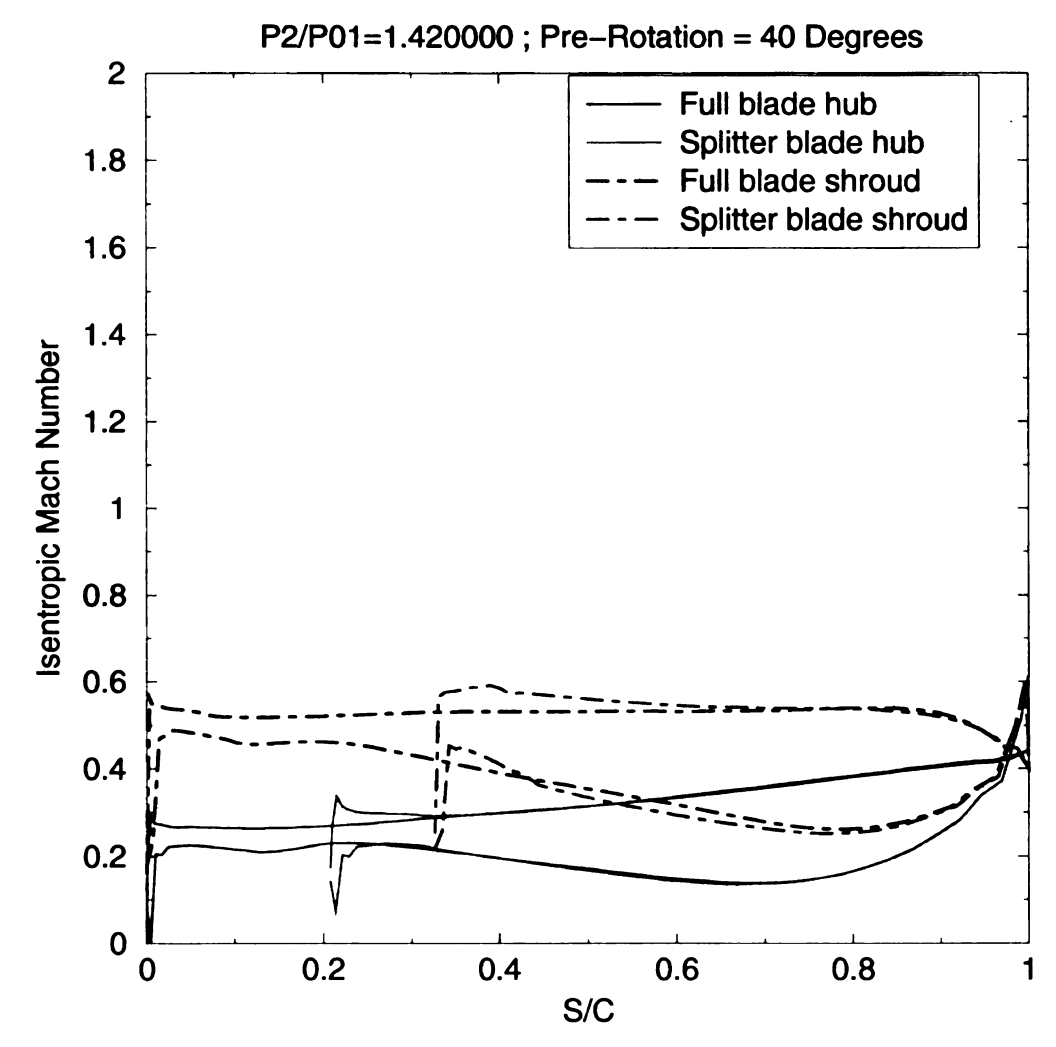


Figure 4.26 (cont'd)

Single Point Optimum, 7 Blades

P2/P01=1.425000; Pre-Rotation = 60 Degrees

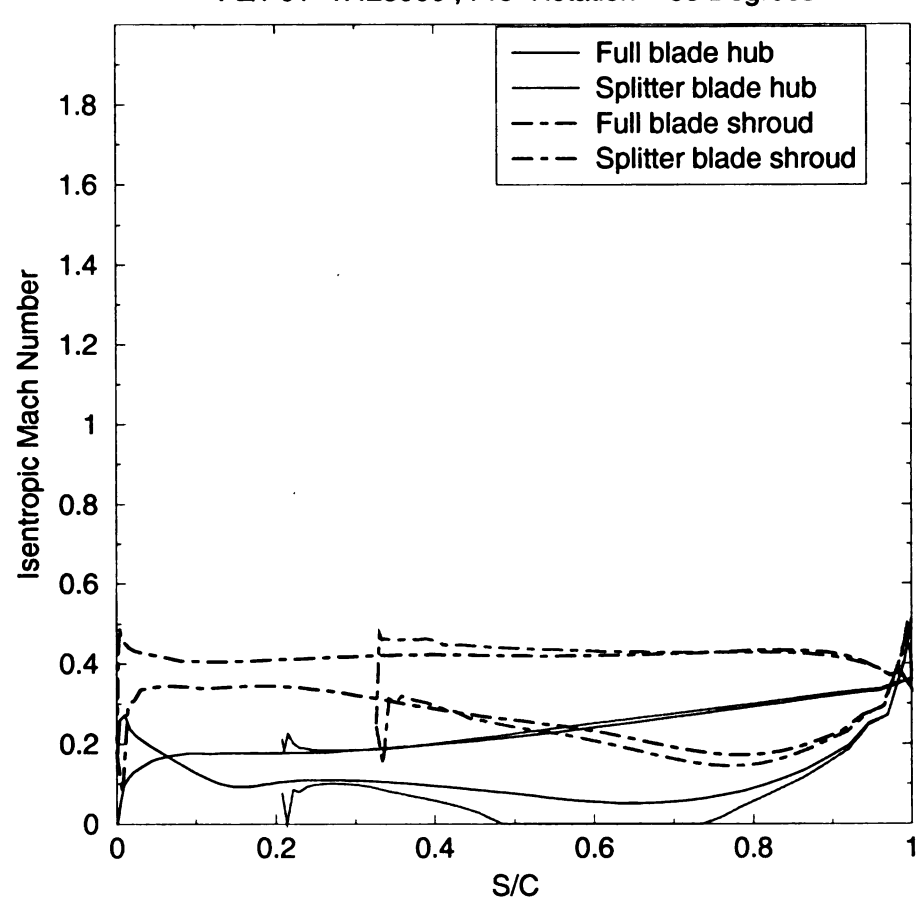


Figure 4.26 (cont'd)

CHAPTER 5

MULTIPOINT OPTIMIZATION

In this chapter the results of the multiple point optimization will be discussed. The design space used is the same as for the single point case and so is the performance prediction. Consequently, these concepts will not be repeated. However, the reader is reminded that the number of Artificial Neural Networks used is now 21, instead of the 7 used for the single point optimization. For more details about the above mentioned, one should consult chapter 4.

5.1 Objective Function and GA settings

5.1.1 Objective Function

As discussed in the previous chapter, the ANN predicts the performance of an individual. This performance is then converted to an objective function with which the genetic algorithm will minimize. The Genetic algorithm mimics biological evolution and thus is a statistical or non-deterministic process. The purpose is that blades will reproduce other better geometries and the poor geometries will tend to die out. This is why the term survival of the fittest is usually used. A somewhat in depth treatment of the operational principle of the GA was given in section 2.3; consequently, we will progress to the specifics that apply to our design case.

The objective function used by the genetic algorithm is displayed below:

$$OF = \sum_{1}^{Numofpo \text{ int } s=3} W_i OP_i = W_1 OP_1 + W_2 OP_2 + W_3 OP_3$$
 [5.1]

$$OP_{i} = \left(W_{massflow}P_{mass_diff}P_{mass_diff}P_{mass_diff} + W_{\eta_{ls}}P_{\eta_{ls}} + W_{lu}P_{lu} + W_{nl}P_{nl}\right)_{i} [5.2]$$

This function is a weighted sum of various penalties used to quantify the performance. A higher value of the objective function implies a lower performance impeller, while a lower value represents good impeller performance. The penalties in equation [5.2] are the same as discussed in section 4.4.1, and as a consequence will not be repeated here.

For the multiple point case various overall weights (W_1, W_2, W_3) were used to represent the various seasons of the year. That is, in the summer one requires more mass flow to cool the building. Even if the summer is shorter than spring and autumn, the air conditioner could possibly waste more energy in that season than in the other two seasons combined. This is simply because more power is required to pump a large amount of Freon through the building and if this is done inefficiently, a lot of energy can be wasted. Thus, for operating point 1, which represents the summer, the overall weight was chosen to be $W_1 = 55$ %, while the others were $W_2=30$ %, $W_3=15$ %. The way in which this was implemented was through the following procedure. This procedure is presented for anyone whom will try to re-create and understand how the author calculated the weights.

First of all, there is no input file to implement these overall weights. Thus, one must calculate manually these weights and put them in the existing input files (weights.in1,

weight.in2, weights.in3). Once the weights are chosen for operating point 1 (Pre-Rotation = 0 Degrees), as seen in the first column of Table 5.1 below, to get the weights for the other two operating points, the following procedure should be consulted. This procedure is applied to the first row of Table 5.1 Finally, the procedure was repeated for the rest of the penalties.

1. To calculate 100 % weight, assuming the weights for operating point 1 are already at 55 %.

$$\frac{500}{0.55} = 909.09$$

2. To Calculate 30 % weight.

$$909.09(0.30) = 276$$

3. To Calculate 15 % weight.

$$909.09(0.15) = 136$$

This was done, because if one multiplies the original values in the first column by 0.30 and 0.15, the values of the penalties can be a little on the low side. Also one does not know what should be the order of magnitude of the Penalty input to the GA. In any event, it can be seen from Table 5.1 and the convergence history, discussed in section 5.2.2, that more emphasis is placed on OP1 (summer) than the other two operating points.

Table 5.1 Weights used in Multiple Point Optimization

Penalty	Weight 1 (OP1)	Weight 2 (OP2)	Weight 2 (OP3)
Mass Flow	500	273	136
Mass Difference	100000	54545	27273
Total to static Efficiency	600	327	164
Loading unbalance at hub	100	54	27
Loading unbalance at shroud	100	54	27
Negative loading at hub	3300	1800	900
Negative loading at shroud	3300	1800	900

5.1.2 GA Settings

Before performing the optimization one must select the GA and ANN settings. The only parameter that was changed for the multiple point optimization was the mutation probability. This is because the optimization system was updated such that it calculated the substring length. Then from GA theory [2], it was advised by the system manager that the following parameters be tried. In any event, the author is unsure of the impact, if any, the change in the mutation probability (from 1 % to 0.45%) had on the results.

Table 5.2 GA and ANN Parameters

Parameter	Settings		
GA			
irestrt	1		
npopsiz	50		
pmutate	0.45%		
maxgen	100		
pcross	75%		
ielite	1		
itourny	1		
pcreep	5%		
lunifrm	0		
nchild	2		
ANN			
TRAINING	80%		
NANN	7		

Where the parameters in the table are defined as follows (see reference [4]):

GA:

- irestrt = 0 for a new GA run; 1 for a restart continuation of a GA run
- npopsiz = The population size of a GA run
- pmutate = Jump mutation probability
- maxgen = The maximum number of generations to be run by the GA
- pcross = Cross over probability
- ielite = 1; Implies that the best individual is replicated into the next generation
- itourny = 1; Implies tournament selection
- pcreep = Creep mutation probability
- iunifrm = 0; Implies single point crossover
- nchild = 2 children are produced per pair of parents

ANN:

- TRAINING = 80 % of all the samples are used for training of the ANN
- NANN = Number of neural networks per operating point.

5.2 Presentation of the Optimization

In this section one will discuss the database creation, the convergence history, and finally compare a few Navier-Stokes results which will lead to the selection of the multipoint optimum. However, one must first mention the operating points that were chosen.

The operating point was chosen near high efficiency plateau as can be seen in the following figure. A designer should optimize at a point with sufficient surge margin.

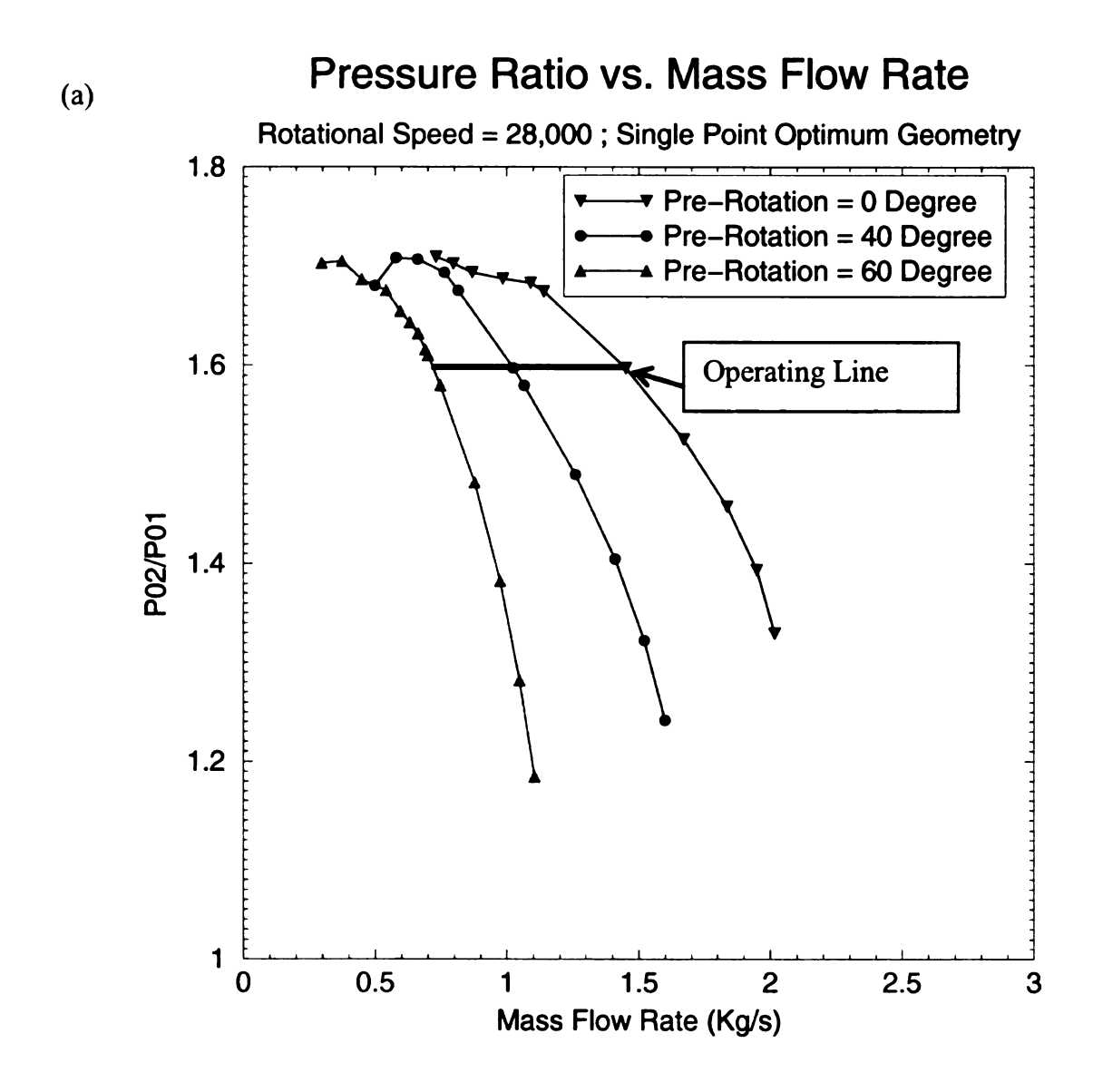


Figure 5. 1 The operating points chosen for optimization. (a). PI (b). TS



(b)

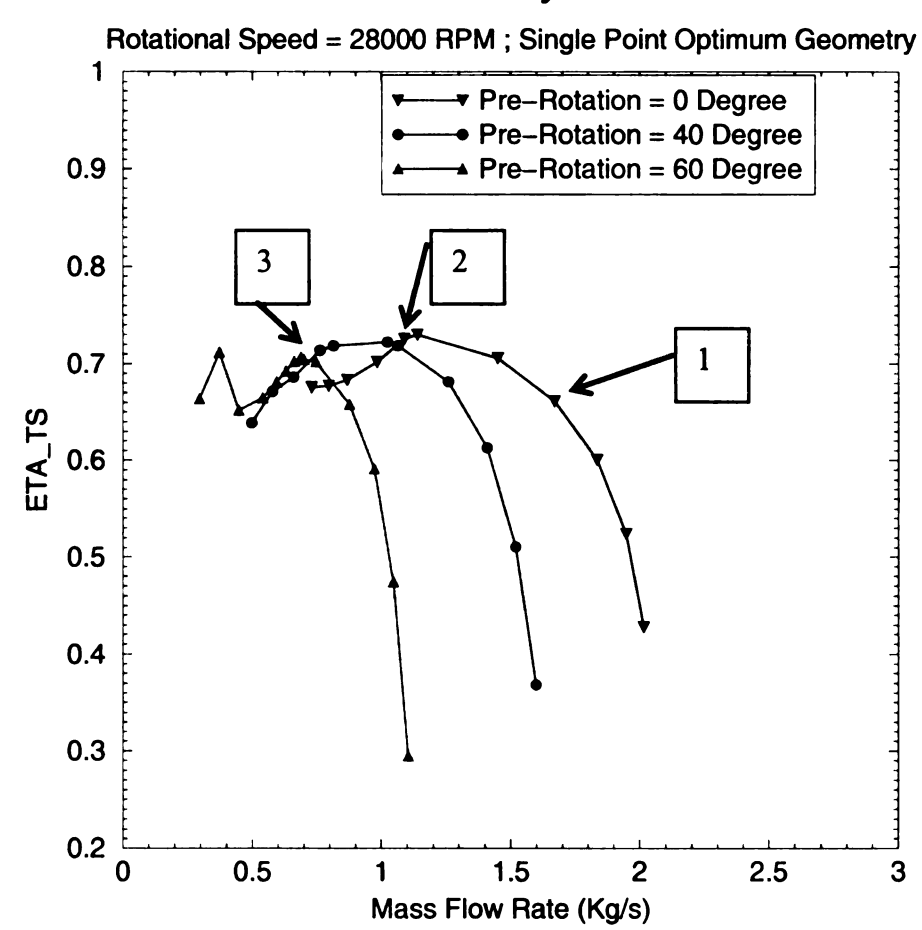


Figure 5.1 (cont'd)

The mass flow required for the first operating point was chosen to be 1.3 Kg/sec. While for operating point 2 it is 1.0 Kg/sec and 0.7 Kg/sec for operating point 3. The efficiency requirement on total-static efficiency was set at 90% as mentioned before in chapter 4. The reason being that one does not expect to improve the total-static by more than 25 points. That is, going from 63% to 90% seems a little unreachable, and it has been observed that is it better to put a value that is within expectation, rather than to just put 100%.

5.2.1 Database

As explained before in the optimization method chapter, the whole original knowledge of the ANN and GA comes from a reference database. The database contains 35 Navier-Stokes calculations per operating point, coming from different geometries representing the design space within the limits defined in chapter 4. The selection of the geometries can be realized in two different ways, either randomly, or using the design of experiment method, DOE technique. It can be used in a wide variety of applications when some parametric analyses are needed. Its aim is to construct a more representative and systematic database, performing a statistical survey of the design parameters. This approach was used for 32 of our samples. Indeed, it presents the disadvantage of considering only to extreme values (25% and 75% over the lower limit) of the parameter's range so that in the end not much is known about the center of the design space. This is why a central point case is run in which the variables are forced to be 50% over the lower limits. Cases 1-32 were given by the DOE, while the other samples that were included were the baseline geometry and the single point optimum geometry.

In the Multi-point optimization, the same geometries that were utilized in the single point case were used for the multi-case. The geometries were simply run at the other prerotation values of 40 and 60 degrees. Finally, tables containing information about the NS computations of the database are displayed below in Tables 5.3, 5.4, and 5.5. Finally, if one takes the time to survey all the tables in the same manner as was done in chapter 4, then it is evident that none of the samples in the database have the optimum combination of characteristics. This is why we will now progress to the results of the optimization in hopes that the system can find the optimum.

Table 5.3 NS results of the Database at IGV Setting Angle = 0 Degrees

DB Sample #	Mass Flow	ETA_TT	ETA_TS	P02/P01	P2/P01	Inlet Lean (Deg)	Outlet Lean (Deg)
1	1.456	0.865	0.680	1.599	1.453	-21.766	45.000
2	1.102	0.717	0.575	1.564	1.437	-13.496	45.000
3	1.311	0.832	0.660	1.574	1.440	-9.928	45.000
4	1.370	0.820	0.675	1.603	1.481	-12.970	45.000
5	1.437	0.826	0.678	1.612	1.486	-6.092	45.000
6	1.350	0.821	0.643	1.585	1.442	-6.751	45.000
7	1.177	0.761	0.617	1.575	1.452	-15.328	45.000
8	1.382	0.852	0.674	1.587	1.448	-5.001	45.000
9	1.187	0.799	0.636	1.563	1.433	-10.028	45.000
10	1.117	0.727	0.585	1.559	1.435	-2.540	45.000
11	1.402	0.851	0.672	1.582	1.443	0.000	42.882
12	1.228	0.729	0.582	1.571	1.441	-2.355	45.000
13	1.037	0.680	0.541	1.542	1.417	-8.831	45.000
14	1.213	0.795	0.631	1.556	1.426	-9.086	45.000
15	1.298	0.791	0.645	1.589	1.465	-20.146	45.000
16	1.413	0.839	0.656	1.600	1.452	-10.480	45.000
17	1.305	0.841	0.670	1.575	1.443	-14.990	45.000
18	1.017	0.697	0.556	1.554	1.428	-17.209	45.000
19	1.313	0.832	0.662	1.568	1.436	-13.680	45.000
20	1.430	0.840	0.693	1.606	1.486	-25.641	45.000
21	1.516	0.836	0.680	1.637	1.501	0.000	14.790
22	1.322	0.818	0.644	1.575	1.437	0.000	43.814
23	1.221	0.777	0.632	1.581	1.458	-6.349	45.000
24	1.362	0.848	0.673	1.580	1.444	-8.861	45.000
25	1.245	0.802	0.634	1.566	1.432	0.000	34.625
26	0.976	0.682	0.542	1.544	1.418	-0.260	45.000
27	1.442	0.842	0.658	1.583	1.439	0.000	27.734
28	1.079	0.698	0.557	1.547	1.423	-8.991	45.000
29	1.295	0.768	0.617	1.595	1.462	0.000	0.649
30	1.323	0.810	0.635	1.565	1.428	0.000	30.363
31	1.252	0.776	0.631	1.574	1.452	-4.616	45.000
32	1.248	0.810	0.642	1.573	1.438	-6.748	45.000
33	1.371	0.821	0.664	1.596	1.466	-6.854	45.000
Single OPT	1.451	0.867	0.705	1.597	1.470	0.000	43.539
Baseline	1.257	0.824	0.635	1.562	1.417	-4.336	45.000

Table 5.4 NS results of the Database at IGV Setting Angle = 40 Degrees

DB Sample #	Mass Flow	IETA TT	ETA TS	P02/P01	P2/P01	Inlet Lean (Deg)	Outlet Lean (Deg)
1.000	1.053	0.891	0.702	1.593	1.451	-21.766	45.000
2	0.678	0.678	0.525	1.586	1.437	-13.496	45.000
3	0.954	0.874	0.694	1.583	1,447	-9.928	45.000
4	0.921	0.826	0.660	1.602	1,464	-12.970	45.000
5	0.938	0.826	0.657	1.603	1,463	-6.092	45.000
6	1.010	0.870	0.679	1.597	1,449	-6.751	45.000
7	0.748	0.726	0.566	1.586	1.440	-15.328	45.000
8	1,013	0.889	0.704	1.595	1.455	-5.001	45.000
9	0.887	0.841	0.668	1.584	1.448	-10.028	45.000
10	0.766	0.728	0.569	1.587	1,441	-2.540	45.000
11	1.011	0.887	0.702	1.587	1,448	0.000	42.882
12	0.814	0.727	0.566	1.588	1,440	-2.355	45.000
13	0.736	0.691	0.536	1.575	1,430	-8.831	45.000
14	0.906	0.842	0.667	1.577	1,441	-9.086	45.000
15	0.807	0.749	0.586	1.590	1.445	-20.146	45.000
16	1.026	0.880	0.689	1.610	1.459	-10.480	45.000
17	0.976	0.880	0.698	1.588	1,450	-14,990	45.000
18	0.679	0.680	0.526	1.585	1.436	-17.209	45.000
19	0.950	0.874	0.697	1.579	1,446	-13.680	45.000
20	1.021	0.877	0.708	1.613	1.478	-25.641	45.000
21	1.136	0.881	0.698	1.626	1.478	0.000	14.790
22	0.971	0.864	0.680	1.587	1.446	0.000	43.814
23	0.815	0.774	0.608	1.592	1.448	-6.349	45.000
24	0.986	0.885	0.704	1.589	1.452	-8.861	45.000
25	0.967	0.862	0.680	1.585	1.446	0.000	34.625
26	0.732	0.729	0.566	1.586	1.438	-0.260	45.000
27	1.053	0.890	0.698	1.587	1.444	0.000	27.734
28	0.760	0.718	0.558	1.579	1.434	-8.991	45.000
29	1.029	0.836	0.661	1.608	1.463	0.000	0.649
30	0.991	0.869	0.684	1.578	1.439	0.000	30.363
31	0.856	0.791	0.625	1.593	1.452	-4.616	45.000
32	0.914	0.847	0.671	1.593	1.453	-6.748	45.000
33	0.979	0.857	0.684	1.604	1.465	-6.854	45.000
Single OPT	1.024	0.897	0.722	1.598	1.465	0.000	43.539
Baseline	0.941	0.869	0.681	1.574	1.433	-4.336	45.000

1	0.718	0.885	0.693	1.606	1.457	-21.766	45.000
2	0.315	0.428	0.291	1.458	1.298	-13.496	45.000
3	0.637	0.833	0.653	1.593	1.448	-9.928	45.000
4	0.526	0.714	0.540	1.595	1.432	-12.970	45.000
5	0.534	0.696	0.526	1.596	1.432	-6.092	45.000
6	0.630	0.809	0.619	1.589	1.433	-6.751	45.000
7	0.378	0.477	0.327	1.464	1.305	-15.328	45.000
8	0.683	0.869	0.685	1.612	1.465	-5.001	45.000
9	0.566	0.779	0.594	1.578	1.423	-10.028	45.000
10	0.404	0.532	0.373	1.486	1.326	-2.540	45.000
11	0.707	0.881	0.690	1.592	1.446	0.000	42.882
12	0.444	0.576	0.429	1.593	1.422	-2.355	45.000
13	0.428	0.575	0.426	1.587	1.416	-8.831	45.000
14	0.655	0.856	0.665	1.589	1,440	-9.086	45.000
15	0.442	0.560	0.399	1,505	1.345	-20,146	45.000
16	0.538	0.787	0.585	1.580	1,412	-10,480	45,000
17	0.662	0.863	0.679	1.604	1.459	-14.990	45,000
18	0.334	0.440	0.299	1.463	1.301	-17.209	45.000
19	0.654	0.858	0.680	1.595	1.455	-13.680	45.000
20	0.568	0.790	0.602	1.599	1.438	-25.641	45.000
21	0.779	0.849	0.656	1.622	1.461	0.000	14.790
22	0.637	0.818	0.631	1.585	1.434	0.000	43.814
23	0.429	0.568	0.404	1.505	1.344	-6.349	45.000
24	0.681	0.887	0.698	1.608	1.461	-8.861	45.000
25	0.708	0.876	0.683	1.596	1.448	0.000	34.625
26	0.434	0.593	0.423	1.518	1.353	-0.260	45.000
27	0.745	0.892	0.690	1.591	1.439	0.000	27.734
28	0.441	0.600	0.445	1.587	1.417	-8.991	45.000
29	0.733	0.814	0.627	1.604	1.447	0.000	0.649
30	0.716	0.881	0.684	1.583	1.436	0.000	30.363
31	0.481	0.662	0.501	1.612	1.443	-4.616	45.000
32	0.538	0.779	0.584	1.576	1.414	-6.748	45.000
33	0.590	0.786	0.597	1.588	1.429	-6.854	45.000
Single OPT	0.701	0.890	0.704	1.610	1.465	0.000	43.539
Baseline	0.657	0.892	0.699	1,596	1.450	-4.336	45.000

5.2.2 Convergence history

In theory, the NS and ANN penalties should overlap each other in order to say that the system has found the optimum geometry, or converged. One can see in Figure 5.2 that the NS and ANN penalties slowly start to come together. A possible reason why the lines do not come fully together could be that other penalties are offsetting each other. For instance, in Figure 5.3 the ANN and NS actually come together at various places. Another reason is that it may not be fully converged because there are a lot of design variables and 3 operating points. Thus, it can be expected that it may really take 100 or more Iterations to fully converge. This however was unfortunately unobtainable due to

lack of time. In the Figures (5.2-5.6), the upper left hand corner represents operating point 1 as defined in Figure 5.1. The other two operating points are also labeled in the figure according to Figure 5.1. Finally, for the sake of completeness, the rest of the convergence histories are listed.

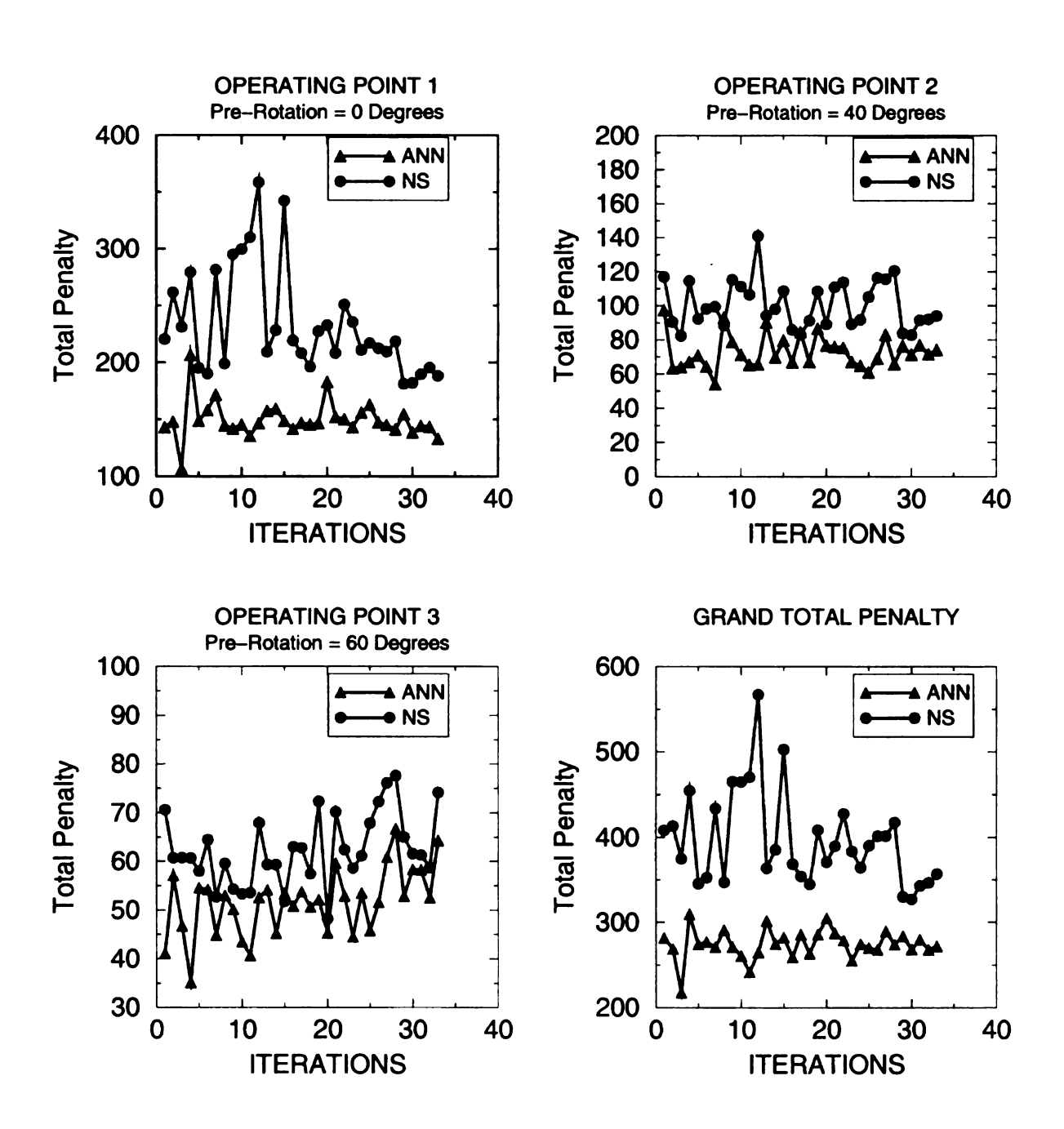


Figure 5.2 Convergence History of Total Penalty at the three operating points.

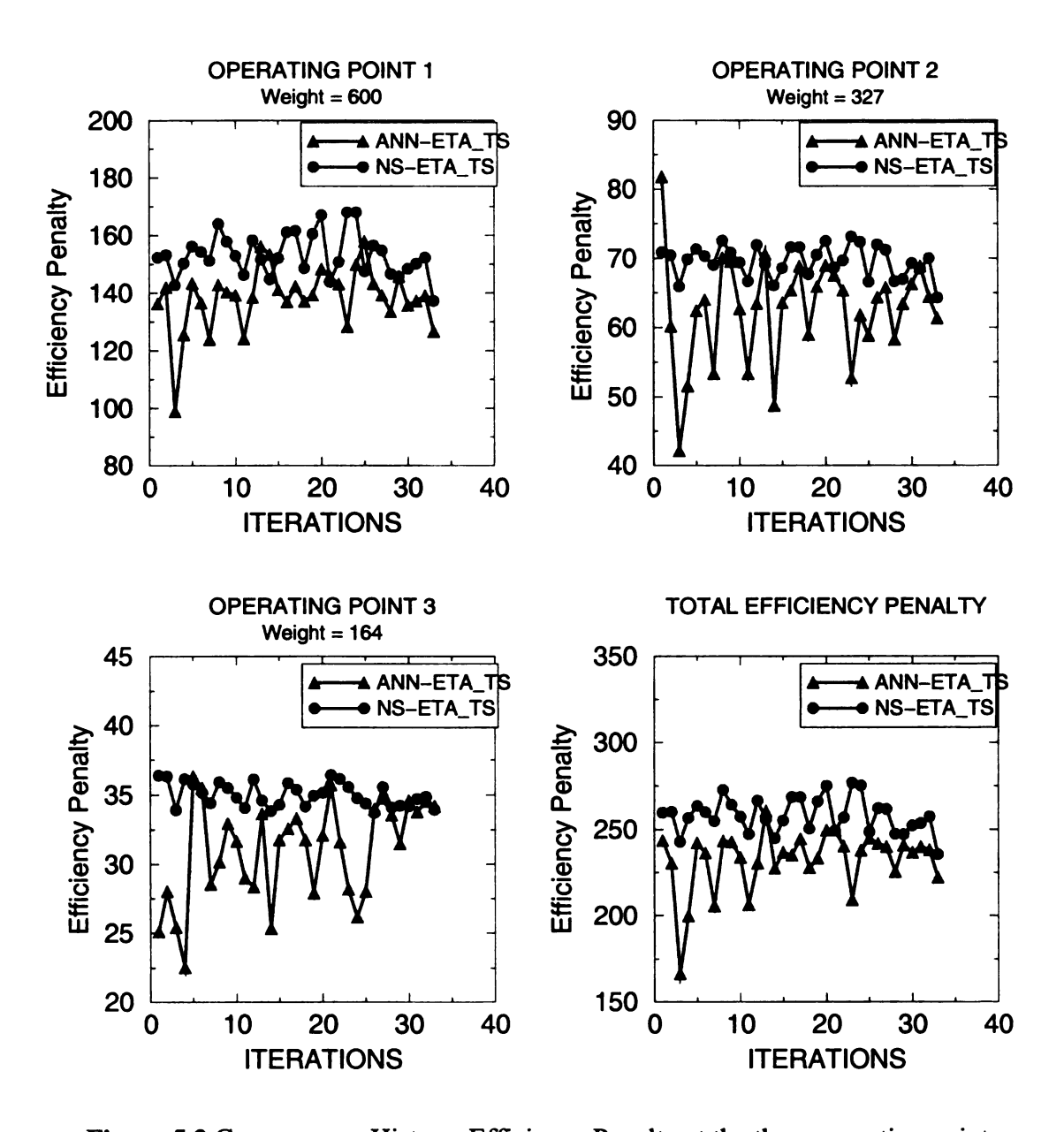


Figure 5.3 Convergence History. Efficiency Penalty at the three operating points.

143

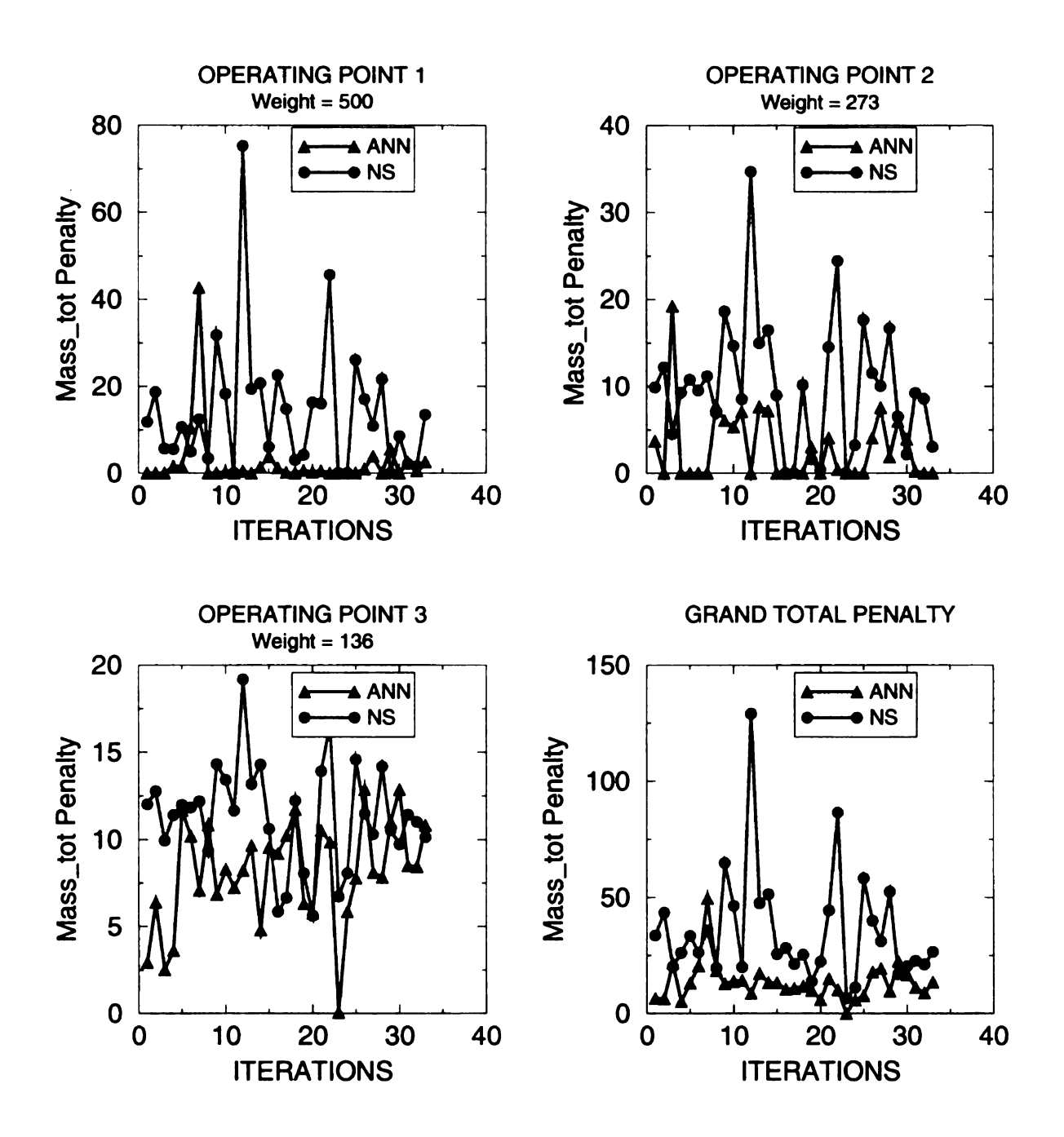


Figure 5.4 Convergence History. Mass Penalty at the three operating points.

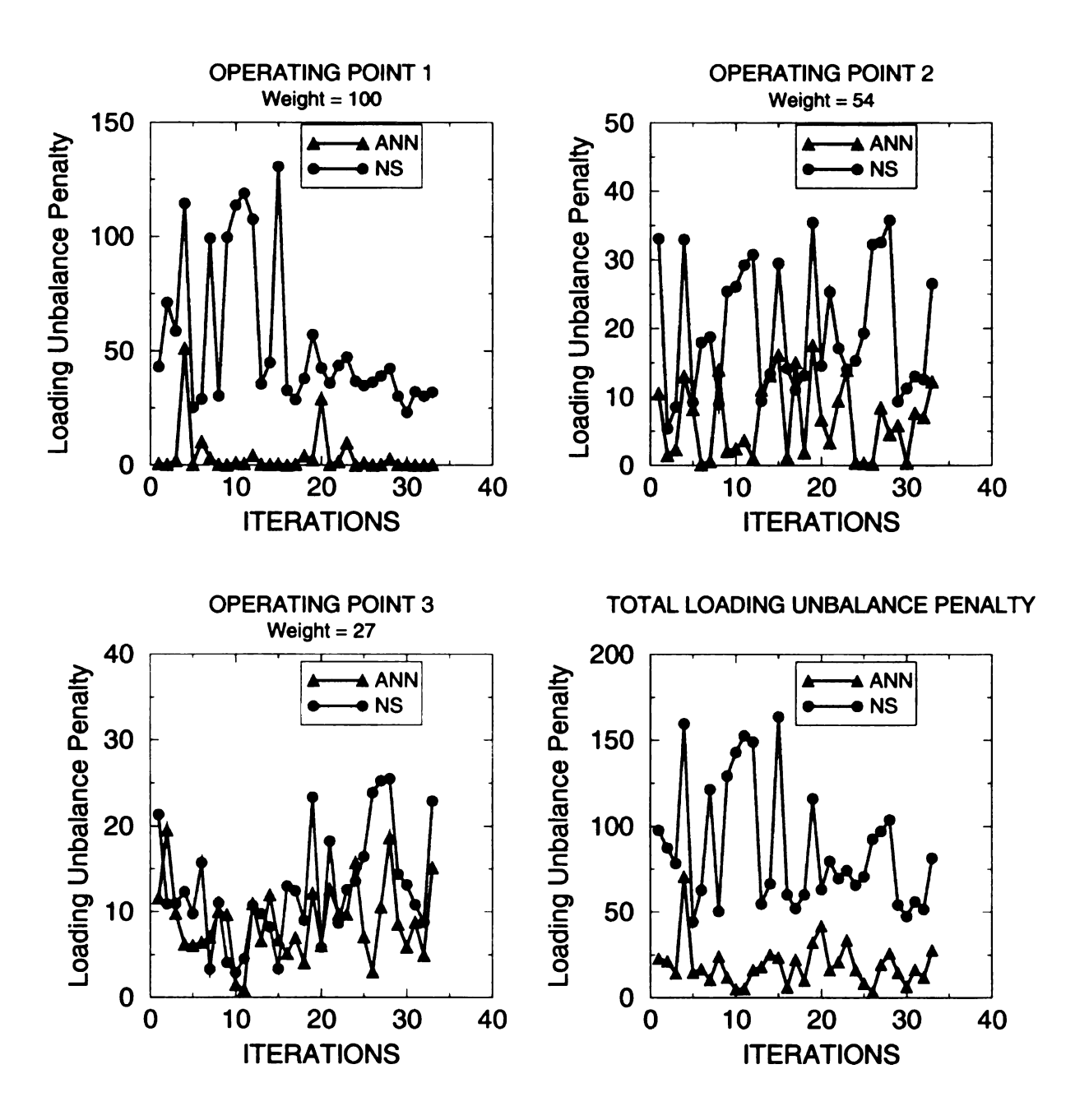


Figure 5.5 Convergence History. Unbalance Penalty at the three operating points.

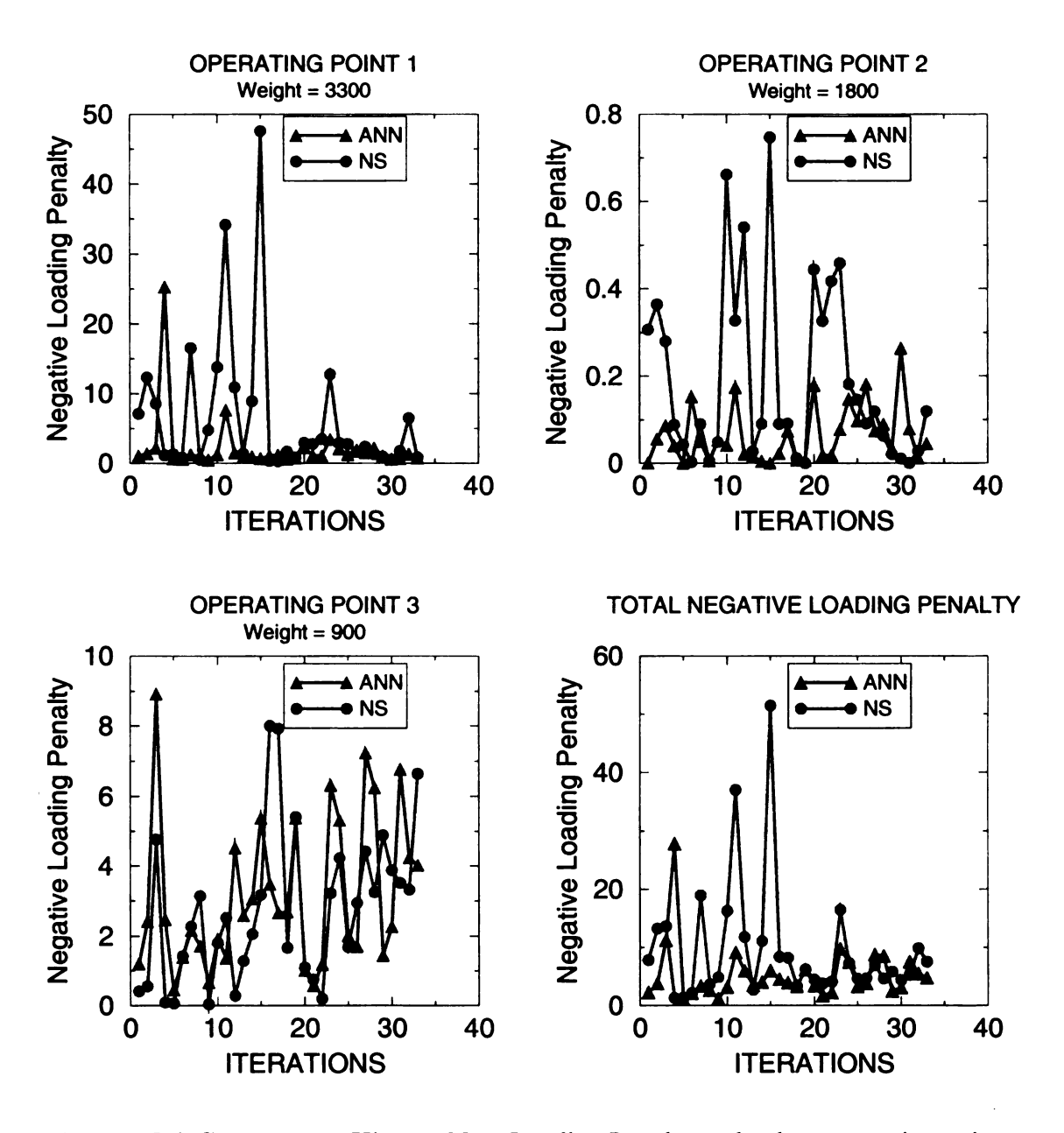


Figure 5.6 Convergence History. Neg. Loading Penalty at the three operating points.

5.2.3 Analysis of Optimized Geometries

If a designer is to select the most important criteria by which to make a selection from a large amount of geometries, it would obviously be the efficiency. In this section we will compare a few geometries that were produced during the optimization process with the aid of Figure 5.7 and Tables 5.6, 5.7, and 5.8.

Figure 5.7 shows the value of the total-total and total-static efficiency versus the number of iterations. The negative iterations represent the NS efficiencies of the database, while the positive values represent the efficiencies obtained during the optimization process. Indeed, this figure resembles the convergence history, but in a way that has more physical meaning to the designer. That is, it is easier to understand efficiencies, rather than penalties.

Looking at the total-total efficiency, one can see that in Figures 5.7a,b that the single point optimum (Iteration -34) has the highest total-static efficiency when compared to the rest of the iterations. This is because the exit width is wider than the rest of the Iterations produced during the optimization. However, at 60 degrees pre-rotation, there is the problem of flow separation at the main blade hub (see fig. 4.26c or 5.10f) which explains why in Figure 5.7c that the total-static efficiency is closer to the efficiencies of the optimized geometries. These optimized geometries all exhibit narrow exit width channels. The reason for the separation could be that the wider exit is causing too much diffusion at 60 degrees pre-rotation. In any event, the single point optimum is clearly not the best candidate for multi-point operation.

Looking at both efficiencies in all three Figures, one can see that Iterations 3, 11, and 33 are clearly set apart from the rest of the geometries. Thus the author will attempt to compare these geometries. However, before doing this, one must say that the contours in Figure 5.8a,c,e are also compared to the baseline and single point optimum contours, where the wide exit contour is the single point optimum. These contours are just to show that the optimized geometry tends to resemble the baseline. In Figure 5.8a,c,e, there is not much variation in the meridional contour to be seen.

Starting with Iteration 3, this geometry has a longer main blade, but a short splitter blade, as can be seen in Figures 5.8a and 5.9a when compared to Iterations 11 and 33 which have the opposite traits. Apart from this, the only real difference between the meridional contours is that the impeller inlet width of Iteration number 33 (Fig 5.8e) is a little smaller than the other two. Since the values of the total-total and total-static efficiencies listed in Tables 5.6, 5.7, and 5.8 are all the around the same value for each of the Iterations, one will try to choose the optimum by means of the Mach number distribution. Of course, the efficiencies change a little from operating point to operating point. This comparison of Mach number distributions takes place just after Figure 5.8.

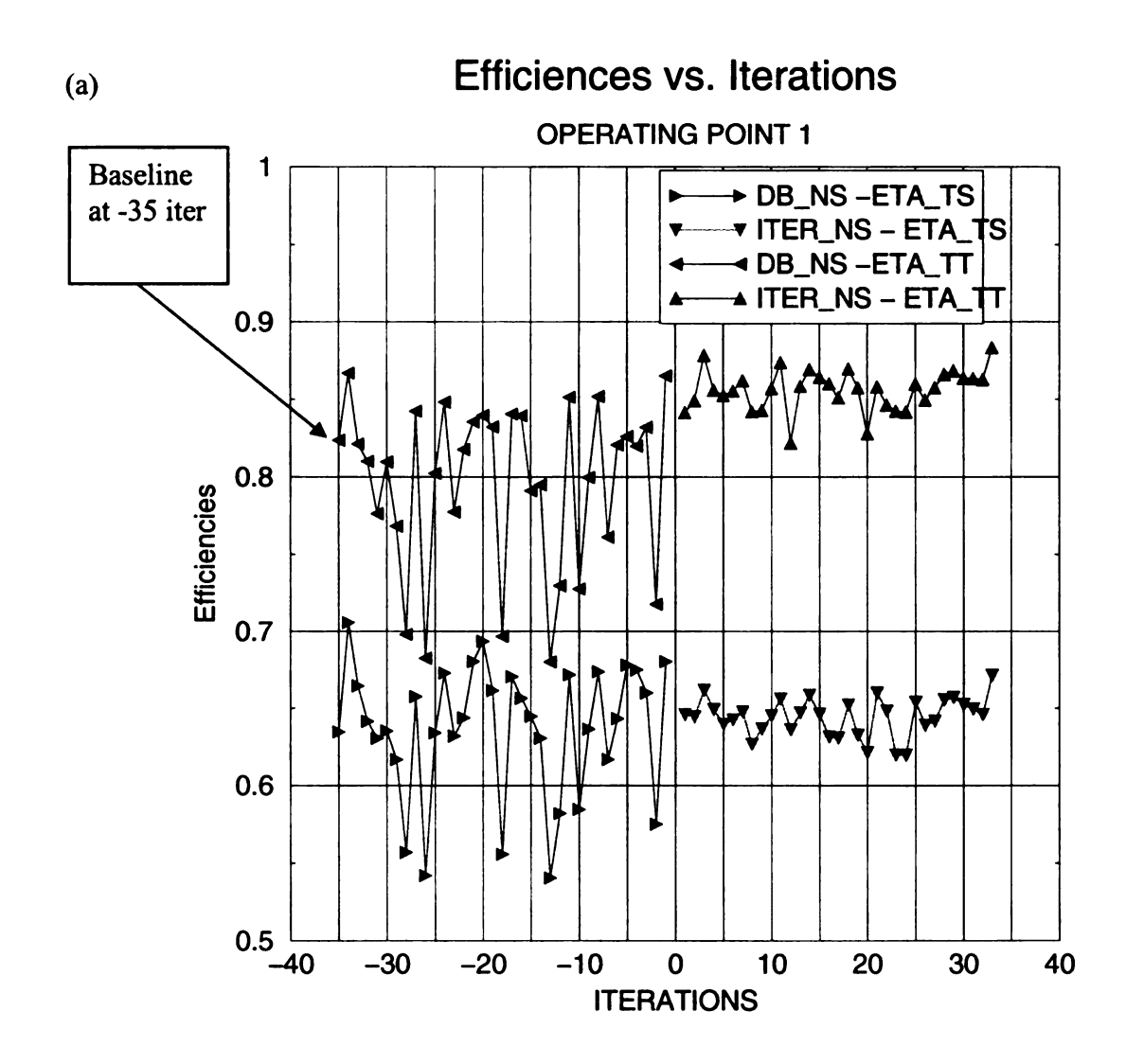


Figure 5.7 Plots of the efficiencies at Various IGV Setting angles. (a) 0° (b) 40° (c) 60°

Efficiences vs. Iterations

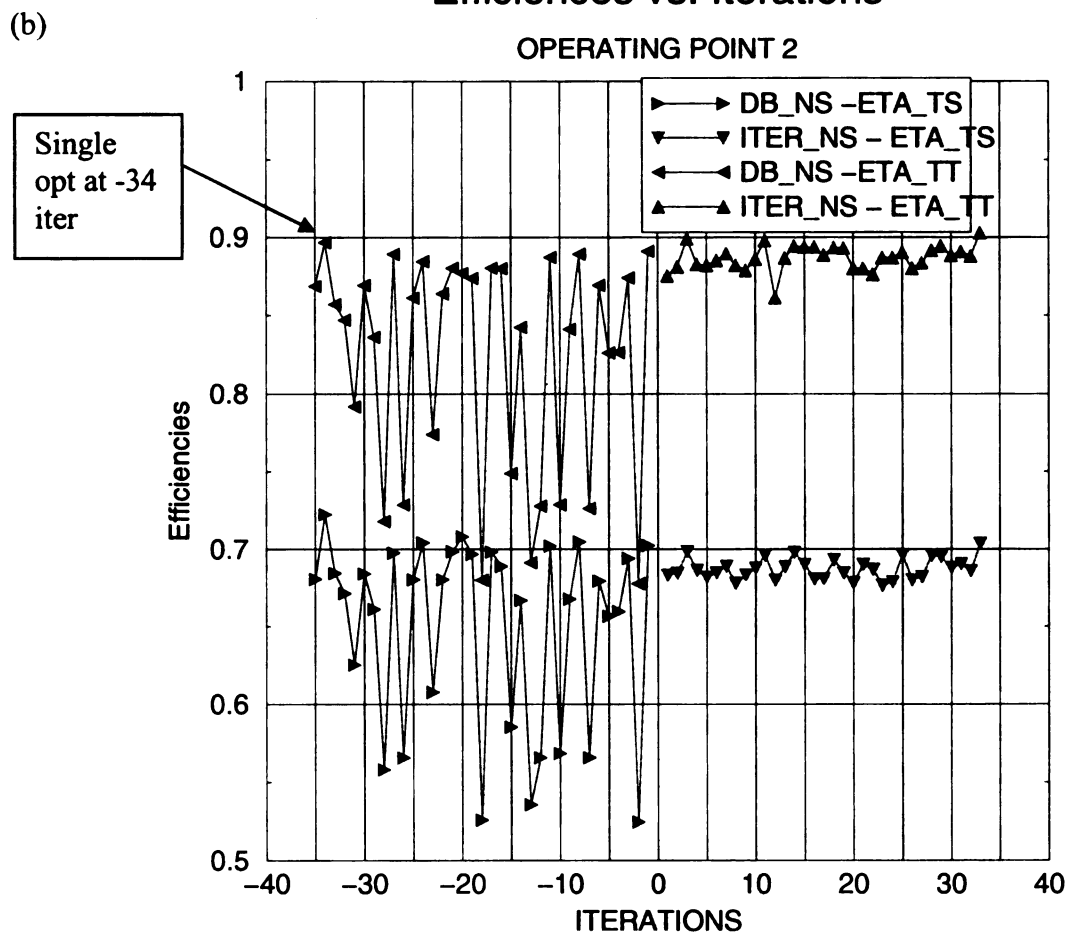


Figure 5.7 (cont'd)

Efficiences vs. Iterations

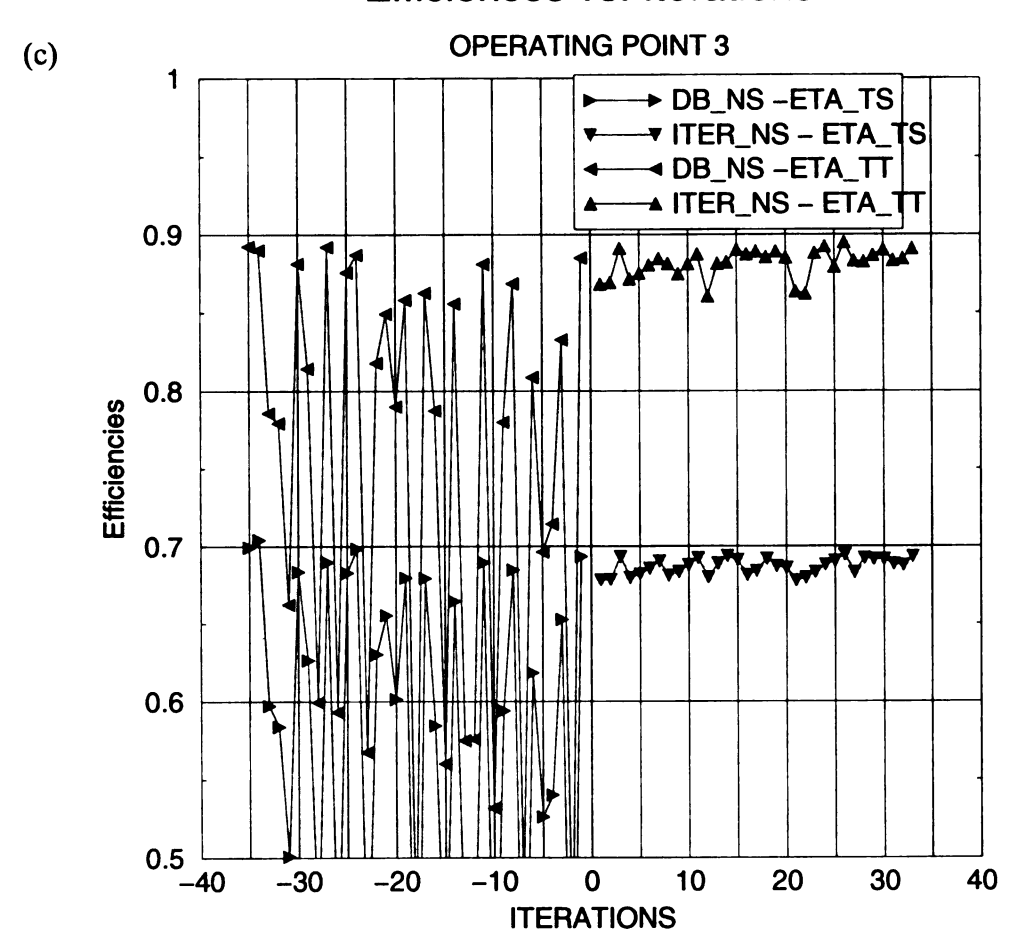


Figure 5.7 cont'd

Table 5.6 NS Results of the Optimizations at Pre-rotation = 0 Degrees

Iteration #	Mass Flow	ETA_TT	ETA_TS	P02/P01	P2/P01	Inlet Lean (Deg)	Outlet Lean (Deg)
1	1.256	0.841	0.646	1.557	1.412	-6.298	45.000
2	1.238	0.849	0.645	1.551	1.402	-7.415	45.000
3	1.328	0.878	0.662	1.558	1.404	-4.984	45.000
4	1.272	0.856	0.649	1.560	1.408	0.000	42.679
5	1.259	0.852	0.640	1.554	1.399	-4.494	45.000
6	1.274	0.855	0.643	1.554	1.399	-5.984	45.000
7	1.255	0.862	0.648	1.549	1.396	-7.603	45.000
8	1.278	0.842	0.627	1.551	1.393	0.000	31.509
9	1.204	0.843	0.637	1.542	1.394	0.000	42.455
10	1.239	0.857	0.645	1.546	1.395	-6.818	45.000
11	1.289	0.874	0.656	1.551	1.397	-7.058	45.000
12	1.091	0.822	0.636	1.529	1.395	0.000	44.050
13	1.236	0.858	0.647	1.547	1.396	-3.270	45.000
14	1.233	0.869	0.659	1.543	1.396	-1.868	45.000
15	1.271	0.864	0.646	1.549	1.394	0.000	41.029
16	1.372	0.860	0.631	1.561	1.394	0.000	17.202
17	1.351	0.851	0.631	1.558	1.397	0.000	18.523
18	1.279	0.870	0.652	1.552	1.397	-2.430	45.000
19	1.324	0.858	0.632	1.552	1.390	0.000	14.359
20	1.355	0.828	0.621	1.563	1.406	0.000	-33.080
- 21	1.245	0.858	0.660	1.554	1.411	-6.329	45.000
22	1.168	0.846	0.649	1.540	1.399	-1.060	45.000
23	1.305	0.842	0.620	1.549	1.387	0.000	-18.049
24	1.296	0.842	0.620	1.543	1.383	0.000	-37.108
25	1.219	0.860	0.654	1.541	1.396	-2.040	45.000
26	1.243	0.850	0.639	1.549	1.397	-3.752	45.000
27	1.259	0.858	0.642	1.550	1.395	-4.859	45.000
28	1.231	0.866	0.656	1.542	1.395	-7.494	45.000
29	1.303	0.868	0.657	1.555	1.403	-2.562	45.000
30	1.335	0.864	0.652	1.562	1.408	-5.211	45.000
31	1.281	0.864	0.650	1.550	1.398	0.000	42.861
32	1.283	0.863	0.646	1.552	1.397	-3.157	45.000
33	1.348	0.884	0.671	1.566	1.413	-7.914	45.000
Single OPT	1.451	0.867	0.705	1.597	1.470	0.000	43.539
Baseline	1.257	0.824	0.635	1.562	1.417	-4.336	45.000

Table 5.7 NS Results of the Optimizations at Pre-Rotation = 40 Degrees

Iteration #	Mass Flow	ETA_TT	ETA_TS	P02/P01	P2/P01	Inlet Lean (Deg)	Outlet Lean (Deg)
1	0.940	0.875	0.683	1.572	1.430	-6.298	45.000
2	0.929	0.881	0.685	1.565	1.423	-7.415	45.000
3	0.965	0.899	0.698	1.565	1.423	-4.984	45.000
4	0.943	0.883	0.686	1.571	1.428	0.000	42.679
5	0.936	0.882	0.682	1.567	1.422	-4.494	45.000
6	0.941	0.885	0.685	1.566	1.422	-5.984	45.000
7	0.934	0.890	0.689	1.561	1.419	-7.603	45.000
8	0.954	0.882	0.678	1.563	1.416	0.000	31.509
9	0.898	0.879	0.683	1.558	1.418	0.000	42.455
10	0.917	0.886	0.688	1.560	1.419	-6.818	45.000
11	0.946	0.898	0.696	1.562	1.420	-7.058	45.000
12	0.822	0.862	0.680	1.551	1.420	0.000	44.050
13	0.916	0.887	0.689	1.561	1.420	-3.270	45.000
14	0.909	0.894	0.698	1.556	1.419	-1.868	45.000
15	0.944	0.894	0.690	1.560	1.417	0.000	41.029
16	1.011	0.894	0.681	1.567	1,415	0.000	17,202
17	1.000	0.889	0.681	1.567	1.418	0.000	18.523
18	0.939	0.894	0.693	1.562	1.420	-2.430	45.000
19	0.979	0.893	0.684	1.561	1.414	0.000	14.359
20	1.015	0.880	0.678	1.569	1.422	0.000	-33.080
21	0.918	0.880	0.690	1.566	1.428	-6.329	45.000
22	0.871	0.876	0.687	1.557	1.422	-1.060	45.000
23	0.988	0.887	0.676	1.559	1.410	0.000	-18.049
24	0.972	0.887	0.679	1.553	1.407	0.000	-37.108
25	0.903	0.891	0.696	1.556	1.420	-2.040	45.000
26	0.932	0.880	0.680	1.564	1.420	-3.752	45.000
27	0.939	0.884	0.682	1.563	1.419	-4.859	45.000
28	0.907	0.892	0.696	1.556	1.419	-7.494	45.000
29	0.956	0.894	0.695	1.565	1.423	-2.562	45.000
30	0.977	0.888	0.688	1.571	1.426	-5.211	45.000
31	0.943	0.891	0.690	1.562	1.420	0.000	42.861
32	0.946	0.888	0.686	1.564	1.419	-3.157	45.000
33	0.972	0.903	0.703	1.570	1.428	-7.914	45.000
Single OPT	1.024	0.897	0.722	1.598	1.465	0.000	43.539
Baseline	0.941	0.869	0.681	1.574	1.433	-4.336	45.000

Table 5.8 NS Results of the Optimizations at Pre-Rotation = 60 Degrees

Iteration #	Mass Flow	ETA_TT	ETA_TS	P02/P01	P2/P01	Inlet Lean (Deg)	Outlet Lean (Deg)
1	0.672	0.868	0.678	1.587	1.441	-6.298	45.000
2	0.665	0.869	0.679	1.581	1.437	-7.415	45.000
3	0.692	0.891	0.693	1.578	1.433	-4.984	45.000
4	0.678	0.872	0.680	1.588	1.441	0.000	42.679
5	0.672	0.875	0.682	1.579	1.435	-4.494	45.000
6	0.674	0.880	0.686	1.577	1.433	-5.984	45.000
7	0.670	0.885	0.690	1.572	1.430	-7.603	45.000
8	0.698	0.882	0.681	1.573	1.426	0.000	31.509
9	0.650	0.875	0.684	1.570	1.429	0.000	42.455
10	0.659	0.881	0.688	1.571	1.430	-6.818	45.000
11	0.676	0.887	0.692	1.574	1.431	-7.058	45.000
12	0.604	0.860	0.680	1.566	1.432	0.000	44.050
13	0.661	0.881	0.689	1.573	1.432	-3.270	45.000
14	0.650	0.882	0.694	1.567	1.431	-1.868	45.000
15	0.686	0.890	0.691	1.572	1.427	0.000	41.029
16	0.731	0.887	0.681	1.575	1.425	0.000	17.202
17	0.724	0.889	0.684	1.578	1.428	0.000	18.523
18	0.670	0.886	0.692	1.573	1.431	-2.430	45.000
19	0.710	0.889	0.687	1.572	1.425	0.000	14.359
20	0.733	0.885	0.686	1.580	1.432	0.000	-33.080
21	0.654	0.864	0.678	1.581	1.440	-6.329	45.000
22	0.629	0.862	0.680	1.572	1.435	-1.060	45.000
23	0.723	0.888	0.683	1.571	1.423	0.000	-18.049
24	0.710	0.892	0.688	1.564	1.419	0.000	-37.108
25	0.648	0.879	0.690	1.568	1.431	-2.040	45.000
26	0.677	0.895	0.695	1.575	1.430	-3.752	45.000
27	0.689	0.883	0.683	1.575	1.428	-4.859	45.000
28	0.651	0.882	0.692	1.569	1.430	-7.494	45.000
29	0.686	0.887	0.691	1.576	1.433	-2.562	45.000
30	0.694	0.890	0.692	1.582	1.435	-5.211	45.000
31	0.678	0.884	0.688	1.573	1.431	0.000	42.861
32	0.682	0.885	0.688	1.576	1.431	-3.157	45.000
33	0.690	0.891	0.693	1.574	1.430	-7.914	45.000
Single OPT	0.701	0.890	0.704	1.610	1.465	0.000	43.539
Baseline	0.657	0.892	0.699	1.596	1.450	-4.336	45.000

Meridional Contours

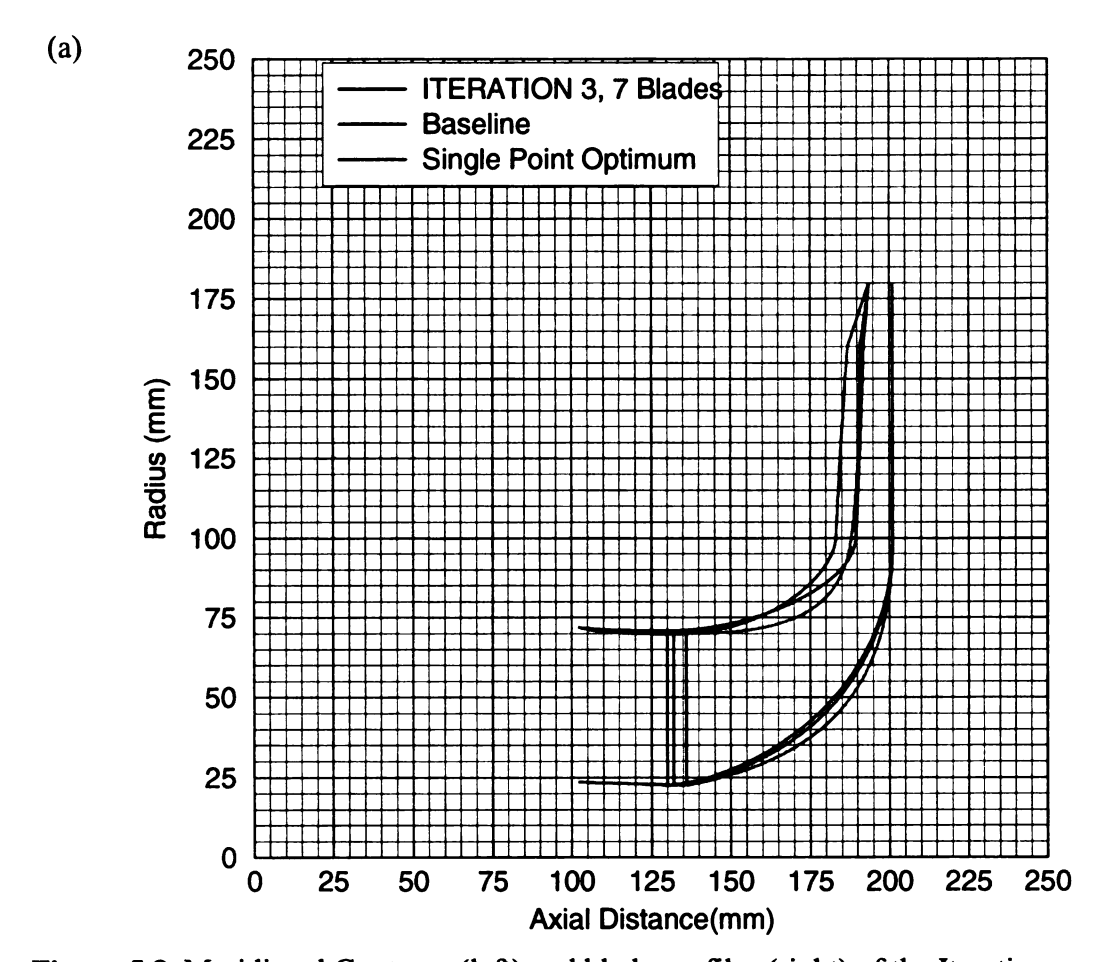


Figure 5.8 Meridional Contours (left) and blade profiles (right) of the Iterations.

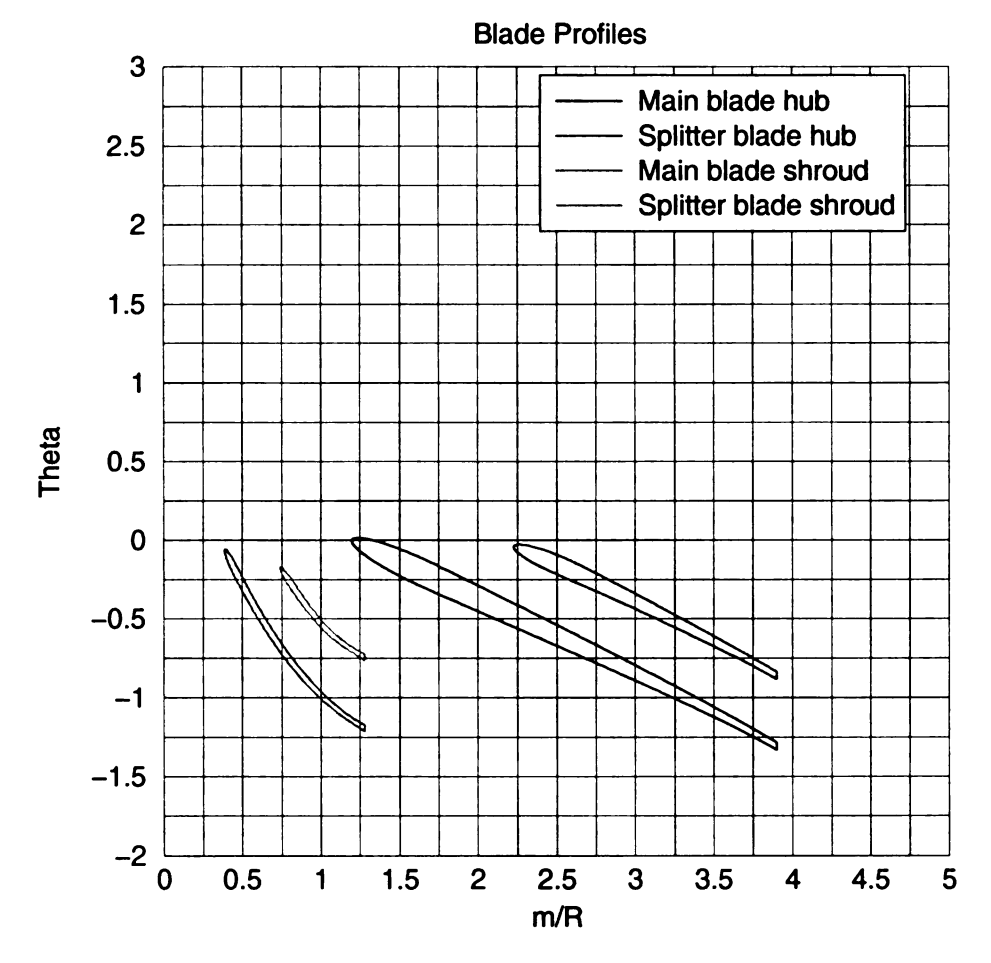


Figure 5.8 cont'd

Meridional Contours

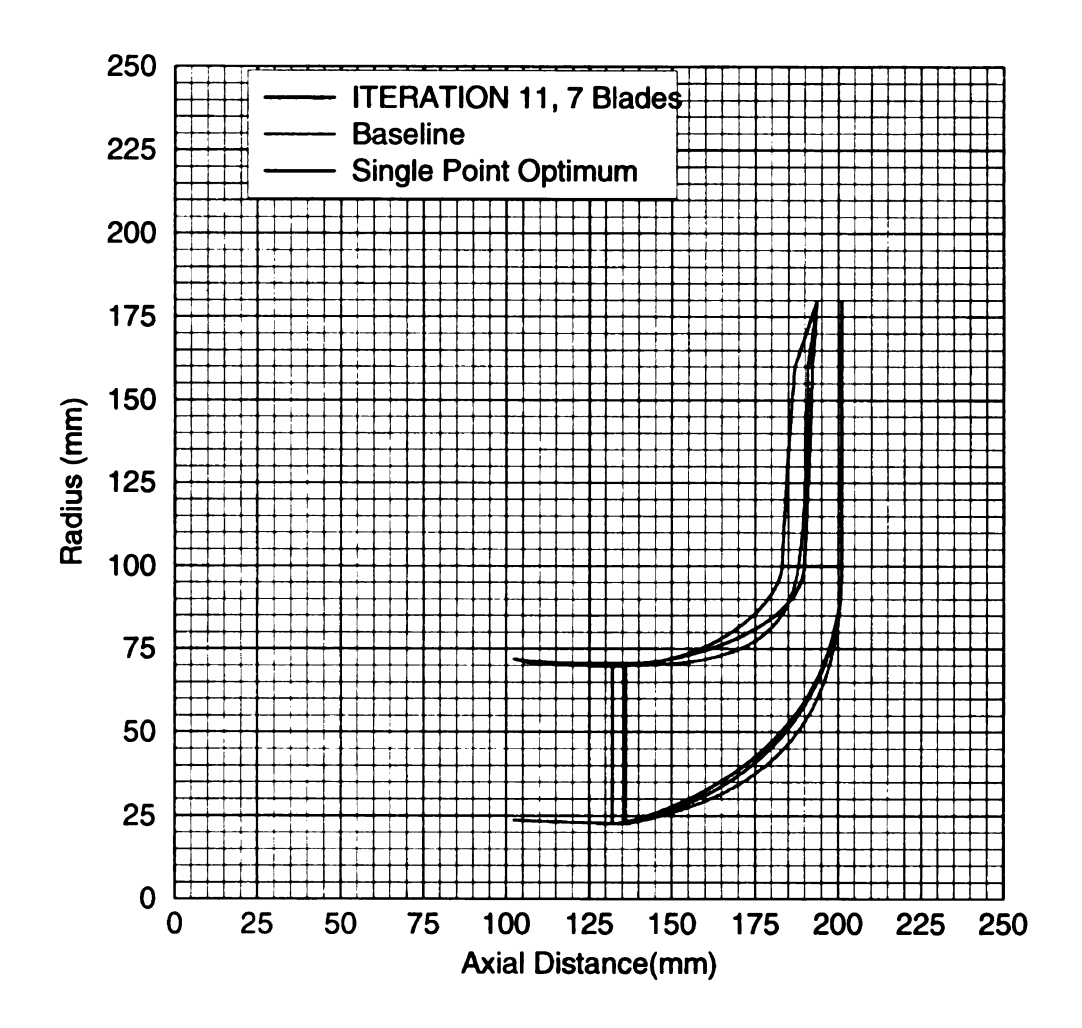


Figure 5.8 cont'd

ITERATION 11, 7 Blades

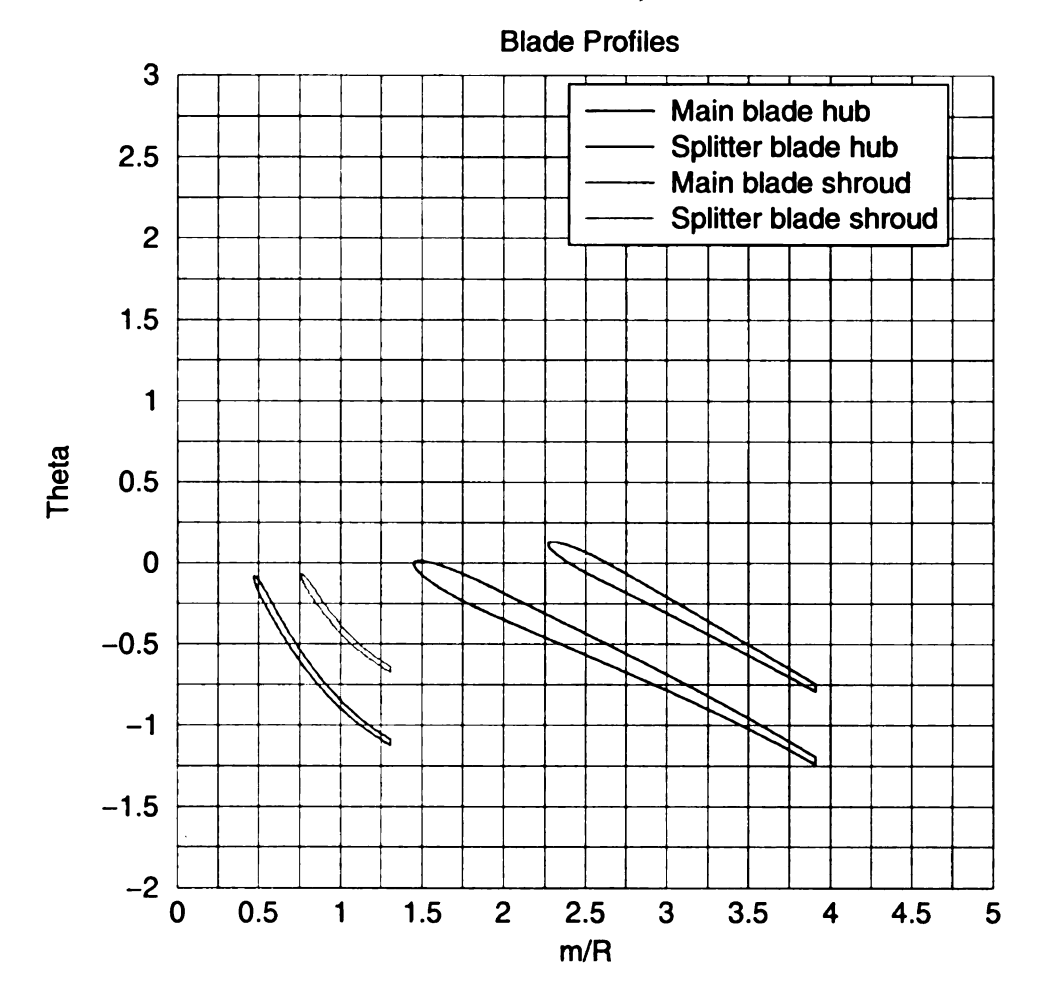


Figure 5.8 cont'd

Meridional Contours

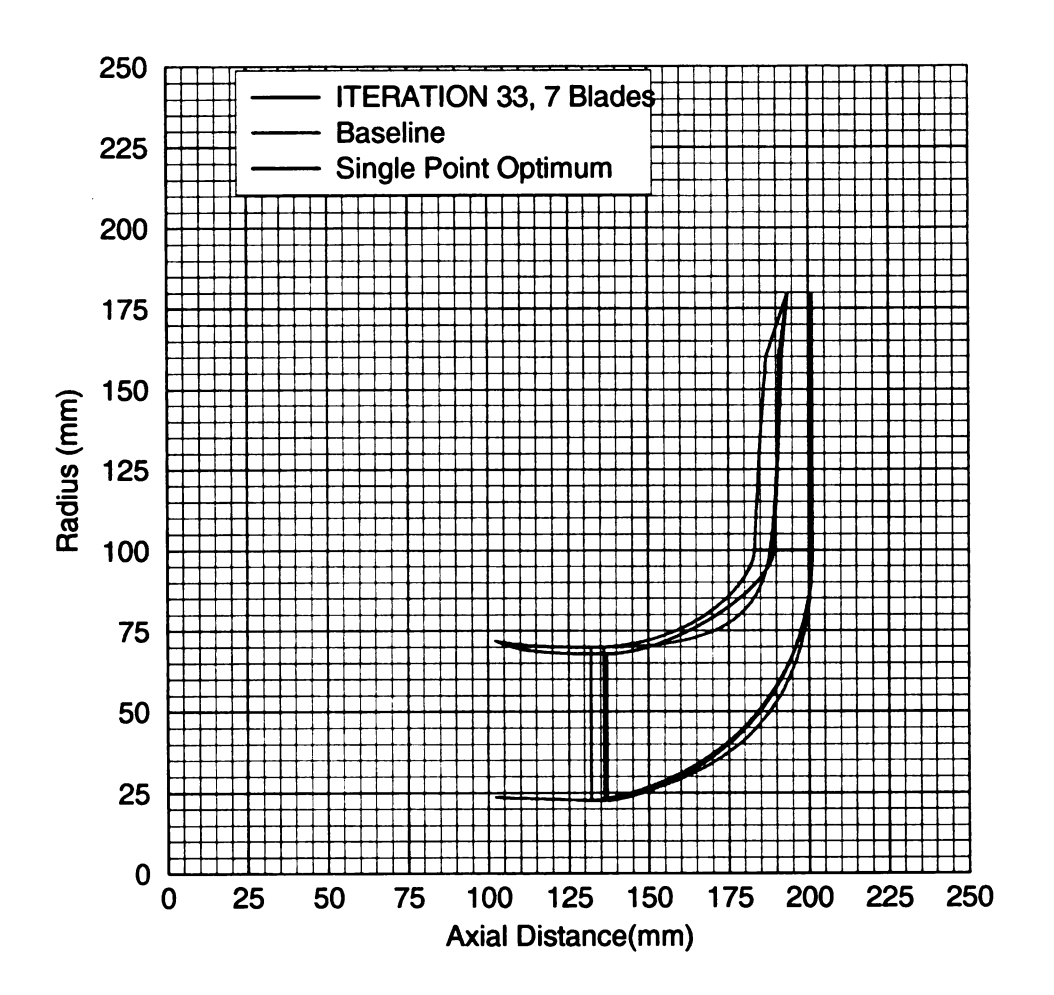


Figure 5.8 cont'd

(f) ITERATION 33, 7 Blades

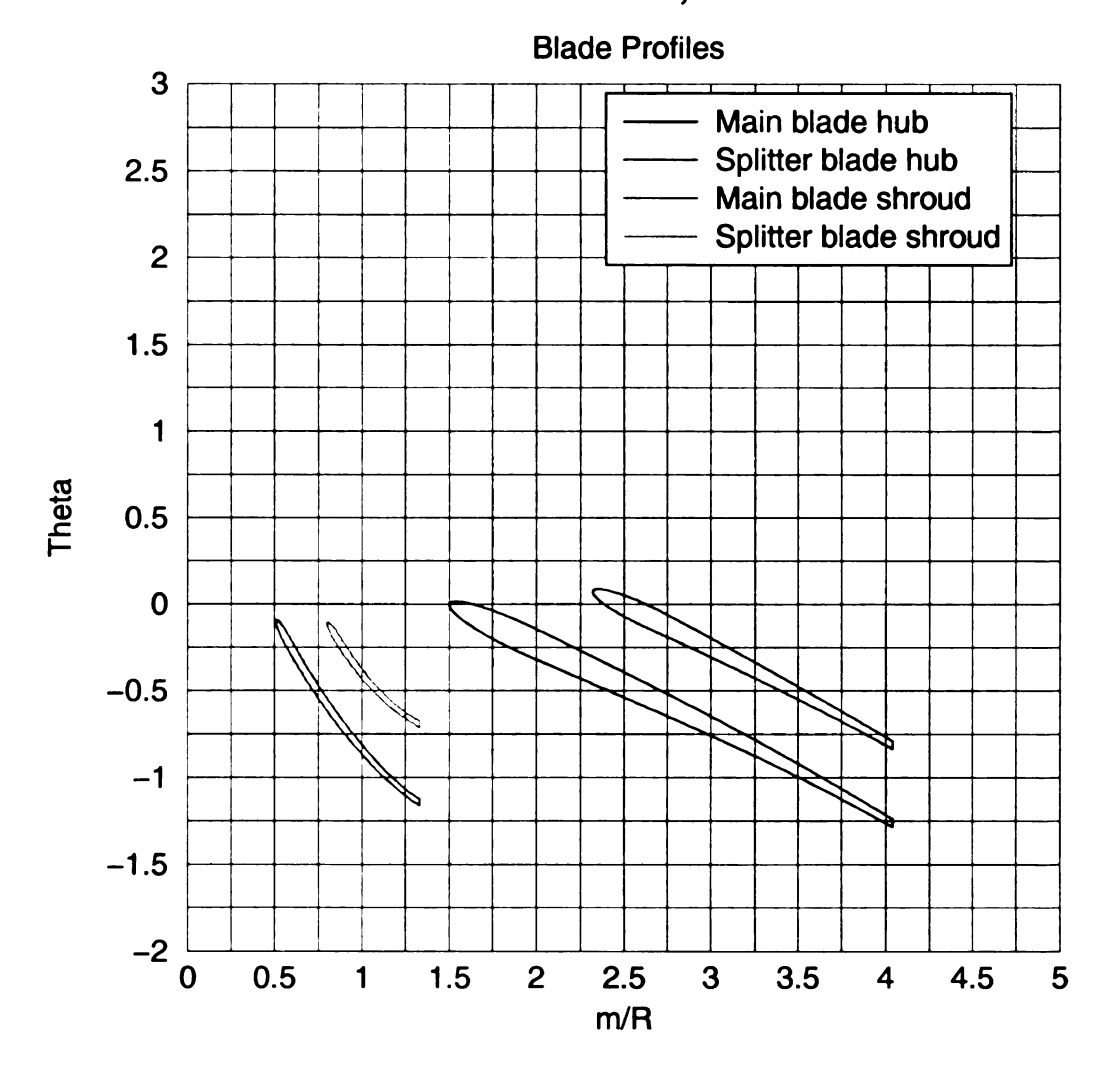


Figure 5.8 cont'd

Looking at Iteration 3, one can see in Figure 5.9(a-c) that the Mach number distributions look quite good at all three operating points. That is, extremely high velocity peaks are not present, there is no loading unbalance. There seems to be a little bit of negative loading at the leading edge of the splitter blade hub of Figure 5.9a. In Figure 5.9c there is negative loading near the leading edge of the main blade hub. The negative loading at 60 degrees pre-rotation was present in all the Iterations that were observed. There must be some problem associated with the highly non-uniform pressure

distribution that is the observed at 60 degrees pre-rotation. On than, these few observations, the Mach number distributions look much better than the baseline (Figure 5.10a-c)

Iteration 11 can be observed in Figure 5.9(d-f). In Figure 5.9d negative loading is present near LE of the splitter blade at the hub. However the rest of the blade distributions look acceptable. That is, no loading unbalance, no extremely high velocity peaks. In Figure 5.9e, the distribution is quite good, perhaps one of the best that has been observed yet. In Figure 5.9f, the distribution looks alright. However, the ever bothersome negative loading is present at full blade hub leading edge

Iteration 33 can be observed in Figure 5.9g-i. In Figure 5.9g the high velocity peaks are not present, which is good. There is no loading unbalance and no negative loading. Continuing on with Figure 5.9h one can see a good distribution. Perhaps, there is not enough diffusion however. Finally in Figure 5.9i, there is still negative loading that is always present, plus a little amount of return flow at the splitter blade hub.

Finally, it is obvious that the Mach number distributions in Figure 5.10 (a-f) are clearly worse than the ones in Figure 5.9. Well, that is if one requires them to be suitable for multiple point operation. So based on Mach number distribution, it looks like Iteration 3 is the best.

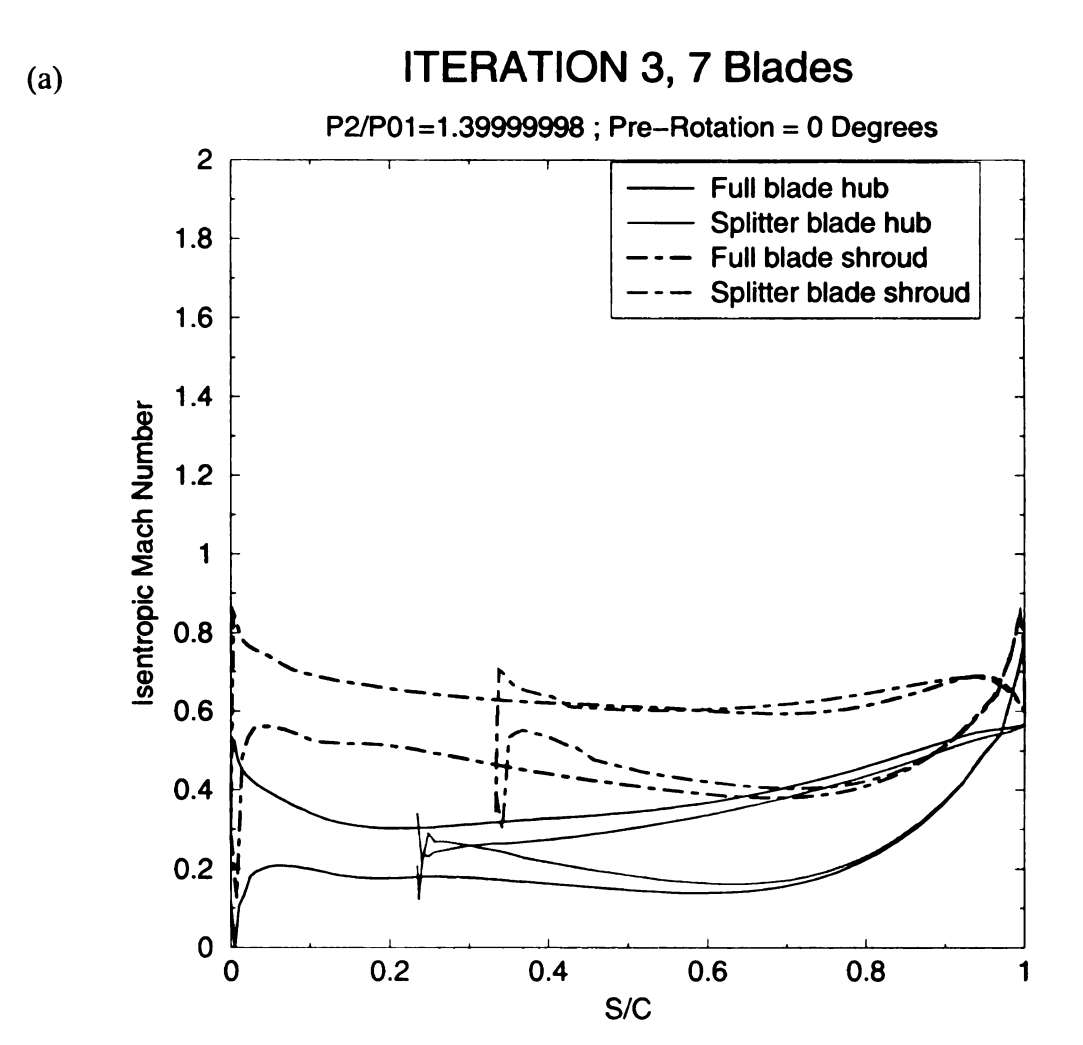


Figure 5.9 Mach number distributions at various IGV settings of Iterations

ITERATION 3, 7 Blades

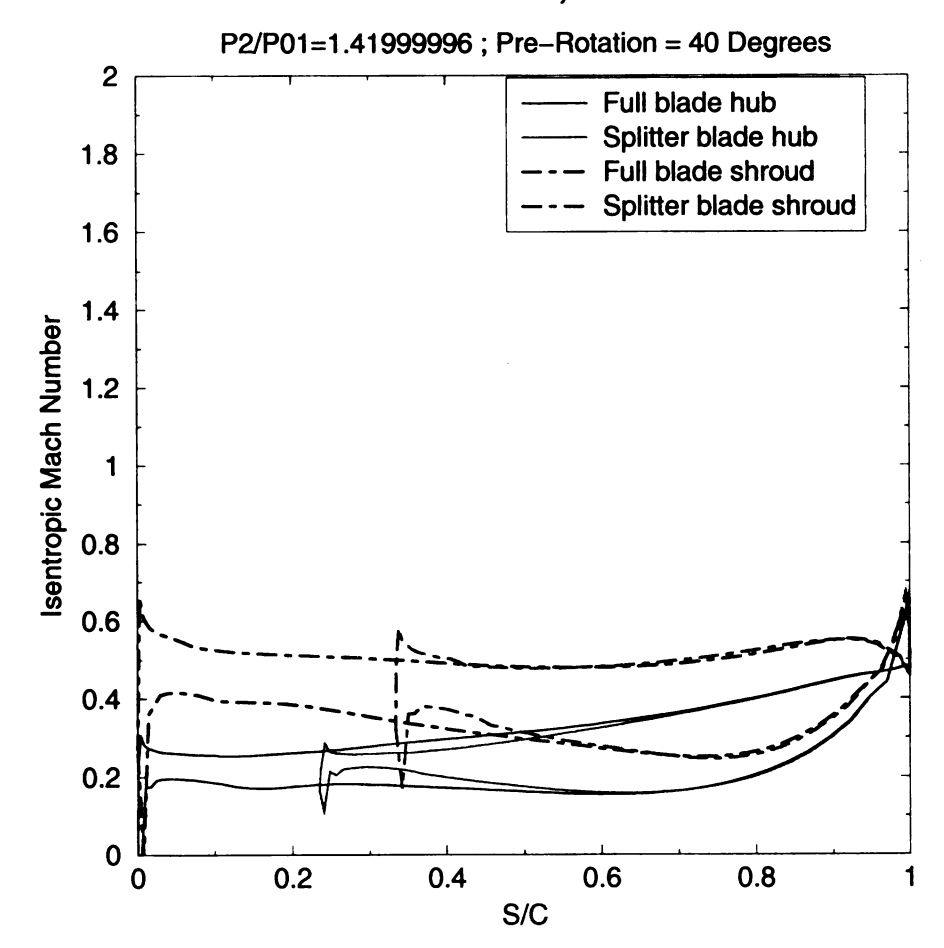


Figure 5.9 Cont'd

(c) ITERATION 3, 7 Blades

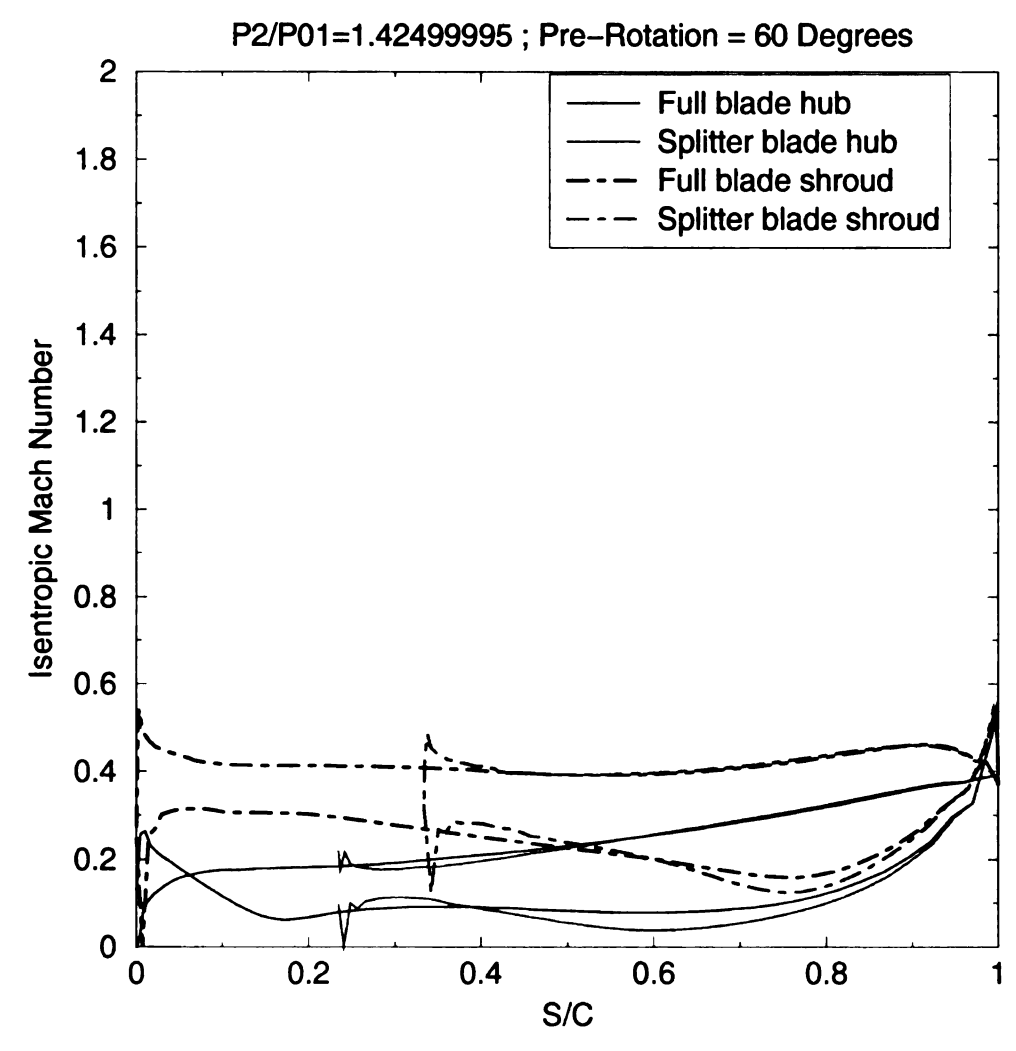


Figure 5.9 Cont'd

(d) ITERATION 11, 7 Blades

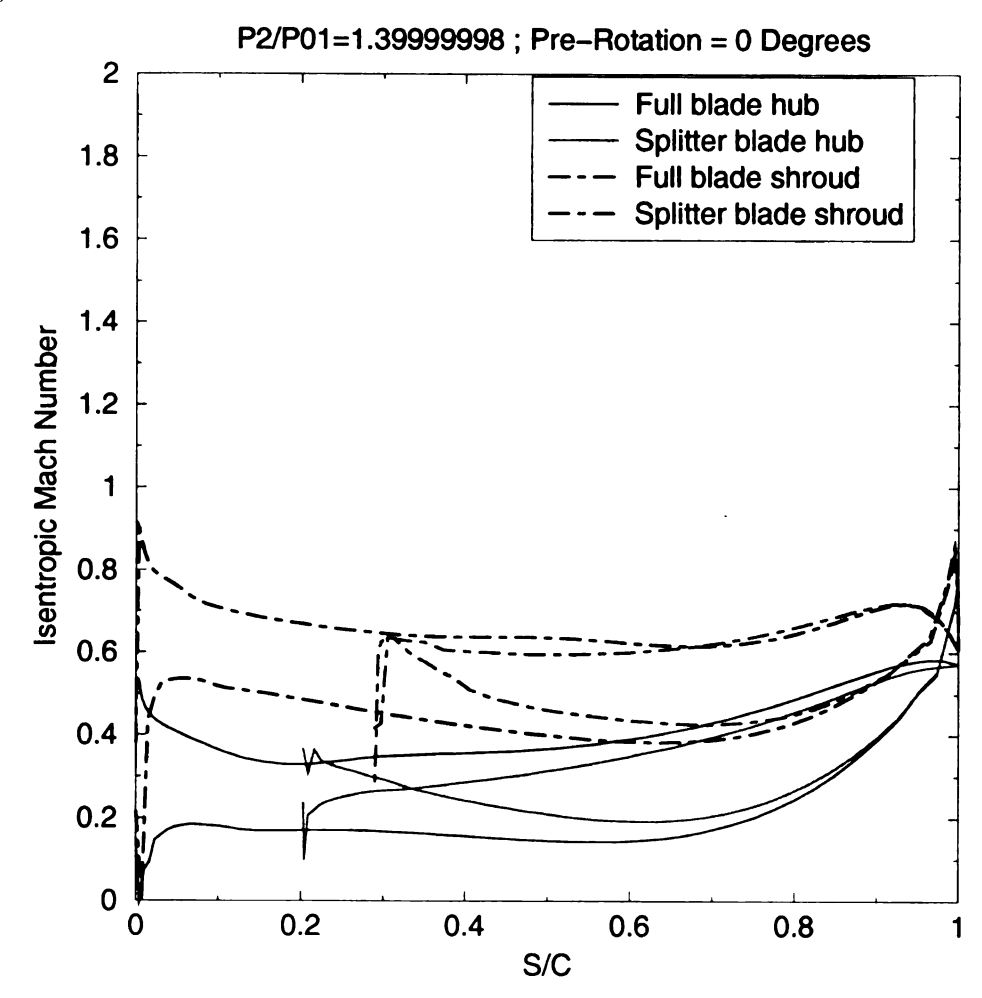


Figure 5.9 Cont'd

(e) ITERATION 11, 7 Blades

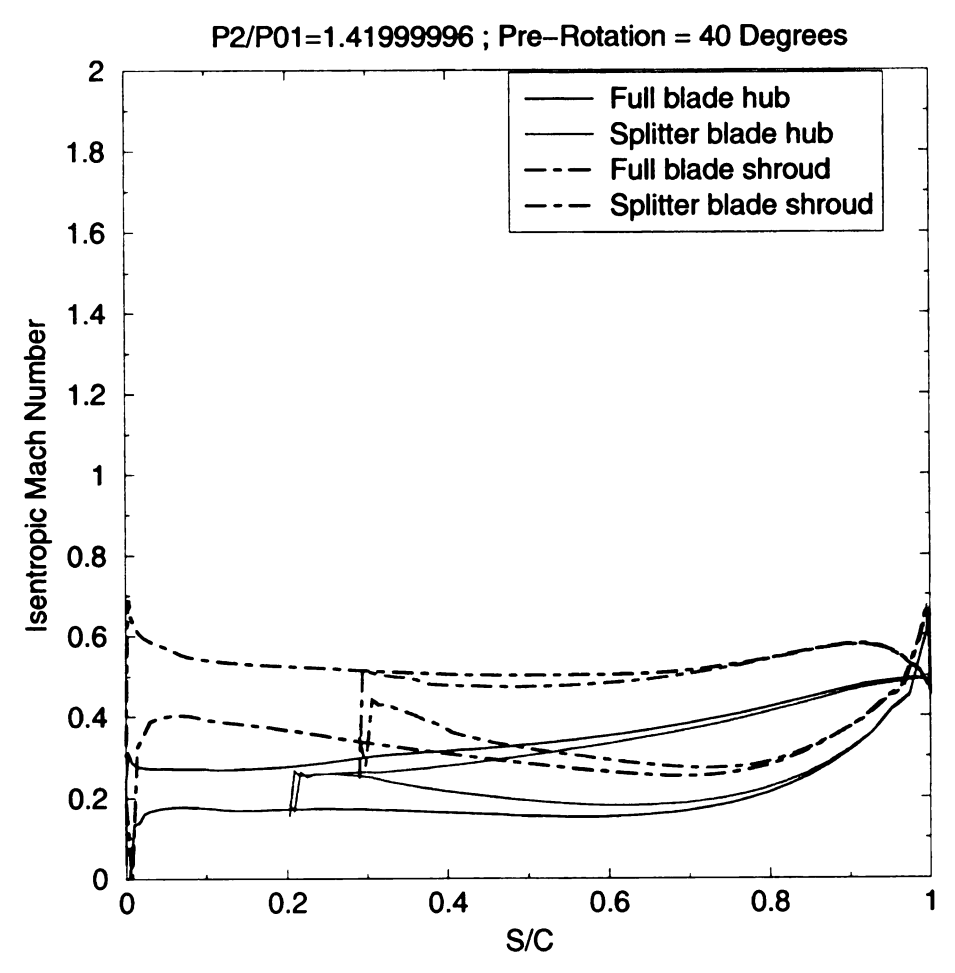


Figure 5.9 Cont'd



(f)

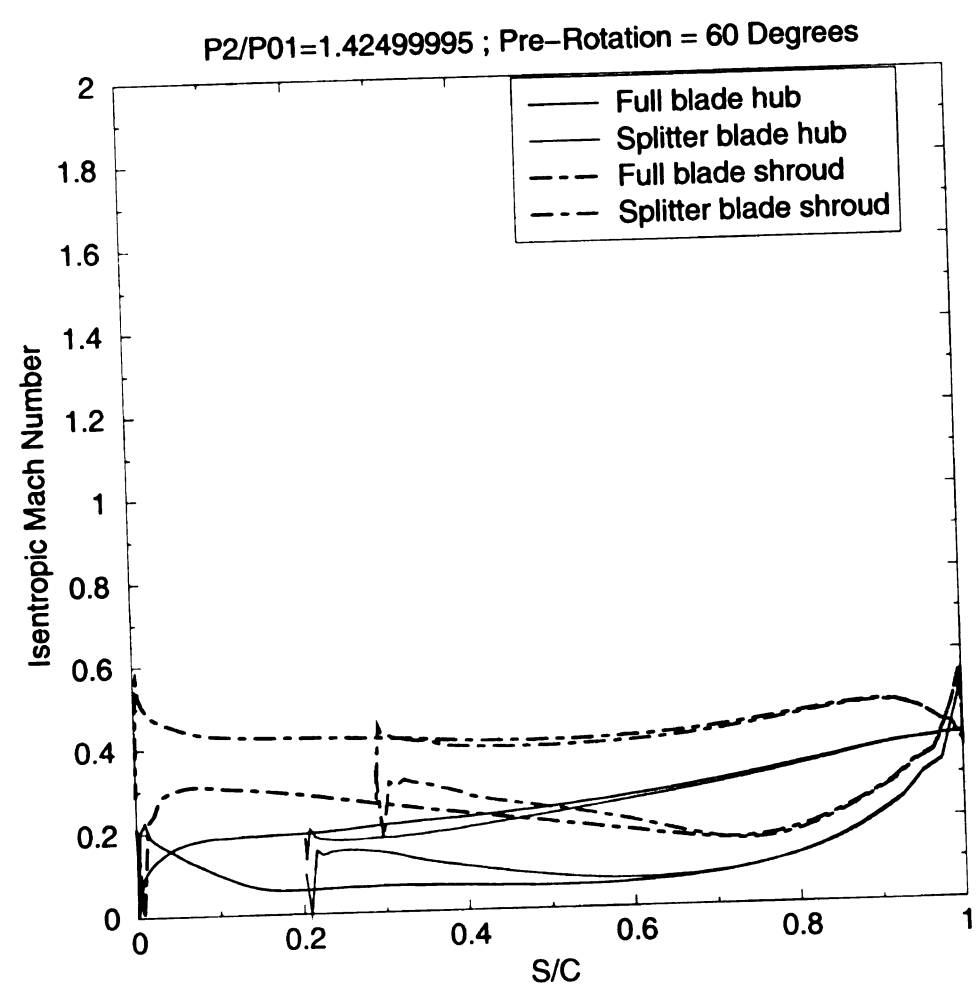


Figure 5.9 Cont'd

ITERATION 33, 7 Blades

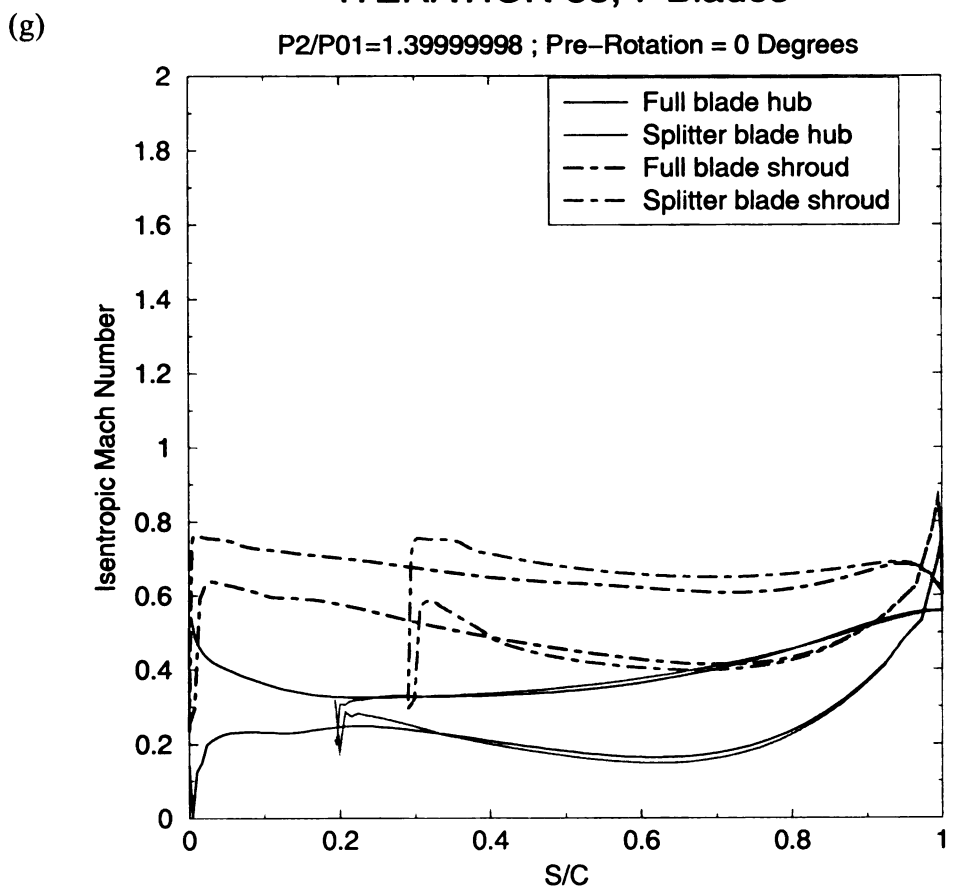


Figure 5.9 Cont'd



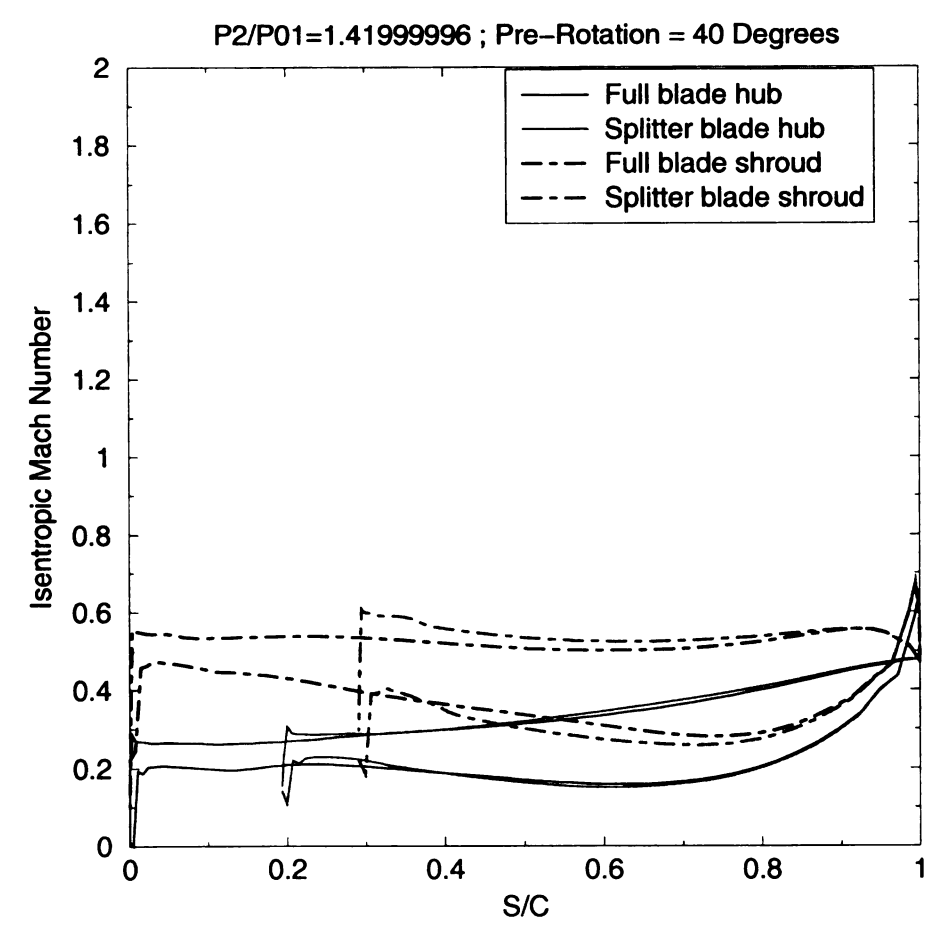


Figure 5.9 Cont'd

(i) ITERATION 33, 7 Blades

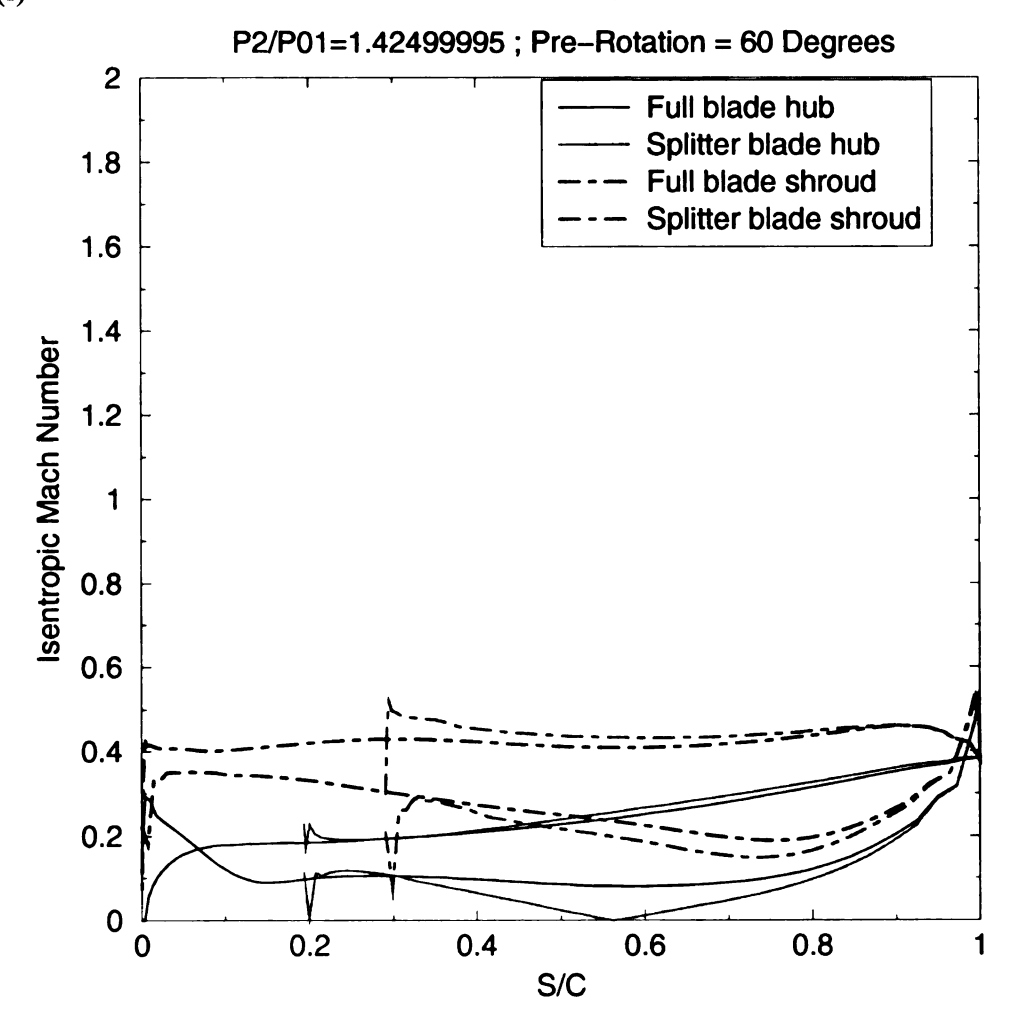


Figure 5.9 Cont'd

Baseline Mach number Distribution (a) Pre-Rotation = 0 Degrees 2 Full blade hub Splitter blade hub 1.8 Full blade shroud Splitter blade shroud 1.6 1.4 Isentropic Mach Number 1.2 1 0.8 0.6 0.4 0.2

0

0

0.2

Figure 5.10 Mach number distributions of the Baseline and Single Point Optimum geometries.

S/C

0.4

0.6

0.8

(b) Baseline Mach number Distribution

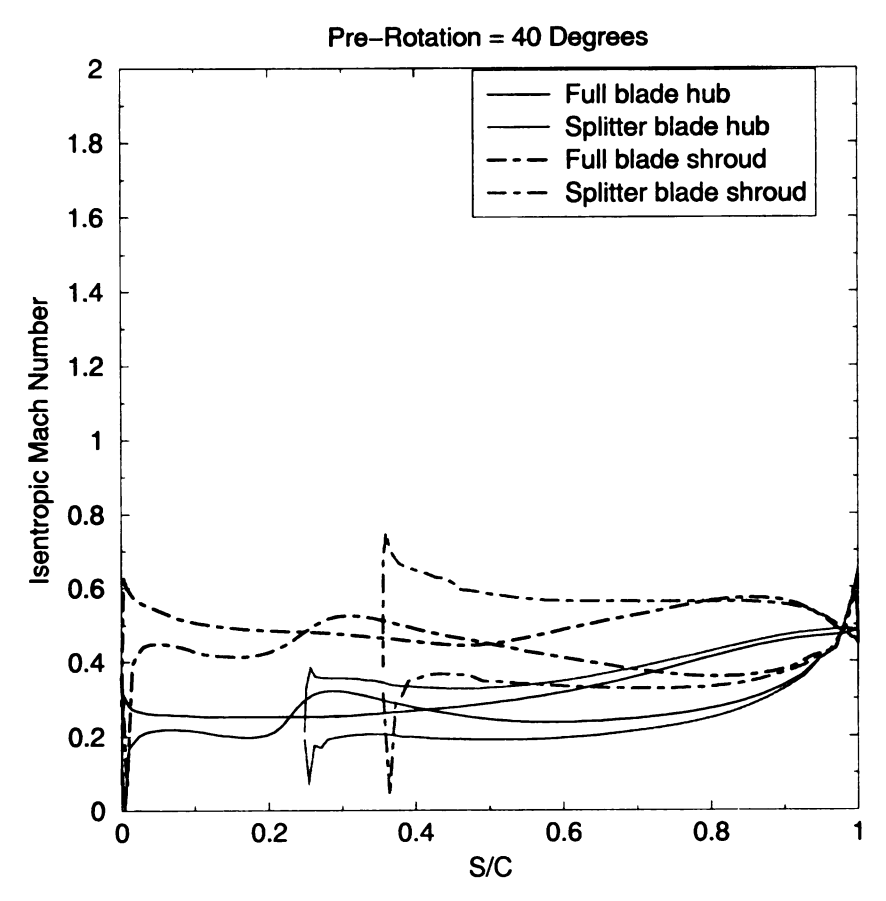


Figure 5.10 cont'd

(c) Baseline Mach number Distribution

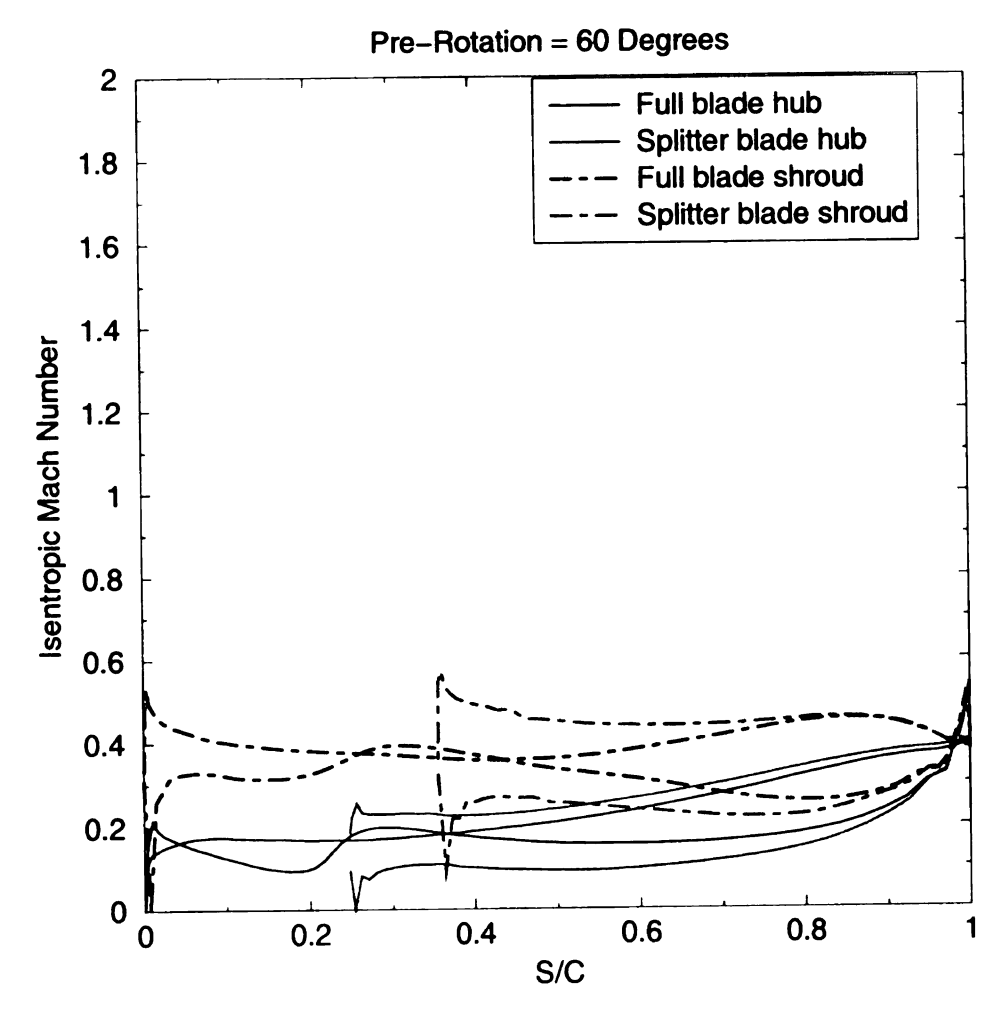


Figure 5.10 cont'd



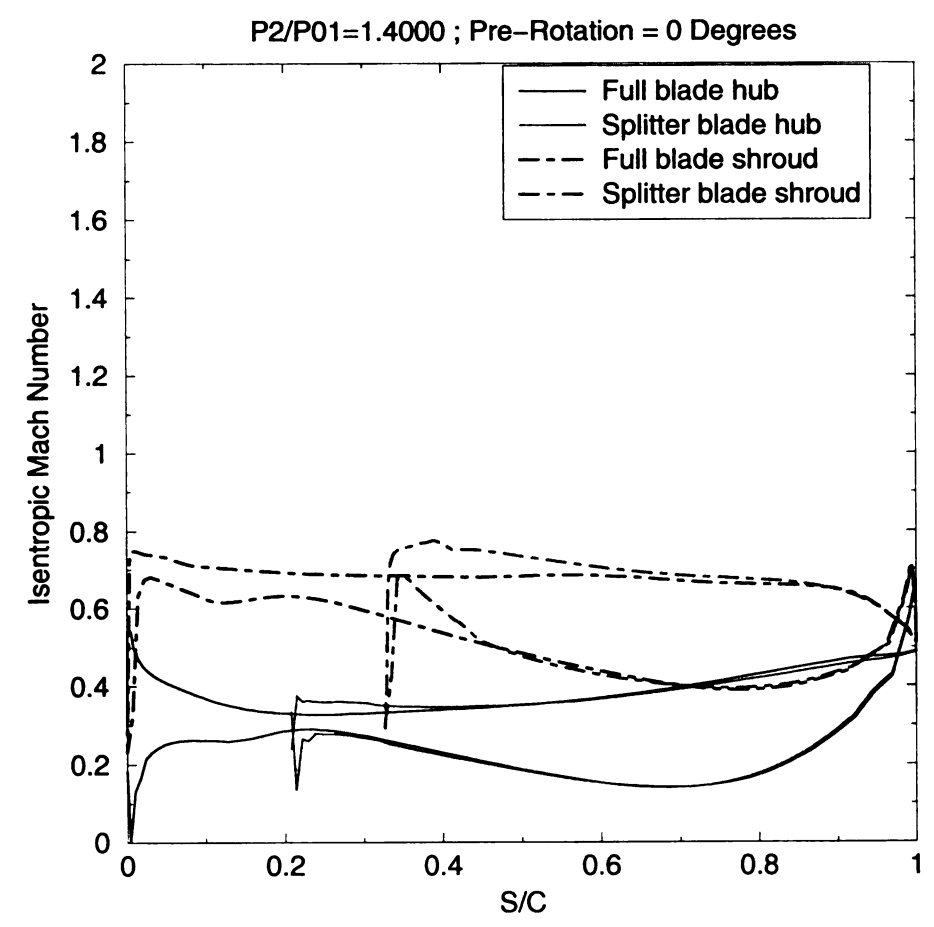


Figure 5.10 cont'd



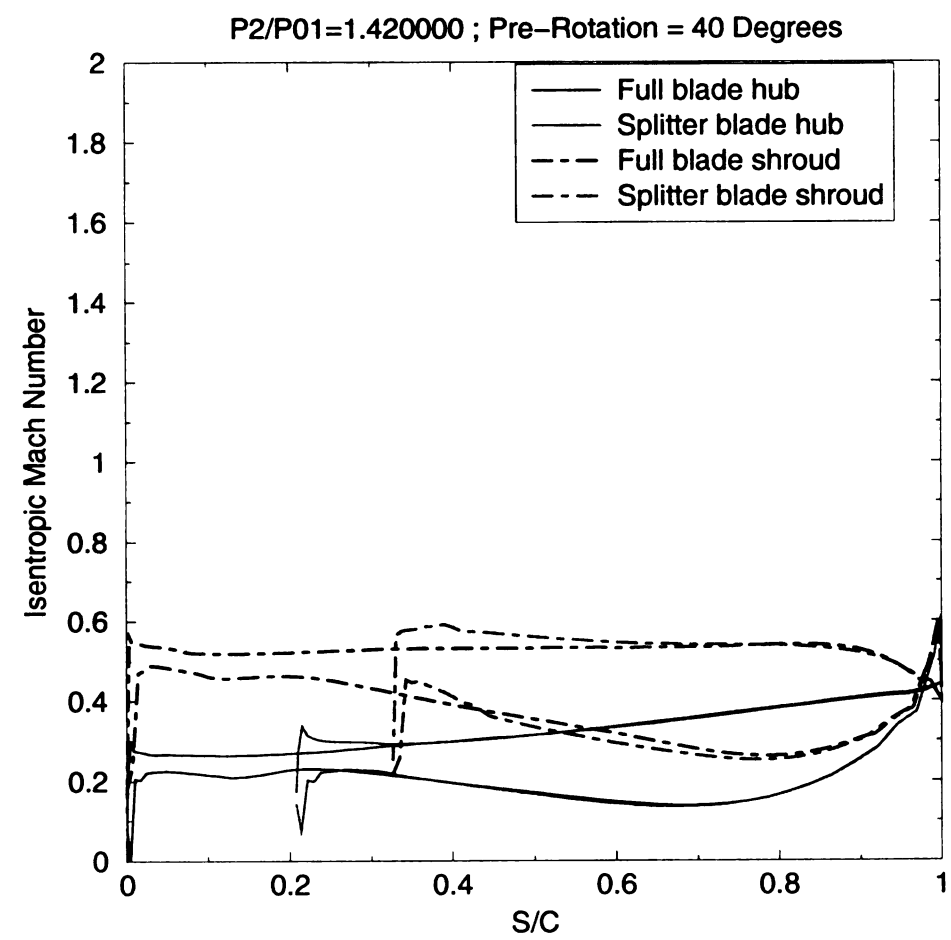


Figure 5.10 cont'd



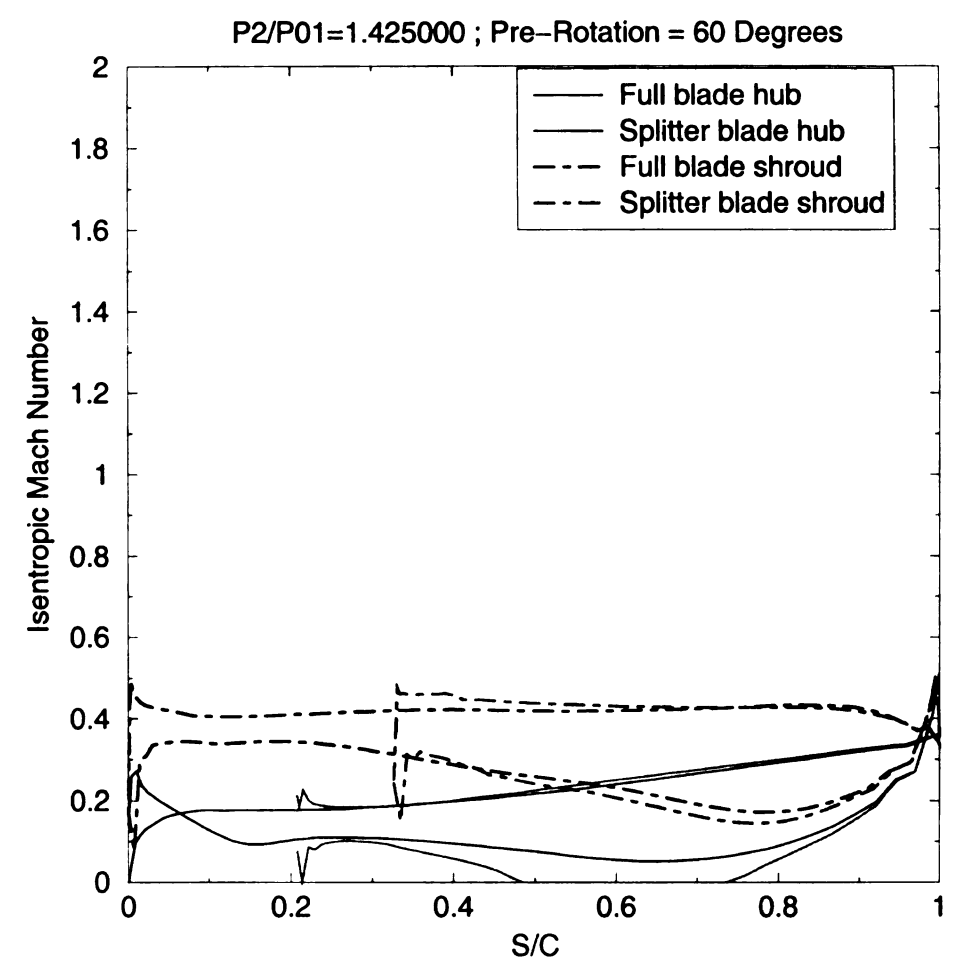


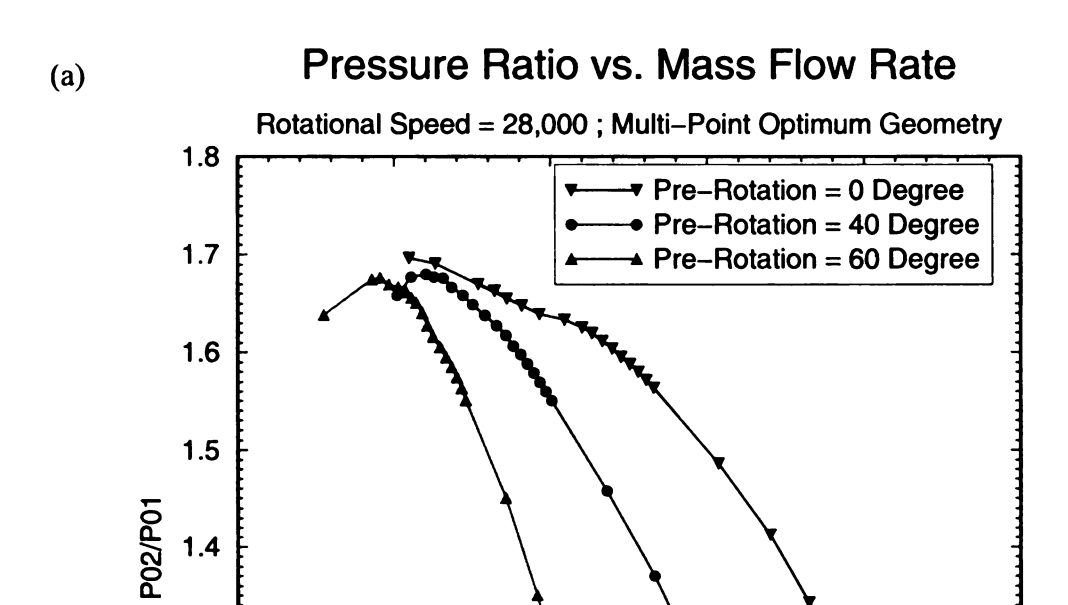
Figure 5.10 cont'd

5.3 Performance of Optimum Geometry and Conclusion

All of the geometries that have been analyzed are rather good, when compared to the baseline. So the question is, how does one select the best one? It is quite difficult to say that there is the ultimate optimum geometry that is by far better than any other one. In fact, there are many suitable candidates for the operation of an air conditioner and other applications. Since the efficiencies are all around the same values, the designer then looks at the Mach number distributions for some insight. Doing this, it is evident Iteration 3 is the best even though Iteration 33 has a slightly higher efficiency. The reason why Iteration 33 was not chosen was because there is a slight local return flow at the splitter blade hub as illustrated above in Figure 5.9i. Finally some characteristics of Iteration 3 and its performance map can be seen Table 5.12 and Figure 5.11.

Table 5.9 Characteristics of the Multi-Point Optimum Geometry

Geometric Characteristics	Control of the Contro
Beta-le-hub	24.98 Degrees
Beta-le-hub-sp	21.31 Degrees
Beta-le-shr	64.56 Degrees
Beta-le-shr-sp	57.38 Degrees
Beta-te	30.00 Degrees
Shroud clearance	0.575 mm
Max Hub Thickness	4 mm
Min Hub Thickness	3 mm
Max Shroud Thickness	3 mm
Min Shroud Thickness	2.5 mm
Percent blade chord length where finishes	25 %
the transition from Max to Min thickness.	
Thickness remains constant from this	
point all the way the trailing edge.	
Impeller Tip Radius	100 mm



1.3

1.2

1.1

1

0

0.5

Figure 5.11 Performance Map: (a) Pressure ratio (b) η_{ts} (c) η_{tt}

Mass Flow Rate (Kg/s)

1.5

2

2.5

Total to Static Efficiency vs. Mass flow rate

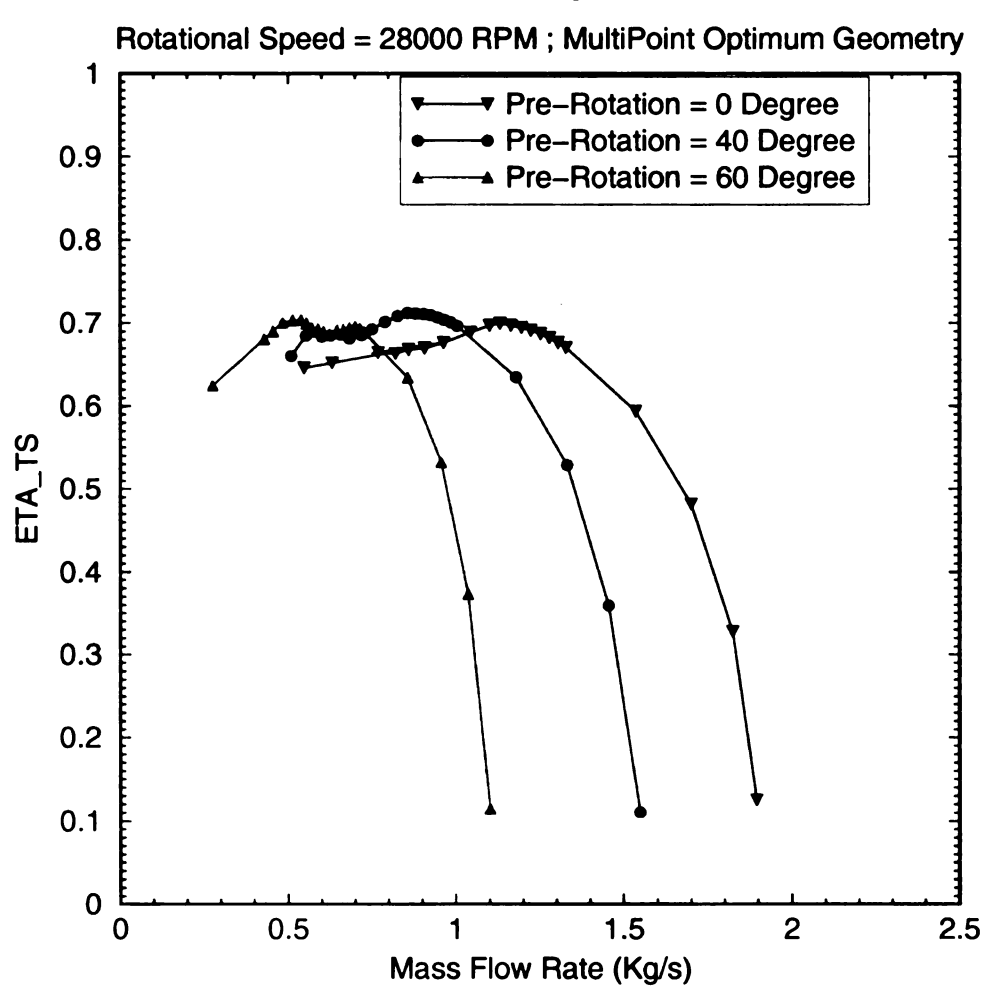


Figure 5.11 cont'd

(c) Total to Total Efficiency vs. Mass flow rate

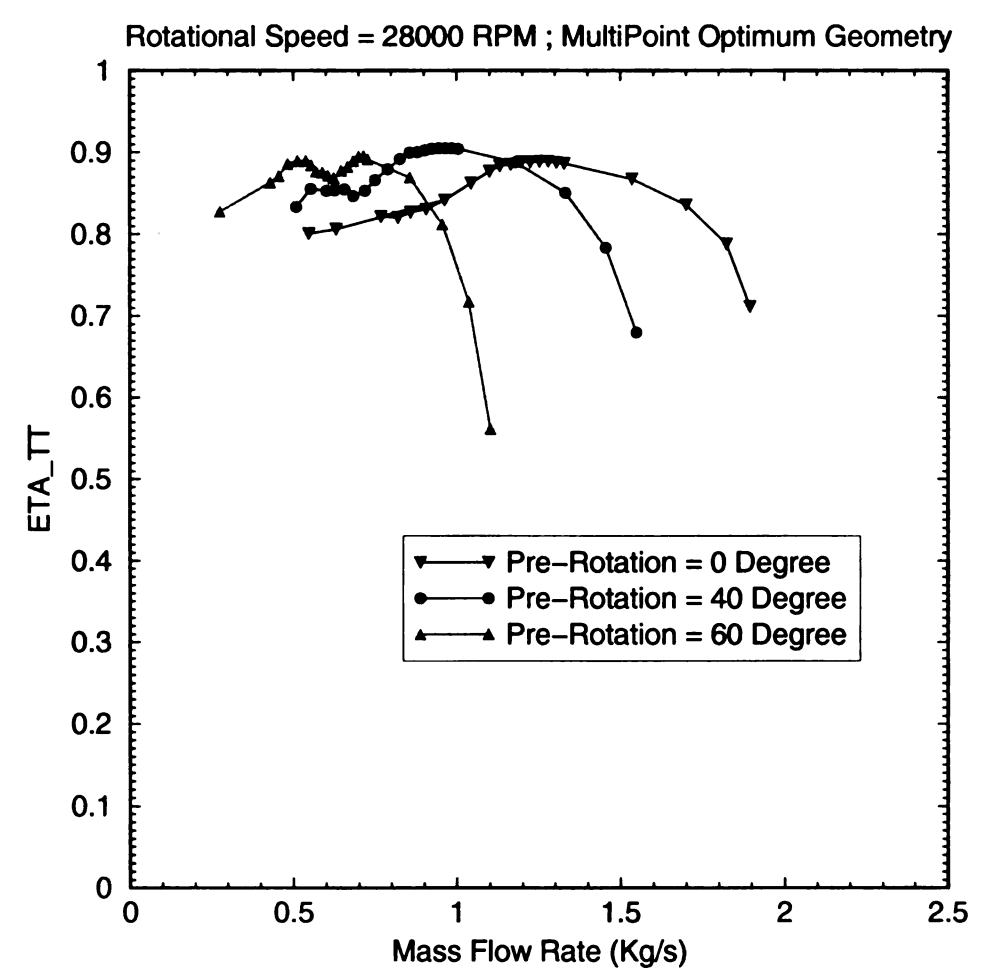


Figure 5.11 cont'd

Thus the multi-point optimum has an efficiency improvement over the baseline at the various operating points. These improvements are:

OP1:

 A 5 point increase in total-total efficiency and almost a 3 point increase in totalstatic efficiency

OP2:

• A 3 point increase in total-total efficiency and almost a 2 point increase in totalstatic efficiency

OP3:

• A 0 point increase in either efficiencies. However, the Mach number distribution for multi-point optimum is better than the baseline distributions. Perhaps there is no improvement because of the fact that the losses coming from the IGV are too high. Another alternative would be that perhaps not enough emphasis or weight was placed at the operating point corresponding to the spring time (Pre-Rotation = 60 Degrees).

CHAPTER 6

OVERALL CONCLUSIONS AND FUTURE WORK

The following conclusions are supported by the results of the study:

Single Point:

- ✓ The total to static efficiency of the impeller was improved by 7 points for the single point case when compared to the baseline. The reason is that the exit width is larger than the baseline, which naturally gives rise to increased total-static efficiency. Another contributor to the increased efficiency is simply that the Mach number distributions are much better than the ones corresponding to the baseline.
- ✓ The total-total efficiency of the impeller was improved by 4 points. Again, the Mach number distributions are much better. That is, no high velocity peaks are observed and thus there should not be any corresponding separation or incidences losses.
- ✓ At 60 degrees Pre-Rotation the single point optimum exhibits separation at the splitter blade hub, thus making it an unsuitable candidate for multi-point operation. A possible reason for the separation can be attributed to the fact the exit width is too wide, which results in too much diffusion.

Multiple Points:

- ✓ The total to static efficiency increased by 3, 2, and 0 points for the pre-rotations of 0, 40, and 60 degrees respectively. That is, relative to the baseline of course. These improvements are less than the single point optimum because of the fact that the geometry has to accommodate for the very non-uniform inlet profile. Even though there is really no improvement in efficiency at the 60 pre-rotation case, the Mach number distribution is improved for all three setting angles.
- ✓ The total to total efficiency increased by 5, 3 and 0 points for the pre-rotations of 0, 40, and 60 degrees. That is, relative to the baseline of course. The improvement is actually greater than for the single point optimum. Of course, if one were to choose a different single point optimum, then it is possible to achieve one more point. This gives rise to the final conclusion

Overall:

✓ It is difficult to determine the ultimate optimum, especially for the single point case. Thus is can be said that there exist many feasible solutions in the design space. Perhaps in the future it will be possible to find the absolute, without a doubt, optimum geometry.

Some suggestions for future work include:

- > Implement for a variable vaned diffuser along with an IGV
- > Implement for a Low solidity diffuser with the IGV
- > Test even more operating points.
- > Perform Multi-disciplinary optimization.

REFERENCES

- 1. Pierret, S. <u>Designing Turbomachinery blades by means of the function</u>
 <u>approximation concept based on Artificial Neural Network, Genetic Algorithm,</u>
 <u>and the Navier-Stokes Equations</u>.
- 2. Van den Braembussche, R. <u>Fast Multidisciplinary Optimization of Turbomachinery Components.</u>
- 3. Doulgeris. <u>Designing Nonsymmetrical IGVs by means of the VKI inverse design</u> method.
- 4. Alsalihi, Z. Optimization of Radial Impellers and Diffusers manual 58-b.
- 5. Alsalihi, Z. TRAF3D SPLITTER-NOSPLITTER MANUAL
- 6. Sapiro, L. Centrifugal Compressors.
- 7. Van den Braembussche, One dimensional design, VKI Course Note 134
- 8. Van den Braembussche, <u>Radial Impeller Design Methodology</u>, VKI Course Note 162
- 9. Van den Braembussche, <u>Design and Optimization of Centrifugal Compressors</u>, VKI Course Note 141
- 10. Simon, H. et al, <u>Improvements in Performance Characteristics of Single-Stage</u> and <u>Multistage Centrifugal Compressors by Simultaneous Adjustments of Inlet</u> Guide Vanes and Diffuser Vanes.
- 11. Cengel and Boles, *Thermodynamics*, 3rd Edition, 1998.
- 12. Van den Braembussche, *Surge and Stall in Centrifugal Compressors*, Pre-Print 1984-15.
- 13. Van den Braembussche, <u>Stability and Range in Centrifugal Compressors</u>, Re-Print 1996-51.

